An Organ-on-a-Chip Model to Study Neuroinflammation

By

NOAH GOSHI
DISSERTATION

Submitted in partial satisfaction of the requirements for the degree of

DOCTOR OF PHILOSOPHY

in

Biomedical Engineering

in the

OFFICE OF GRADUATE STUDIES

of the

UNIVERSITY OF CALIFORNIA

DAVIS

Approved:

Erkin Seker, Chair

Pamela Lein

Karen Moxon

Committee in Charge

2022

An Organ-on-a-chip Model to Study Neuroinflammation

Abstract

Neuroinflammation plays a significant role in a wide range of neurological disorders, from neurodegenerative diseases to cancer, affecting millions of people worldwide. As a result, there is a critical need to better understand the mechanisms underlying neuroinflammation and its relationship to different disease states. Organ-on-a-chip platforms can aid in this research by striking a balance between recapitulating relevant cell-cell interactions found *in vivo*, while reducing the complexity of the system to allow for more controlled mechanistic studies. In this work, we developed an organ-on-a-chip model to study neuroinflammation, with a particular focus on modeling how different disease states are able to propagate to synaptically connected, but anatomically remote regions of the brain. We used theoretical, computational, and experimental methods to optimize a two-chamber microfluidic device to maintain two distinct primary neural cultures that are chemically isolated but synaptically connected. Additionally, we demonstrate the ability to record robust extracellular electrophysiological signals from axons connecting the two cell populations for 60 days *in vitro* using an integrated surface-patterned microelectrode array. In tandem, we developed and characterized an enhanced cell culture model comprised of neurons, astrocytes, and microglia that more faithfully mimics the *in vivo* neuroinflammatory response (both neurotoxic and neuroprotective) to a variety of neuroinflammatory stimuli. This “tri-culture” is established and maintained through the use of a specifically designed, serum-free media making the tri-culture particularly amenable to high-throughput experiments and integration into complex culture platforms for studying a wide range of neurological diseases.

Acknowledgements

I am extremely grateful to my Ph.D. advisor Professor Erkin Seker for his continuous support and guidance throughout my Ph.D. studies. His mentorship and encouragement helped me develop as a researcher and overcome the many obstacles along this journey. I would also like thank him for always being there and offering invaluable advice that I will always remember. I am forever grateful for his mentorship and support.

I would also like to express my gratitude to my long-term collaborators, Professor Pamela Lein, Dr. Ana Cristina Goncalves Grodzki, Dr. Felipe da Costa Souza, Dr. Sunjay Sethi, Dr. Hao Chen, and Harman Panesar for their guidance and expertise. I would especially like to thank Dr. Rhianna Morgan whose advice and feedback has greatly influenced much of this work.

I would also like to thank my qualifying exam and dissertation committee members, Professor Pamela Lein, Professor Karen Moxon, Professor Weijian Yan, Professor Johannes Hell, and Professor Eduardo Silva for their astute insights and suggestions.

Furthermore, I would like to thank my Master's advisor Professor Samuel Kassegne for inspiring me to continue education and pursue a doctoral degree. I would also like to thank Dr. Maria Vomero for bringing me into the field of neuroengineering and also encouraging me continue my studies.

I would also like to thank all the past and current members of the Seker Lab and office mates here at UC Davis. A big thank you to Dr. Jovana Veselinovic, Dr. Zidong Li, Dr. Mashari Alangari, Dr. Zimple Martharu, Alexander Hampe, Gregory Girardi, Heyhyun Kim, Alex Gardner, Said Md Shahriar, Darius Rudominer, Kavya Somayajula, Sachit Nagella, and Suzan AlMashtoub for making my time at UC Davis unforgettable. I would also like to thank Barath Palanisamy not only for his outstanding contributions, but more importantly for helping me become a better mentor and person.

I would like to thank my family for their continuous support throughout my long academic journey. I would also like to thank my wife Nadia for her patience and unwavering support. None of this would have been possible without your love and encouragement. Finally, I would like to thank my children Marcel and Matteo for being a constant source of inspiration and joy throughout this long journey.

Table of Contents

List of Acronyms

4',6-diamidino-2-phenylindole	DAPI
Action Potential	AP
Alzheimer's Disease	AD
Apolipoprotein E	APOE
Blood-Brain Barrier	BBB
Calcitonin Gene-Related Peptide	CGRP
Central Nervous System	CNS
Colony Stimulating Factor 1 Receptor	CSF1R
Conoly Stimulating Factor 1	CSF1
Cysteine-Cysteine Chemokine Ligand 21	CCL21
Damage Associated Molecular Patterns	DAMPs
Days *In Vitro*	DIV
Deionized Water	DI water
Diameter	Ø
DL-Thereo-β-Benzyloxyaspartic Acid	TBOA
Dulbecco's Phosphate-Buffered Saline Solution	DPBS
Excitatory/Inhibitory Ratio	E/I Ratio
Flagellin from *Salmonella typhimurium*	FLA-ST
Heat-Killed *Listeria monocytogenes*	HKLM
High Molecular Weight	HMW
High-Mobility Group Box Protein 1	HMGB1
Inter-Spike Interval	ISI
Lipopolysaccharide	LPS
Low Molecular Weight	LMW
Microelectrode Array	MEA
Middle Cerebral Artery Occlusion	MCAO
Mitogen-Activated Protein Kinase	MAPK
N-Methyl-D-Aspartate	NMDA
Nuclear-Factor κB	NF-κB
Oligodendrocyte Precursor Cells	OPCs
Oligodendrocytes	OLs
Paraformaldehyde	PFA
Pathogen Associated Molecular Patterns	PAMPs
Pattern-Recognition Receptors	PRRs
Polydimethylsiloxane	PDMS
Poly-L-Lysine	PLL
Substance P	SP
Toll-Like Receptors	TLRs
Traumatic Brain Injury	TBI

List of Figures

Chapter 1: Introduction

Neuroinflammation is present in most, if not all, pathological conditions in the central nervous system (CNS), either acting as the primary driver of these conditions, or as a response to neurodegeneration or disruption of homeostasis following disease progression [1–3]. *In vivo*, neuroinflammation is a highly complex process that depends on both the interaction between neurons and glial cells and the overall structural and cellular architecture of the CNS. For example, a number of studies have reported the presence of neuroinflammation in remote regions of the CNS following a focal brain lesion [4–7]. These observations are examples of the phenomenon known as diaschisis, in which neurophysiological changes occur in anatomically remote, but synaptically connected regions of the brain following a focal insult or injury [8,9]. These regions of secondary neuroinflammation are typically too distant from the initial injury site for diffusion of soluble factors through the brain parenchyma to be a significant contributor, while also too specific in location for systemic disorders or blood-brain barrier (BBB) breakdown to be the probable cause. Therefore the leading hypothesis is that the interconnecting neurons themselves are propagating or transmitting these neuroinflammatory cues [4,9–11]. Neuroinflammation has also been linked to neurodegenerative diseases and is now thought to play an active role in Alzheimer's disease (AD) progression through the secretion of pro-inflammatory and neurotoxic factors that have been shown to increase tau phosphorylation and Aβ production [12–18]. Additionally, neuroinflammation is the driving force behind to Aβ clearance early in AD, and disruption to the early immune response has been shown to exacerbate AD progression [13,19–21]. There is also significant evidence to suggest that aggregated tau can be transferred between synaptically connected neurons, and these aggregates can seed new tau aggregates in a prion-like fashion [22–25].

And while there is significant evidence of this neuronal mediated transmission of neuroinflammation and neurodegenerative diseases from both animal studies and clinical observations [26,27], the highly complex and interconnected processes that dictate these phenomenon *in vivo* makes studying the underlying cellular and molecular level mechanisms extremely challenging. One such technology that can aid in this discovery are organ-on-a-chip platforms, which strike a balance between recapitulating relevant cell-cell interactions found in vivo, while reducing the complexity of the system to allow for more controlled mechanistic studies.

1.1 Propagation of Neuroinflammation Via Axonal Projections

While there are many CNS pathologies demonstrate the complexity of neuroinflammation *in vivo*, the propagation or transmission of neuroinflammation within the CNS through neuronal connections may be one the clearest and highlights the influence of cellular crosstalk and architecture on the observed neuroinflammatory response. Much of the research demonstrating the transmission or propagation of neuroinflammation to remote regions of the CNS has involved the induction of a focal cerebral ischemia in rodent models and tracking neuroinflammatory and other structural changes in remote neural populations [4]. For example, Nagasawa and Kogure found significant neuron death in the ipsilateral thalamus and substantia nigra following a middle cerebral artery occlusion (MCAO) that was not observed in the contralateral side [28]. Additionally, they reported that no changes in cerebral blood flow was observed in the ipsilateral thalamus or substantia nigra during the transient MCAO, further supporting their conclusion that the neuronal damage and neurophysiological changes were caused by synaptic connections to the ischemic foci. Similarly, other groups have found neural degeneration and other markers of neuroinflammation such as astrocyte and microglia activation in the ipsilateral thalamus [29–32] and hippocampus [33–36] following MACO. More recently researchers have reported that the application of known pro-resolving neuroinflammatory treatments such as minocycline [37] and

resolving D1 [38] reduce the neuroinflammatory response in these secondary injury sites, and this reduction can lead to improved functional recovery [38].

In addition to animal studies, there are a number of clinical observations that report a similar induction of neuroinflammation in remote regions of the brain following a focal ischemia or traumatic brain injury [39]. There have been multiple reports of acute degeneration of the ipsilateral thalamus following an infarct in the territory of the middle cerebral artery [27,40,41]. Similarly, there are many reports of degeneration of the ipsilateral substantial nigra following striatal infarction [42,43]. However, while there are many clinical examples and animal studies demonstrating secondary neuroinflammation in regions that are synaptically connected to original injury site, clinicians and researchers have largely been unable to predict the extent of this secondary neuroinflammation based on the initial injury or its impact on functional outcomes. Therefore, there is a need to better understand the cellular and molecular mechanisms underlying the propagation of neuroinflammation in order to elucidate the role of this phenomenon plays on the functional outcome and recovery following stroke or traumatic brain injury (TBI).

There are multiple theories on the underlying mechanisms behind the induction of neuroinflammation in remote regions of the CNS. One hypothesis is that pro-inflammatory neuropeptides such as substance P (SP) and calcitonin gene-related peptide (CGRP) may be involved due to their role in neuropathic pain in the periphery [44]. SP and CGRP are released in response to noxious stimuli in unmyelinated sensory nerve fibers, and lead to tissue inflammation and pain [45–49]. Furthermore, these neuropeptides have also been shown to be released in the CNS [50,51]. The release of SP in the CNS following TBI has been shown to activate both astrocytes and microglia, disrupt the BBB and increase the infiltration of circulating immune cells into the CNS [52–54]. Another potential peptide is cysteine-cysteine chemokine ligand 21 (CCL21), which has been shown to activate microglia, and may be responsible for the remote activation of microglia in the thalamus following spinal cord injury [55]. Additionally, fractalkine (CX3CL1) is another protein that has been implicated in the induction of neuroinflammation in

remote regions of the CNS. Fractalkine is expressed by neurons in the CNS and is found in both a membrane-bound and soluble form, while its corresponding receptor (CX3CR1) is primarily expressed by microglia [56,57]. When under stress due to insult or injury neurons can release soluble fractalkine, which serves as a powerful neuroinflammatory signal for microglia [58]. This process is thought to play a role in neuropathic pain, in which dysfunction to peripheral neurons leads to an increase in soluble fractalkine in the dorsal horn, which in turn leads to the activation of microglia and a neuroinflammatory response [59,60].

Another popular theory hypothesizes that Wallerian degeneration or retrograde degeneration is responsible for the observed neurophysiological changes in remote regions of the CNS following focal insult or injury [4,39]. In addition to directly causing neuron degeneration, the release of alarmin or damage associated molecular patterns (DAMPs) such as ATP, DNA and heat-shock proteins by the degenerating neurons can activate toll-like receptors (TLRs) which are widely expressed on microglia, astrocytes, and other cells of the innate and adaptive immune system [61,62]. The binding of these ligands to TLRs leads to the activation of the nuclear-factor κB (NF-κB) and p38α mitogen-activated protein kinase (MAPK) pathways, activation of which triggers release of proinflammatory cytokines and mediators such as TNF-α, IL-1β, and MCP-1 [63–67]. Additionally, activated microglia and astrocytes can also produce neurotoxic nitric oxide and reactive oxygen species [68,69], damage the BBB [70], and recruit circulating immune cells [71]. Additionally, several studies have suggested that this theory is responsible for the degeneration of neurons in the corticospinal tract following an infarct in the territory of the middle cerebral artery, and the extent of this secondary degeneration can predict the motor function outcome [72–74].

The final theory suggests that the initial injury can lead to increased neural activity in the secondary region, either by increasing the excitability of excitatory neurons projecting from the initial injury site, or by reducing or eliminating the projections of inhibitory neurons [4,9]. This increase in neural activity can lead to the overactivation of neurons in the secondary region

leading to calcium dysregulation and eventual degeneration in a phenomenon known as excitotoxicity [75,76]. This theory is supported by several studies that show reduced signs of neuroinflammation in secondary regions following the local application of the N-Methyl-D-aspartate (NMDA) receptor antagonist MK-801 [4,77].

While there is significant evidence to suggest that neurons are capable of transmitting neuroinflammatory signals and play a predominant role in the propagation of neuroinflammation to remote regions of the CNS. However, much of the research investigating this phenomenon has been conducted *in vivo*, where there are a number of competing and confounding mechanisms that influence neuroinflammation. Therefore, there is a need for a new method to study the propagation of neuroinflammation to remote regions in the CNS that can isolate the neuron-mediated transmission of neuroinflammation from other factors found *in vivo*, and thereby allow researchers to gain a better understand the underlying mechanisms behind this phenomenon.

1.2 Organ-on-a-Chip Models of the CNS

Organ-on-a-chip models (also known as microphysiological systems) are a popular way of increasing the physiological relevance of *in vitro* studies while still maintaining the ability to perform highly specific cellular and molecular level experiments. These models typically involve the use of microfabricated devices that aim to replicate the structural and cellular level architecture of the *in vivo* environment [78]. Organ-on-a-chip models of the CNS can largely be classified into two distinct categories, the first aims to model the BBB, while the second attempts to capture the cellular architecture to recreate different neural networks [79].

The BBB is a critical component of the neurovascular unit that tightly controls the transport of ions, neurotransmitters, macromolecules, and cells between the blood and brain. It primarily consists of brain microvascular endothelial cells, pericytes, and astrocytes along with the extracellular matrix that maintain this highly selective barrier [80]. Degradation of this barrier plays a significant role in the progression of many neurological diseases and also present a major

challenge to the uptake of pharmaceuticals into the CNS [81,82]. Organ-on-a-chip models of the BBB are typically based on the Boyden chamber assay, which was initially designed for cell migration studies, and involves the use of a thin membrane with micropores that cells are able to transverse [83]. Current organ-on-a-chip models of the BBB use similar membranes integrated into microfluidic platforms [84]. In these devices, brain microvascular endothelial cells are cultured on one side of the membrane and astrocytes and pericytes are cultured on the other side [85–87]. Additionally, fluid flow can be applied to the endothelial side of the device to simulate the flow through the blood vessels, and this shear stress has been shown to improve the tightness of the barrier [88].

The second major category of organ-on-a-chip models of the CNS are devices that attempt to model neural network formation or known synaptic pathways in the brain [79]. Many of these devices are based on a compartmentalized neural culture platform developed by Taylor *et al*, to physically separate neurons and axons for axon transport and axon regeneration studies [89,90]. These culture platforms consist of two large cell culture chambers (which house the cell somas) and are connected by an array of microchannels that, due to their reduced height, only allow neurites to pass through. Other groups have adapted this general principle to design devices to reconstruct directional neural networks. For example, Peyrin *et al* used tapered microchannel designs to form “axon diodes” that would allow axons to pass through the microchannels in one direction, but not the other [91]. Using this device, they were able to form a unidirectional synaptic connection between the two culture chambers to mimic the corticostriatal network. Other groups used devices with different microchannel lengths to achieve similar unidirectional connectivity to mimic corticostriatal [92] and nigro-striatal pathways [93].

1.3 Cell Culture Models of Neuroinflammation

While the microengineering and microfabrication of organ-on-a-chip devices is an important aspect to increase the physiological relevance of *in vitro* models of the CNS, an equally

important aspect of CNS organ-on-a-chip technology is the cell culture model used within the device. Of the many different cells found within the CNS, neurons, astrocytes, and microglia are the three primary CNS specific cells most closely associated with neuroinflammation. Additionally, microglia and astrocytes have also been shown to be critical players in maintaining homeostasis in the CNS. It has also been shown that crosstalk between neurons, astrocytes, and microglia plays a significant role both in maintaining homeostasis and during neuroinflammation, with some signals requiring direct cell-cell contact (**Figure 1.1**). Therefore, when cell culture systems are used to model neuroinflammation, it is important to consider not only cellular composition, but also spatiotemporal factors.

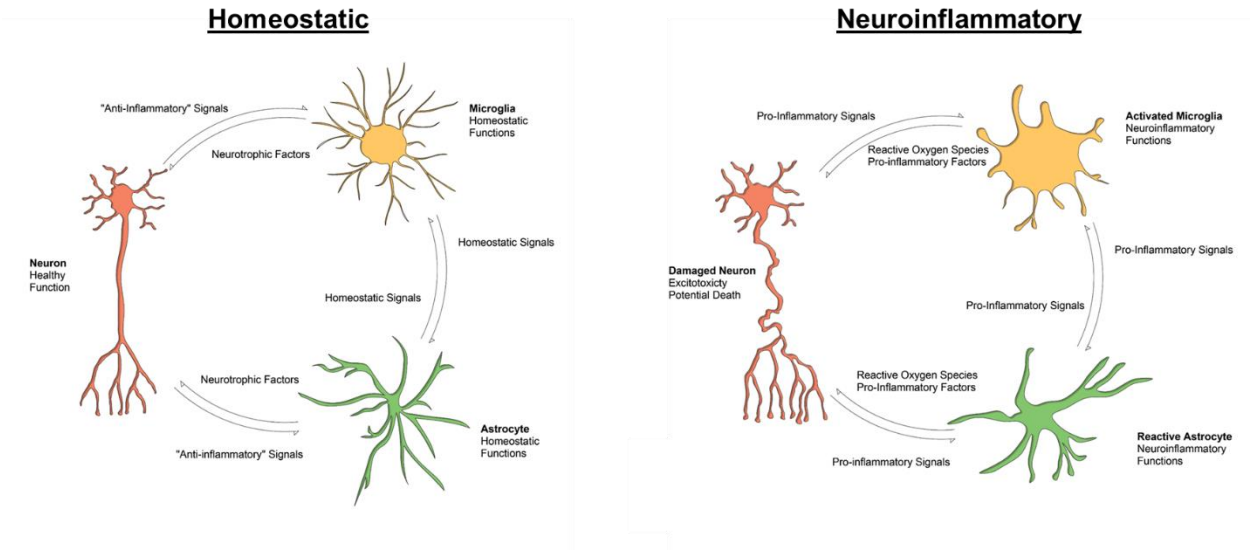

Figure 1.1: The importance of cellular crosstalk between neurons, astrocytes, and microglia in both homeostatic and neuroinflammatory conditions.

Current *in vitro* methods of studying neuroinflammation are primarily split into three categories. The first uses separate isolated cultures on neurons and glial cells to determine the effect of secreted factors on neurons or glial cells [94,95]. This is a popular method to identify the role of individual glial cells and specific factors on the neuroinflammatory response. For example, Liddelow *et al* demonstrated that microglia secrete three specific factors (IL-1α, TNF, and C1q) that are necessary and sufficient to induce a neurotoxic astrocyte phenotype, which they labeled

as “A1.” They exposed purified microglia cultures to lipopolysaccharide (LPS), and transferred the conditioned media to isolated astrocyte cultures and observed a distinct change in the transcriptomic profile associated with neurotoxic astrocytes. Additionally, they were able to demonstrate that by adding the aforementioned factors to the astrocyte culture, they could replicate that change in transcriptomic profile and neurotoxic phenotype [96]. In other studies, the application of conditioned media from an LPS treated BV-2 microglia cell line induced the production of nitric oxide in healthy NSC-34 cells (motor neuron cell line) [97], and a similar effect was observed from primary cultures, where LPS-conditioned media from microglia cultures lead to neurotoxicity when added to primary neuron cultures [98]. Finally other groups have attempted to determine the role that microglia play during excitotoxic events by treating isolated microglia cultures with kainic acid and other excitatory ligand-gated ion channel receptor agonists [98–100]. These studies have shown that the secreted factors found in the microglia conditioned media increase neuron death, leading the authors to suggest that microglia play a neurotoxic role during excitotoxic events. However more recent studies have suggested that microglia actually play a neuroprotective role during excitotoxicity through mechanisms mediated by the direct contact of microglia and damaged axons [101–103]. These contradictory results highlight some of the inherent limitations in this method, most notably the inability to observe the effects of membrane-bound or cell proximity-dependent mechanisms and the fact that the concentration of secreted cytokines transferred between cultures may not be physiologically relevant.

An alternative method to overcome some of the limitations of the media transfer method of modeling neuroinflammation is through culturing multiple types of neurons and glial cells in the same culture [94,104]. This has become one of the most popular methodologies to study neuroinflammation *in vitro*, with many reports using co-culture methods to investigate the neuroinflammatory response to LPS [96,105–107], proteins associated with neurodegenerative diseases such as amyloid-β and α-synuclein [108,109], and viral infection [110,111]. However, one of the major limitations in these co-culture models is the difficulty in effectively culturing

neurons and microglia together for extended periods of time. This is largely due to the high serum concentrations required by microglia in culture that can be toxic to neurons. This limits the time that microglia and neurons can be cultured together, with most cultures only being used for 24-72 hours [112–114]. Additionally, as the BBB tightly controls the what proteins are able to enter the CNS, and therefore the high serum concentration in the media is likely causing the microglia to be in an already activated state [115]. Conversely, culture conditions for neurons and astrocytes are similar, these co-cultures can be studied over extended time scales, and are a well-established method of studying neuroinflammation *in vitro* [116–120]. However, none of the aforementioned co-culture models are able to capture the important interplay between neurons, astrocytes, and microglia.

An alternative to the use of dissociated cells is the use of organotypic slice cultures, which maintain the three-dimensional architecture and cellular composition of the native tissue. These models are often considered the “gold standard” for modeling the CNS in culture [121], however they also present some specific drawbacks when studying neuroinflammation. In particular, the trauma caused by preparation of the organotypic culture leads to neuron degeneration and activation both astrocytes and microglia [122–124]. Additionally, astrocytes migrate to the edge of the organotypic culture and form a glial-scar like layer that encases the slice [122,124–126]. This encapsulation inhibits the diffusion of neuroinflammatory treatments added to the culture and makes determining the true response of the slice culture to the stimuli more difficult. In addition, organotypic slice cultures require specialized culture setups that make them difficult to incorporate into organ-on-a-chip devices.

Therefore, there is a need for new cell culture models on neuroinflammation that can be incorporated in the organ-on-a-chip devices that are also capable of capturing the important cellular communication of neurons, astrocytes, and microglia required to recapitulate the *in vivo* neuroinflammatory response.

1.4 Dissertation Objectives

The overall goal of this dissertation is to develop the foundation for an organ-on-a-chip system that is capable of modeling the complex neuroinflammatory conditions found *in vivo*, with a particular focus on how neuroinflammatory and neurodegenerative disease state are able to propagate to different regions of the brain. This organ-on-a-chip system must be able to capture enough of the structural architecture and direct cell to cell communication to faithfully mimic the more intricate aspects of neuroinflammation while still enabling researchers to use of highly directed cellular and molecular level experiments to gain a better understanding of the underlying mechanisms. This goal is accomplished through the following objectives:

1: Engineer and fabricate an organ-on-a-chip device that can capture the cellular architecture to model the propagation of neuroinflammation to anatomically remote but synaptically connected regions of the CNS.

The goal of this objective was to develop a microfluidic platform that was capable of effectively maintaining two neural cultures that are chemically isolated but synaptically connected. The microfluidic platform is based on the compartmentalized neural culture devices first developed by Taylor *et al* [127], but theoretical, computational, and experimental methods were used to determine the optimal microchannel geometry to extend the capabilities of these devices for the long-term study of synaptically-connected neural populations. Reducing microchannel height to ~1.5 μm proved to be a simple and effective method to dramatically improve both the fluidic isolation and cellular confinement of these devices, thereby making these devices an effective platform for studying the propagation of neuroinflammation. Additionally, robust extracellular electrophysiological signals were recorded from axons connecting the two cell populations for 60 days *in vitro* using an integrated surface-patterned microelectrode array (MEA), further extending the capabilities of this style of device (**Chapter 3**).

2: Develop and characterize an enhanced cell culture model to study neuroinflammation that can be incorporated into organ-on-a-chip platforms.

The goal of this objective was to develop and characterize an enhanced cell culture model of neuroinflammation that not only could capture the cellular crosstalk between neurons, astrocytes, and microglia that is required to faithfully mimic the *in vivo* neuroinflammatory response, but also be incorporated efficiently into complex organ-on-a-chip devices. This was accomplished by combining a well characterized neuron-astrocyte co-culture medium [120] with additional factors that have been shown to support isolated microglia survival in culture [115]. This new serum-free culture medium was capable of supporting a healthy population of neurons, astrocytes, and microglia. Additionally, this "tri-culture" more faithfully mimics the *in vivo* neuroinflammatory response to a variety of neuroinflammatory stimuli as compared to the more common neuron-astrocyte co-culture model of neuroinflammation (**Chapter 4**). As this tri-culture is established and maintained simply through the use of the specifically designed culture medium, it is particularly amenable to high-throughput experiments and integration into more complex culture platforms and extracellular recording systems for studying a wide range of neurological diseases, and these capabilities are highlighted in **Chapters 5 & 6**.

Chapter 2: Methodology

2.1 Culture Media Preparation

Base media (plating medium and co-culture medium) were prepared as previously described [120]. Briefly, plating medium consisted of Neurobasal A culture medium supplemented with 2% B27 supplement, 1x GlutaMAX, 10% heat-inactivated horse serum, and 20 mM HEPES at pH 7.5, while the co-culture medium consisted of Neurobasal A culture medium supplemented with 2% B27 supplement and 1x GlutaMAX (all from ThermoFisher). The tri-culture medium consisted of supplementing the co-culture medium with 100 ng/mL mouse IL-34 (R&D Systems), 2 ng/mL TGF-β (Peprotech), and 1.5 µg/mL ovine wool cholesterol (Avanti Polar Lipids). Due to the limited shelf life of IL-34 and TGF-β, the tri-culture medium was made fresh each week.

2.2 Primary Cortical Culture

All procedures involving animals were conducted in accordance with the National Institutes of Health Guide for the Care and Use of Laboratory Animals following protocols approved by the University of California, Davis Institutional Animal Care and Use Committee. Timed-pregnant Sprague Dawley rats were purchased from Charles River Laboratory (Hollister, CA). All animals were housed in clear plastic shoebox cages containing corn cob bedding under constant temperature (22 ± 2 ^{o}C) and 12 h light-dark cycle. Food and water were provided ad libitum. Primary cortical cultures were prepared from postnatal day 0 rat pups as previously described [128]. Neocortices from all pups in the litter were pooled and dissociated and plated at a density of 550-650 cells/mm^2 on substrates precoated with 0.5 mg/mL of poly-L-lysine (Sigma) in B-buffer (3.1 mg/mL boric acid and 4.75 mg/mL borax, Sigma) for 4 h at 37^{o}C and 5% CO_2 then washed with sterile deionized (DI) water and covered with plating medium. Primary cortical cells were plated in plating medium and allowed to adhere for 4 h before the medium was changed to the co- or tri-culture medium. Half-media changes were performed at twice weekly with the respective media types.

2.3 Microfabrication

2.3.1 MEA Fabrication

Custom MEAs were designed to be compatible with a previously described custom rig to interface with an RHD2132 Intan amplifier (Intan Technologies) [129]. The MEAs were designed with a 4 x 8 array of electrodes (32 total) each with a diameter (Ø) of 20 µm and an interelectrode pitch of 130 µm. The electrodes and traces (250 nm-thick Au over a 160 nm-thick Cr adhesion layer) were sputter-deposited on borosilicate glass wafers (500 µm thick, University Wafers) and patterned using standard lift-off techniques). SiO_2 was deposited via PECVD to serve as the insulation layer. Finally, the electrode sites were lithographically patterned and opened via a brief immersion in buffered oxide etch. Glass cloning cylinders (8 mm x 6 mm inner Ø, Sigma) were then fixed over the MEA using sterile vacuum grease (Dow Corning).

2.3.2 Microfluidic Platform Fabrication

The fabrication of the microfluidic platforms followed standard soft lithography techniques. Briefly, master molds containing the different platform geometries were fabricated by patterning two layers of SU-8 (Kayaku Advanced Materials) on a silicon wafer using standard photolithography techniques. The first layer defined the interconnecting microchannels and was fabricated using SU-8 6005 deposited with different spin rates to achieve a final thickness of 1.5, 3, or 6 µm. The second layer defined the cell culture chambers and was fabricated using SU-8 2050 with a final thickness of 75 µm. Following the patterning of the cell culture chamber layer, the master molds were hard-baked for 1 h at 250 ºC. All dimensions of the microfluidic platform master molds were confirmed using a Bruker Dektak XT profilometer following the hard-bake.

The master molds were placed in a 100 mm-diameter (Ø) petri dish and premixed (1:10 w/w curing agent to base) polydimethylsiloxane (PDMS; Slygard 184, Dow Corning) was poured over the mold and placed in a vacuum chamber to remove any bubbles. The PDMS was then placed on a 90 ºC hotplate for 2.5 h to cure. The PDMS platforms were removed from the master

mold and fluidic ports to access the cell culture chambers were opened using a 3 mm Ø biopsy punch. PDMS platforms were reversibly bonded to poly-L-lysine (PLL) coated glass coverslips, following the aforementioned coating methods, but were air dried following the sterile DI water wash. To produce reversibly bonded devices, the PDMS platforms were sterilized with 70% EtOH followed by treatment in an air plasma cleaner at 10 W for 2 min. The PDMS platforms were then sealed over the PLL coated glass coverslips and glass cloning cylinders were fixed over each of the fluidic ports using sterile vacuum grease to form the final device.

2.3.3 Integrated MEA and Microfluidic Platform Fabrication

Compatible MEAs and microfluidic platforms were fabricated following the same procedures outlined above. Each MEA contained an array of 8 microelectrodes in each cell culture chamber, and an array of 16 microelectrodes placed under the microchannels, with microelectrodes having a surface area of 400 μm^2. To form the final integrated microfluidic device, the MEAs were treated with air plasma to be permanently bonded to the corresponding “MEA” style microfluidic platform. Both the MEA and PDMS platforms were sterilized with 70% EtOH and the surfaces were activated with air plasma at 30 W for 2 min. The MEA was then covered with 70% EtOH and the PDMS platform was placed over the MEA and aligned under a microscope. The aligned device was placed in a vacuum chamber for 1 h to remove the EtOH solution and permanently bond the MEA and PDMS platform. The bonded devices were then treated with air plasma at 30 W for 10 min to make the surfaces hydrophilic and glass cloning cylinders were fixed over the fluidic ports. Finally, PLL solution was added to the device and incubated for 4 h and washed with sterile DI water to coat the interior surfaces of the device.

2.4 Neuroinflammatory Challenges

To simulate bacterial infection, cultures were challenged with LPS (3.0 × 106 EU/mg; Sigma) that was reconstituted in sterile Dulbecco’s phosphate-buffered saline solution (DPBS) with calcium and magnesium (DPBS+; Sigma) as a stock solution of 1 mg/mL and stored at −20

°C. Following the DIV 7 media change, each well was spiked with LPS solution to a final concentration of 5 µg/mL or an equal volume of sterile DPBS+ as vehicle control.

To simulate mechanical injury, a scratch was made in the cultures following the DIV 7 media change. A cross (~ 200–300 µm wide) was scratched in the center of each well using a sterile 200 µL micropipette tip.

Excitotoxicity was triggered by adding varying concentrations of glutamate to the cultures. Prior to each experiment, a fresh 50 mM solution of L-glutamic acid (Sigma) in DPBS+ was prepared. This 50 mM solution of L-glutamic acid was diluted with sterile DPBS+ to 100 × stocks. At DIV 7, half of the medium was removed from each well and stored at 37 °C. The glutamate solutions were diluted 1:100 directly into the cultures; vehicle controls received an equal volume of sterile DPBS+. Glutamate-exposed cultures were incubated at 37 °C for 1 h. For co-cultures, the media collected from the cultures prior to the addition of glutamate was combined with an equal volume of tri-culture medium that had twice the concentration of supplemental factors (4 ng/mL TGF-β, 200 ng/mL IL-34, and 3 µg/mL cholesterol) to create a tri-culture medium that contained any secreted factors from the co-culture, while the stored tri-culture media was combined with an equal volume of standard tri-culture medium. Following 1 h incubation, the medium from each well was completely removed and quickly replaced with the appropriate medium type for the culture condition.

To demonstrate the capability of the tri-culture as a high-throughput screening platform, we challenged the culture to a suite of nine TLR agonists. The TLR agonists used were as follows (all purchased from InvivoGen): Pam3CSK4 (TLR1/2 agonist), heat-killed L*isteria monocytogenes* (HKLM, TLR2 agonist), Poly(I:C) both high molecular weight (HMW) and low molecular weight (LMW, TLR3 agonist), lipopolysaccharide (LPS, TLR4 agonist), flagellin from *Salmonella typhimurium* (FLA-ST, TLR5 agonist), FSL1 (TLR6/2 agonist), R848 (Resiquimod, TLR7/8 agonist), and ODN1826 (TLR9 agonist). Prior to use, all ligands were reconstituted in sterile DI water at 200x (the maximum working concentration) and stored at -20ºC. To spike the cultures,

at DIV 7 half the medium was removed from each well and replaced with an equal volume of medium that contained a 2x working concentration of a TLR agonist or an equal volume (~1/200 of the medium volume) of sterile DI water to act as the vehicle control. The cultures were then maintained for 48 h.

2.5 Immunostaining

At the conclusion of the experiment, the cell cultures were washed 3 times with 37 ºC DPBS+ and fixed using 4% w/v paraformaldehyde (PFA; Affymetrix) in PBS for 2.5 h. Fixed cells were washed twice with 0.05% v/v Tween20 (Sigma) solution in DPBS+, followed by a 3 min permeabilization with 0.1% v/v Triton X-100 (ThermoFisher) solution in DPBS+ and two additional washes with Tween20 solution. Samples were blocked with a solution of 0.5% v/v heat-inactivated goat serum (ThermoFisher) and 0.3 M glycine (Sigma) in DPBS+ (blocking buffer) for 1 h. Following the blocking step, samples were incubated for 1 h in primary antibody solution containing a combination of the following antibodies: mouse anti-βIII tubulin (ThermoFisher), rabbit anti-GFAP (ThermoFisher), chicken anti-Iba1 (Abcam), mouse anti-PSD-95 (ThermoFisher), rabbit anti-VGlut1 (ThermoFisher), and chicken anti-MAP2 (Abcam) in blocking buffer. Samples were then washed 3 times with Tween20 solution before a 1 h incubation with secondary antibody solution containing a combination of goat anti-mouse antibodies conjugated to AlexaFluor 647 (ThermoFisher), goat anti-rabbit antibodies conjugated to AlexaFluor 488 (ThermoFisher), and goat anti-chicken antibodies conjugated to AlexaFluor 555 (ThermoFisher). Following incubation with secondary antibody solution, the samples were washed 3 times with DPBS+. Lastly, samples were incubated for 5 min with a 4’,6-diamidino-2-phenylindole (DAPI) solution (Sigma) to stain cell nuclei, followed by an additional Tween20 solution wash before mounting them onto glass slides using ProLong Gold Antifade Mountant (ThermoFisher).

2.6 Methods to Quantify Neuroinflammation in Culture

2.6.1 Morphological Analysis

For morphological analysis, cultures were fixed with 4% w/v PFA solution and stained as described above. All sample images were acquired with a Zeiss Observer D1 inverted fluorescence microscope at 100x or 200x magnification and analyzed using ImageJ. The cell number/mm^2 of different cell types was determined by manually counting the number of nuclei that were co-localized with β-III tubulin (neurons), GFAP (astrocytes), or Iba1 (microglia) from the 100x magnification images. The average astrocyte/microglia areas were determined by manually tracing the outline of astrocytes/microglia from 200x magnification images and determining the area inside the trace. Percent area coverage of neurons or astrocytes was determined through the use of the Huang auto-thresholding method on the β-III tubulin (neuron) or GFAP (astrocyte) channel. A minimum of three predetermined fields were analyzed per well to account for variability within the individual cultures, and when determining average astrocyte/microglia areas at least two cells were quantified per field of view.

2.6.2 Apoptosis Assay

Triggered irreversible apoptosis was quantified using the Caspase-Glo® 3/7 Assay System (Promega) according to the manufacturer's protocol. Luminescence was measured using a H1 hybrid microplate reader (BioTek Instruments).

2.6.3 Calcium Imaging

Prior to imaging, tri- and co-cultures were loaded with cell-permeant Fluo-4 AM calcium indicator (Thermo- Fisher) following the manufacturer's protocol. To determine the effect of glutamate on calcium fluxes in the tri- and co-cultures, each culture type was spiked with varying concentrations of L-glutamic acid (Sigma) in DPBS+ or an equal volume of DPBS+. For each well, prior to the addition of the glutamate solution, a fluorescence image at 200x magnification was taken, after which the shutter to the light source was closed, and the glutamate solution was

added to the well. Following a 2- min incubation in the glutamate solution, a second fluorescence image was taken over the same field-of-view with the same exposure time and was used to compare the change in fluorescence intensity following the addition of glutamate.

2.6.4 Cytokine Profile

Following the DIV 7 media change, co- or tri-cultures were incubated with 5 µg/mL LPS or vehicle control for 48 h. Following incubation, the conditioned media was spun down to remove any cells, and the supernatant containing the conditioned media was stored at -80 °C until analyzed. The proteome profile was determined using a Proteome Profiler Rat XL Cytokine Array (Bio- Techne) in conjugation with the IRDye® 800CW (Bio- Techne) for use with the LI-COR Odyssey® Imaging System. Relative concentrations of each cytokine in conditioned media were determined using ImageJ to compare the total pixel intensity from each spot. Hierarchical cluster analysis was performed using the MATLAB (2019a) bioinformatics toolbox.

2.6.5 Live/Dead and Apoptosis Analysis

Following the 48 h exposure to TLR agonists, each well was incubated with both Hoechst 33342 (ThermoFisher) and propidium iodide (ThermoFisher) both directly added to the medium to yield working concentrations of 1 µg/mL and 1 µM respectively, and incubated for 20 min at room temperature. Late stage apoptotic cells were quantified via annexin V staining using the ab176749 Apoptosis/Necrosis Assay Kit (Abcam) according to the manufacturer's protocol. All sample images were acquired with a Zeiss Observer D1 inverted epi-fluorescence microscope at 100x or 200x magnification and analyzed using ImageJ. The number of live/dead cells and percent area positive for annexin V staining were quantified using custom ImageJ macros provided in the Appendix.

2.7 Synaptic Puncta Quantification

To quantify synaptic puncta density cultures were fixed with 4% w/v/ PFA solution as immunostained as described above. All sample images were acquired using a Leica TCS SP8

STED 3X microscope with a 63x/1.4 oil immersion objective. The images were thresholded to determine the number of excitatory pre-synaptic puncta (VGlut1) and post-synaptic puncta (PSD-95), and the number of mature synapses were quantified by determining the number of co-localized puncta. These values were then correlated with dendrite length to determine the number of puncta or mature synapses per 100 µm of dendrite length. Five predetermined fields were analyzed per well to account for variability within the individual cultures.

2.8 Electrophysiological Recording and Analysis

For electrophysiology measurements, the devices were placed on a custom-built rig and maintained at 37 ºC and 5% CO_2 during the recordings. Recordings were performed at a sampling frequency of 30 kHz using an RHD2132 Intan amplifier (Intan Technologies). Half-media changes were performed 24 h prior to each recording except for LPS treated conditions, in which the half-media change was performed 24 h prior to the baseline measurement.

Feature extraction from the recordings was done using Offline Sorter and NeuroExplorer (Plexon). Spikes were detected following a filtering (300 Hz high pass) using a threshold of ±8x standard deviation of the noise. Channels that showed less than 10 spikes per 10 min recording were discarded from the analysis. The number of active electrodes for each array was determined as the number of electrodes with at least 10 spikes detected during the 10 min recording. Overall synchrony of the active electrodes within each device was determined using the SPIKE-distance methodology [130] using the PySpike Python package [131]. Bursts were classified using the *max interval* method in NeuroExplorer using previously defined parameters [132,133]. Briefly these parameters were; (i) maximum initial inter-spike interval (ISI) of 0.1 s, (ii) maximum end ISI of 0.25 s, (iii) minimum inter-burst interval of 0.5 s, (iv) minimum burst duration of 0.05 s, and (v) minimum number of spikes in bursts of 6 spikes, and were used to determine the percentage of spikes in bursts, average burst duration, and average ISI within bursts at a per electrode basis. Spike

frequency and burst features were determined on a per electrode basis, but statistical analysis was performed on a per device basis by taking the overall mean from the active electrodes.

To determine the average peak-trough duration we first sorted the threshold spikes using the valley-seeking algorithm in OfflineSorter (Plexon) with a Parzen multiplier of 2.0. Due to the relatively large distance between the electrodes and low seeding density, nearly every electrode only displayed one cluster, however on occasion two duplicate clusters were found due to the use of dual thresholds during spike detection (±8σ). As these two clusters clearly belonged to the same group, one cluster was disregarded from the analysis. The average peak-trough duration of each cluster was then calculated via OfflineSorter.

2.9 Statistical Analysis

When comparing the response of the tri- and co-cultures to different treatments, a two-way ANOVA was used. If the interaction was determined not significant ($p < 0.05$), then the analysis of the main effects was used to compare the two treatments. If a significant interaction was found, analysis of the simple main effects was conducted via a post hoc Tukey test or Holm-Bonferroni method. A one-way ANOVA test was used when comparing multiple groups against a single treatment, and differences between groups were identified by a post hoc Tukey test or Dunnett's test. A two-tailed Student's t-test assuming unequal variances was used when only two groups were analyzed.

To compare change in the different spike features based on culture type or condition, each data set was fitted using a linear mixed effects model (treating the individual devices as a random effect) with a b-spline basis to account for the overall shape of the plots. We then compared the estimated marginal means from the fitted curves at each timepoint or pre-determined timepoints and adjusted for multiple comparisons using the Holm-Bonferroni or Tukey's method. In all cases a p-value < 0.05 was considered significant. All statistical analyses were performed in R or MATLAB.

Chapter 3: Influence of Microchannel Geometry on Microfluidic Device Performance for Long-Term Studies of Connected Neural Populations

The central nervous system (CNS) is extremely complex, with each neuron communicating with hundreds to thousands of other neurons via synaptic connections [134]. In addition, glial cells are in constant contact with neurons, and any disruption or dysregulation within this highly interconnected system can lead to disease states. This high complexity and interconnectivity has led to disproportionally high failure rates of late phase clinical trials targeting neurological disorders [135]. One common approach to overcome this challenge has been the development of organ-on-a-chip models with electrophysiological read-out capabilities [136], which can be used to gain a better understanding of specific cellular and molecular mechanisms behind many neurological and neurodegenerative diseases. These models aim to reduce the complexity of the system as compared to *in vivo* models, while still maintaining many of the critical characteristics of the *in vivo* microenvironment (e.g., presence of relevant glial cells, mature neuronal networks, and distinct neural populations), and thereby allow researchers to conduct highly directed cellular level experiments with increased physiological relevance.

One popular example of an organ-on-a-chip model to study the CNS was first described by Taylor *et al* [90], and involves the use of polydimethylsiloxane (PDMS) based microfluidic culture platforms to physically separate the cell bodies of neurons and their axons. These culture platforms consist of two large cell culture chambers (which house the cell somas) and are connected by an array of microchannels that, due to their reduced height, only allow neurites to pass through. Additionally, fluidic isolation of one chamber (primary) can be achieved by increasing the volume of media in the opposing chamber (secondary), thereby driving a hydrostatic pressure driven flow through the microchannels counteracting any diffusion from the primary chamber to the secondary chamber. These devices were initially used to study isolated axons, along with their growth and regeneration following injury [127]. Researchers have

subsequently adapted the original design for use in myriads of other studies including the formation of directional neural networks [91–93], investigating the transport and propagation of neurodegenerative disease related proteins [137–142], studying the spread of glutamate-induced ecotoxicity [143], and the innervation of non-neuronal cell cultures [144,145]. While many great insights have been gained from these studies, the fundamental design of the platform - in particular the geometry interconnecting microchannel array - has largely been unchanged and may not be suitable for every application, especially for chronic studies that are necessary for recapitulating mature neuronal networks.

In this chapter we investigate the influence of microchannel geometry on device performance particularly in the context of long-term studies (1+ month) of synaptically-connected yet fluidically-isolated neural populations. Compared to acute studies, maintaining fluidic isolation becomes much more challenging as the fluid flow through the microchannels that counteracts diffusion is no longer negligible and may significantly alter the concentration of effector molecules. Additionally, for long-term studies, the inclusion of glial cells in the neuronal culture has been shown to improve the overall health of the culture and neuron function [132,146]. Of the different glial cells that are included in these mixed cultures, astrocytes, which contain fine processes with similar diameters to axons [147], are able to extend processes a significant distance into the microchannels, which may confound experimental results. Here, we cultured primary rat cortical neurons and astrocytes in microfluidic culture platforms with varying microchannel dimensions to systematically compare the influence of microchannel dimensions and initial seeding densities, on the fluidic properties of the platform and the ability for neurons, astrocytes, and nuclei to enter and cross through the microchannels. In addition, we study the influence of microchannel geometry on the electrophysiological recording fidelity. We demonstrate that microchannel height has an outstanding impact on the fluidic properties of the platform, while the seeding density can be used to adjust the number of astrocyte processes entering the microchannels. Using this information, we designed platforms that enable chronic studies, and demonstrate that neural

activity can be recorded from these platforms (from electrodes placed under the cell culture chambers and microchannels) for at least 59 days *in vitro* (DIV) with more than an order of magnitude enhancement in signal-to-noise ratio in microchannels and significantly higher number of active electrodes. This study demonstrates the importance that small changes in microchannel dimensions can have on the overall performance of commonly-used microfluidic neural cell culture platforms and concludes with considerations for designing similar organ-on-a-chip devices for long-term neural culture and electrophysiology.

3.1 Meta-Analysis of Reported Microchannel Geometries in Compartmentalized Neural Culture Devices

We performed a meta-analysis of over 200 unique research articles using similar organ-on-a-chip devices and found that ~70% articles used devices with geometries identical to the original devices described by Taylor *et al* [90,127], irrespective of cell type (CNS vs PNS), presence of glial cells, and experimental objective (**Figure 3.1**). Additionally, for the studies that used microchannels with different dimensions, nearly all of them used devices with larger microchannels, and in general there was limited discussion regarding the change over the common microchannel dimension. In the original device, the microchannels were 3 µm x 8-10 µm (height x width), with lengths ranging from 150-900 µm [90,127]. The small height of the microchannels was largely effective at preventing the soma of the neurons (with average diameter's ranging from 7-58 µm) [148] from entering the microchannels, while allowing axons and dendrites (with diameters ranging 0.2-2.2 µm) [148,149] to easily enter and cross through the channels. The range of lengths were used to differentiate axons from dendrites, as it was noted that dendrites were unable to fully pass through microchannels greater than 450 µm in length [127]. Taken together, the meta-analysis suggests that the majority of researchers use the original device dimensions, and the reasons for using a specific channel dimensions are rarely discussed, even though these dimensions likely play a significant role in the device function.

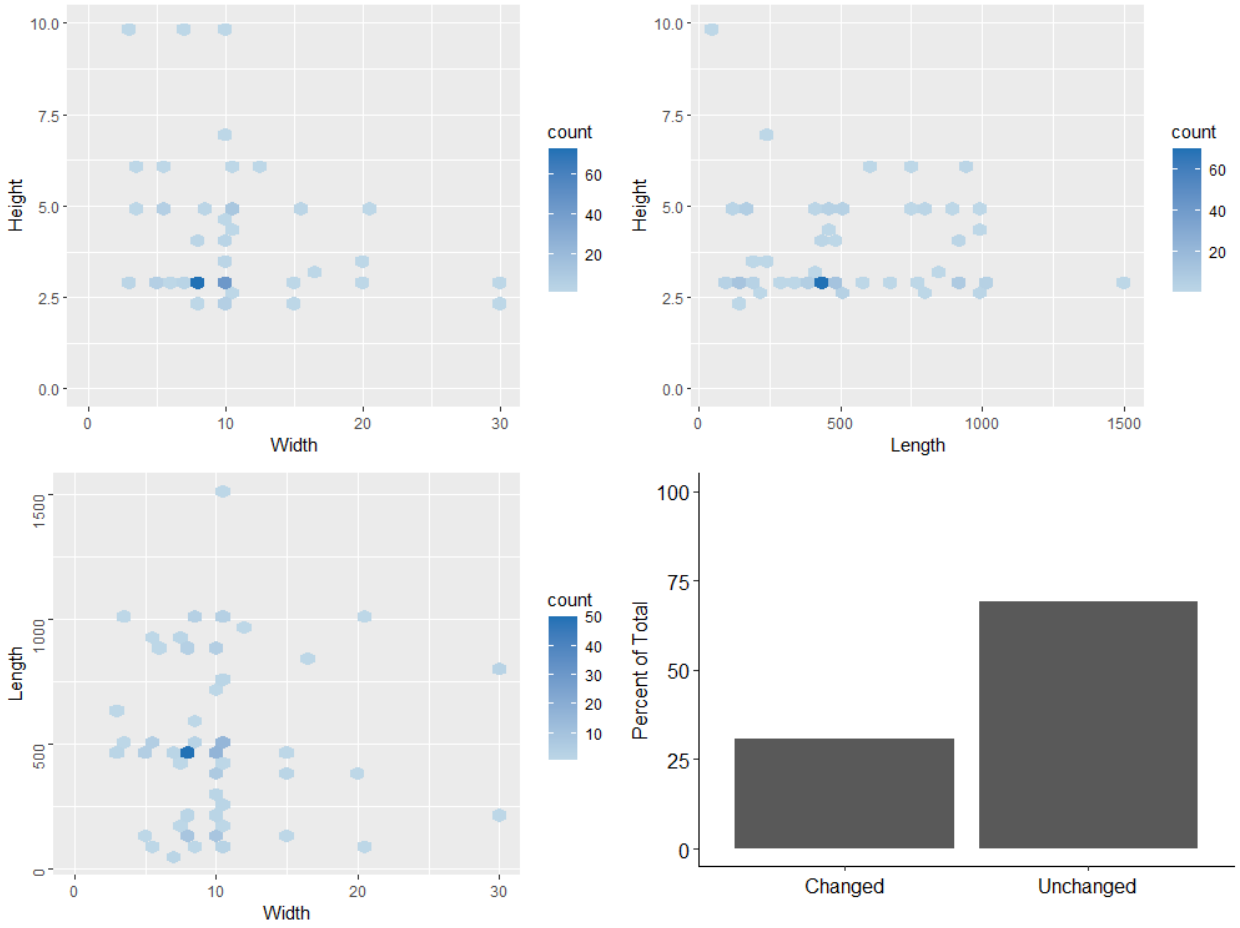

Figure 3.1: Analysis of different microchannel dimensions reported in publications using "axon compartmentalization" style microfluidic devices. Most common microchannel dimensions were 3 µm x 8 µm x 450 µm (H x W x L), which are the original dimensions reported by Taylor *et al*. and are the dimensions of commercially available devices (Xona Microfluidics), with ~70% of all studies use microchannel dimensions of 3 µm x 8 µm x 450-1000 µm. The bottom-right plot illustrates the percentage of the cited papers that use the same original dimensions or different dimensions than the original. (A full list of references used to generate this data can be found in **Appendix I**).

3.2 Microfluidic Platform Designs

Multiple microfluidic devices with varying microchannel dimensions were designed in order to assess the influence of microchannel geometry on different properties of the device (**Figure 3.1**). "Array" style devices were designed to investigate the cellular response to different microchannel geometries. Each array device contained 4, 25 microchannel arrays with widths of 2, 5, 10, and 15 µm. Additionally, these devices were designed with microchannel lengths of 500, 1000, and 1500 µm and heights of 1.5, 3, and 6 µm. "Full" style devices were used to determine

the influence of microchannel geometries (of a single channel width per device) on the fluidic properties of the devices. These devices each had 101 microchannels with dimensions of 10 µm x 1000 µm x 1.5 or 6 µm (width x length x height). Finally, “MEA” style devices contained an array of 25 microchannels with dimensions of 5 or 10 µm x 1000 µm x 1.5 µm (width x length x height), which were bonded over custom microelectrode arrays (MEAs) designed for integration into the microchannel devices. All these devices were fabricated following the methods outlined in the previous chapter.

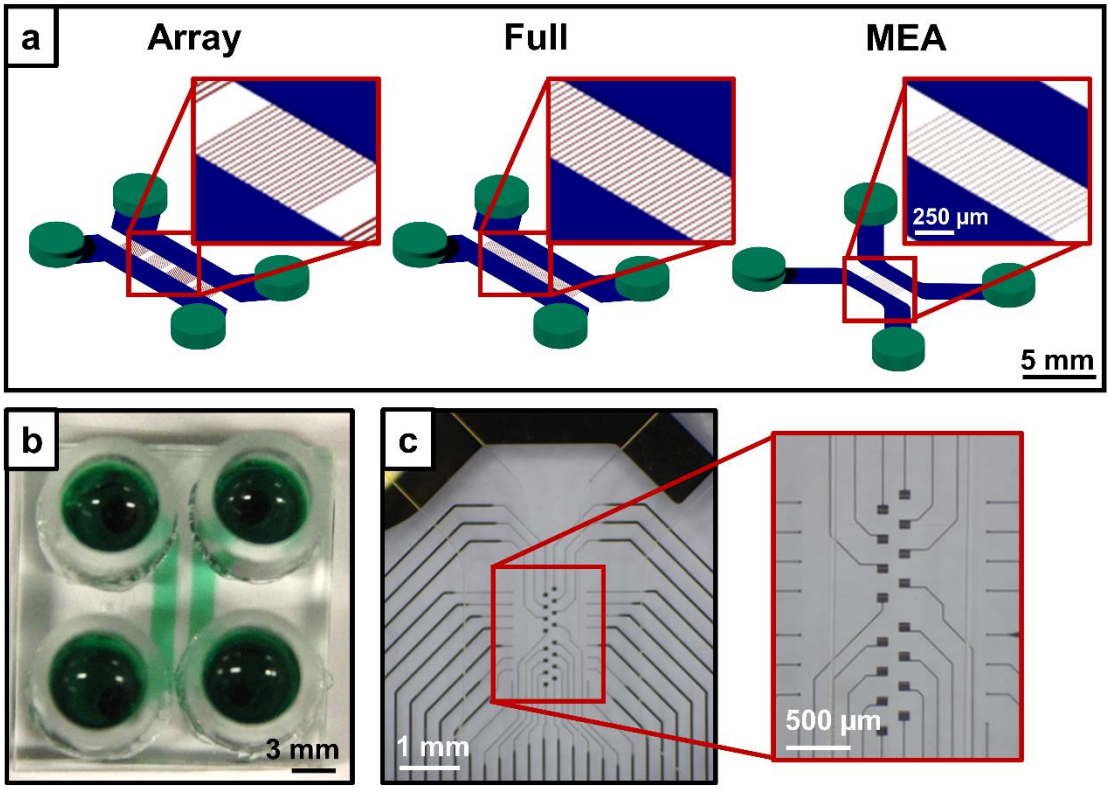

Figure 3.2: Examples of different microfluidic platforms used in this study. (a) 3D renderings of the three styles of microfluidic platforms. The microchannels are shown in red with dimensions of 1.5-6 µm x 2-15 µm x 500-1500 µm (height x width x length) depending on the design. The cell culture chambers are shown in blue with a height of 75 µm. The fluidic access ports are shown in green and created via biopsy punch (3 mm Ø) over which glass cloning cylinders (6 mm Ø, 8 mm height) were affixed to increase the overall media volume capacity. (b) An example of a fully assembled device with affixed cloning cylinders. (c) An example of an “MEA” style device with the integrated MEA.

3.3 Influence of Microchannel Height on the Stability of Soluble Factor Concentrations in the Chambers

Initial studies using microfluidic devices with microchannel geometries as described in literature revealed significant limitations in translating these compartmentalized neural culture devices for chronic studies of connected neural populations. In particular, we discovered that we were unable to induce a neuroinflammatory or cytotoxic response in the treatment chamber even when using extreme treatments such as 100 μM glutamate (**Figure 3.3**). As this effect was observed across a number of different neuroinflammatory and cytotoxic treatments, we hypothesized that fluid flow between the cell culture chambers required to counteract diffusion and maintain the fluidic isolation of the treatment chamber may be significantly altering the concentrations of the added neuroinflammatory and cytotoxic stimuli. While many papers using these devices highlight and employ the fluidic isolation capabilities of these devices, the volume of fluid flow between the cell culture chambers less studied. Additionally, these devices were originally designed for acute studies (minutes to hours), and therefore the impact of the fluid flow between the chambers at longer timescales (days to weeks) may not have been considered in the original design.

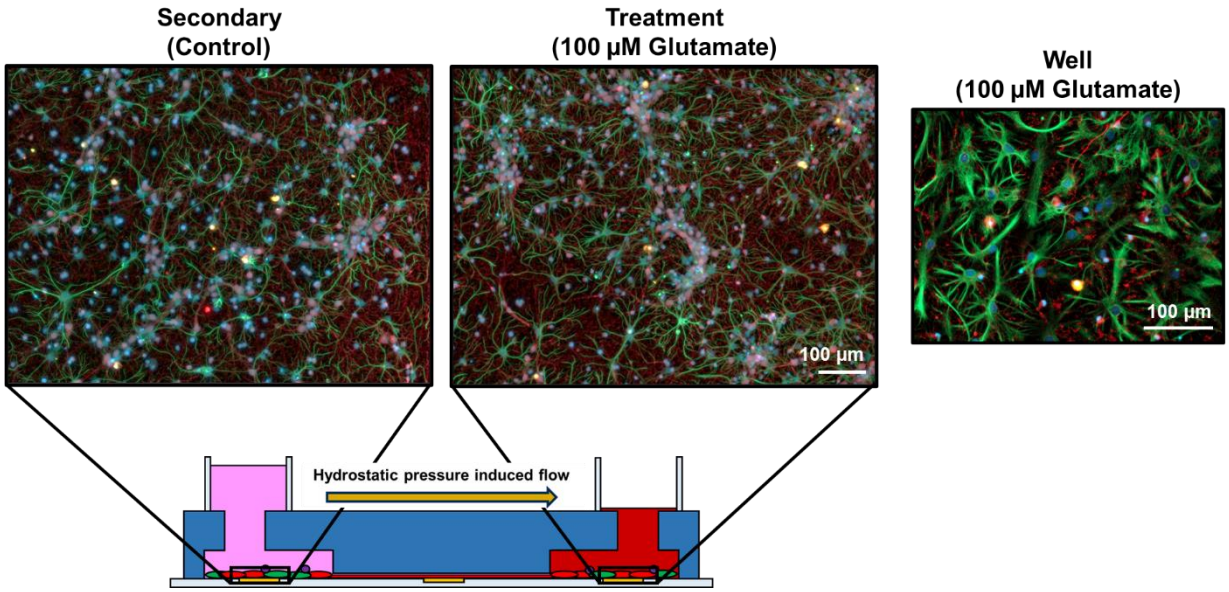

Figure 3.3: Example images of the impact of 100 µM glutamate treatment on a primary cortical culture for 48 h in the microfluidic device (left) and in a standard multi-well plate. The cultures were immunostained for neurons – anti-βIII-tubulin (red) and astrocytes – anti-GFAP (green) and the general nuclear stain DAPI (blue).

3.3.1 Theoretical and Computational Modeling

In order to determine the effect of altering microchannel geometry on the fluid flow through the microchannels, we estimated the volumetric flow rate through the microchannels using analytical and computational models.

Analytical modeling of the fluidic properties of the devices was done using previously described electrical circuit analogies, treating the interconnecting microchannels as resistors and the open wells containing media as capacitors [150]. The dimensions of the model were the same as the "full" device with 101 microchannels with widths of 10 µm and lengths of 1000 µm. **Figure 3.4** shows the circuit diagram of the electrical circuit analogy of the microfluidic device with the four wells modeled as capacitors (C1-C4) and the interconnecting microchannels modeled as resistors (MC1-MC101). An initial volume differential of 150 µL per cell chamber (75 µL per well) was used to drive the hydrostatic pressure-induced flow, which amounted to a height differential of ~2.65 mm using the 6 mm inner Ø of the cloning cylinders.

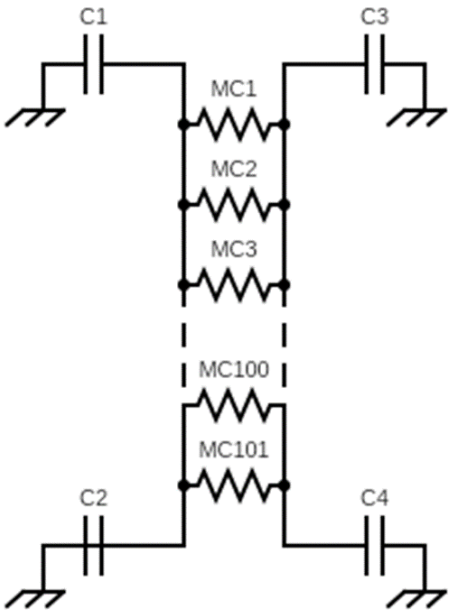

Figure 3.4: Electric circuit analogy used to estimate the fluid flow through the microchannels.

The change in volume between the chambers over time can be found using the following equation

$$V(t) = \frac{\Delta V}{2}\left(1 - e^{-\frac{2t}{RC}}\right)$$

Where ΔV is the initial volume differential between the chamber, R is the hydraulic resistance through the microchannels, and C is the "capacitance" of the wells. The hydraulic resistance through rectangular microchannels can be estimated using the following equation

$$R_H = \frac{12\mu L}{wh^3\left(1 - 0.630\left[\frac{h}{w}\right]\right)}$$

Where w, L, and h are the width, length, and height of the microchannel respectively, and μ is the dynamic viscosity. C is defined as the change in stored volumetric flow rate due to change in pressure and can be calculated for an open well as

$$C = \frac{\Delta V}{\Delta P} \propto Area_{Well}$$

Computational modeling was done in COMSOL Multiphysics 5.5 solving for the Navier-Stokes equations to model the pressure driven flow through the microchannels in a full 3D model of the “full” device with the following geometry: Chamber height: 75 µm, Channel length: 1000 µm, Channel width: 10 µm, Channel height: variable, 101 channels (**Figure 3.5**). The boundary conditions were set as follows: Inflow (Blue) with a set pressure equal to the volume differential of 150 µL per chamber (75 µL per well), Outflow (opposing “openings”), No Flux (all other surfaces). The model was solved for steady state, and the volumetric flow rate was determined by taking the average velocity at the outflow multiplied by the surface area of the outflow boundaries.

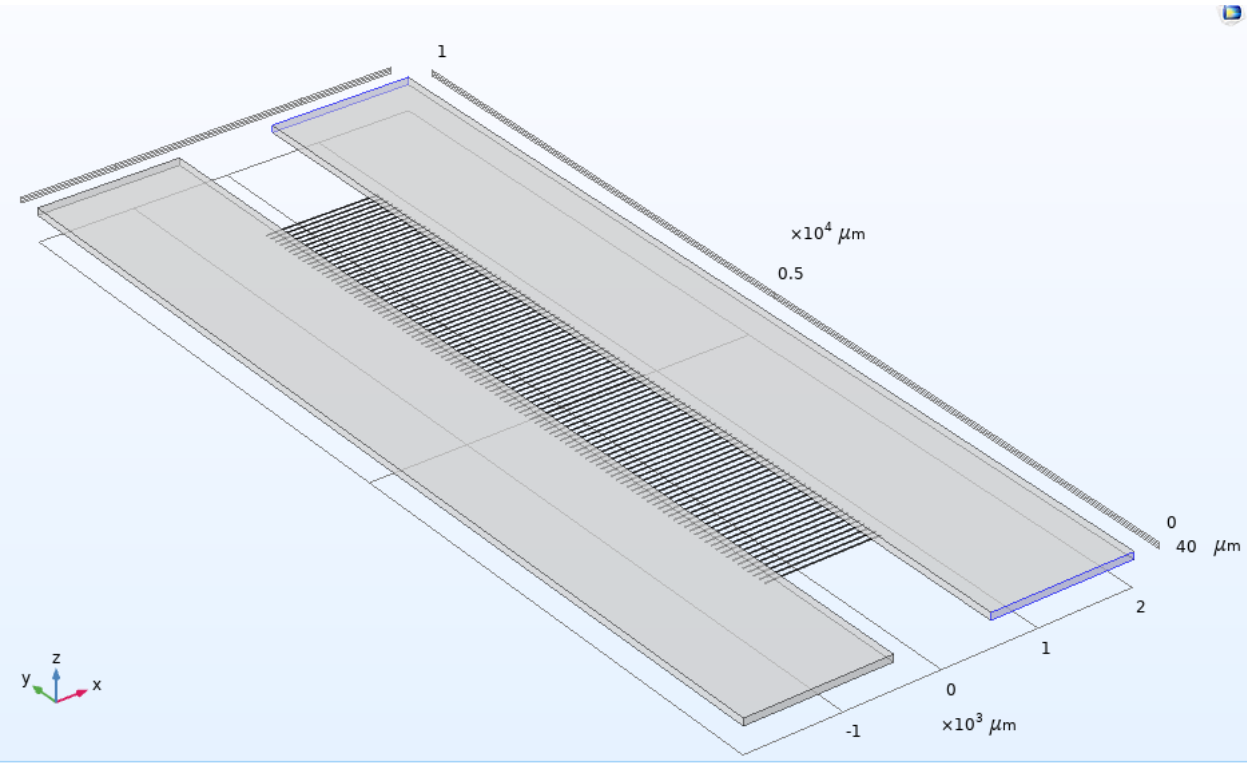

Figure 3.5: 3D geometry of the COMSOL model.

Using these models, we determined that of the three microchannel dimensions, microchannel height had the largest influence on the estimated fluid flow. This is largely due to the cubic relationship between the height of a rectangular microchannel and its hydraulic

resistance. **Figure 3.6** shows the estimated volumetric flow rate through “full” style devices (10 µm width x 1000 µm length, with 101 microchannels) with varying heights and an initial volume differential of 75 µL per well or ~2.65 mm difference in height. When the microchannel height was increased to 5 µm, ~18 µL flowed between the chambers within only 24 h. While this volume appears negligible, the volume of each cell culture chamber of the full device is ~2.45 µL, resulting in the entire volume of the cell culture chamber being overturned every ~3.25 hours. Additionally, the results from the electric circuit analogy and 3D COMSOL model show good agreement with each other, and the higher values estimated by the COMSOL model can be attributed to the fact that the COMSOL model was solved for steady-state, and thus the pressure between the chambers did not decrease with the change in volume differential. The results from these models suggest that reducing the heigh of the microchannel may be a promising method to improve the fluidic properties of this style of organ-on-a-chip devices for long-term studies of connected neural populations

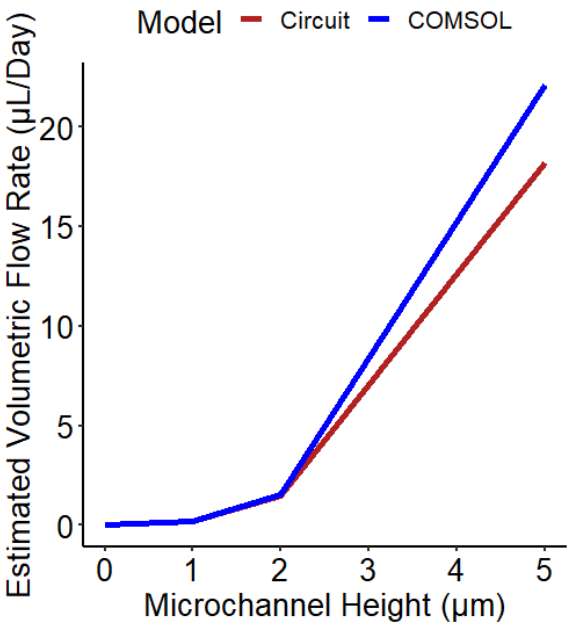

Figure 3.6: Estimated volumetric flow rate for the first 24 h given by electrical circuit analogy or 3D computational model (COMSOL).

3.3.2 Experimental Confirmation

In order to experimentally confirm the results from the electric circuit analog and computational model, that is, whether dilution of the treatment chamber soluble factors is significant due to the media flow, we seeded primary cortical cells at a density of 3 x 10^6 cells/mL in both cell culture chamber of "full" style devices with microchannel heights of 1.5 μm and 6 μm. After allowing the cells to adhere, 150 μL of GM was added to each well connected to the "secondary" chamber, while 75 μL GM with 50 μM cytosine arabinoside (AraC) was added to each well connected to the "treatment" chamber. The devices were maintained for 48 h with no media changes, after which they were fixed and immunostained. At this concentration AraC acts as a neurotoxic factor [151], and thus we would expect to see significant neuron death in the treatment chambers. As expected, we observed significant neural death in the treatment chamber of microfluidic platforms with microchannel heights of 1.5 μm, however we did not see any neural death in the treatment chambers of the devices with microchannel heights of 6 μm (**Figure 3.7a**). In order to quantify neuronal cell viability, we compared the percent area of each field-of-view stained for β-III tubulin with a circularity less than 0.2 using ImageJ (**Figure 3.7b**). The circularity cutoff was used to eliminate the contribution of cell debris from apoptotic/necrotic neurons, which still stained for β-III tubulin, but lacked long cellular processes, and therefore had high circularity values. A two-way ANOVA indicated a significant interaction between chamber (treatment vs. secondary) and microchannel height on the percent area covered by neurons (p = 0.0095). Analysis of the simple main effects (using Tukey's method to account for multiple comparisons) revealed a significantly reduced percent area coverage of neurons in the treatment chamber as compared to the secondary chamber in the devices with a 1.5 μm microchannel height (p = 0.0057). However, in the devices with 6 μm tall microchannels, we observed no significant difference (p = 0.99) in the neuron percent area coverage, indicating that the flow between the chambers was enough to "wash-out" the AraC from the treatment chamber preventing the neurotoxic effect. Additionally, we did not see a significant difference in the neuron coverage

between the control chambers of the different devices (p = 0.85) indicating that reducing microchannel height does not negatively influence the fluidic isolation of the treatment chamber.

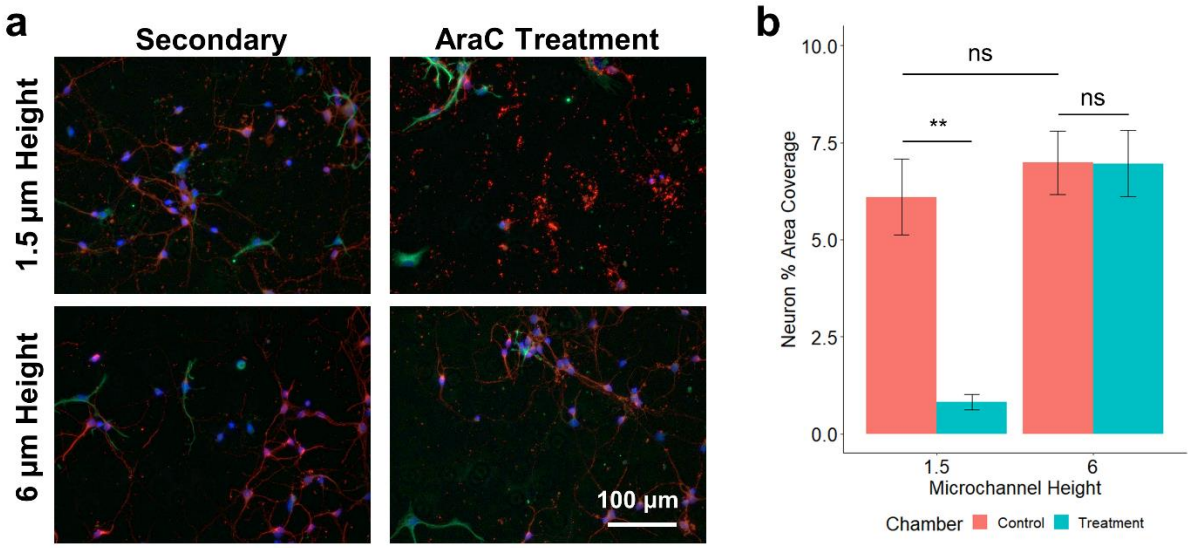

Figure 3.7: (a) Representative fluorescence images from the different cell culture chambers following 48 h exposure to 50 µM AraC in the treatment chamber. The cultures were immunostained for neurons – anti-βIII-tubulin (red) and astrocytes – anti-GFAP (green) and the general nuclear stain DAPI (blue). (b) Quantification of the percent area coverage of neurons with a circularity cutoff of 0.2 to eliminate cellular debris (mean ± SEM, n = 3 from two independent dissections). ** $p < 0.01$.

We also observed similar results from established (DIV14) cultures in devices with 1.5 µm tall channels, with severe neuronal death isolated to the treatment chamber following a 4 day excitotoxic challenge, whereas cultures in devices with 6 µm tall channels show no cell death in either chamber (**Figure 3.8**)**.** These results indicate that reducing the height of the microchannels can significantly improve the fluidic properties of these devices, especially during extended treatment times. Furthermore, as half-media changes are required every 3-4 days to maintain the cultures, it is expected that the robust fluidic isolation observed in the 1.5 µm microchannel height devices can be maintained indefinitely, as the volume differential between the chambers can naturally be “reset” every 3-4 days. Finally, axonal growth into the channels likely further improves the fluidic isolation between the chambers by reducing the effective channel cross-section available for fluid flow, thereby increasing the hydraulic resistance.

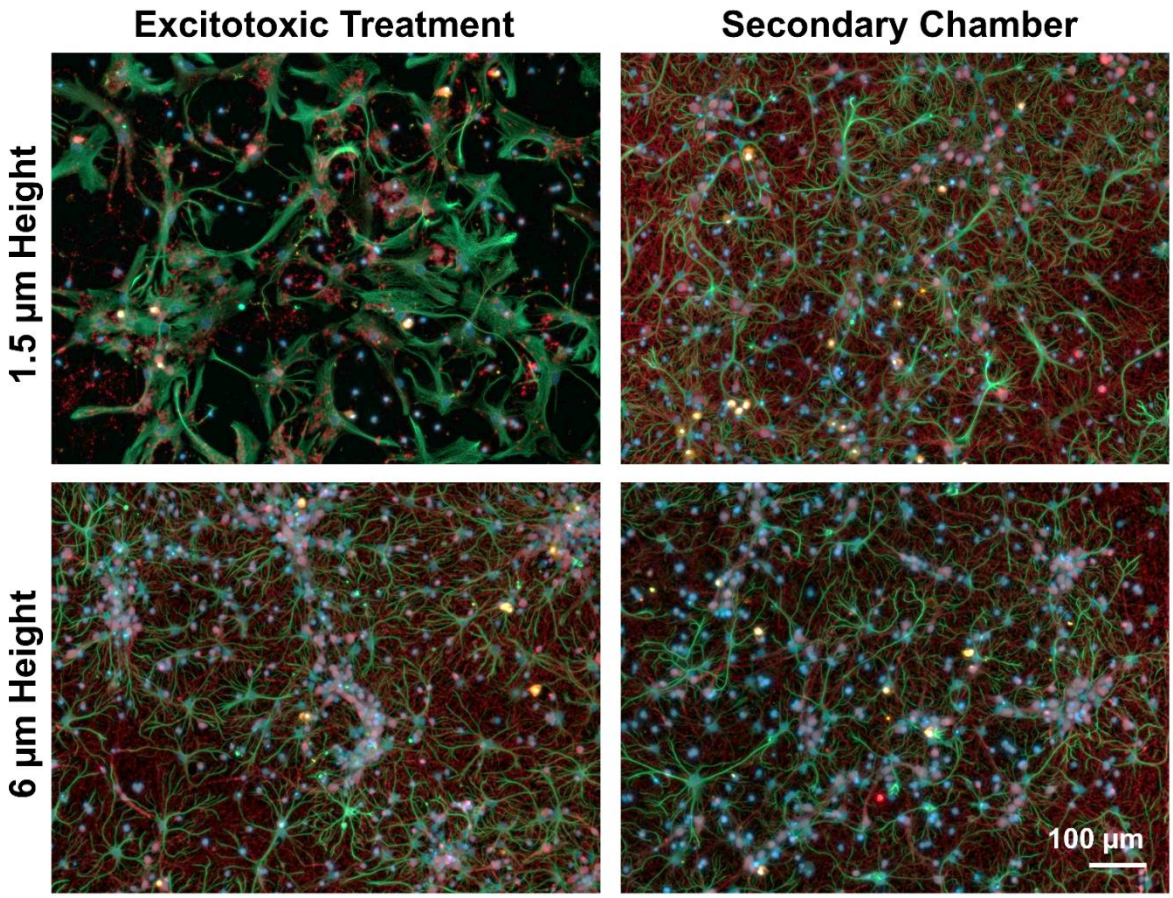

Figure 3.8: Representative fluorescence images from the different cell culture chambers in microfluidic platforms with either 1.5 µm tall microchannels (top) or 6 µm tall microchannels (bottom) following a 4-day excitotoxic treatment (100 µM glutamate). The cultures were immunostained for neurons – anti-βIII-tubulin (red), astrocytes – anti-GFAP (green), microglia – anti-Iba1 (orange), and the general nuclear stain DAPI (blue).

3.3.3 Influence of Reducing Volume Differential

An alternative method to reduce the flow between the chambers during fluidic isolation that has been used by some researchers is decreasing the volume difference between the control and treatment chambers [142,143]. While this method is effective in reducing the fluid flow by reducing the pressure differential, we found that this comes at the expense of fluidic isolation (**Figure 3.9**). We observed a similar reduction in fluid flow between the chambers by reducing the hydrostatic pressure differential in devices with 6 µm tall microchannels to ~0.71 mm as compared to devices with 1.5 µm tall microchannels with a more standard hydrostatic pressure differential

(~2.83 mm). However, we also observed diffusion of dye molecules from the treatment chambers within the microchannels of the reduced-volume differential devices. This was not observed in devices with 1.5 µm or 6 µm tall microchannels that maintained the more standard hydrostatic pressure differential. This suggests that reducing microchannel height as opposed to reducing the hydrostatic pressure differential is the better solution to reduce the fluid flow through the microchannels when absolute fluidic isolation of the treatment chamber is critically important.

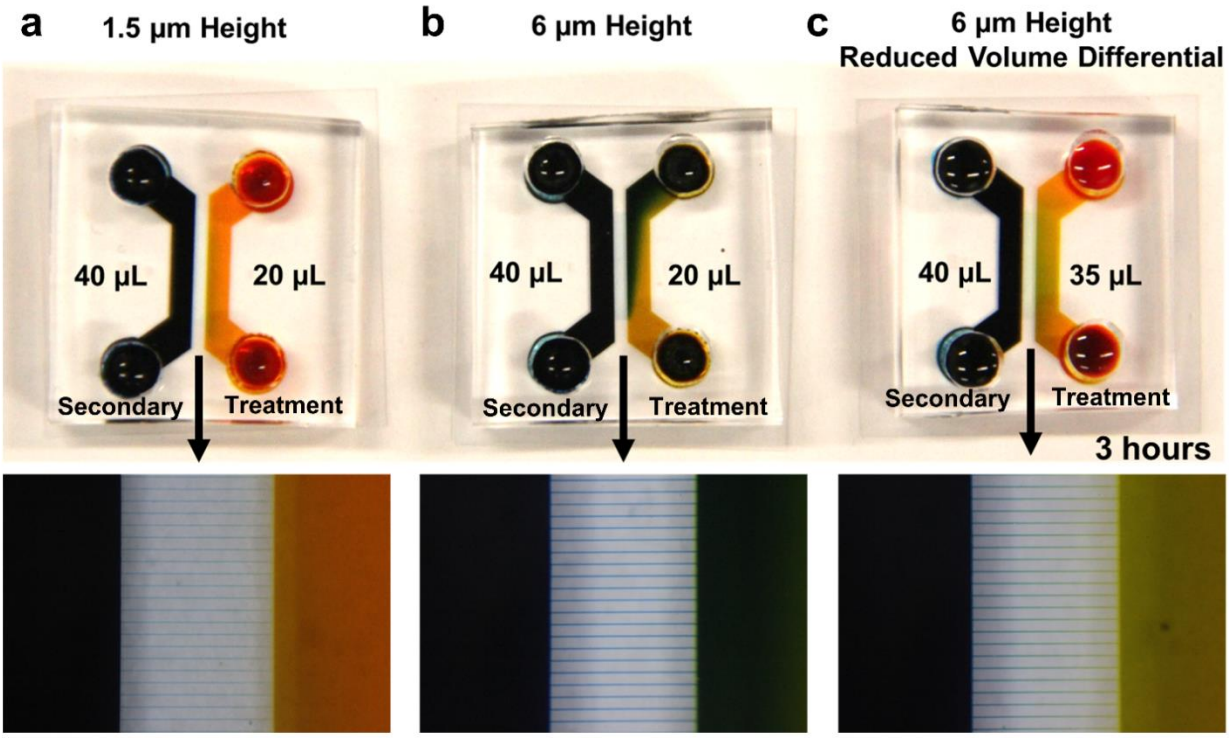

Figure 3.9: Comparing the fluid flow and fluidic isolation of different devices after 3 hours. In these devices a volume differential of 20 µL equated to a height differential of ~2.83 mm, while a volume differential of 5 µL equated to a height differential of ~0.71 mm. (a) For 1.5 µm height devices with a 20 µL volume differential we see both good fluidic isolation (negligible diffusive transport) and minimal flow between the chambers. (b) For the 6 µm height device and 20 µL volume differential there was good fluidic isolation, but significant flow between the chambers. (c) When the volume differential was reduced, the flow between the chambers was also reduced, but some of the dye from the isolated chamber (yellow) can be seen diffusing into the microchannels.

Ultimately, the results from this section indicate that reducing the height of the microchannels in these compartmentalized organ-on-a-chip devices is a simple and effective way of reducing the fluid flow between the cell culture chambers while maintaining a high degree of

fluidic isolation in the treatment chamber, and thereby significantly improve the fluidic properties of these devices for long-term studies of connected neural populations.

3.4 Cell Culture Response to Changes in Microchannel Geometry

Changes in microchannel geometry has the potential not only to influence the fluidic properties of the device, but also how the cells interact with the microchannels. In particular, there was concern that reducing microchannel height may impede the ability for axons to cross through the microchannels. In order to quantify the cellular response to changes in microchannel geometry, we compared the response of the primary cortical cells cultured in “array” style devices to a number of different variables including microchannel width, length, and height along with the initial seeding density. One chamber of the device was seeded with 20 µL of cortical cells at high (20×10^6 cells/mL) and low (3×10^6 cells/mL) concentrations. A seeding volume of 20 µL was chosen as preliminary studies indicated that higher seeding volumes lead to a more even distribution of cells within the chamber, without altering the plating density. Nevertheless, multiple designs of each “array” style device were fabricated, in which the order of arrays of microchannels were randomly placed along the device to account for any uneven distribution of seeding density. The cortical cells in these devices were maintained for 14 DIV, after which they were fixed, and the different culture responses were quantified. Four different responses were quantified by determining: (i) the number of microchannels with at least 1 axon crossing the entire length of the channel, (ii) the number of nuclei that entered or crossed through the microchannels, (iii) the number of channels that had at least 1 astrocyte process entering the channel, (iv) the length that the astrocyte process extended into the microchannels (**Figure 3.10**).

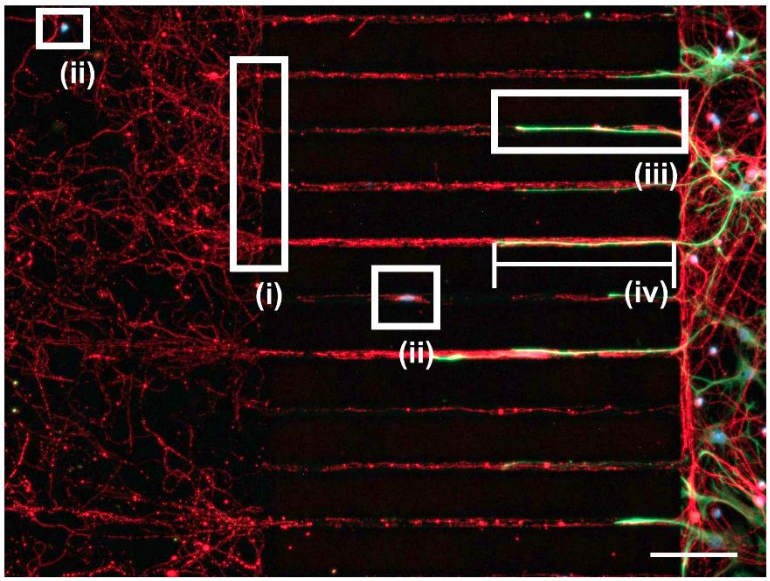

Figure 3.10: Representative fluorescence image illustrating the different cellular responses to varying device parameters. The cultures were immunostained for neurons – anti-βIII-tubulin (red) and astrocytes – anti-GFAP (green) and the general nuclear stain DAPI (blue). The responses quantified are as follows: (i) the number of microchannels with at least 1 axon crossing the entire length of the channel, (ii) the number of nuclei that entered or crossed through the microchannels, (iii) the number of channels that had at least 1 astrocyte process entering the channel, (iv) the length that the astrocyte process extended into the microchannels. Scale bar = 100 µm.

3.4.1 Axon Crossing Microchannels

One critical parameter determining the functionality of these organ-on-a-chip devices is the ability for axons to cross through the microchannels and thereby synaptically connect the two neural populations. Our results indicate that for most microchannel geometries, by DIV14 axons are able to consistently cross through all available microchannels, especially at higher seeding densities (**Figure 3.11a**). However, we observe a clear reduction in the number of microchannels with axon crossings at small channel widths (2 µm) and long channel lengths (1500 µm), which is exacerbated at low seeding densities. These observations were confirmed by hierarchical regression analysis (**Figure 3.12a**), which indicates that the most significant variables, in order of importance, were seeding density, microchannel width, and microchannel length. Interestingly, microchannel height, while still significantly improving the adjusted R^2 coefficient of the regression model, had the least impact on the ability for axons to cross through the microchannels (**Figure**

3.11a & 3.12a). It has been shown that axons from cortical neurons have heights of less than 1 µm when cultured on planar surfaces [152], and therefore axons were not physically excluded from the microchannels even at the lowest tested height. Additionally, while percentage of microchannels with at least one axon crossing did not substantially increase as microchannel widths increased above 5 µm, we did observe that microchannels with increased widths had a larger number of axons crossing through each individual microchannel.

3.4.2 Soma confinement in chambers

The ability to effectively confine the somas from each cell population to their respective chamber is another critical aspect to the effectiveness of these devices. Although the height of the most reported microchannel geometries are smaller than the size of neurons and glial cells (**Figure 3.1**), there are a number of reports of showing significant populations of neurons or glial cells that pass through similarly designed microchannels [153–156]. We found that microchannel height had a significant impact on the soma confinement capabilities of the device (**Figure 3.11b**) and was the most significant factor in explaining the observed variance (**Figure 3.12b**). Additionally, increasing the seeding density ubiquitously increased the number of non-confined cells across all conditions, and was the second most important factor identified by hierarchical regression analysis (**Figure 3.11b & 3.12b**). For devices seeded at 20 x 10^6 cells/mL the average number (and ± standard error of the mean) of non-confined cells averaged across all microchannel widths and lengths, were 0.25 ± 0.65, 31.78 ± 30.28, and 145.36 ± 161.93 for devices with microchannel heights of 1.5, 3, and 6 µm respectively. These values dropped to 0.21 ± 0.44, 4.28 ± 7.29, and 19.29 ± 24.20 when the initial seeding density was reduced to 3 x 10^6 cells/mL. Microchannel width and length also played a significant role in determining the effectiveness of the cellular confinement of the devices, but their effect was only observed at larger channel heights and higher seeding densities (**Figure 3.11b & 3.12b**).

Interestingly, while we initially expected to see similar numbers of cells entering or crossing through the microchannels with similar cross-sectional areas (i.e., 5 µm wide x 6 µm tall vs 10 µm wide x 3 µm tall), we observe that microchannel height plays a substantially greater role in determining if cell nuclei can enter the microchannels. Microchannels with heights of 1.5 µm showed a near complete confinement of nuclei within the seeded cell culture chamber, regardless of seeding density or other microchannel dimensions. It has been shown that nuclei in cultured cells can undergo large deformations in width and length to pass through confined microchannels but show a lesser ability to adjust nuclei height [157]. It has also been shown that compressing the nuclei of HeLa cells below 3.5 µm leads to nuclear lamina rupture, nuclear blebbing, and alterations in gene expression [158]. This suggests that for these devices, reducing microchannel heights below 3 µm may be an effective way to ensure near total confinement of cells within their seeded chambers. Additionally, we observed that the loss of somal confinement occurred rapidly following cell seeding, most likely due to cells flowing into the channels during the initial seeding. This observation is supported by comparing the overall ratio of neurons to astrocytes that were not confined to the seeded cell chamber. Averaged across all conditions, the ratio of neurons to total cells was 0.92 ± 0.08. While it has been shown that small populations of cultured neurons can migrate in response to specific stimuli, the large majority of cultured neurons are considered non-motile [159,160]. Conversely, astrocytes have been shown to migrate readily even in the absence of stimulation [161], and therefore we would expect a higher ratio of non-confined astrocytes to neurons if post-seeding migration was dominant. This suggests that cell confinement may not be a critical factor if each chamber is seeded with cells from the same initial population, however in instances where two distinct cell populations are seeded in opposing chambers, reducing microchannel height to prevent cellular cross-contamination is critical.

3.4.3 Astrocytes permeating microchannels

Many studies have demonstrated that culturing neurons with other glial cells can improve the overall health of the neuronal cultures especially at later timepoints (> 28 DIV) [132,146,162]. Previous studies along with our own preliminary experiments indicated that microglia, mature oligodendrocytes (OLs), and oligodendrocyte precursor cells (OPCs) do not interact significantly with the microchannels [163–165], however astrocytes are able to extend processes significant distances into the microchannels. Therefore, we wanted to quantify the astrocyte response to different microchannel geometries. We observed that seeding density was the primary factor in determining the percentage of microchannels containing at least one astrocyte process (**Figure 3.11c & 3.12c**), accounting for nearly 50% of the variance. As astrocytes account for only ~20% of the cells seeded, it is unsurprising that increasing the number of astrocytes close to the microchannels has the largest effect. The addition of microchannel width, length, and height to the regression model each improves the adjusted R^2 value of the model by a statistically significant amount (**Figure 3.12c**), where microchannel height had the least impact on the ability for astrocyte processes to enter the channel. Similar to axons, this is most likely due to the fact that cultured astrocytes have an average height of less than 1 µm [147], and therefore would largely be unaffected by the reduction in channel height. All four parameters significantly influenced the length that astrocyte processes extended into the microchannel, but compared to the other culture responses, the proportion of the variance explained by these four parameters was substantially less (adj R^2 for the full model = 0.11) (**Figure 3.12d**). However, we observed that astrocytes were able to extend processes up to ~450 µm into the microchannels with the largest cross-sectional areas (6 µm x 15 µm). This suggests that when co-culturing neurons and astrocytes together in these devices, microchannel lengths should be a minimum of 1000 µm to prevent the formation of astrocyte-astrocyte gap junctions, which may confound experimental results that assume only synaptic connectivity between the chambers.

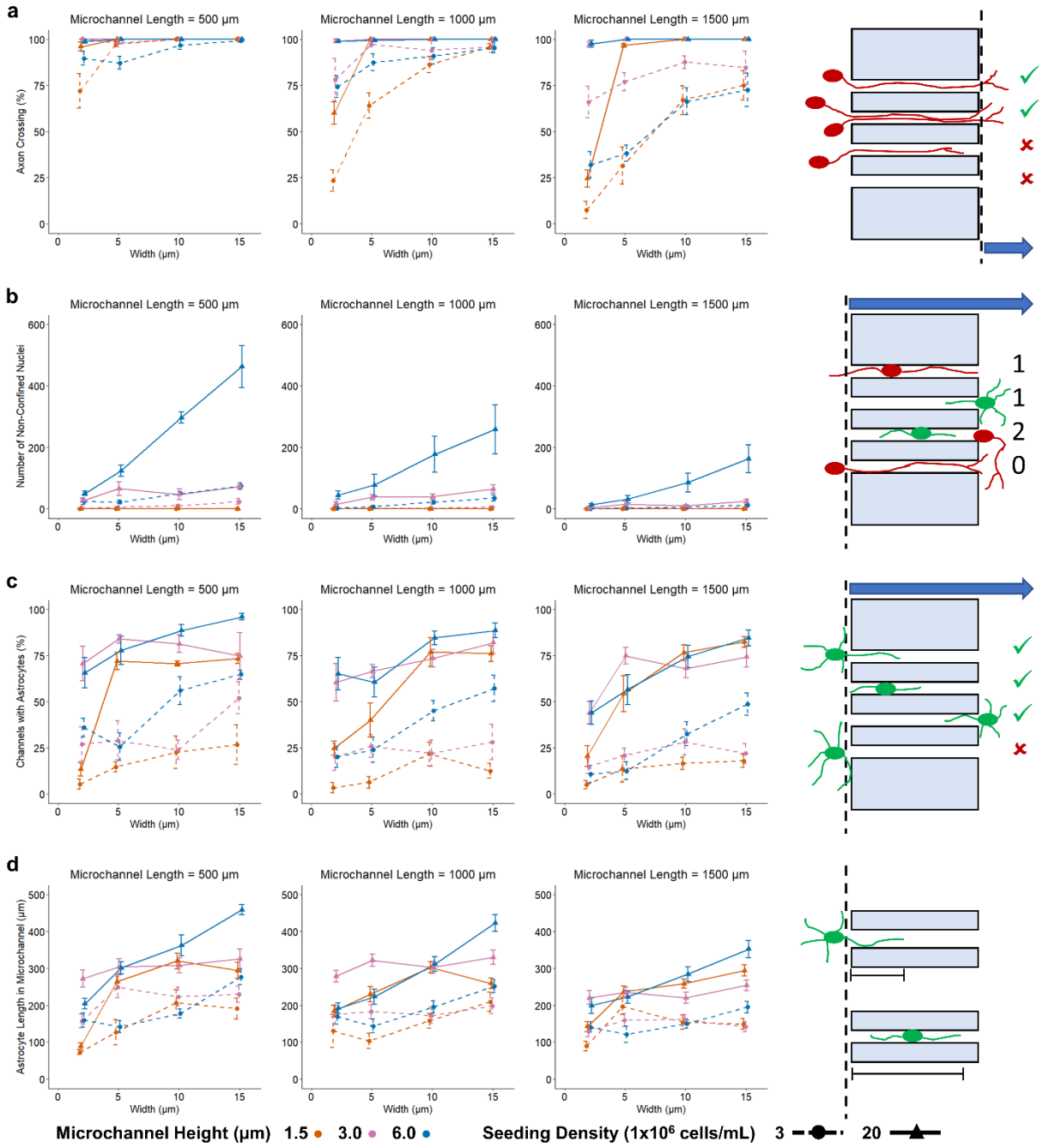

Figure 3.11: Quantification of (a) the percentage of microchannels with at least one axon crossing the entirety of the channel, (b) The number of non-confined cell bodies (nuclei), (c) the percentage of microchannels that contained at least one astrocyte process, and (d) the length that the astrocyte process extended into the microchannels to varying device parameters (mean ± SEM, *n* = 4-8 from two independent dissections). For the quantification of astrocyte length, only channels that contained at least one astrocyte process were analyzed. A schematic representation of how each response was quantified is shown in the right-most column.

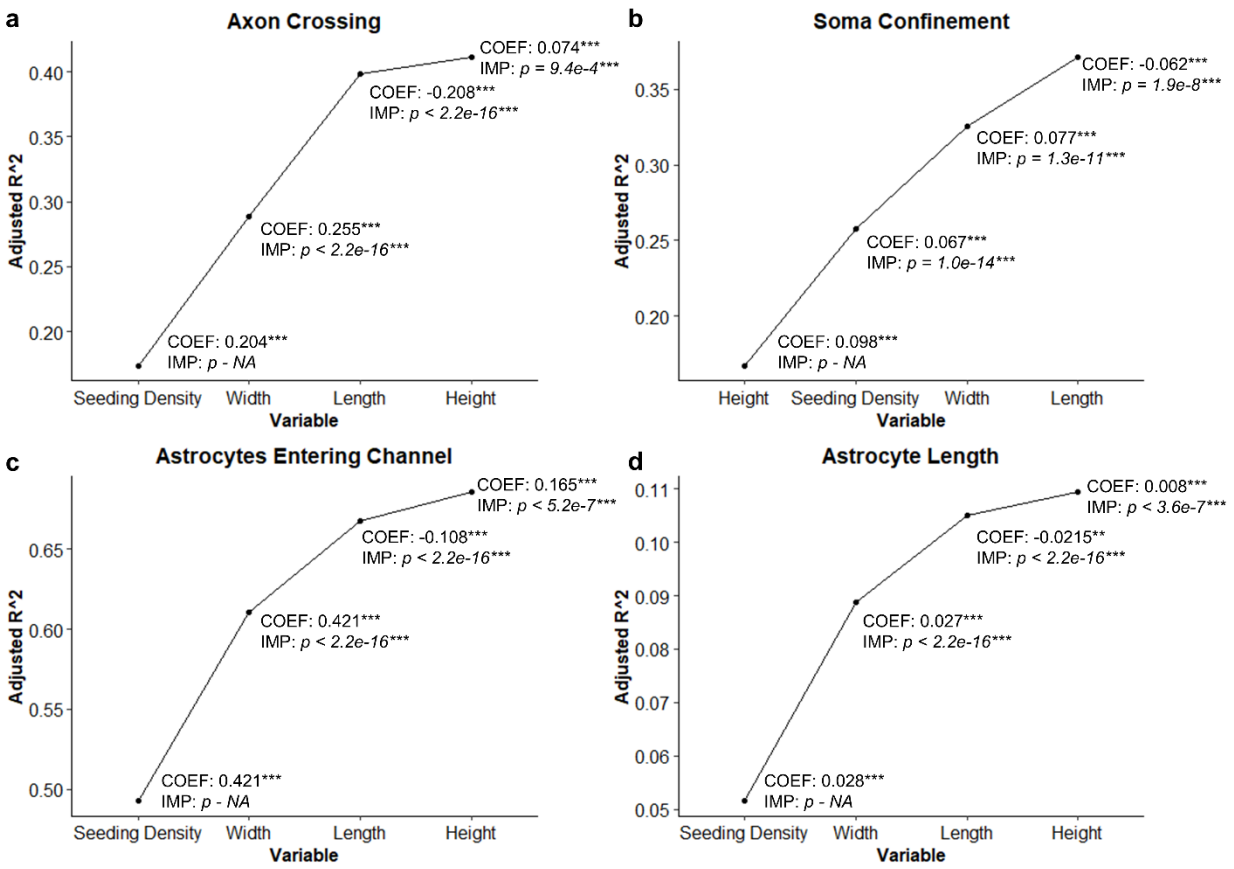

Figure 3.12: Plots showing the change in the adjusted R^2 following the addition of each variable in the stepwise linear regression model for (a) the percentage of microchannels with at least one axon crossing fully through the microchannel, (b) the number of nuclei not confined to the initial seeding chamber, (c) the number of microchannels with at least one astrocyte process in them, and (d) the length that the astrocyte process extended into a microchannel. IMP indicates the *p-value* for the improvement in adjusted R^2 due to the addition of the respective variable. COEF indicates the coefficient of that variable in the full model with all four variables included. *$p < 0.05$, **$p < 0.01$, ***$p < 0.001$.

3.5 Influence of Microchannel Geometry on Electrophysiological Recording Fidelity

Extracellular recording from neural cultures seeded onto MEAs in a well format have been widely used to study the development of neural circuit activity and responses to various pharmaceutical and pathological stimuli [166]. Similarly, MEAs can be integrated into microfluidic neural culture devices to record neural activity from synaptically-connected neural populations along with the interconnecting axons. While most research in this area has primarily been to demonstrate the ability to record large single unit recordings from axons within microchannel

[167–169] or study the rate of action potential (AP) propagation along axons [170,171], some researchers have begun to study the electrophysiological response of neurons cultured in these chambers to compartmentalized treatments [172,173] or develop directional neural networks [174,175]. For studying connected neural populations for longer durations (1+ month), it is necessary to determine the impact on microchannel geometry on electrophysiological recording fidelity. We seeded primary cortical cells at a concentration of 3 x 10^6 cells/mL and cultured them in "MEA" style devices integrated with a 32 channel MEA (16 electrodes were placed under the microchannels, and 8 were placed in each chamber) (**Figure 3.2c**). Based on our previous results, we narrowed down the fabricated devices to two microchannel geometries. All microchannels had lengths of 1000 µm to prevent astrocyte gap junction formation between the chambers and heights of 1.5 µm to minimize cell nuclei entering the chambers and improve fluidic isolation, informed by the studies above. The devices contained microchannels with either 5 µm or 10 µm channel widths, and the dimensions of the corresponding electrodes were adjusted to ensure a 400 μm^2 exposed electrode area. Additionally, the number of microchannels in the device was reduced from 101 to 25 and the surface area of each cell culture chamber was reduced to increase the likelihood of neurons attaching close to the chamber electrodes.

At DIV 59 the cultures maintained within the devices appeared healthy with robust neural processes and non-activated astrocyte morphologies [146] (**Figure 3.13a**) and showed robust neural activity recorded from electrodes in both the chamber (**Figure 3.13b**) and under the microchannels (**Figure 3.13c**). Initially, the percentage of active electrodes (electrodes recording at least 10 spikes during the 10 min recording) increased for all electrode types (electrodes placed under 10 µm-wide microchannels, 5 µm-wide microchannels, and within cell culture chambers), with almost 100% active channels by DIV 17 for the microchannel electrodes (**Figure 3.13d**). This increased percentage of active electrodes in the microchannels is likely due to the microchannels guiding the axons directly over the electrode sites, eliminating the stochastic effect of neuron-electrode proximity required for electrodes in the chambers. At early (DIV 7) and middle (DIV 21)

timepoints when the cultures are maturing and reaching maturity respectively, there is no difference between the percentage of active channels in 10 µm and 5 µm wide microchannels (p = 0.48 at DIV 7 & p = 0.59 at DIV 21). However, the percentage of active electrodes begin to decline at a much more rapid rate for 5 µm-wide microchannel electrodes as compared to electrodes under the 10 µm-wide channels, and by DIV 56 we observe a significant difference in the percent active electrodes ($p < 0.0001$). The decline in the number of active channels over time is not unexpected as it has been shown that the overall health of primary cortical cultures begins to decline around 28-35 DIV [129,132]. We expect that over time the axons in the microchannel may begin to deteriorate as the overall health of the neuron declines, and as the 10 µm wide microchannels contain more axons, this decrease is less pronounced as recording neural activity from only a single healthy axon is required to classify an electrode as active.

We see a similar relationship between electrode types when comparing changes in spike frequency (**Figure 3.13e**). Once again, for microchannels, there is an initial increase in firing rate as the culture matures followed by a decrease as the culture ages. The significant differences in estimated marginal means at DIV 21 between the microchannel and chamber electrodes ($p <$ 0.0001 for both 5 µm and 10 µm microchannels) can be attributed to recording from multiple axons within the microchannels. This also supports previous studies that show the AP from one axon within a microchannel does not depolarize other axons within the microchannel [168,170]. Unlike the number of active channels, there was no difference in firing rate between the 5 µm and 10 µm-wide microchannels at DIV 56 (p = 0.32). This difference can partially be attributed to the fact that non-active channels were excluded from the spike frequency analysis, and therefore contributions from rapidly degrading axons were not included in the analysis. Unlike the recordings from the microchannels, the firing rate of neurons in the chamber was relatively stable following the initial rise as the culture matured. This indicates that the neurons in the culture chambers may remain relatively healthy, but over time a portion of the axons within the microchannels begin the degrade.

We report significant increases in SNR (**Figure 3.13f**) and noise (**Figure 3.13g**) from electrodes within the microchannels as compared to those in the cell culture chambers. This is in line with previous reports showing increased SNR and noise floors from electrodes placed within microchannels [168–170]. The increase in noise can largely be attributed to the increase in electrode impedance due to the added electrical resistance along the length of the microchannel [168]. Similarly the increased resistance in the microchannel due to the spatial confinement leads to an increase in the spike amplitude [169]. Additionally, large numbers of neurites and astrocytes can block both sides of the microchannels essentially creating a high-resistance seal, which can dramatically increase the spike amplitude and lead to the much larger SNR seen in the microchannels (with a roughly order of magnitude difference at DIV 21) [169]. Interestingly, we saw a decrease in SNR over time in the 5 µm microchannels that was not observed in the 10 µm microchannels. As the microchannel geometries do not change over the course of the experiment, this may be attributed to a loss of the high-resistance seal in the 5 µm microchannels.

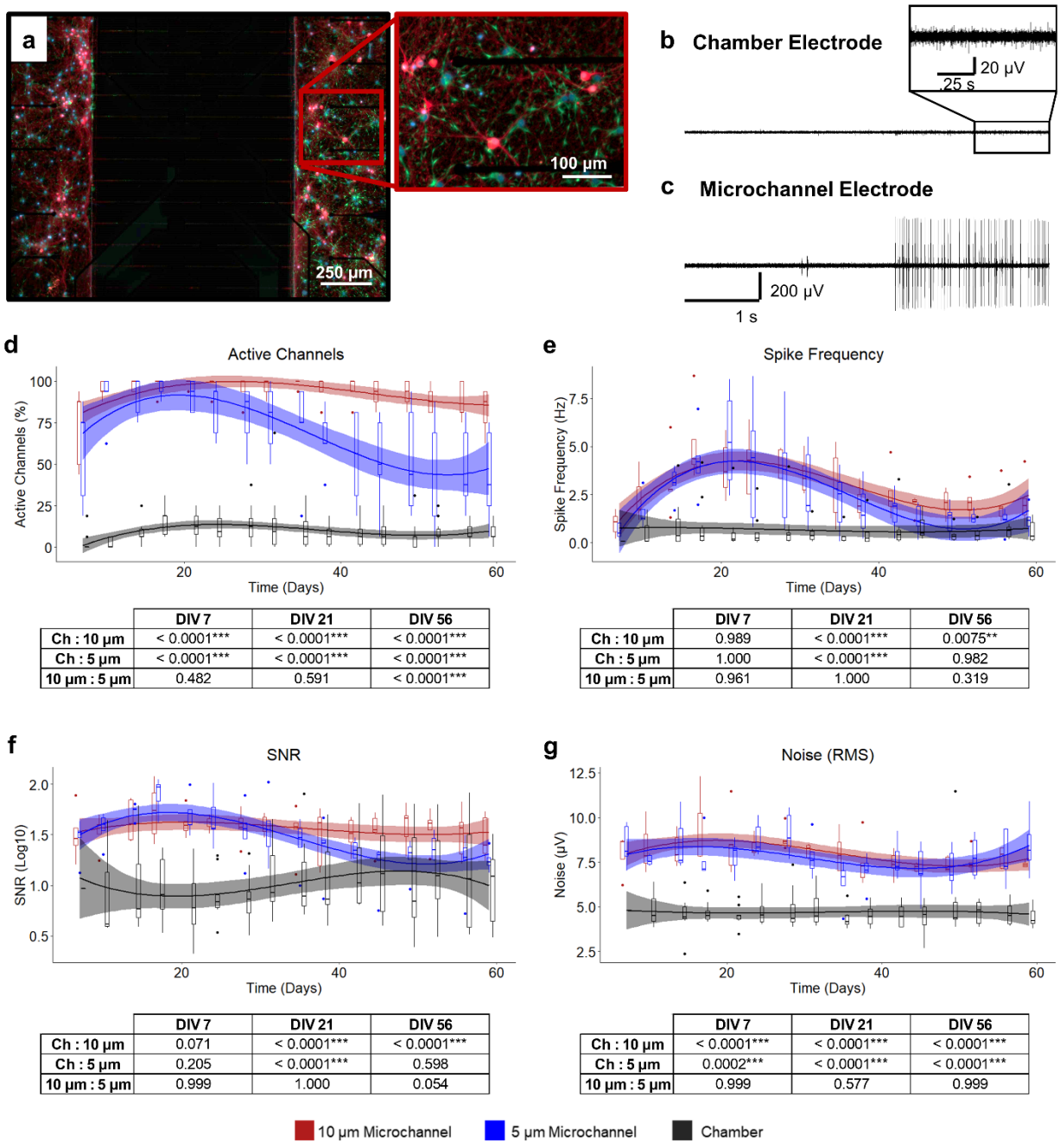

	DIV 7	DIV 21	DIV 56
Ch : 10 µm	< 0.0001***	< 0.0001***	< 0.0001***
Ch : 5 µm	< 0.0001***	< 0.0001***	< 0.0001***
10 µm : 5 µm	0.482	0.591	< 0.0001***

	DIV 7	DIV 21	DIV 56
Ch : 10 µm	0.989	< 0.0001***	0.0075**
Ch : 5 µm	1.000	< 0.0001***	0.982
10 µm : 5 µm	0.961	1.000	0.319

	DIV 7	DIV 21	DIV 56
Ch : 10 µm	0.071	< 0.0001***	< 0.0001***
Ch : 5 µm	0.205	< 0.0001***	0.598
10 µm : 5 µm	0.999	1.000	0.054

	DIV 7	DIV 21	DIV 56
Ch : 10 µm	< 0.0001***	< 0.0001***	< 0.0001***
Ch : 5 µm	0.0002***	< 0.0001***	< 0.0001***
10 µm : 5 µm	0.999	0.577	0.999

Figure 3.13: (a) Representative fluorescence image of cortical cells cultured in the "MEA" style device for 59 DIV. The cultures were immunostained for neurons – anti-βIII-tubulin (red) and astrocytes – anti-GFAP (green) and the general nuclear stain DAPI (blue). Representative recordings taken at DIV 59 from an electrode placed (b) within the cell culture chamber and (c) under a microchannel. Comparisons of the (d) percent active channels, (e) spike frequency, (f) SNR, and (g) RMS noise from electrodes placed under 10 µm wide microchannels (red), 5 µm wide microchannels (blue), and within the cell culture chambers (black). The solid lines show the fitted linear mixed effects model (treating the individual devices as a random effect) with a b-spline basis. The shaded regions are the 95% confidence interval. The tables show the p-values comparing the estimated marginal means of the fitted curves at pre-determined timepoints. (n = 5, from two independent dissections). $^{**}p < 0.01$, $^{***}p < 0.001$.

We also compared a number of different electrophysiological features (percentage of spikes in bursts, within burst ISI, and burst duration) to assess culture maturation and stability over time (**Figure 3.14a-c**). As expected, we see an increase in the percentage of spikes in bursts across all electrode types as the cultures mature. Additionally, over time we see a similar change in the percent of spikes in bursts as with the firing rate. Within microchannels, the percentage of spikes in bursts begins to decrease, presumably as some axons within the microchannels begin to degrade. In contrast, within the chamber, the values remain relatively constants, again suggesting that the neurons in the culture chambers remain healthy over the extended culture times. We also observe minimal changes over time for the within-burst ISI and burst duration, which also suggests that the cultures are healthy over the 59 DIV.

Finally, we compared the overall synchrony in devices with 5 µm and 10 µm-wide channels to assess the network development and stability over time (**Figure 3.14d**). We calculated the overall synchrony by comparing the dissimilarity of the spike trains of active channels using the SPIKE-distance method [130,131] (with values closer to 1 indicating higher levels of synchronization between the spike trains of active channels). While we observed an increase in synchrony for both devices as the cultures matured, the devices with 10 µm wide channels reached a higher degree of synchronization (p = 0.035 at DIV 56). This is presumably due to the increased number of axons crossing through the wider microchannels and form a more robust network between the two separated chambers. We also observed that for both devices the synchrony plateaued following the initial rise, suggesting that the network is stable over the extended culture times. Overall, these results suggest that increasing microchannel width may improve network formation between the microchannels and improve electrophysiological recording fidelity within the microchannels.

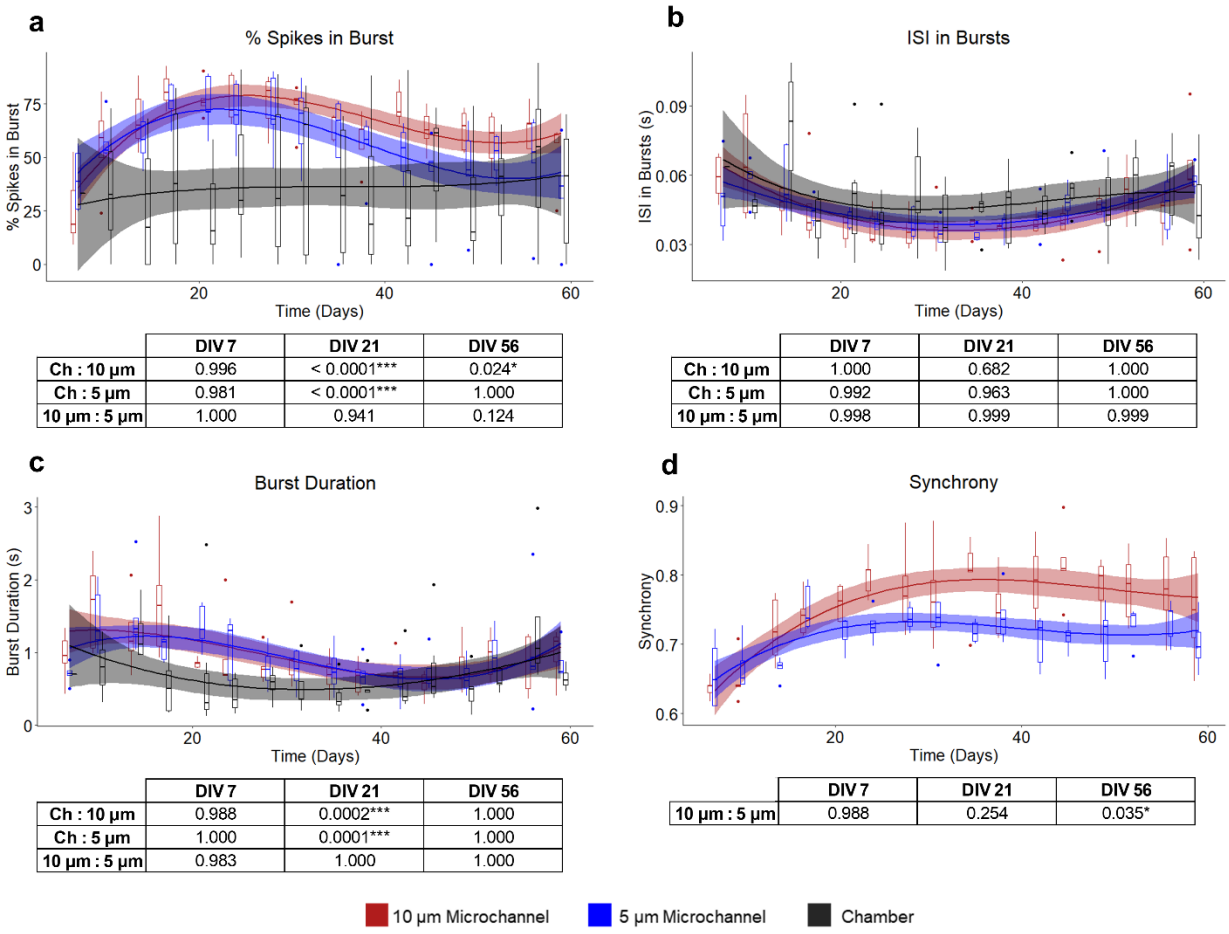

	DIV 7	DIV 21	DIV 56
Ch : 10 µm	0.996	< 0.0001***	0.024*
Ch : 5 µm	0.981	< 0.0001***	1.000
10 µm : 5 µm	1.000	0.941	0.124

	DIV 7	DIV 21	DIV 56
Ch : 10 µm	1.000	0.682	1.000
Ch : 5 µm	0.992	0.963	1.000
10 µm : 5 µm	0.998	0.999	0.999

	DIV 7	DIV 21	DIV 56
Ch : 10 µm	0.988	0.0002***	1.000
Ch : 5 µm	1.000	0.0001***	1.000
10 µm : 5 µm	0.983	1.000	1.000

	DIV 7	DIV 21	DIV 56
10 µm : 5 µm	0.988	0.254	0.035*

Figure 3.14: Comparisons of the (a) percentage of total spikes in bursts, (b) within-burst ISI, and (c) burst duration from electrodes placed under 10 µm wide microchannels (red), 5 µm wide microchannels (blue), and within the cell culture chambers (black). (d) Comparing the overall synchrony in devices with 10 µm-wide microchannels (red) and 5 µm-wide microchannels (blue). The solid lines show the fitted linear mixed effects model (treating the individual devices as a random effect) with a b-spline basis. The shaded regions are the 95% confidence interval. The tables show the p-values comparing the estimated marginal means of the fitted curves at pre-determined timepoints. (n = 5, from two independent dissections). $^{**}p < 0.01$, $^{***}p < 0.001$.

3.6 Conclusions

In this study, we have demonstrated the significant impact of small changes in microchannel geometry can have on the overall device functionality of commonly used microfluidic neural culture platforms. In particular, we studied how microchannel geometry influenced the cellular confinement, axon crossings, fluidic properties, and electrophysiological recording fidelity when using these devices. It is important to note that all experiments in this study

were performed using cortical cells from neonatal rats. While the size distribution of neurons and astrocytes in mice and rats are similar, the axon diameter and overall astrocyte size of human cells tends to skew slightly larger [149,176–178]. As the size difference between neuronal cells from rodents and humans are relatively minimal (for example over 95% axons from rat [149], mouse [176], and human [178] cortical neurons are less than 1.5 µm) we do not expect the cell source to significantly impact the results from this study. Additionally, as both human neurons and astrocytes are larger than their rodent counterparts, the overall conclusions drawn from this study should remain applicable across species. Below, we describe how each design factor can influence device functionality and summarize general design rules for different experimental objectives (**Figure 3.15**).

i) **Microchannel Height:** It is best to keep microchannel height as small as possible, ideally around 1.5 µm. Reducing microchannel heights to this value significantly reduces the number of cell bodies that can enter the microchannels (improving cellular confinement) while minimally impacting the ability for axons to enter the channels. Additionally, there is a significant reduction in the volumetric flow rate through the microchannels when a hydrostatic pressure differential is maintained. This is especially critical for long-term studies, where fluid flow between the chambers can significantly alter the concentration of soluble factors added to the fluidically isolated chamber. In general, we do not recommend increasing microchannel height above 1.5 µm, with the exception that if peripheral neurons are being cultured taller microchannels may be required to accommodate the larger axon diameters [179]. In this case the initial seeding density should be reduced to minimize the number of cells that enter the microchannels, and treatment times should be kept to a minimum to minimize changes in the effector molecule concentration.

ii) **Microchannel Length:** For long-term experiments studying connected neural populations, in which both neurons and astrocytes will be added to both sides of the

microchannels, it is important that the microchannels are at least 1000 μm in length to prevent the formation of astrocyte-astrocyte gap junctions within the microchannels. For experiments in which cells are cultured on only one side of the microchannels or when only neurons are being cultured, the previous recommended length of 450-500 μm should be used to prevent dendrites from crossing through the channels [90].

iii) **Microchannel Width:** For extended studies of connected neural populations, we suggest a microchannel width of at least 5 μm to ensure robust connectivity between the chambers. Increasing microchannel width beyond 5 μm can improve the long-term electrophysiological recording fidelity, at the cost of increasing the number of axons in each microchannel. If robust synaptic connectivity between the chambers is desired, increasing the number of axons in each microchannel is beneficial and there is little to no drawback from increasing microchannel width. If the experiment requires a single axon to be present in each microchannel (i.e., single axon imaging or electrophysiological recording studies) reducing the microchannel width down to 2 μm may be worthwhile. If this is the case, increasing the initial seeding density can be used to counteract the reduced axon crossings and improve the overall connectivity between the chambers.

iv) **Initial Seeding Density:** The initial seeding density can largely be used as a tool or countermeasure to reduce some of the negative side effects of altering microchannel geometries. Increasing seeding density can be used to increase the number of axons crossing the microchannels when using devices with small microchannel widths or very long microchannel lengths. Alternatively, reducing the seeding density can improve the cellular confinement of devices with large microchannel heights. Additionally, reducing initial seeding density can substantially reduce the number of astrocyte processes within the microchannels.

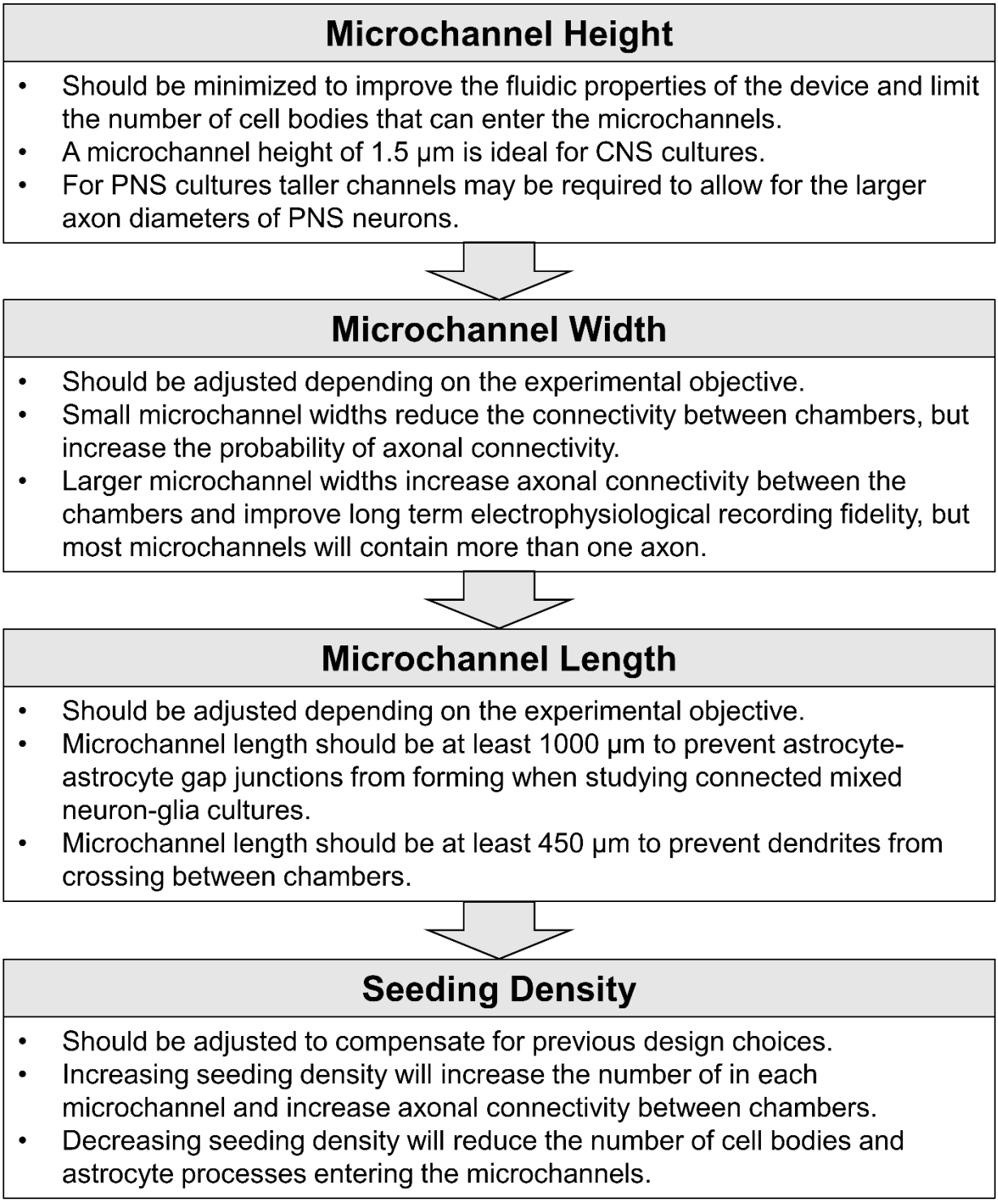

Figure 3.15: A summary of general step-wise design rules for different experimental objectives.

Chapter 4: Development and Characterization of a Primary Tri-Culture of Neurons, Astrocytes, and Microglia to Study Neuroinflammation

Neuroinflammation is present in most, if not all, pathological conditions in the central nervous system (CNS), either acting as the primary driver of these conditions, or as a response to neurodegeneration or disruption of homeostasis following disease progression [1–3]. Following insult or injury to the CNS, the two primary cell types associated with neuroinflammation, microglia and astrocytes, become “activated,” as indicated by changes in their morphology and phenotype [180–182]. Previously, activated astrocytes and microglia were dichotomously classified as either neurotoxic (A1/M1) or neuroprotective (A2/M2) depending on the mode of activation, however recent evidence suggests that both astrocytes and microglia display a wide range of phenotypes depending on the activating stimuli [183–185]. Furthermore, crosstalk between neurons, astrocytes and microglia has been shown to play a significant role in the observed neuroinflammatory response [186,187].

While there are a number of *in vivo* models to study neuroinflammation, in vitro models are often used to investigate specific molecular pathways. Current cell culture models of neuroinflammation typically consist of cultures of individual cell types with conditioned media from one cell type transferred to cultures of another cell type [94,188,189]. While these models have provided significant insights into neuroinflammatory processes [96], these models contain inherent limitations, most notably the inability to observe the effects of membrane-bound or cell proximity-dependent mechanisms and the fact that the concentration of secreted cytokines transferred between cultures may not be physiologically relevant. An alternative model involves seeding microglia over a previously established primary neuron culture to observe the effect of this cell-cell interaction of a short period of time (24- 72 h) [112–114]. In addition to the limited time-scale of this model, the culture media used to support the microglia prior to their addition to the neuronal culture typically contains a high concentration of serum, likely causing the microglia

to be in an already activated state before their addition to the neuronal cell cultures [115]. Co-cultures of neurons and astrocytes are another established method of studying neuroinflammation in vitro [116–118,129]. As the culture conditions for neurons and astrocytes are similar, these co-cultures can be studied over extended time scales [116,129]. However, none of the aforementioned neuroinflammatory models are able to capture the important interplay between neurons, astrocytes and microglia. Thus, there is need for new, multicellular culture systems that are capable of modeling the neuroinflammatory impact of crosstalk between different cells in the CNS. This need was highlighted in a recent review on the current tools and methods for studying glia [94].

To address the shortcomings of existing *in vitro* models of neuroinflammation, we developed an enhanced cell culture model comprised of the three major cell types associated with neuroinflammation – neurons, astrocytes and microglia. Primary rat cortical cells were maintained in a serum-free culture media developed to support all three cell types. We demonstrate that this "tri-culture" can be maintained for at least 21 days *in vitro* (DIV), without any deleterious effect of the continuous presence of microglia on the overall health of the neurons in the tri-culture. The tri-culture contains a similar relative percentage of neurons and displays a similar amount of neurite growth as compared to the microglia-free, neuron-astrocyte co-cultures. Furthermore, we demonstrate that the tri-culture system responds to several pro-inflammatory stimuli, including lipopolysaccharide (LPS), mechanical trauma, and excitotoxicity, in a manner similar to that observed *in vivo*.

4.1 Tri-Culture Media Formulation

We hypothesized that a tri-culture of neurons, astrocytes, and microglia could be maintained through the use of a specialized media formulation consisting of a well-established and commercially available neuron-astrocyte co-culture medium [190] supplemented with 100 ng/mL IL-34, 2 ng/mL TGF-β and 1.5 µg/mL cholesterol. These three factors were chosen as they

have been identified as key factors in supporting serum-free cultures of isolated microglia [19]. Additionally, these three factors each of these three factors have been associated with improved neuron health and survival, and therefore we thought that these factors could be added to the co-culture medium without negatively impacting the overall health of the culture. In particular, it has been shown that TGF-β enhances the effect neurotrophic factors and improves the survival of cultured neurons maintained with low concentrations of neurotrophins [63,64], while exogenous cholesterol is thought to play a significant role in neural cholesterol homeostasis [65]. Activation of CSF1R on neurons via CSF1 or IL-34 has been shown to increase neuron survival following kainic acid induced excitotoxicity [44], while activation via CSF1 leads to reduced apoptosis in cultured neurons in a dose dependent manner [66]. We decided to include IL-34 instead of CSF1 in the tri-culture medium, as IL-34 is more widely expressed in the cortex of postnatal mice [67,68].

In order to test this hypothesis, we cultured primary dissociated cortical cells from neonatal rats for 7 days in the either the neuron-astrocyte co-culture media or that media supplemented with different combinations of the aforementioned factors (**Figure 4.1**). As the three media supplements present in the tri-culture have been shown to support isolated microglia and are found in astrocyte conditioned media [19], we were interested to see if the neurons or astrocytes might be constitutively secreting any of these factors in the tri-culture, thereby making their addition to the tri-culture media redundant.

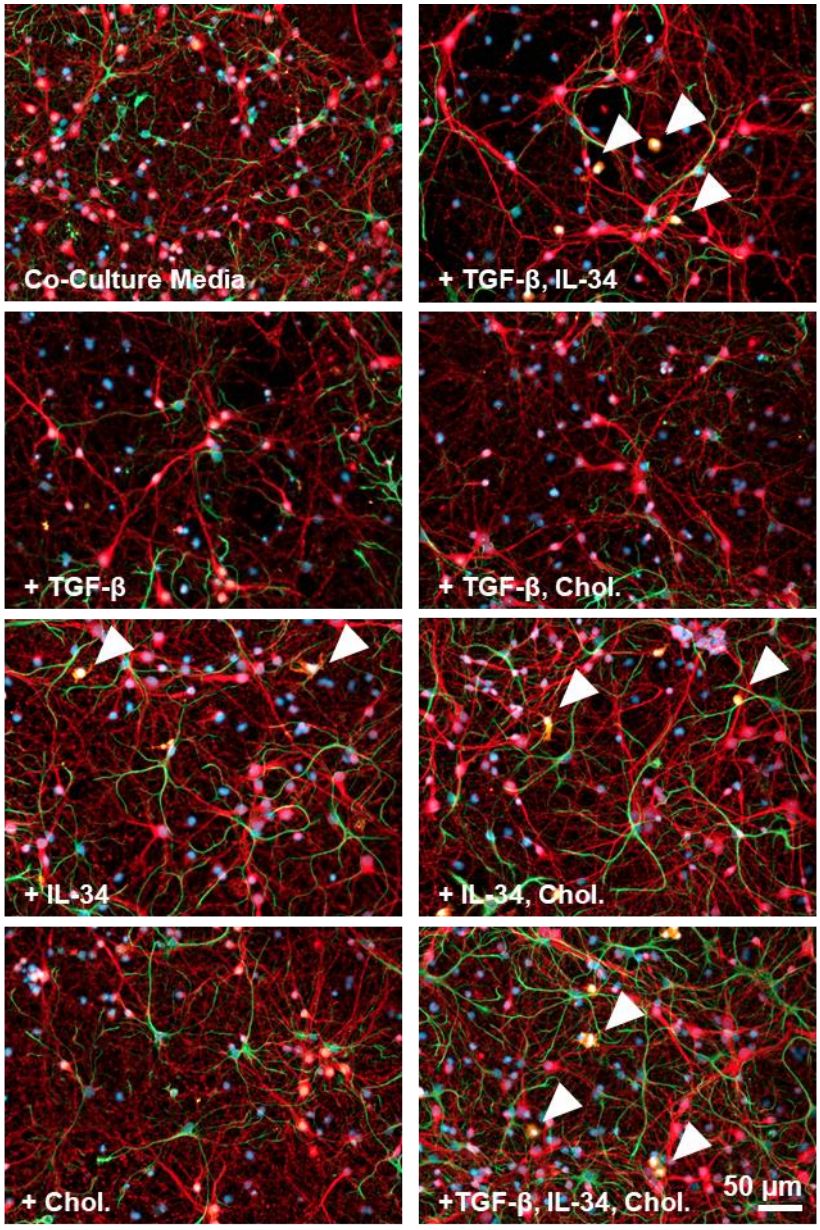

Figure 4.1: Representative images of cultures maintained with co-culture media and different combinations of TGF-β, IL-34, and cholesterol. The cultures were immunostained for neurons – anti-βIII-tubulin (red), astrocytes – anti-GFAP (green), microglia – anti-Iba1 (orange) and the general nuclear stain DAPI (blue). Cells stained with Iba1 are highlighted with arrows.

An exploratory study unambiguously indicated that IL-34 was required for microglia survival (**Figure 4.2**); however, the additional presence of TGF-β or cholesterol did not appear to impact the number of microglia present in the culture. Additionally, neither TGF-β nor cholesterol allowed for microglia survival on their own. Previous studies have indicated that the activation of

the colony stimulating factor 1 receptor (CSF1R) via colony stimulating factor 1 (CSF1) or IL-34 is required for microglia viability both *in vitro* and *in vivo* [57–59], and therefore its requirement in the tri-culture media was not unexpected.

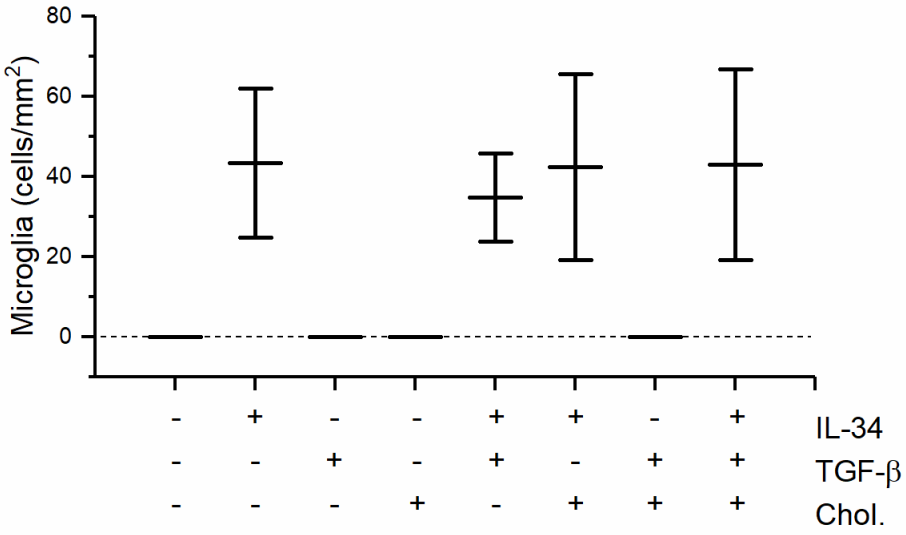

Figure 4.2: Tri-culture media supplement requirements for microglia survival at DIV 7. The results indicate that IL-34 is required for microglial survival in the tri-culture. The figure shows the mean ± SD of the technical replicates (n = 4) of a single biological replicate.

In order to determine if either TGF-β or cholesterol was required to maintain physiologically active microglia, we challenged cultures maintained under different combinations of TGF-β and cholesterol plus IL-34 with 5 µg/mL of LPS. LPS is a potent activator of neuroinflammation and neuronal apoptosis, which acts through the toll-like receptor 4 (TLR4) found only on microglia in the CNS [30,31]. As expected, LPS did not increase caspase 3/7 activity in neuron-astrocyte co-cultures relative to the vehicle control. However, cultures grown in the presence of different combinations of the tri-culture factors responded to LPS with increased caspase 3/7 activity (**Figure 4.3**). In particular, cultures exposed to all 3 co-factors (IL-34, cholesterol and TGF-β) showed a significant increase in caspase 3/7 activity following the addition of LPS ($p = 0.0081$). Cultures maintained in the co-culture medium spiked with a subset of the co-factors (IL-34 alone, IL-34 plus cholesterol or IL-34 plus TGF-β) all showed increased caspase

3/7 activity, but a post hoc Tukey test did not reveal any significant differences between these cultures and either the co- or tri-culture. However, the fact that the change in caspase 3/7 activity of these cultures more closely resembled that of the co-culture (p = 0.99, 0.91 & 0.95 respectively) than that of the tri-culture (p = 0.064, 0.16, and 0.16 respectively), indicates that the microglia present in these cultures are most likely not physiologically active.

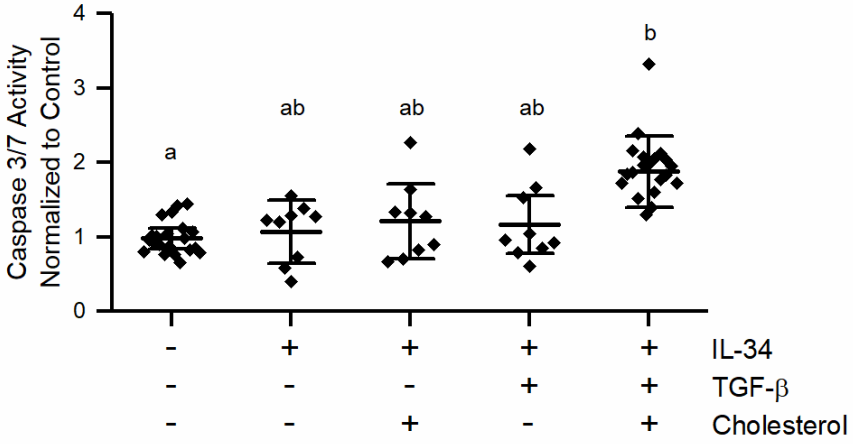

Figure 4.3: Comparing the effects on apoptosis following a 48 h incubation with 5 µg/mL LPS on DIV 7 cortical cultures maintained in different media types (mean ± SD, n=3-6). The letters above the bars indicate statistically distinct groups (p < 0.05), while the points indicate the values of the technical replicates.

While the addition of TGF-β or cholesterol did not seem to be a requirement for microglia viability in the tri-culture, both factors proved critical in maintaining physiologically active microglia. It has been shown that TGF-β can induce a quiescent microglia phenotype in vitro [60], and it may even be required for cultured microglia to maintain their gene expression profile [61]. Excess cholesterol in the culture media may also be beneficial for maintaining a functional microglia gene expression profile as it reduces the expression of apolipoprotein E (ApoE) [62], which is critical for lipid transport, but it is also inversely correlated with the expression of microglia signature genes [61]. The results from this study indicated that all three factors are required to support a healthy tri-culture of neurons, astrocytes, and microglia.

4.2 The Tri-Culture Supports Neurons, Astrocytes, and Microglia *In Vitro*

Primary cortical cells taken from neonatal rats were cultured in our previously described neuron-astrocyte co-culture media, or in our tri-culture media consisting of the co-culture media supplemented with 100 ng/mL IL-34, 2 ng/mL TGF-β and 1.5 µg/mL cholesterol. Immunostaining for Iba1 revealed that there was a significant population of microglia at both DIV 7 and 14 in the cultures maintained in the tri-culture media, which are absent from cultures maintained in the co-culture medium (**Figure 4.4a-c**). A two-way ANOVA did not establish a significant interaction between the time in culture and media type on the number of microglia present in the culture ($p = 0.44$). Analysis of the main effects indicated that the tri-cultures had significantly more microglia present than the co-cultures ($p = 0.0025$); however, the time in culture did not impact the number of microglia ($p = 0.44$). The total number of microglia in the tri-culture accounted for ~7-8% of the total cell population (**Figure 4.4c**) in agreement with microglia numbers reported in vivo [191,192].

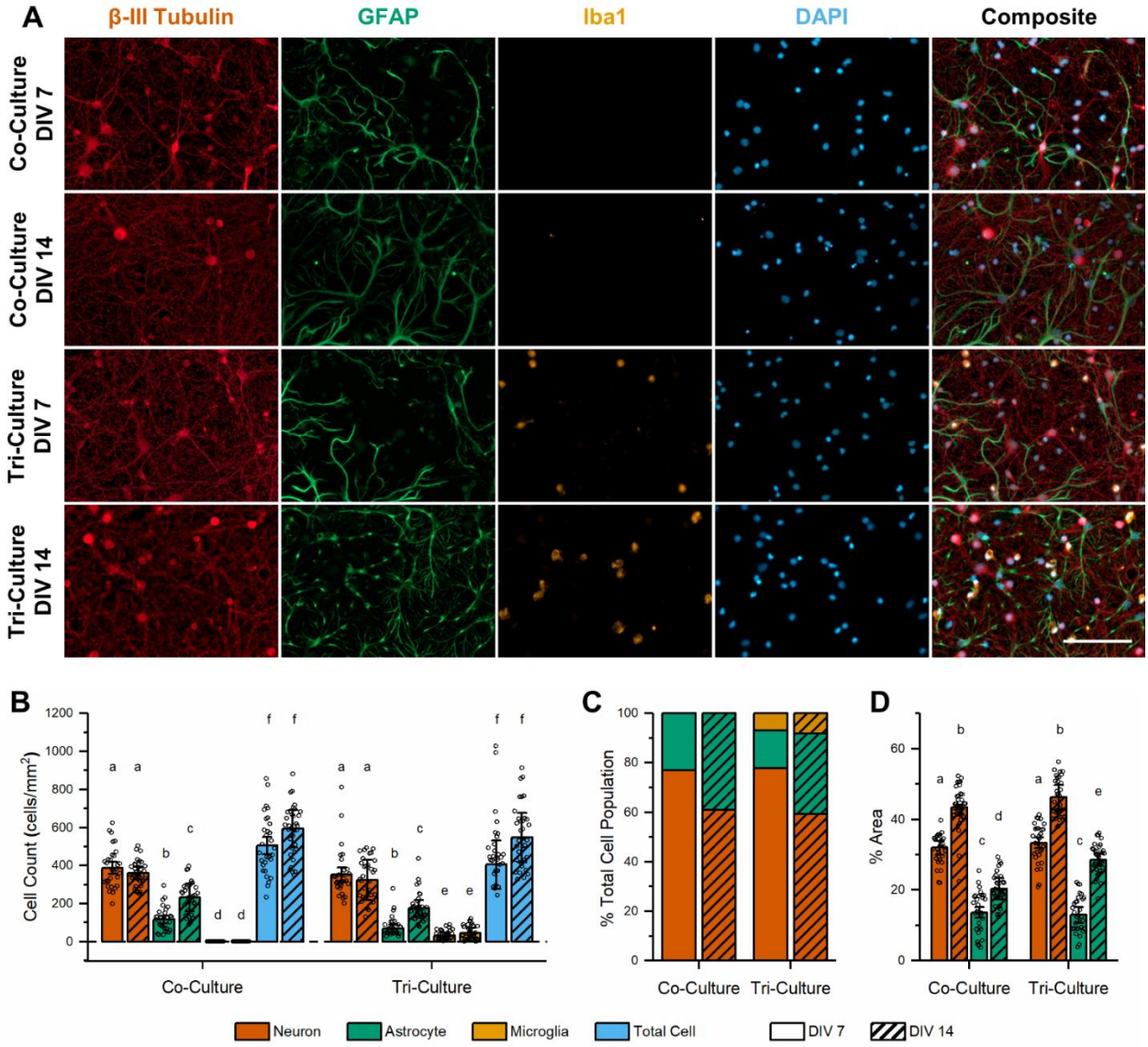

Figure 4.4: Tri-culture media is capable of supporting neurons, astrocytes and microglia. (**a** Representative fluorescence images of the tri- and co-cultures at DIV 7 and 14. The cultures were immunostained for the three cell types of interest: neurons – anti-βIII-tubulin (red), astrocytes – anti-GFAP (green), microglia – anti-Iba1 (orange), general nuclear stain DAPI (blue). Microglia are present in the tri-culture at both time points, but are absent in the co-culture. Scale bar = 100 µm. (b) Quantification of the number of each cell type and total number of cells per mm^2 for each condition shown in Figure 4.4A (mean ± SD, n=3). (c) Percent of total cell population represented by each cell type in co-culture vs. tri-culture conditions (d) Quantification of the percent area coverage of the neurons and astrocytes in the co- and tri-cultures at DIV 7 and 14 (mean ± SD, n=3). (b&d) The letters above the bars indicate statistically distinct groups ($p < 0.05$), while the points indicate the values of the technical replicates.

Immunostaining for β-III tubulin to label neurons and GFAP to label astrocytes revealed a healthy population of both neurons and astrocytes in both the tri- and co-cultures (**Figure 4.4a**). The number of neurons present was not affected by either the media type or time in culture (**Figure 4.4b**, $p = 0.44$ and $p = 0.31$ respectively). Additionally, neurite outgrowth (measured as the percent of the area stained for β-III tubulin as compared to the total image area) was not statistically different between the co- and tri-cultures (**Figures 4.4d**, $p = 0.13$), and the neurons continue to produce new projections through DIV 14 as determined by the significant increase in neuron percent area coverage from DIV 7 to 14 ($p = 1.04 \times 10^{-5}$). Furthermore, by DIV 14, we observed the co-localization of f-actin and β-III tubulin indicating the presence of dendritic spines (**Figure 4.5**). As no mitotic inhibitors were added to the culture media, the number of astrocytes significantly increased in both culture types from DIV 7 to 14 (**Figure 4.4b** $p = 0.0023$). While the analysis of the main effects from the two-way ANOVA did not reveal a significant difference in astrocyte population between the two culture types ($p = 0.062$), the results suggest that the tri-cultures may contain a lower number of astrocytes than the co-cultures. Unlike the neurons, the astrocyte percent area coverage showed a significant interaction between the culture type and time in culture (**Figure 4.4d**, $p = 0.0077$), with the tri-culture having a similar astrocyte percent area coverage to the co-culture at DIV 7 ($p = 0.90$), but a significantly higher astrocyte percent area coverage at DIV 14 ($p = 0.0076$).

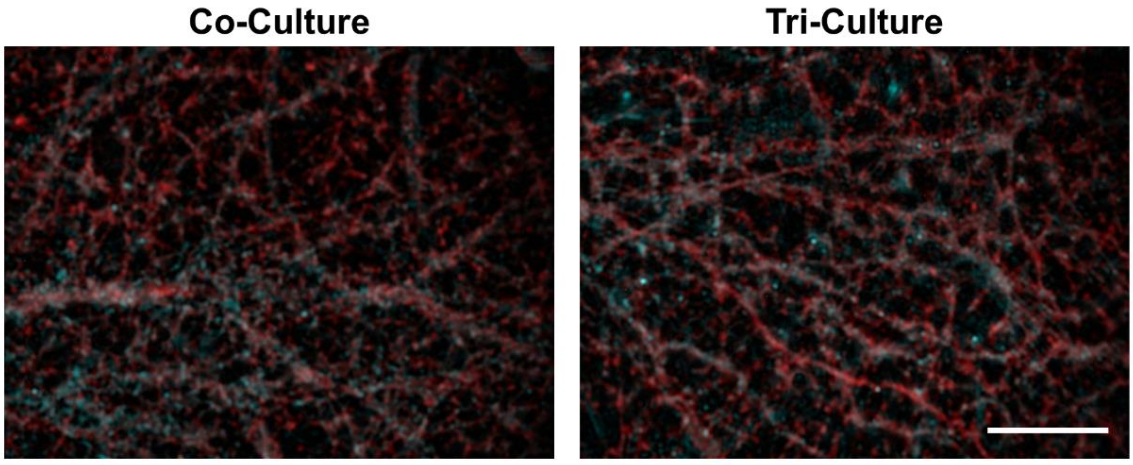

Figure 4.5: Immunostained images of the co- and tri-cultures at DIV 14 showing the co-localization of f-actin (cyan) and β-III tubulin (red) indicative of dendritic spines. Scale bar = 20 µm.

We observed that the tri-culture contains all three cell types, and that the continuous presence of microglia did not impact the number of neurons or neurite outgrowth. However, we did observe a slight decrease ($p = 0.062$) in the number of astrocytes in the tri-culture as compared to the co-culture, which might be due to the presence of TGF-β in the tri-culture media, which has been shown to reduce astrocyte proliferation [193]. Additionally, we observed a significant increase in the percent area coverage of the astrocytes at DIV 14. However, this increase is due in part to the large number of fine astrocyte processes seen in the DIV 14 tri-culture, which is overvalued by the auto-thresholding process used to calculate these values. We also observed a small portion of cells in both the tri- and co-cultures (~2%) that were not immunoreactive for antibodies that selectively label neurons, astrocytes or microglia (**Figure 4.6a**). These unidentified cells may be oligodendrocyte precursor cells based on immunoreactivity for NG2 (**Figure 4.6b**) [194]. It is likely that the lack of a mitotic inhibitor may have allowed a small portion of these cells to survive, as they are not observed in neuron-astrocyte co-cultures treated with mitotic inhibitors [116]. Furthermore, we do not expect that the presence of NG2-glia would impact the observed differences in the inflammatory response between the co- and tri-cultures as both cultures have a similar population of NG2- immunopositive cells. However, as there is evidence that NG2-glia

can play a role in neuroinflammation [194–196], in future studies it may be beneficial to attempt to increase the number of NG2-glia to physiologically-relevant levels to attain an even more complete cell culture model of neuroinflammation.

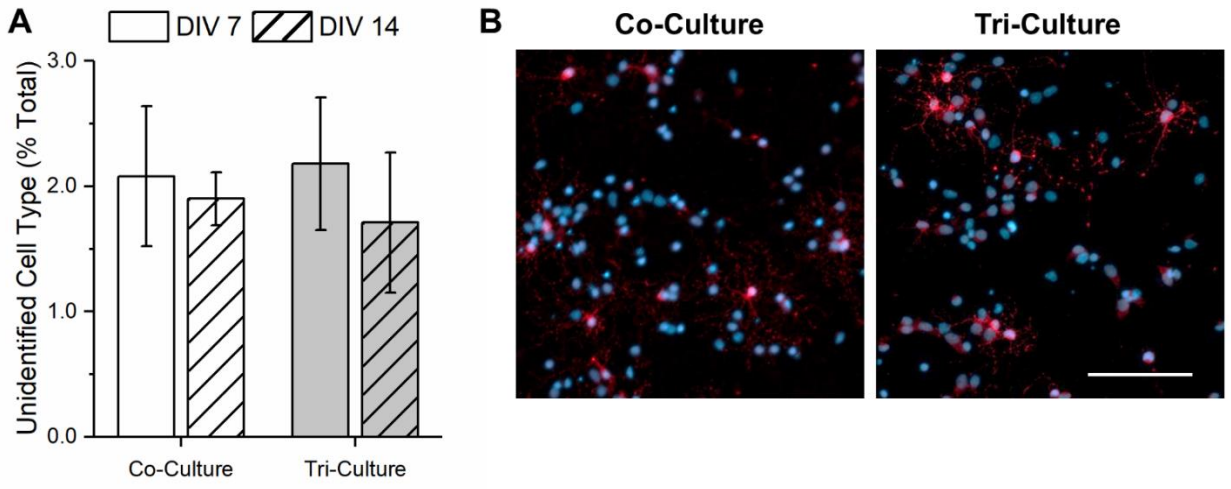

Figure 4.6: There are approximately 2% of the total cell population that was not clearly identifiable as neurons, astrocytes or microglia. (a) Mean ± SD of cells from each culture type not reactive for antibodies selective for neurons, astrocytes or microglia (n = 3). (b) Representative images from DIV 7 co- and tri-cultures immunostained for NG2 (red), a biomarker of oligodendrocytes, and reacted with DAPI (blue), scale bar = 100 µm.

Ultimately, the results from these experiments demonstrate that the tri-culture medium is capable of supporting neurons, astrocytes, and microglia, and that the continuous presence of microglia in the culture does not have a negative impact on the overall health of the neurons and astrocytes.

4.3 Tri-Culture Response to Neuroinflammatory Stimuli

After demonstrating that the tri-culture medium was capable of supporting a healthy population of neurons, astrocytes, and microglia, we then characterized the tri-culture to several neuroinflammatory stimuli, including exposure to LPS, mechanical injury and excitotoxic challenges. We compared the response of the tri-cultures to that of the neuron-astrocyte co-cultures to these different neuroinflammatory insults and found that the presence of microglia

changes the response in each case. Moreover, the response of the tri-culture to these neuroinflammatory challenges are more in line with what is reported *in vivo* and in slice culture models.

4.3.1 Response to LPS

The use of LPS to stimulate a neuroinflammatory response is well characterized method used by researchers to study a wide range of neuroinflammatory and neurodegenerative conditions [197], including Alzheimer's disease (AD) [198], Parkinson's disease (PD) [199] and even mood disorders such as clinical depression [200]. Therefore, we determined the response of the tri-culture model to LPS. As stated previously, a 48 h incubation with 5 µg/mL LPS significantly increased caspase 3/7 activity in the tri-culture model relative to the neuron-astrocyte co-culture (**Figure 4.3**). This is in agreement with previous studies that show LPS induces a neurotoxic pro-inflammatory condition both in vitro and in vivo via apoptotic caspase-3 mediated mechanisms [96,201,202]. Immunohistochemical analyses (**Figure 4.7**) reveal clear morphological changes in both astrocytes and microglia in the tri-culture after exposure to LPS. Astrocytes in the tri-culture showed reduced ramification, increased process length and hypertrophy, all of which are hallmarks of reactive astrocyte morphology [203]. The increased process length and hypertrophy result in an overall increase in astrocyte area (**Figure 4.8a**) that was significantly higher in tri-cultures exposed to LPS relative to tri-cultures exposed to vehicle ($p = 0.0030$) or astrocytes in the co-culture exposed to LPS ($p = 0.0039$). Additionally, there was no change in the morphology or average area of astrocytes in the co-cultures exposed to LPS or vehicle ($p = 0.90$). The size of microglia also significantly increased in tri-cultures exposed to LPS as compared to vehicle control tri-cultures (**Figure 4.8b**, $p = 0.0052$).

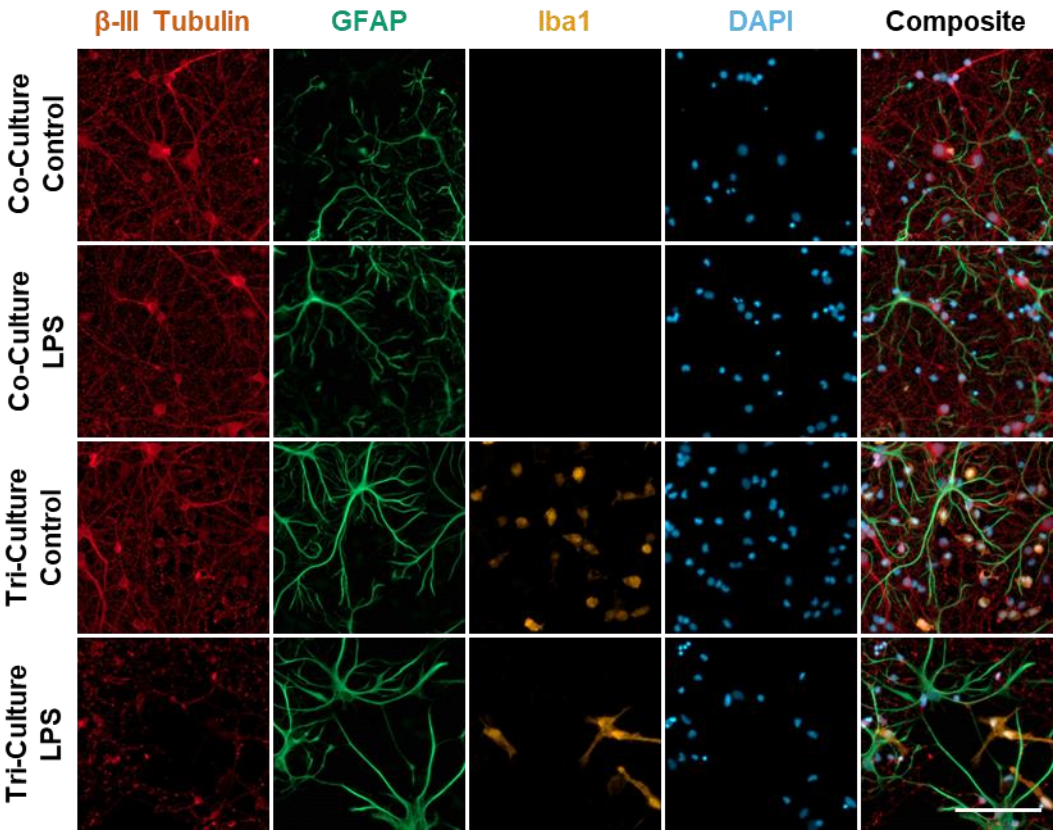

Figure 4.7: Representative fluorescence images of the tri- and co-cultures after a 48 h incubation with 5 µg/mL LPS or vehicle. The cultures were immunostained for the three cell types of interest: neurons – anti-βIII-tubulin (red), astrocytes – anti-GFAP (green), microglia – anti-Iba1 (orange) and the general nuclear stain DAPI (blue). Scale bar = 100 µM.

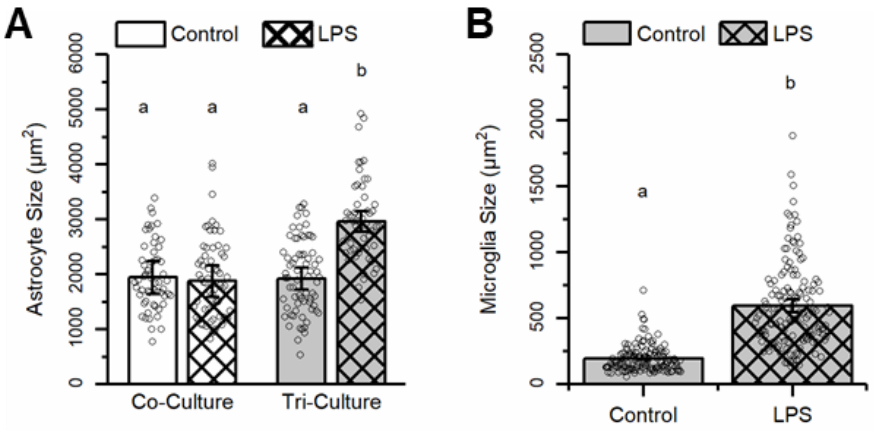

Figure 4.8: (a) A comparison of the average astrocyte area from the different conditions (mean ± SD, n=3). (b) Comparing the average microglia size in tri-cultures exposed to LPS vs. vehicle (mean ± SD, n=3). The letters above the bars indicate statistically distinct groups ($p < 0.05$), while the points indicate the values of the technical replicates.

In addition, we compared the cytokine secretion profiles of the control and LPS-exposed tri- and co-cultures using the proteome profiler rat XL cytokine array (Bio-Techne). Of the 79 cytokines detected by the array, 34 were detected at a relative concentration greater than 10% of the maximum in at least one of the samples. A hierarchical cluster analysis was performed on the results from these 34 cytokines (**Figure 4.9a**), which revealed three distinct expression profiles. In general, these profiles consist of cytokines secreted by both the co- and tri-cultures (green) and those only secreted by the tri-culture. This second group of cytokines can be further subdivided into cytokines that are secreted in relatively equal concentrations by the control and LPS-exposed tri-cultures (orange) and cytokines having increased expression in the LPS-exposed tri-cultures (purple). As expected, the co-cultures did not respond to LPS, leading to a nearly indistinguishable cytokine profile as compared to the control co-culture exposed only to vehicle.

All cytokines secreted by both the tri- and co-cultures have been shown to be expressed by either neurons or astrocytes in non-inflammatory conditions [204–208], with the exception of adiponectin, which is found in the CSF of healthy individuals but has not been shown to be expressed by neurons or astrocytes [209]. Additionally, with the exception of CX3CL1, these cytokines appear to be constitutively expressed by astrocytes and microglia as neither the media type nor the addition of LPS had an impact on their concentration in the conditioned media. Interestingly, we see a significant decrease in CX3CL1 concentration in the tri-culture as compared to the co-culture (**Figure 4.9b**, $p = 0.0051$). Additionally, we observe the presence of IGF-1 in the control tri-culture conditioned media that is not present in either the co-culture or the LPS-exposed tri-culture (**Figure 4.9g**, $p = 0.0010$ and $p = 0.0010$ respectively).

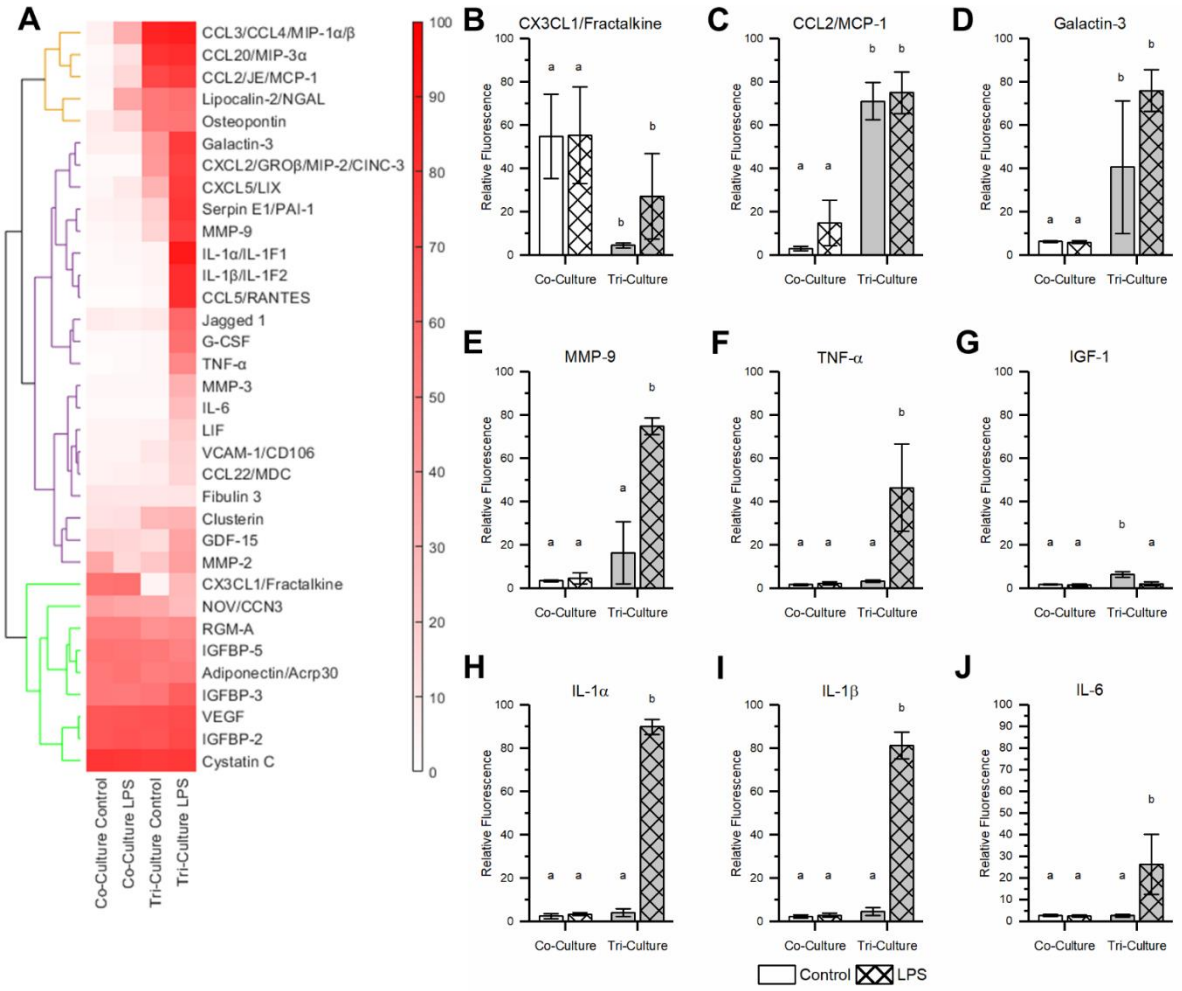

Figure 4.9: Comparing the proteomic profile of the conditioned media from co- and tri-cultures after 48 h incubation with 5 µg/mL LPS. (a) Heat map showing the relative cytokine concentrations scaled from 1 to 100. Proteins with a relative concentration of less than 10% of the maximum for all treatments were not included in the heat map, but can be found in (**Figure 4.10**). Hierarchical cluster analysis revealed three major groups of cytokines consisting of cytokines present in the conditioned media from all culture types (green), cytokines with increased expression in both control and LPS challenged tri-culture (orange) and cytokines with increased expression only in the LPS exposed tri-cultures (purple). (b-j) The relative concentrations of specific cytokines of interest. All graphs display mean ± SD (n = 3). The letters above the bars indicate statistically significant differences ($p < 0.05$, 2-way ANOVA with the Tukey test used to analyze the simple main effects if necessary).

Of the cytokines present in the tri-culture conditioned media that do not increase in expression in response to LPS, all have been shown to be secreted by microglia, and are also linked to neuroinflammatory states [210–214]. In the case of CCL2, CCL3, and CCL20, the concentration of these cytokines in the conditioned media are at the upper limit of the array under control conditions, thus, an increase in concentration in response to LPS may not have been

detected. However, there are a significant number of pro-inflammatory cytokines that are present in the conditioned media only after treatment with LPS, including many of the hallmark pro-inflammatory cytokines secreted by activated microglia. In particular, levels of TNF-α, IL-1α, IL-1β and IL-6 are significantly increased in the conditioned media of tri-cultures challenged with LPS (**Figure 4.9f-j**, $p = 0.0033$, $p = 0.0010$, $p = 0.0010$, $p = 0.013$ respectively). These four cytokines are consistently secreted by microglia in response to LPS in a variety of experimental conditions and are often used as biomarkers to indicate neuroinflammatory or neurodegenerative disorders [215].

In response to LPS, the tri-culture displays many classic hallmarks of neuroinflammation including increase in caspase 3/7 activity, astrocyte hypertrophy and the secretion of a number of pro-inflammatory cytokines. However, while we do see evidence of neurodegeneration and neurite loss in the LPS-exposed tri-cultures (**Figure 4.7**), the extent of the damage is significantly less severe than what is observed in vivo. This may be because microglia require co-activation with both LPS and INF-γ (secreted by circulating leukocytes) to produce the severe neurotoxic effects seen in vivo [216]. In the absence of leukocytes, no INF-γ is produced by the tri-culture in response to LPS (**Figure 4.10**) leading to a less severe response. We also observe an increase in microglia area in response to LPS, contradictory to the decrease in microglia area typically observed in vivo as the microglia transition from a highly ramified to amoeboid morphology [217]. However, the morphology of the microglia following exposure to LPS is consistent with previous in vitro experiments, with the microglia showing a distinct polarity and the formation of large lamellipodia [218–220], which accounts for the increase in area. We believe that this difference may not be due to a difference in microglia function but a result of the change from a 3D to 2D environment. In both instances, microglia become activated and prepare to migrate towards the site of injury. In the 3D environment, this involves the transformation from a ramified to amoeboid morphology to allow for the free movement through the parenchyma, while in the 2D environment this involves the extension of lamellipodia.

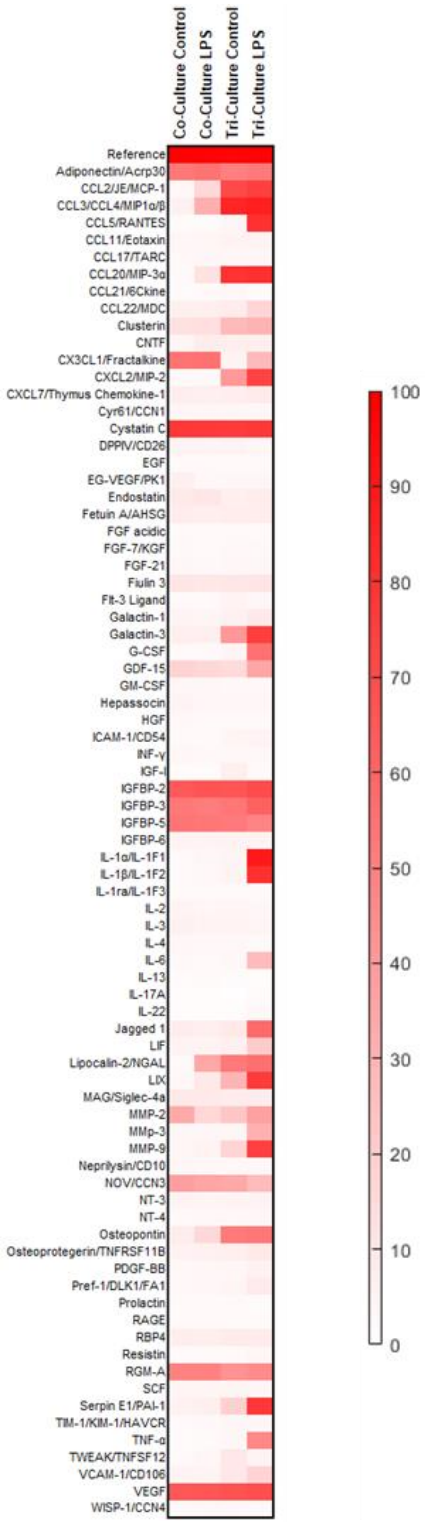

Figure 4.10: Complete proteomic profile from **Figure 4.9.**

4.3.2 Response to Mechanical Injury

In order to simulate a mechanical injury, we performed a scratch assay by drawing a pipette tip through co- and tri-cultures at DIV 7. Scratch assays are a common method used to model and measure cell migration [221], and have also been used to simulate mechanical injuries, such as the trauma induced by the insertion of therapeutic implants, on cultured neurons and glial cells [222–224]. At 48 h following the scratch injury, we see that a significant population of microglia migrated into the damaged area (**Figure 4.11a**). In the tri-culture injury model, while the microglia that migrate into the injury site do not have a statistically significant larger surface area than the microglia in the control condition (**Figure 4.11d**, $p = 0.078$), they do show a trend of having a slightly larger surface area than microglia in the non-injured tri-culture.

Glial scarring is another aspect of the inflammatory response to mechanical injury, and it consists of the formation of a glial sheath consisting mostly of reactive astrocytes that encapsulate the damaged tissue, isolating it from healthy tissue [182]. While the formation of a glial scar may take weeks to fully mature, reactive astrocytes begin to migrate towards injury site in less than 24 h [182]. We observed this in the tri-culture as astrocytes began to migrate into the scratched area; in contrast, in the co-culture, the percent area coverage by astrocytes in the scratched area was almost non-existent (**Figure 4.11c**, $p = 0.032$). Additionally, at 48 h following the scratch injury, caspase 3/7 activity was increased in both the tri- and co-cultures; however, the presence of microglia appeared to amplify a neurotoxic inflammatory response to the scratch, leading to a greater increase in caspase 3/7 activity in the tri-culture (**Figure 4.11b**, $p = .035$).

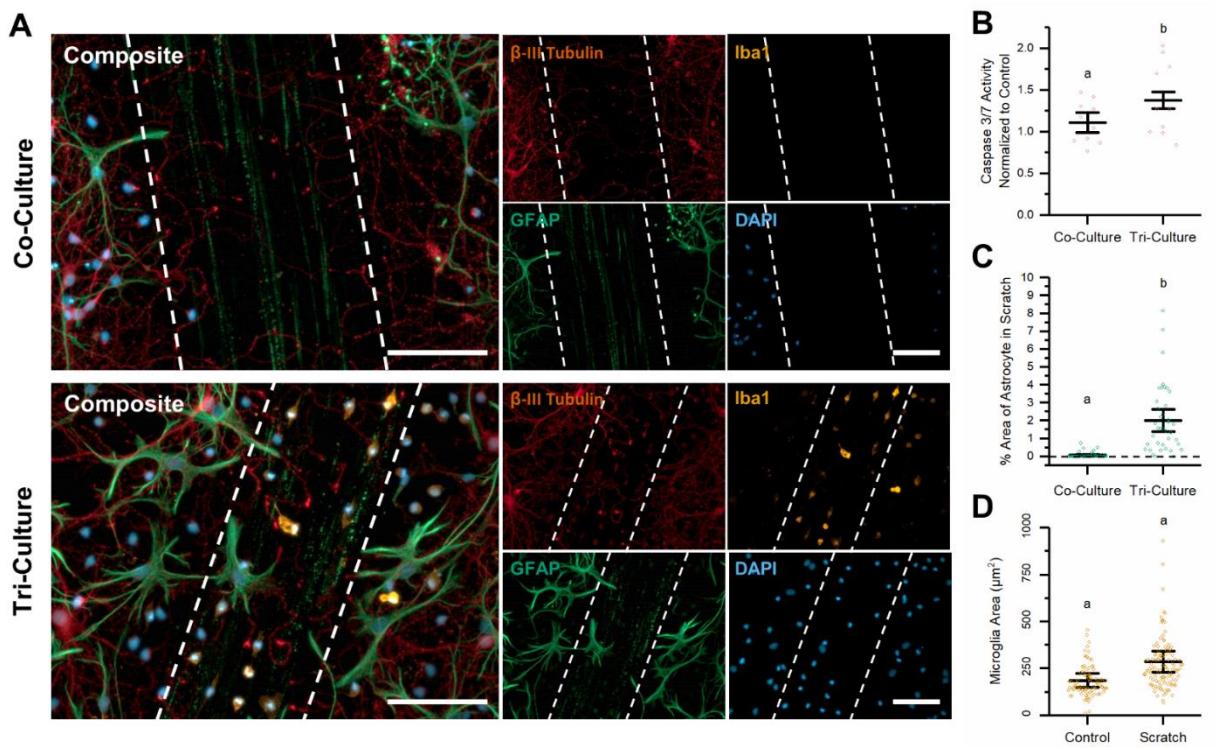

Figure 4.11: Comparing the effects from a simulated mechanical trauma (scratch) on co- and tri-cultures. (a) Representative fluorescence images of the co- and tri-cultures at 48 h following the simulated mechanical trauma. The dashed lines in the image highlight the area that was damaged by the scratch. The cultures were immunostained for the three cell types of interest: neurons – anti-βIII-tubulin (red), astrocytes – anti-GFAP (green), microglia – anti-Iba1 (orange) and the general nuclear stain DAPI (blue). Scale bar = 100 µM. (b) There was a significant increase in caspase 3/7 activity in the tri-culture as compared to the co-culture 48 h after the simulated mechanical trauma. (c) Comparing the percent area coverage of astrocytes in the scratched area between the co- and tri-cultures 48 h following the scratch. (d) Difference in the microglia area in the control and scratched tri-cultures. (b-d) All graphs display mean ± SD (n = 3), while the points indicate the values of the technical replicates. The letters above the bars indicate statistically significant differences ($p < 0.05$) as found by a t-test assuming unequal variances.

The neuroinflammatory response to the mechanical trauma caused by the implantation of therapeutic electrodes is a highly complex process, with both microglia and astrocytes responding to alarmins released by damaged cells to initiate an inflammatory cascade. Activated microglia display a wide range of phenotypes with overlapping gene expression profiles, and microglia polarization is no longer classified along a binary “M1 (neurotoxic) /M2 (neuroprotective)” scale based on the presence of specific markers [183,225]. However, following the implantation of therapeutic electrodes, it is generally hypothesized that microglia play a pro-inflammatory and neurotoxic role through the secretion of reactive oxygen species and pro-inflammatory cytokines,

such as TNF-α, IL-1β and IL-6, along with the recruitment of circulating immune cells [182,226]. The increased caspase 3/7 activity in the tri-culture 48 h following the scratch injury is in line with the hypothesized neurotoxic role of microglia during these types of injuries. Additionally, the tri-culture is capable of modeling the early stages of glial scarring, which is a major factor in the functional recovery following mechanical trauma [227,228] and a primary reason for the loss of functionality of therapeutic neural implants [229]. We observe a significantly higher coverage of astrocyte processes in the scratched area in the tri-culture as compared to the co-culture. In the tri-culture, we also find microglia in the scratched area, and these microglia appear to have a larger surface area, most likely due to the extension of lamellipodia as the microglia migrate into the scratched area. Microglia are thought to migrate into injury site and secrete factors that lead to increased astrocyte migration towards the injury [228]. One such factor is matrix metalloprotease 9 (MMP-9), which is secreted by microglia in response to neuroinflammatory factors [230] and has been implicated in the migration of astrocytes and initial formation of the glial scar [231]. We observed that MMP-9 is secreted in tri-cultures, but not in co-cultures in response to LPS (**Figure 4.9e**).

4.3.3 Response to Glutamate Induced Excitotoxicity

At DIV 7, tri- and co-cultures were exposed to varying concentrations of glutamate for 1 h to simulate an excitotoxic event. Following glutamate exposure, both tri- and co-cultures were maintained for 48 h in tri-culture medium to eliminate the additional factors in the tri-culture medium as potentially confounding factors in the response. In particular, TGF-β [232] and IL-34 [233] have been shown to be neuroprotective during excitotoxicity. We observed no microglia in the co-culture media at the end of the experiment, further confirming that the co-culture medium is incapable of supporting even an insignificant microglia population.

Our results suggest that microglia in the tri-culture play a significant neuroprotective role during excitotoxic events. We observed significant neuronal cell loss and astrocyte hypotrophy in

neuron-astrocyte co-cultures treated with 25 μM glutamate, which is significantly reduced in similarly treated tri-cultures (**Figure 4.12a**). As glutamate concentrations increased, astrocytes in the co-culture became progressively more reactive, evidenced by increasing hypertrophy and loss of processes. This resulted in a significant increase in astrocyte surface area following treatment with 10 μM and 25 μM glutamate, which is not observed in the tri-culture (**Figure 4.12b**, $p = 0.0022$ and $p = 0.0010$ respectively). In order to quantify neuronal cell viability, we compared the percent area of the field-of-view stained for β-III tubulin with a circularity less than 0.2. The circularity cut-off was used to eliminate cell debris from apoptotic/necrotic neurons, which still stained for β-III tubulin, but lacked long cellular processes, and therefore had high circularity values. Across all concentrations of glutamate that were tested (5, 10 and 25 μM), there was significantly more neuronal cell loss in the co-culture then in the tri-culture (**Figure 4.12c**, $p = 0.017$, $p = 0.0010$ and $p = 0.0017$ respectively). Furthermore, we observed that the neuron percent area significantly decreased in the co-cultures upon exposure to increasing concentrations of glutamate. In contrast, significant decreases in the neuron percent area were observed in tri-culture only at the highest concentration of glutamate. Surprisingly, unlike exposure to LPS or mechanical trauma, the exposure of the tri-cultures to glutamate did not appear to change the morphology of the microglia (**Figure 4.12d**). Specifically, the average microglia area did not change following treatment with different concentrations of glutamate ($p = 0.81$).

We also confirmed that the tri-culture was electrophysiologically active via calcium imaging. For both the co- and tri-cultures we observed spontaneous calcium influxes at DIV 7. Additionally, we compared the response of both culture types to varying concentrations of glutamate (**Figure 4.12e**). Analysis of the main effects did not identify a significant difference in the response of the tri-culture and co-cultures to different concentrations of glutamate ($p = 0.78$). Additionally, for both culture types, we observed a significant change in fluorescence intensity across a wide range of glutamate concentrations ($p = 1.73 \times 10^{-15}$) indicating that the

neuroprotective effect was a result of the presence of microglia in the tri-culture and was not due to a depressed neuronal response to glutamate.

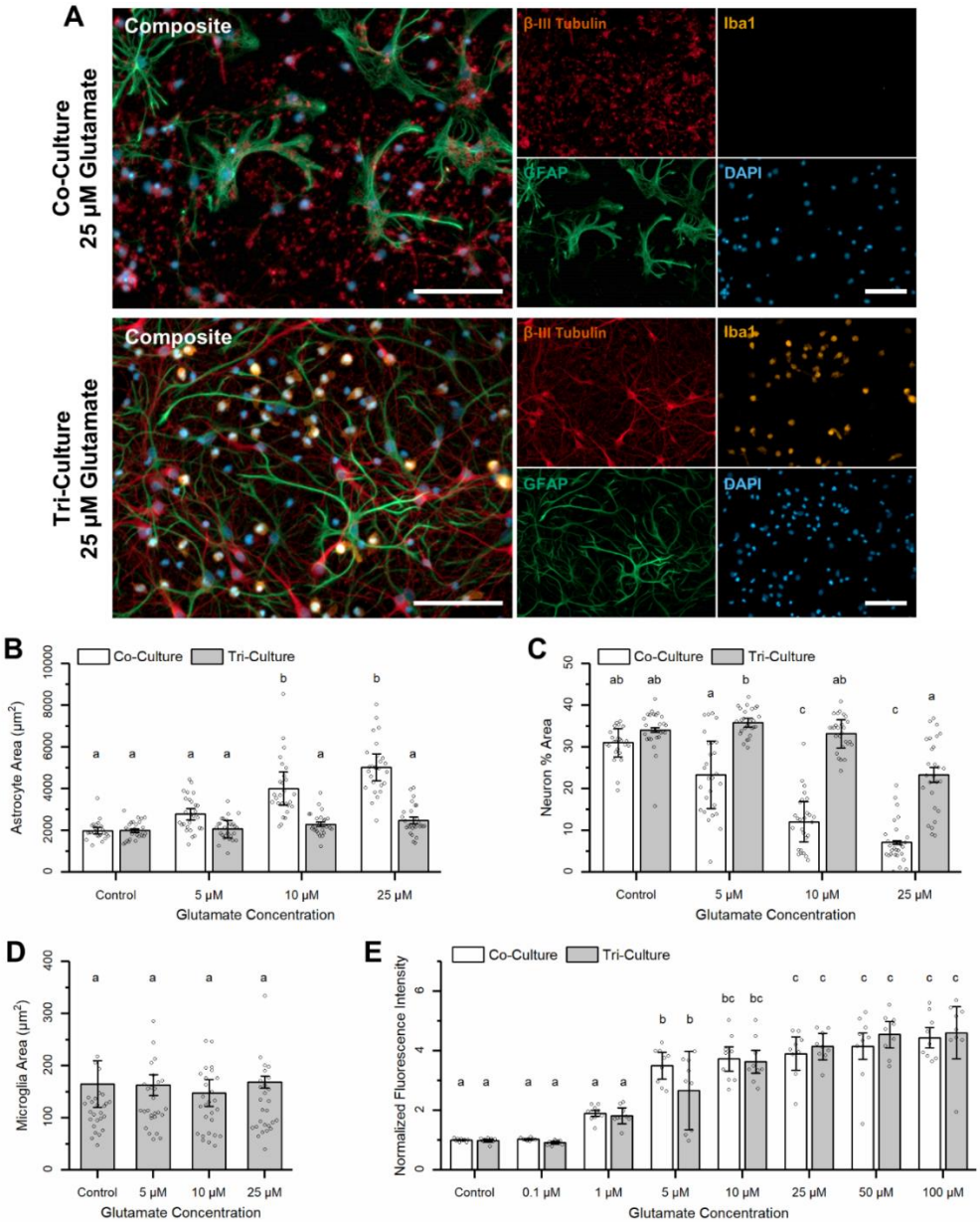

Figure 4.12: (a) Representative fluorescence images of the co- and tri-cultures at 48 h following exposure to 25 µM glutamate for 1 h. The cultures were immunostained for the three cell types of interest: neurons – anti-βIII-tubulin (red), astrocytes – anti-GFAP (green), microglia – anti-Iba1 (orange) and the general nuclear stain DAPI (blue). Scale bar = 100 µM. (b) Comparing the average astrocyte area between the co- and tri-cultures following challenges with different concentrations of glutamate. A full analysis of the simple main effects can be found in supplementary data table 1. (c) The neuron percent area coverage, with a 0.2 circularity cut-off to eliminate cell debris, following excitotoxic challenge. (d) The average microglia surface area did not change following treatment with different concentrations of glutamate. (e) Calcium imaging results showing the change in fluorescence intensity following treatment with different concentrations of glutamate. All graphs display mean ± SD (n = 3), while the points indicate the values of the technical replicates. The letters above the bars indicate statistically significant differences ($p < 0.05$).

The tri-culture model is especially useful in modeling the glial response to glutamate induced excitotoxic events. Both astrocytes and microglia are thought to play a neuroprotective role during excitotoxic events through mechanisms that are difficult to capture in other models. Astrocytes are responsible for maintaining glutamate homeostasis in the CNS through the uptake of extracellular glutamate by membrane transporters, and the failure of these transporters are linked to excitotoxic pathologies [99,234]. Furthermore, blocking these glutamate transporters with DL-Threo-β-Benzyloxyaspartic acid (TBOA) leads to excitotoxicity induced neural death in otherwise healthy hippocampal slices [235] and increased neural death in neuron-astrocyte co-cultures exposed to glutamate [143]. While the exact mechanisms responsible for the neuroprotective response of microglia to excitotoxicity are not fully understood, it has been shown that the microglia migrate towards hyperactive neurons in response to ATP and glutamate released by these neurons [101–103]. These microglia have been shown release small quantities of TNF-α that provide protection to neurons from NMDA-induced excitotoxicity [236] and directly contact damaged axons to repolarize and rescue hyperactive neurons [102]. We observed a significant decrease in the number of neurons lost in the tri-culture as compared to the co-culture following exposure to glutamate (**Figure 4.12c**), indicating that the tri-culture is able to capture the complex interactions between the microglia and neurons that potentiate this neuroprotective response. Additionally, we observed that the average microglia area did not change in response to exposure to different concentrations of glutamate, which is in line with previous research suggesting morphologically resting/ramified microglia can serve a neuroprotective role during excitotoxic events [103].

4.4 Microglia Improve the Overall Health of Primary Cortical Cultures

Our previous experiments demonstrated that the tri-culture is better able to mimic the *in vivo* neuroinflammatory response than standard neuron-astrocyte co-cultures, and that the

continuous presence of microglia did not negatively impact the overall health of the culture. Here we show that the presence of microglia in the tri-culture may actually improve the overall health of the culture, and this improvement can be attributed to the crosstalk between neurons and microglia in the culture.

In order to verify that it was the presence of microglia themselves, and not the additional factors added to the tri-culture medium that was responsible for the improvement in culture health, we compared the total cell death of the co-culture (**Figure 4.13b**) to both the tri-culture (**Figure 4.13a**) and cultures maintained in the co-culture medium supplemented with TGF-β, cholesterol, or both factors at concentrations used in the tri-culture medium (**Figure 4.13c**). We did not compare conditions with IL-34 as we have shown earlier that IL-34 alone is sufficient and necessary for microglia survival *in vitro*, and the present goal was to determine if the additional factors in the tri-culture media (TGF-β and cholesterol) in the absence of microglia had an effect on culture health. We saw a significant reduction in cell death in the tri-culture (1.63 ± 0.32 % dead cells) as compared to the co-culture (22.33 ± 0.44 % dead cells, $p < 1.0 \times 10^{-7}$). Additionally, there was no change in cell death when TGF-β (23.06 ± 0.86 % dead cells), cholesterol (20.89 ± 1.10 % dead cells), or both factors (24.46 ± 0.67 % dead cells) were added to the co-culture medium, which all showed significant increase in cell death as compared to the tri-culture ($p < 1.0 \times 10^{-7}$ for all conditions vs tri-culture). In addition, we observe a significant decrease in caspase 3/7 activity in the tri-culture as compared to the co-culture (**Figure 4.14**, $p = 0.0031$). These results clearly indicate that the overall health of the culture is improved in the tri-culture, and it is a function of the presence of microglia and not due to the additional factors added to the tri-culture medium.

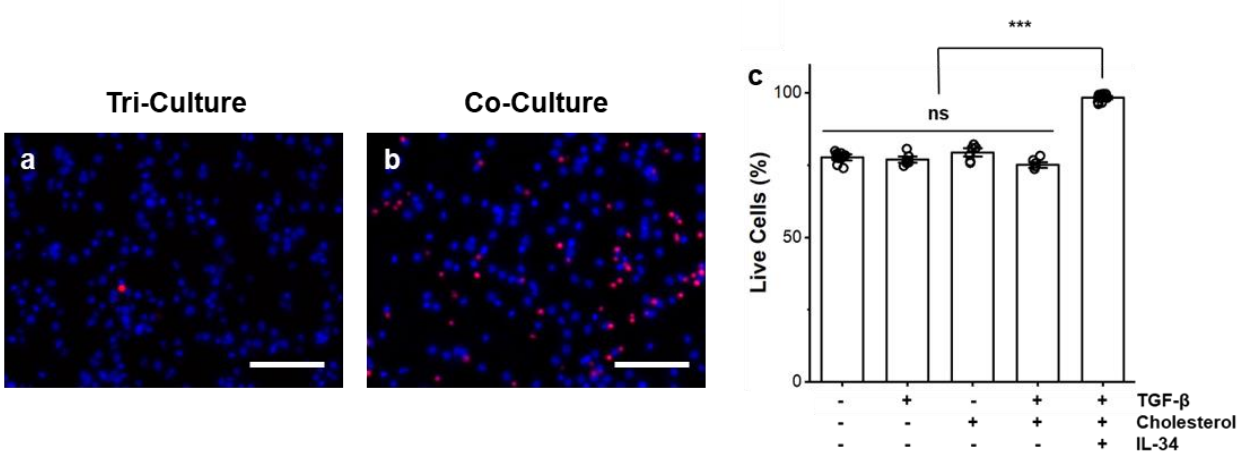

Figure 4.13: Representative images of (a) tri-cultures and (b) co-cultures stained with Hoechst 33342 (Live, blue) and propidium iodide (Dead, red). (c) Comparison of the influence of TGF-β and increased cholesterol concentration on cell death in the absence of microglia as compared to the co-culture and tri-culture (containing all three additional factors). Data presented as mean ± SEM (n = 4-8 wells from two independent dissections) with individual data points plotted, ***$p < 0.001$ (as determined by *post hoc* Tukey's test). Scale bar = 100 µm.

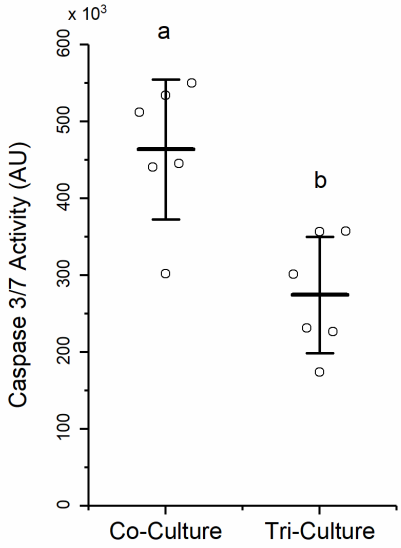

Figure 4.14: The tri-culture shows reduced caspase 3/7 activity at DIV 9 (n = 6). The letters above the bars indicate statistically distinct groups ($p < 0.05$), while the points indicate the values of the technical replicates.

Crosstalk between different cell types in the CNS is integral in maintaining homeostasis, and we observe evidence of that crosstalk in the tri-culture. The tri-culture showed low concentrations of CX3CL1 in the conditioned media, which was elevated in both the co-culture

conditions and the LPS exposed tri-culture (**Figure 4.9b**). CX3CL1 is expressed primarily by neurons in the CNS, and is found in both a membrane-bound and soluble form. Membrane bound CX3CL1 is important for microglia regulation, and thought to hold the microglia in resting state, while soluble CX3CL1 acts as a powerful chemoattractant for microglia and is also secreted by neurons and glial cells during neuroinflammatory conditions [187,237,238]. As microglia are an integral part of CNS homeostasis, the high concentration of CX3CL1 in the co-culture might be a compensatory response to the lack of microglia as co-cultures attempt to recruit them. The lack of CX3CL1 in the conditioned media from the control tri-cultures suggests that the majority of CX3CL1 in tri-cultures is membrane-bound and is interacting with the microglia in the tri-culture to hold them in a non-activated state. In response, the microglia secrete the neurotrophic factor, IGF-1 [239,240], which was only found in the control tri-culture conditioned media (**Figure 4.9g**). IGF-1 has been indicated as a trophic factor produced by microglia in postnatal (P3-7) mice that significantly increases the survival of layer V cortical neurons [239]. These experiments highlight the importance of cellular crosstalk between neurons, astrocytes, and microglia not only in neuroinflammatory conditions, but also in homeostatic conditions. Additionally, we suggest that crosstalk between neurons and microglia may play a significant role in the observed increase in overall culture health of the tri-culture.

4.5 Conclusions

The tri-culture model presents multiple advantages over other methods used to study neuroinflammation *in vitro*. The most obvious benefit is the presence of neurons, astrocytes and microglia in the same cell culture from the same tissue, which will allow researchers to study the complex interplay between these cells that leads to different responses to inflammatory stimuli. Additionally, the use of a single culture (as opposed to using conditioned media to mimic the influence of cell types absent in the culture) allows for the observation of cell-cell interactions and other mechanisms with spatiotemporal nuances that may be lost when using models involving

multiple different types of cultures. Another major benefit of the tri-culture model is its relative simplicity. The only modification needed to establish and maintain the tri-culture model is the use of a specialized tri-culture medium. Compared to other models that involve multiple cultures or the addition of cells at specific time points during culture, the simplicity of this tri-culture model lends itself to high-throughput experiments, and, therefore, it may be an effective tool in the early screening of potential therapeutic molecules. Importantly, this tri-culture model is also amenable to experiments involving more complex culture setups, such as microfluidic and organ-on-a-chip devices [78]. Ultimately, we believe that the neuron, astrocyte and microglia tri-culture described in this chapter can be a useful tool to study neuroinflammation *in vitro* with improved accuracy in predicting *in vivo* neuroinflammatory phenomena.

Chapter 5: Electrophysiological Characterization of the Tri-Culture

In vitro models of the central nervous system (CNS) are powerful tools that allow researchers to conduct highly directed cellular level experiments to study the cellular and molecular pathways underlying many neurological disorders. However, there are inherent limitations within these models that limit their physiological relevance, most notably researchers much ensure that the appropriate cell types are included within their culture model to effectively recapitulate the *in vivo* disease state. This is especially true for CNS models as crosstalk between neurons and glia play significant roles in both pathological conditions [2,14,182,241,242] and maintaining homeostasis [183,243]. Microelectrode array (MEA) technology is a popular method to study *in vitro* neural networks, as it provides a non-invasive method to simultaneously record electrophysiological activity from multiple sites [244,245]. This allows researchers to conduct longitudinal studies to study neural network formation [246,247] and disruption caused by neurotoxic compounds [248–250] and proteins associated with neurodegeneration [251–253]. Nevertheless, the physiological relevance of these studies is still largely dependent on the cell types present within the culture and may not fully recapitulate the *in vivo* response [254]. Therefore, there has been significant effort in developing new CNS culture models and characterizing the spatial and temporal aspects of the electrophysiological recordings both during spontaneous activity and in response to stimuli. This includes studying the neural activity from cultures of neurons from different regions of the brain (cortex [190,244,255] vs hippocampus [256,257]), neurons cultured with supporting glial cells such as astrocytes [129] and oligodendrocytes [132], and human primary [258] or stem cell derived [259,260] neurons. Additionally, electrophysiological recording from complex *in vitro* models such as 3D [261,262] and organ-on-a-chip [263,264] models have been studied to further improve the physiological relevance of *in vitro* neural models.

In the previous chapter we described a neuron, astrocyte, and microglia tri-culture to study neuroinflammation *in vitro* [146], which is maintained by culturing primary cortical neurons from neonatal rats in a serum-free culture medium specifically designed to support all three cell types. We have demonstrated that the tri-culture model better mimics the neuroinflammatory response to a number of stimuli including lipopolysaccharide (LPS) exposure, mechanical trauma, glutamate induced excitotoxicity as compared to neuron-astrocyte co-cultures. In this chapter we further explore the capabilities of the tri-culture by characterizing the neural functionality of the system. We compared the extracellular recordings taken over 21 days *in vitro* (DIV) between the tri- and co-cultures to determine the effect of microglia on network formation and neuron function. We demonstrate that many features of neural activity remain similar between the tri- and co-cultures (% active channels, spike frequency, and burst characteristics), suggesting that the presence of microglia do not adversely affect the neuronal function. The tri-culture shows increased synchrony at early timepoints compared to the co-culture, which may indicate faster maturation of network activity in the tri-culture configuration. Additionally, analysis of the action potential waveform characteristics reveals that the tri-cultures contain an increased excitatory/inhibitory (E/I) neuron ratio that more closely resembles the ratio found *in vivo*, and this observation is supported by synaptic staining. We also incorporated the tri-culture into compartmentalized organ-on-a-chip devices that separate the neural axons and somas using microchannels [90,264], and recorded robust neural activity from these platforms. Finally, we demonstrate the ability to observe changes in neural activity in response to known inflammatory stimuli (LPS exposure).

5.1 MEA Design and Fabrication

Custom MEAs were designed and fabricated following the protocols described in the methodology chapter (**Chapter 2.3.1-2.3.3**). Standard (well) MEAs were designed with a 4 x 8 array of electrodes (32 total) each with a diameter (Ø) of 20 µm and an interelectrode pitch of 130

μm (**Figure 5.1**). We also fabricated microfluidic platforms with integrated MEAs following the designs described for the 10 μm wide microchannel platforms in **Chapter 3.5** (**Figure 5.2**).

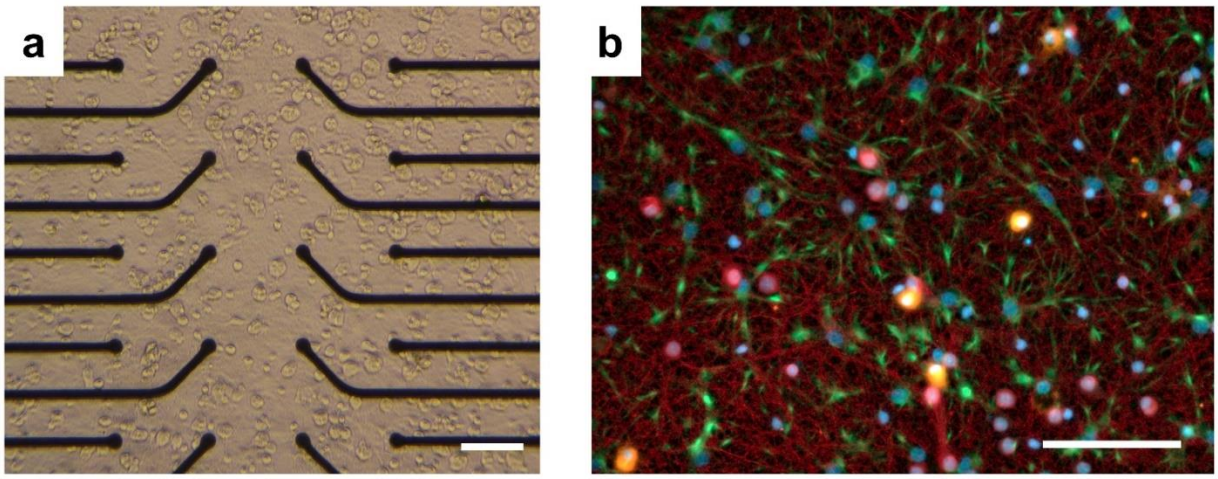

Figure 5.1: (a) Bright-field and (b) epifluorescence images of the tri-culture at DIV 21 on the well MEA. The cultures were immunostained for the three cell types of interest: neurons—anti-βIII-tubulin (red), astrocytes—anti-GFAP (green), microglia—anti-Iba1 (orange), and the general nuclear stain DAPI (blue). Scale bar = 100 μM.

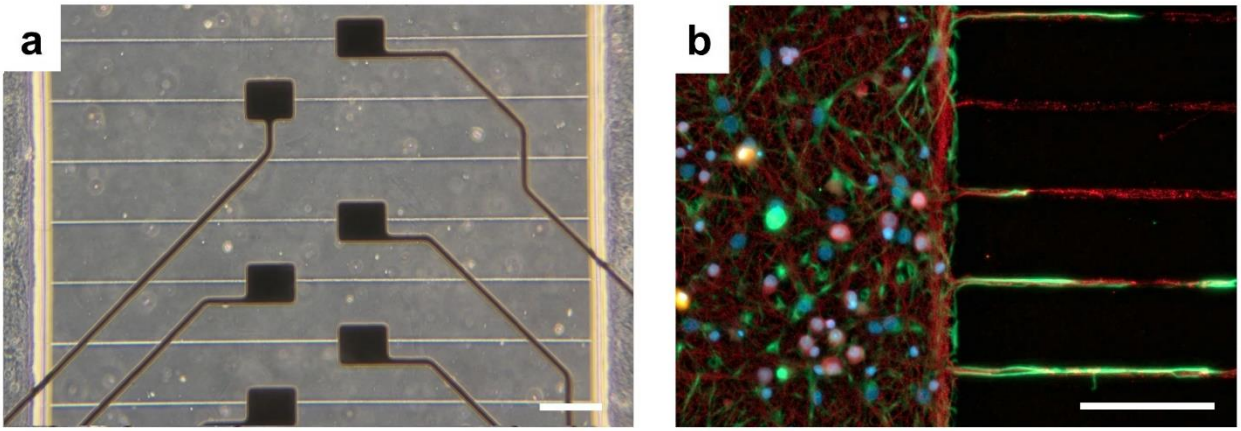

Figure 5.2: (a) Bright-field and (b) fluorescence images of the tri-culture at DIV 21 in the platform MEA with microfluidic encapsulation. The cultures were immunostained for the three cell types of interest: neurons—anti-βIII-tubulin (red), astrocytes—anti-GFAP (green), microglia—anti-Iba1 (orange), and the general nuclear stain DAPI (blue). Scale bar = 100 μm.

5.2 Extracellular Recordings

We recorded spontaneous neural activity from DIV 7 to DIV 21 from both tri- and co-cultures to determine if there was any discernible difference in culture maturation or network formation (**Figure 5.3a,b**). As expected, we observed a significant increase in the percentage of active channels in both the tri- and co-culture from DIV 7 to DIV 21 (**Figure 5.3c**). However, we did not find a significant difference in the percentage of active channels between the tri- and co-cultures at any timepoint. We saw a similar trend in spike frequency for both the tri- and co-cultures (**Figure 5.3d**), with no differences between the tri- and co-cultures. However, in this case the increase in spike frequency was more subtle, and therefore we did not observe a significant increase between DIV 7 and later timepoints with the exception of the tri-culture at DIV 21 (p = 0.0076). We also compared other electrophysiological features used to determine culture maturation and stability over time (**Figure 5.4**), such as the percent of spikes in bursts, burst duration, and ISI within bursts. Both the tri- and co-cultures showed a significant increase in the percentage of spikes in bursts indicating that the cultures were maturing as expected; however, there was no difference between the two cultures (**Figure 5.4a**). Similarly, we saw no difference between the average burst duration and within burst ISI between the two culture types (**Figure 5.4b,c**), and for both the co- and tri-culture these values remained stable over time, suggesting no degradation in neural health over the 21 DIV window. Finally, we compared network formation in the tri- and co-cultures by assessing the synchrony of the spike trains from the active electrodes in each culture using the SPIKE-distance method [130,131]. It is important to note that the SPIKE distance method is a measurement of spike-train dissimilarity given on a scale of 0-1. Therefore, in order to measure the synchrony of the culture, we subtracted the SPIKE distance value from 1, with values closer to 1 indicating increased synchrony in the culture. We observed a significant increase in synchrony over time in both the co- and tri-cultures indicating robust network formation (**Figure 5.3e**). While there was no significant difference in the synchrony between the tri- and co-

culture, we saw evidence of increased network formation in the tri-culture at earlier timepoints, with a trend towards increased synchrony in the tri-culture at DIV 10 (p = 0.11).

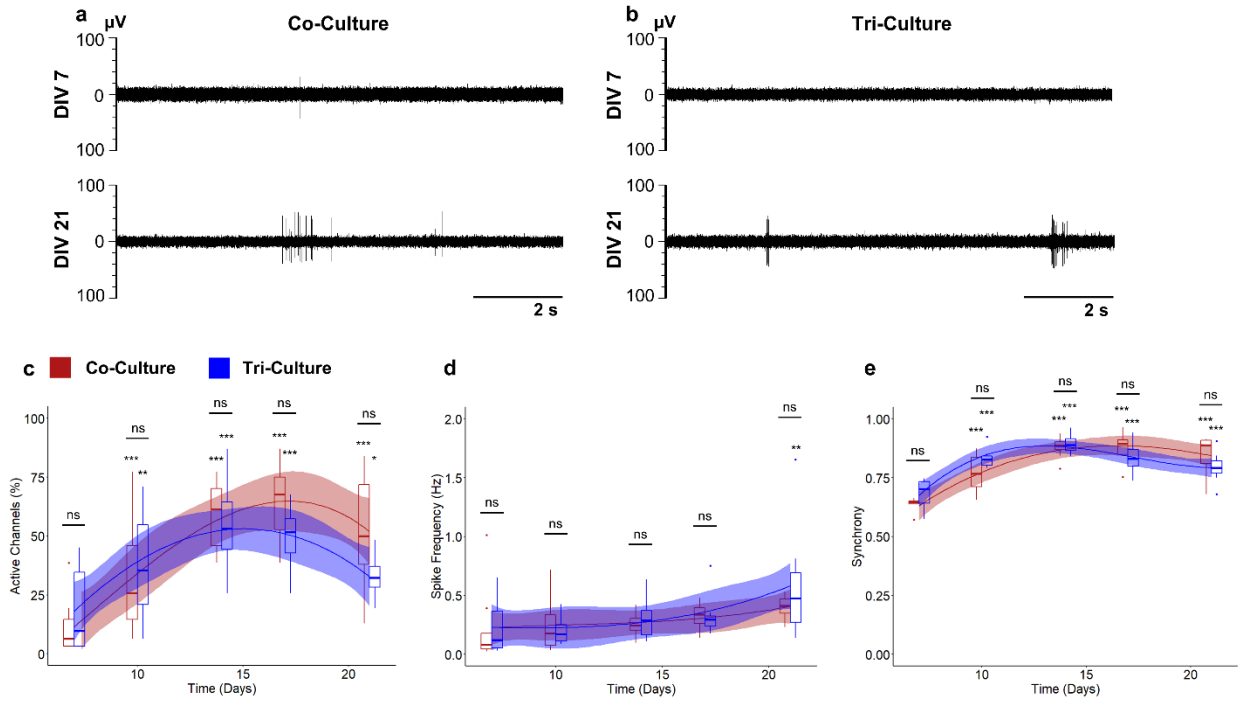

Figure 5.3: Representative extracellular recordings taken at DIV 7 and DIV 21 from (a) co-cultures and (b) tri-cultures. Comparisons of the (c) percent active channels, (d) spike frequency, and (e) synchrony between co-cultures (red) and tri-cultures (blue). The solid lines show the fitted linear mixed effects model (treating individual cultures as a random effect) with a b-spline basis. The shaded regions are the 95% confidence interval. An asterisk above an individual box indicates a significant difference of the estimated marginal means of the fitted curves between that timepoint and DIV 7 of the same culture type, while the bars indicate the significance between the co- and tri-culture at that timepoint (n = 8, from three independent dissections). *p < 0.05, **p < 0.01, ***p < 0.001, ns indicates no significant difference.

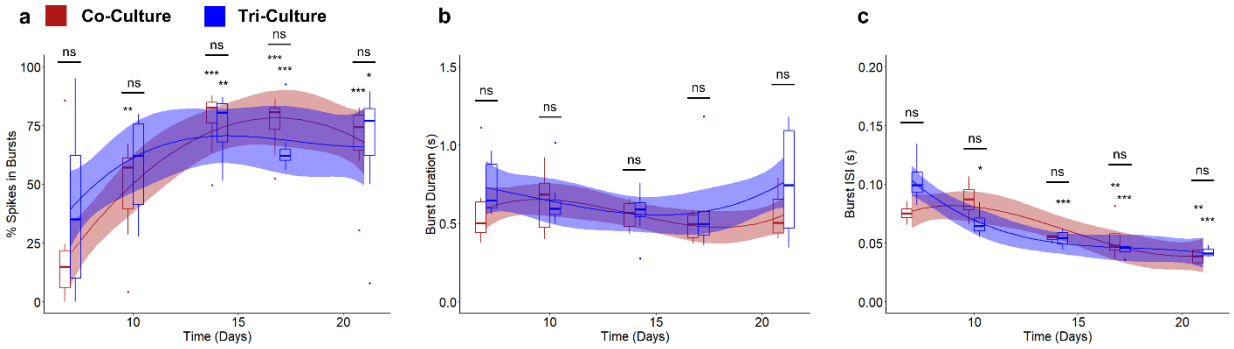

Figure 5.4: Comparisons of the (a) percent spikes in bursts, (d) burst duration, and (e) ISI within bursts between co-cultures (red) and tri-cultures (blue). The solid lines show the fitted linear mixed effects model (treating individual cultures as a random effect) with a b-spline basis. The shaded regions are the 95% confidence interval. An asterisk above an individual box indicates a significant difference of the estimated marginal means of the fitted curves between that timepoint and DIV 7 of the same culture type, while the bars indicate the significance between the co- and tri-culture at that timepoint (n = 8, from three independent dissections). *$p < 0.05$, **$p < 0.01$, ***$p < 0.001$, ns indicates no significant difference.

As expected, we observed many of the common indicators of neural network formation and maturation including an increase in the number of active channels, increased spike frequency, and increased synchrony in both the tri- and co-culture over time (**Figure 5.3**), indicating that the microglia within the tri-culture did not disrupt culture maturation or health. Similarly, we observed no significant differences between the tri- and co-cultures when comparing any of the aforementioned indicators of culture maturation (**Figure 5.3**) or other electrophysiological features (**Figure 5.4**) at any timepoint, which was somewhat surprising considering the significant role microglia are known to play in synaptic plasticity. However, we did see a trend towards increased neuronal network maturation in the tri-culture, as the synchrony of the tri-culture was increased at earlier timepoints (DIV 10, $p = 0.11$), but this increase was not statistically significant (**Figure 5.3e**). Additionally, we saw some evidence that the tri-culture had an increase in spike frequency at DIV 21 as only the tri-culture showed a significant increase in spike frequency between DIV 7 and DIV 21 ($p = 0.0076$ vs $p = 0.51$ for the co-culture), but once again there was no significant difference in spike frequency between the tri- and co-cultures at DIV 21 (**Figure 5.3d**).

5.3: Incorporation into Microfluidic Platforms

In order to further investigate some of the non-statistically significant, but important trends we previously observed, we compared the spontaneous neural activity from tri- and co-cultures maintained in microfluidic devices, as these devices showed improved electrophysiological recording fidelity from co-cultures in **Chapter 3.5**. We once again demonstrate that both the tri- and co-cultures show significant increase in the percentage of active channels over time with no significant difference between the cultures (**Figure 5.5a**). However, using the microfluidic device, we found that both the tri- and co-cultures show significant increases in spike frequency from axons within the microchannels over time, and we observed significantly higher spike frequencies in the tri-culture at DIV 17 and 21 (p = 0.016 and p = 0.0017 respectively; **Figure 5.5b**). Additionally, we observed no differences among other electrophysiological features (percent spikes in bursts, burst duration, and within burst ISI; **Figure 5.6**) and spike train synchrony (**Figure 5.5c**) between the tri- and co-cultures, once again suggesting minimal differences in culture maturation and stability between the tri- and co-cultures, with the exception of increased spike frequency in the tri-culture.

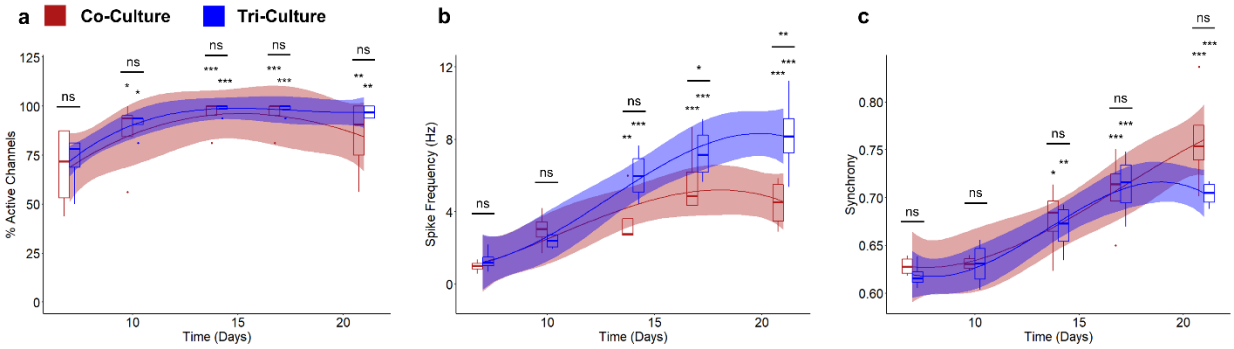

Figure 5.5: Comparisons of the (a) percent active channels, (b) spike frequency, and (c) synchrony between co-cultures (red) and tri-cultures (blue) cultured in a two-chambered microfluidic device. The solid lines show the fitted linear mixed effects model (treating individual cultures as a random effect) with a b-spline basis. The shaded regions are the 95% confidence interval. An asterisk above an individual box indicates a significant difference of the estimated marginal means of the fitted curves between that timepoint and DIV 7 of the same culture type, while the bars indicate the significance between the co- and tri-culture at that timepoint (n = 5, from two independent dissections). *p < 0.05, **p < 0.01, ***p < 0.001, ns indicates no significant difference.

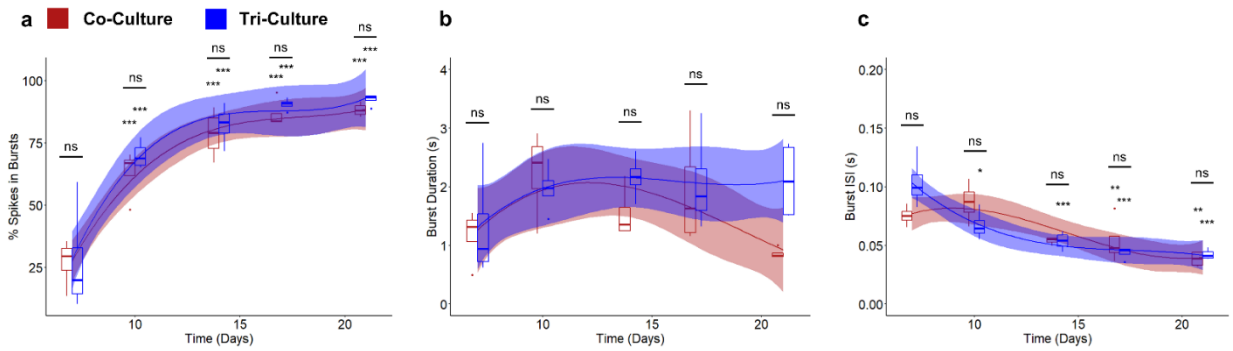

Figure 5.6: Comparisons of the (a) percent spikes in bursts, (d) burst duration, and (e) ISI within bursts between co-cultures (red) and tri-cultures (blue) cultured in a two chambered microfluidic device. The solid lines show the fitted linear mixed effects model (treating individual cultures as a random effect) with a b-spline basis. The shaded regions are the 95% confidence interval. An asterisk above an individual box indicates a significant difference of the estimated marginal means of the fitted curves between that timepoint and DIV 7 of the same culture type, while the bars indicate the significance between the co- and tri-culture at that timepoint (n = 5, from two independent dissections). *$p < 0.05$, **$p < 0.01$, ***$p < 0.001$, ns indicates no significant difference.

This enhancement in recording fidelity allowed us to not only observe the expected increase in spike frequency in both the tri- and co-cultures indicative of culture maturation [265,266], but also revealed a significant increase in the spike frequency of the tri-culture at later timepoints (**Figure 5.5b**), which is in line with the observations from the recordings taken from standard MEAs (**Figure 5.3d**). Furthermore, incorporation of the tri-culture into the microfluidic device was straightforward as it only required the use of a specialized culture medium, highlighting the tri-culture's amenability to complex culture setups such as microfluidic devices and organ-on-a-chip platforms.

5.4 Synaptic Density

In order to determine the cause of increased spike frequency in the tri-culture at later timepoints, we compared synapse formation between the tri- and co-cultures over 21 DIV (**Figure 5.7a**), as microglia are known to play a significant role in synapse formation and elimination during postnatal development [267–269]. A two-way ANOVA revealed that there was no significant interaction between culture type and time in culture on the density of post-synaptic marker PSD-95 (**Figure 5.7b**) and excitatory pre-synaptic marker VGlut1 (**Figure 5.7c**) puncta (p = 0.46 and

p = 0.36 respectively). Simple main effects analysis revealed no significant difference between the density of PSD-95 and VGlut1 puncta based on culture (p = 0.26 and p = 0.15 respectively) but did reveal a significant difference based on time in culture (p = 0.0032 and p = 00.15 respectively). We also compared the number of co-localized puncta as a measurement of mature excitatory synapses [270,271] (**Figure 5.7d**). Once again, a two-way ANOVA revealed no-significant interaction between culture type and time in culture on the number of mature excitatory synapses (p = 0.22), and simple main effects analysis revealed a significant difference increase in mature excitatory synapses based on time in culture (p = 0.0066) but not based on culture type (p = 0.21).

Interestingly, the 2-way ANOVA did not establish an interaction between time in culture and culture type (tri- vs co-culture) when comparing the density of pre-synaptic, excitatory post-synaptic, or co-localized puncta (**Figure 5.7b-d**), and main effects analysis did not reveal a significant difference between the tri- and co-cultures for any of the conditions. This was an unexpected finding as previous *in vitro* studies have shown that IL-10 secreted from microglia increase spine density and excitatory synapses [272]. However, in that study the microglia and neurons were physically separated, with the microglia grown on a porous insert that was added to the isolated neuron culture at a later timepoint, preventing their physical contact, and it has been shown that direct microglia contact with synapses can lead to synaptic elimination [273,274]. While we did not observe a significant difference between the tri- and co-culture, we do observe a trend towards increased excitatory post-synaptic puncta at DIV 21 in the tri-culture (**Figure 5.7c**). Additionally, we observe that the tri-culture continues to show increased co-localized puncta over the 21 DIV, while the number of co-localized puncta appears to plateau at DIV 14 (**Figure 5.7d**). The fact that we only observed a subtle change in synaptic density and excitatory pre-synaptic puncta may be due to the fact that the microglia and neurons are in close approximation in the tri-culture leading to a balance of increased synaptogenesis due to IL-10 secretion by microglia and synaptic pruning due to the direct contact of microglia and synapses.

Furthermore, astrocytes have also been shown to play a significant role in synaptic plasticity [275], and since both the tri- and co-cultures contain astrocytes, the influence of the microglia may be less apparent.

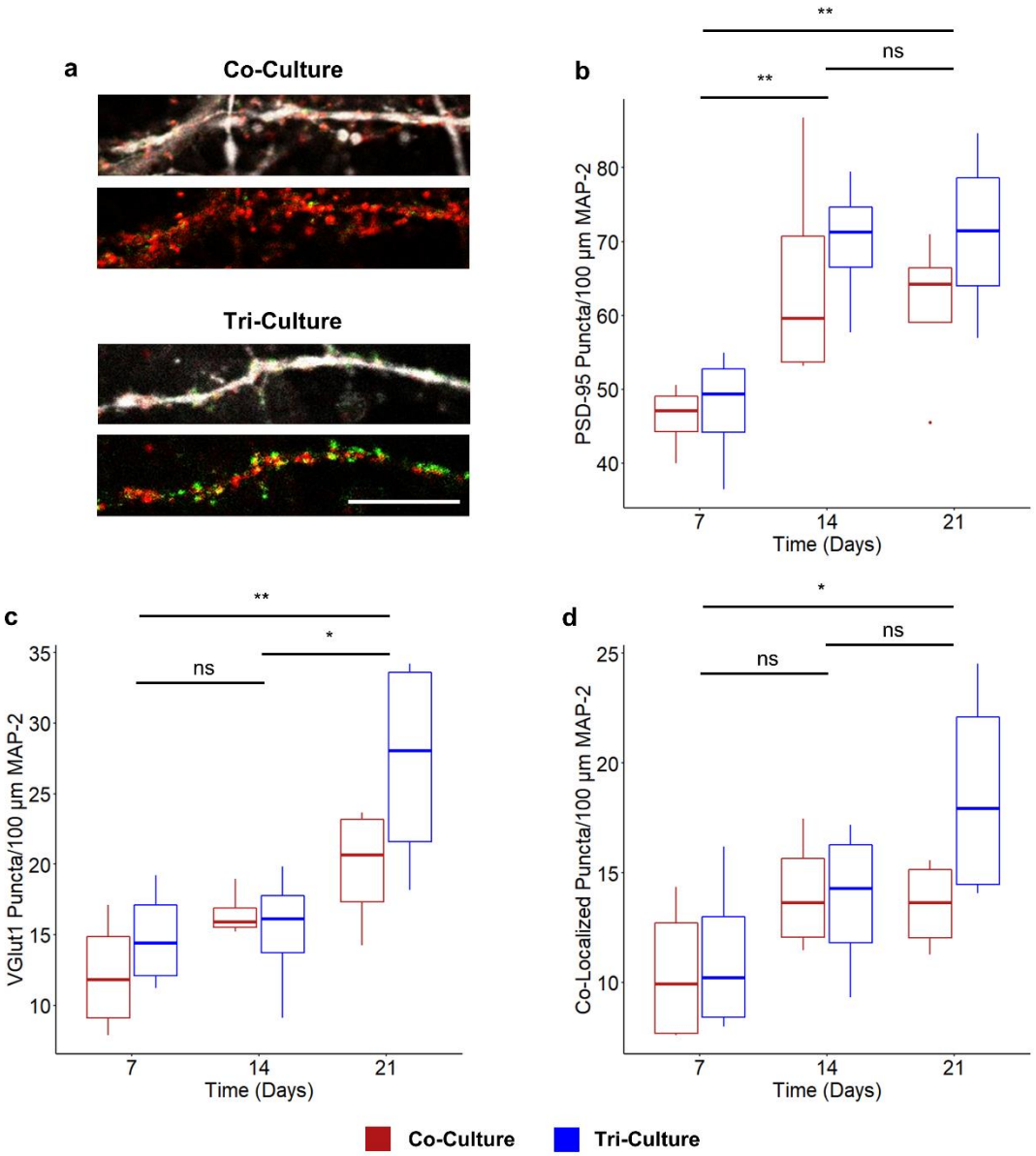

Figure 5.7: (a) Representative fluorescence images of co- and tri-cultures at DIV 21. The cultures are stained for the excitatory pre-synaptic marker VGlut1 (Green), post-synaptic marker PSD-95 (red). The above image also shows the co-localization with MAP-2 (white). (scale bar = 10 µm). Comparison of the density of (b) PSD-95 puncta, (c) VGlut1 puncta, and (d) co-localized puncta. In all three cases a two-way ANOVA found no interaction between culture type and time in culture, and therefore the asterisk indicates the significance of the main effect between timepoints (n = 4, from two independent dissections). *p < 0.05, **p < 0.01, ns indicates no significant difference.

5.5 Excitatory vs. Inhibitory Neurons

While we did not observe any statistically-significant differences in synapse formation between the tri- and co-culture, we do see evidence of increased excitatory synapse formation at DIV 21 and a significant increase in spike frequency in the tri-culture. As the cortex contains both excitatory and inhibitory neurons, we were interested in seeing if the aforementioned differences could be attributed to changes in the ratio of excitatory to inhibitory neurons (E/I ratio). We found a bimodal distribution of the peak-trough duration of the averaged spike waveforms from 249 units recorded from both tri- and co-cultures (**Figure 5.8**). The first peak is centered at a peak-trough duration of ~220 µs, which correlates well with narrow-spiking inhibitory interneurons, while the second peak is centered at a peak-trough duration of ~380 µs, which correlated with broad-spiking excitatory neurons [276–278]. Additionally, the average spike waveforms from these two groups correlated well with previously described narrow-spiking and broad-spiking waveforms (**Figure 5.9a**) [277,278].

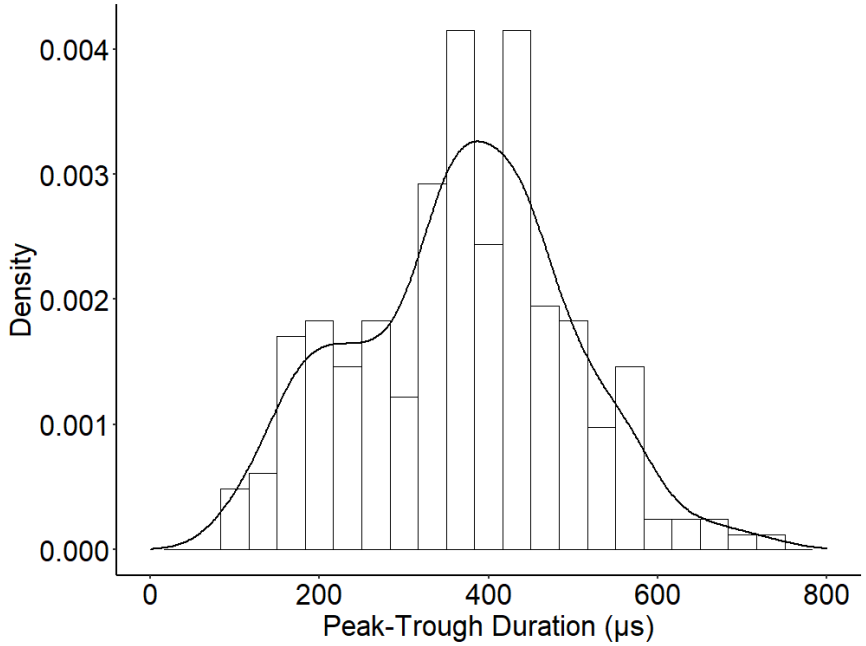

Figure 5.8: Density histogram of the peak-trough durations of the averaged spike waveforms from 249 units recorded from both co- and tri-cultures. We observe one peak at ~220 µs and the second at ~380 µs.

Using the density histogram as a guide, we classified units as either inhibitory (peak-trough duration < 280 μs) or excitatory (peak-trough duration > 280 μs). We observed a significant increase in E/I ratio of recorded units in the tri-culture (86.91 ± 3.27% excitatory neurons) as compared to the co-culture (68.83 ± 5.55% excitatory neurons; p = 0.016) (**Figure 5.9b**). Interestingly, E/I ratio of the tri-culture more closely resembles the E/I ratio of the cortex *in vivo* (~80% excitatory) [279]. However, we cannot be sure if this apparent increase in excitatory neurons in the tri-culture is due to an actual increase in the number of excitatory neurons in the tri-culture or due to a relative increase in the number of excitatory neurons incorporated into the neural network. It has been shown that GABAergic neurons may be less healthy than glutamatergic neurons in culture potentially due to changes in ion channel expression [280], and it may be possible that the microglia in the tri-culture are inducing apoptosis in the weakened GABAergic neurons. Alternatively, it has also been shown that glutamatergic neurons are much more dependent on glial support and the secretion of the thrombospondin family of extracellular matrix proteins to establish functional glutamatergic synapses [280], and therefore the presence of microglia in the tri-culture may further enhance the incorporation of excitatory neurons into the neural network. Additionally, microglia are known to regulate perineuronal nets (PNNs), which stabilize synapses and have been shown to appear in cortical neuron cultures [281]. These PNNs primarily associate with narrow-spiking inhibitory neurons, leading to their over incorporation into neural networks when microglia are not present [268]. Since microglia are present in the tri-culture, they may be able to regulate the PNNs, thereby allowing increased incorporation of excitatory neurons into the neural network and increasing the apparent E/I ratio to values closer to what is observed *in vivo*.

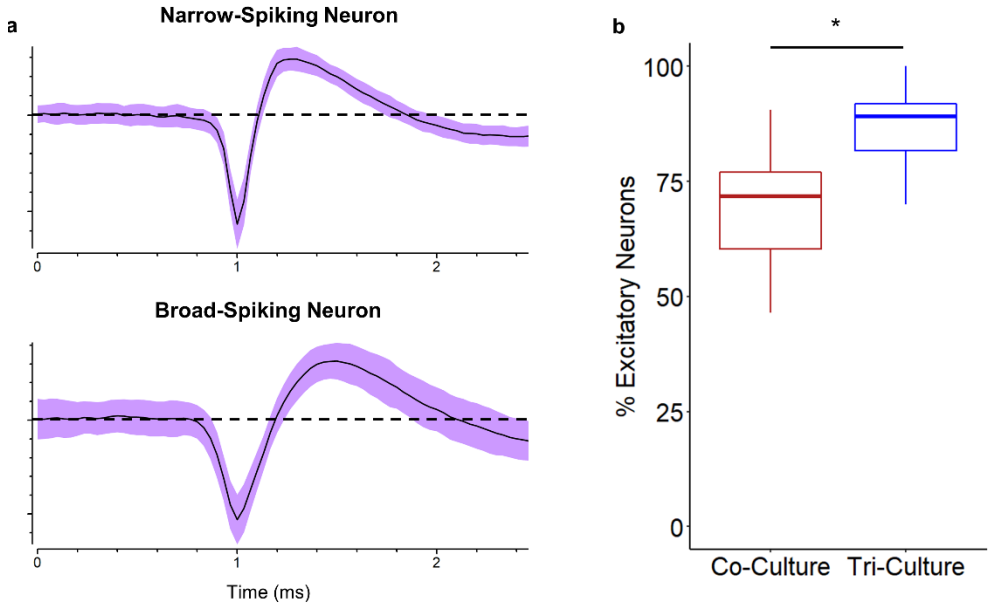

Figure 5.9: Comparison of the E/I ratio in tri- and co-cultures at DIV 21. (a) representative waveforms of narrow-spiking and broad-spiking neurons recorded at DIV 21. The line represents the average spike waveform, while the shaded region is one standard deviation. (b) Percent excitatory neurons in the tri- and co-cultures at DIV 21 (n = 8, from three independent dissections). *$p < 0.05$.

5.6 Influence of LPS Exposure

Finally, we investigated the tri-culture's ability to detect changes in neural activity in response to neuroinflammatory stimuli. We therefore challenged the tri- and co-culture with 5 µg/mL LPS and monitored the change in neural activity over 72 hours. As stated in the previous chapter, LPS is a well characterized activator of neurotoxic neuroinflammation that acts through the TLR4, which is found on microglia, but not neurons and astrocytes [218,282]. Activation of microglia by LPS leads to the secretion of proinflammatory cytokines [146,215], neuronal apoptosis [201,202], and the induction of a neurotoxic "A1" astrocyte phenotype [96]. Additionally, we have demonstrated a significant increase in apoptosis and cell death in tri-cultures treated with 5 µg/mL LPS at 48 h [146,283].

As expected, there was no change in the neural activity in the co-culture in response to LPS, as LPS acts through the toll-like receptor 4 (TLR4) that is not expressed by neurons or astrocytes. Conversely, we observe a significant decrease in both active channels (**Figure 5.10a**)

and spike frequency (**Figure 5.10b**) in the tri-culture following exposure to LPS. Additionally, we begin to see a trend towards a reduction in spike frequency beginning at 3 h (p = 0.17) before there is any change in the number of active channels (p = 0.71). As we observed that the spike frequency decreases at a more rapid rate than the number of active channels, this suggests that changes in neural activity can be detected prior to changes in neuronal health. Unfortunately, we were unable to compare other electrophysiological features (percent spikes in bursts, burst duration, and within burst ISI) and spike train synchrony, due to the dramatic reduction in active channels in the tri-culture following exposure to LPS limiting our ability to effectively characterize these features. Nevertheless, these results demonstrate that monitoring extracellular recordings from MEAs is a powerful method to non-invasively study the effect of neuroinflammation *in vitro*, especially when combined with our previously described tri-culture of neurons, astrocytes, and microglia that more faithfully represents the *in vivo* neuroinflammatory response.

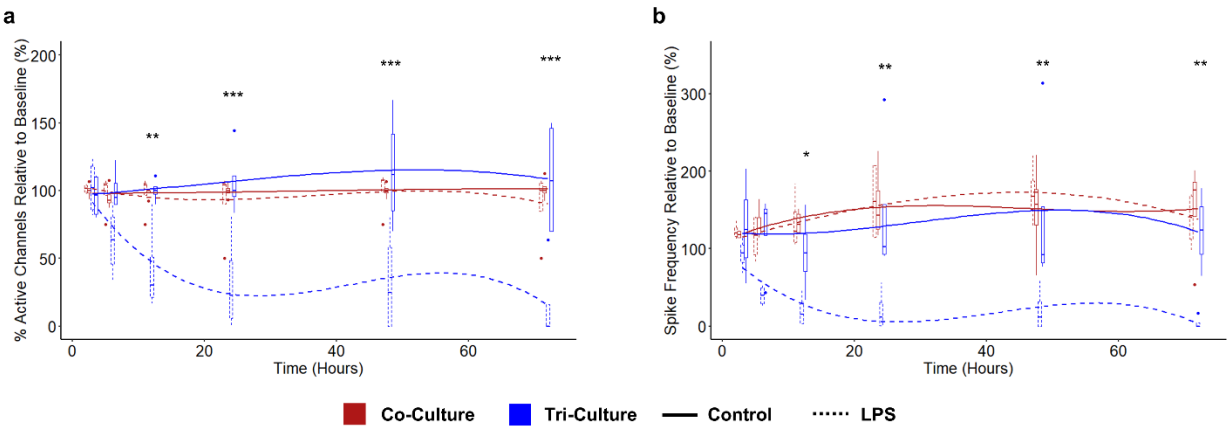

Figure 5.10: Comparing the change in (a) percent active channels and (b) spike frequency following exposure to 5 µg/mL LPS between co-cultures (red) and tri-cultures (blue). The lines show the fitted linear mixed effects model (treating individual cultures as a random effect) with a b-spline basis. Asterisks indicate a significant difference in the estimated marginal means of the fitted curves between control and LPS treated tri-cultures at that timepoint (n = 4, from two independent dissections). *p < 0.05, **p < 0.01, ***p < 0.001.

5.7 Conclusions

In this chapter, we characterized the neural activity and network maturation in a tri-culture of neurons, astrocytes, and microglia. We showed that the presence of microglia in the tri-culture had minimal impact on the formation and stability of neural networks, with the exception of an increase in spike frequency in the tri-culture. Additionally, characterization of the average spike waveforms revealed that the tri-culture had an E/I ratio much closer to that found in the rat cortex. Finally, we demonstrated that the improved neuroinflammatory response of the tri-culture can be captured via extracellular recordings as indicated by a significant decrease in both active channels and spike frequency following exposure to LPS. We expect that the electrophysiological read-out from the tri-culture will be useful for continuous and non-invasive studies in the context of neuroinflammation and neurodegeneration, where the presence of microglia imparts the ability to capture both neurotoxic and neuroprotective phenomena observed *in vivo*.

Chapter 6: Tri-Culture-Based Screening of the Neuroinflammatory Response to Toll-like Receptor Activation

Toll-like receptors (TLRs) are an evolutionarily conserved class of pattern-recognition receptors (PRRs) that recognize a multitude of pathogen associated molecular patterns (PAMPs) produced by bacteria, viruses, and fungi and are significantly involved in the innate immune response [284]. Additionally, TLRs recognize endogenous damage-associated molecular patterns (DAMPs) such as extracellular matrix components, high-mobility group box protein 1 (HMGB1), and mitochondrial DNA [285]. While TLR expression is primarily associated with macrophages, neutrophils, and other cells associated with the innate immune system, TLRs are expressed in many other cell types including both neurons and glial cells in the CNS [286,287]. Additionally, CNS-specific factors such as $A\beta_{1-42}$ along with DAMPs from damaged or necrotic neuronal cells have been shown to activate TLRs on both neurons and glial cells leading to a robust neuroinflammatory response [3,288]. However, the exact nature of the neuroinflammatory response to the activation of different TLRs is debated. This can in part be attributed to limitations in *in vitro* methodologies that are often limited to the culturing of a single cell type. For example, in one study, astrocyte cultures spiked with the TLR3 ligand poly (I:C) showed increased gene expression for many neurotrophic factors and the conditioned media promoted neuron survival in an organotypic culture [289]. Conversely, a similar study conducted on isolated microglia showed a significant increase in the secretion of pro-inflammatory factors such as TNF-α and IL-6 [290]. Therefore, there is a need to better understand the relative contributions of different CNS cells on the observed neuroinflammatory response to TLR activation.

In this study, we investigate the response of the tri-culture and neuron-astrocyte co-cultures to a suite of TLR agonists and quantify the response of both cultures using a number of known neuroinflammatory markers including changes in cell death, apoptosis, and astrocyte and microglia morphology. As the tri-culture is produced by taking primary cortical cells from neonatal

rats and maintaining them in a serum-free culture medium that was specifically designed to support all three cell types, when compared to other mixed culture models that require the separate maintenance and addition of cells at specific time points, the relative simplicity of this tri-culture model makes it well suited for high-throughput experiments and an effective model for the early screening of therapeutic molecules. We observe significant differences in the neuroinflammatory response between the co- and tri-cultures to nearly all tested TLR agonists, highlighting the role of microglia in neuroinflammatory processes. Additionally, we observe changes in microglia morphology in response to the activation of all tested TLRs (1-9), suggesting that rat microglia express TLR1-9 in agreement with previous studies on mouse [291] and human [290] microglia TLR expression. The results highlight the influence of cell culture composition on the neuroinflammatory response to different TLR agonists and emphasize that the microglia are required to observe many of the more neurotoxic aspects of neuroinflammation in response to TLR activation found *in vivo*.

6.1 Influence of TLR Agonists

6.1.1 Influence of TLR Agonists on Cell Death

In order to determine the role of microglia on the overall neuroinflammatory impact of TLR activation, we compared the response of both the co- and tri-cultures to an array of known TLR agonists at a range of concentrations (**Figure 6.1**). These concentrations were individually chosen for each TLR agonist based on concentrations that have been shown to elicit a response from immune cells and covered two orders of magnitude [146,292–297]. As expected, we observed a significant increase in cell death in the tri-culture following a 48 h incubation with LPS (TLR4 agonist) at all concentrations ($p < 2 \times 10^{-16}$, $p = 1.1 \times 10^{-5}$, and $p = 6.6 \times 10^{-4}$ when incubated with 5 µg/mL LPS, 500 ng/mL , and 50 ng/mL respectively) as compared to the vehicle, which was not observed in the co-culture ($p = 1.0$ for all concentrations). We also observed a significant increase in cell death following treatment with the highest concentration of HKLM (1×10^8 cells/mL, TLR2

agonist) in the tri-culture (p = 9.04 x 10^{-4}), and while treatment with 1 x 10^8 cells/mL HKLM did show an increase in cell death in the co-culture, this increase did not prove to be statistically significant (p = 0.10). Interestingly, we saw a non-monotonic relationship between HMW poly (I:C) (TLR3) treatment concentration and cell death, where treatment with 1 µg/mL HMW poly (I:C) induced a significant increase in cell death (p = 5.45 x 10^{-9}) while the 10 µg/mL and 100 ng/mL treatment concentrations did not result in cell death (p = 0.21 & 1.0 respectively). For the co-culture, treatment with 10 µg/mL HMW poly (I:C) led to a significant reduction in cell death (p = 0.023), which was the only instance of a reduction of cell death across all conditions. Additionally, for the co-culture there were trends towards increased cell death following treatment with 100 ng/mL Pam3SK4 (TLR1/2 agonist, p = 0.066), 1 x 10^8 cells/mL HKLM (TLR2 agonist, p = 0.10), and 100 ng/mL FSL1 (TLR6/2 agonist, p = 0.14).

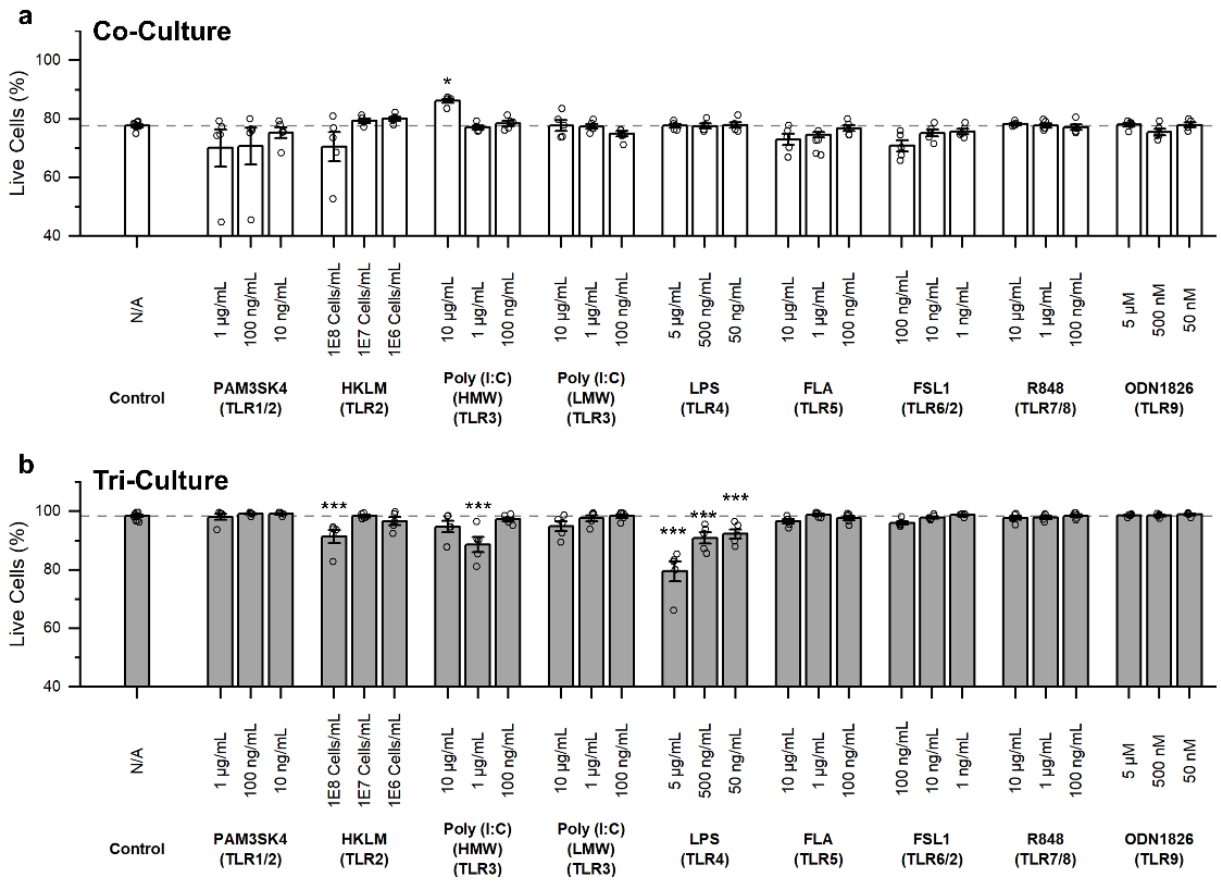

Figure 6.1 Influence of TLR agonist treatment on cell death as quantified by staining the cultures with Hoechst 33342 (all nuclei) and propidium iodide (nuclei from dead cells). The overall percentage of live cells in (a) co-cultures and (b) tri-cultures following TLR agonist treatment. Data shown as mean ± SEM (n = 6 wells from two independent dissections) with individual data points plotted, *$p < 0.05$, **$p < 0.01$, ***$p < 0.001$ (as determined by a one-way ANOVA followed by Dunnett's test vs vehicle control).

6.1.2 Influence of TLR Agonists on Apoptosis

Motivated by the influence of TLR agonist treatment on cell death in both the co- and tri-culture configurations, we studied if TLR agonist treatment induced other, potentially subtle, changes in the cultures. Therefore, we compared the amount of Annexin V staining (a marker for apoptosis) in both the co- and tri-cultures in response to TLR agonist treatments. Specifically, we treated the cultures with the highest concentration of each TLR agonists along with 1 µg/mL HMW poly (I:C) as we observed a difference in cell death in the tri-culture at this concentration that was not observed at the higher concentration. We observed significantly more Annexin V staining in the control conditions of the co-culture (12.27 ± 0.72 %) as compared to the tri-culture (7.05 ±

0.51 %, $p = 5.61 \times 10^{-5}$) (**Figure 6.2a&b**) in agreement with our previous study which used caspase 3/7 activity to quantify apoptosis [146]. Similar to cell death, we observed a significant decrease in the Annexin V staining in the co-culture treated with the 10 µg/mL HMW poly (I:C) (TLR3 agonist) as compared to the control ($p = 3.55 \times 10^{-4}$, **Figure 6.2c**) that was not observed in the tri-culture ($p = 0.99$, Figure 3d). For the tri-culture we observed a significant increase in Annexin V staining following treatment with 10 µg/mL R848 (TLR7/8 agonist, $p = 0.036$, **Figure 6.2d**). Additionally, we saw a trend towards increased Annexin V staining following treatment with 5 µg/mL LPS (TLR4 agonist, p = 0.094) and 1 µg/mL HMW poly (I:C) ($p = 0.17$). Overall, we observe that compared to the co-culture, the tri-culture shows a more robust an increase in Annexin V staining in response to TLR agonist treatment (**Figure 6.3**).

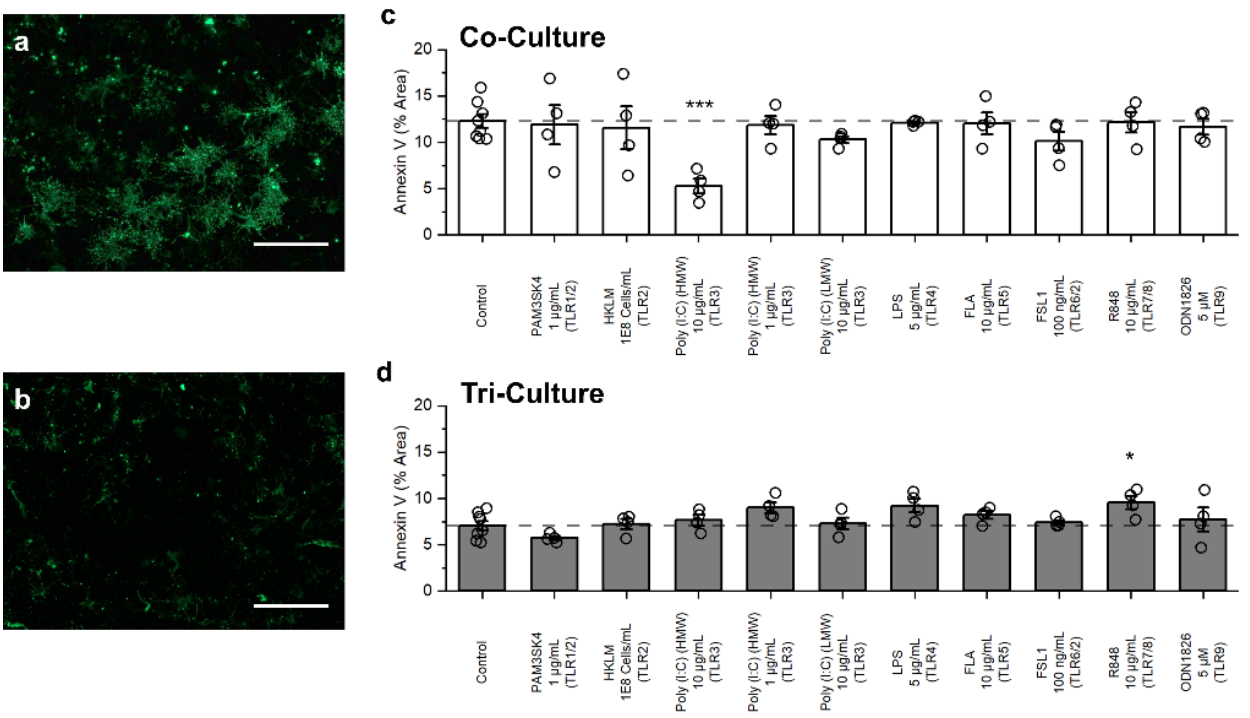

Figure 6.2. Influence on TLR agonist treatment on Annexin V staining. Representative fluorescence images of the (a) co-culture and (b) tri-culture at DIV 9. Quantification of the amount of Annexin V staining in the (c) co-cultures and (d) tri-cultures following 48 h exposure to TLR agonists. Data presented as mean ± SEM (n = 4 wells from two independent dissections) with individual data points plotted, *$p < 0.05$, **$p < 0.01$, ***$p < 0.001$ (as determined by a one-way ANOVA followed by Dunnett's test vs vehicle control). Scale bar = 100 µm.

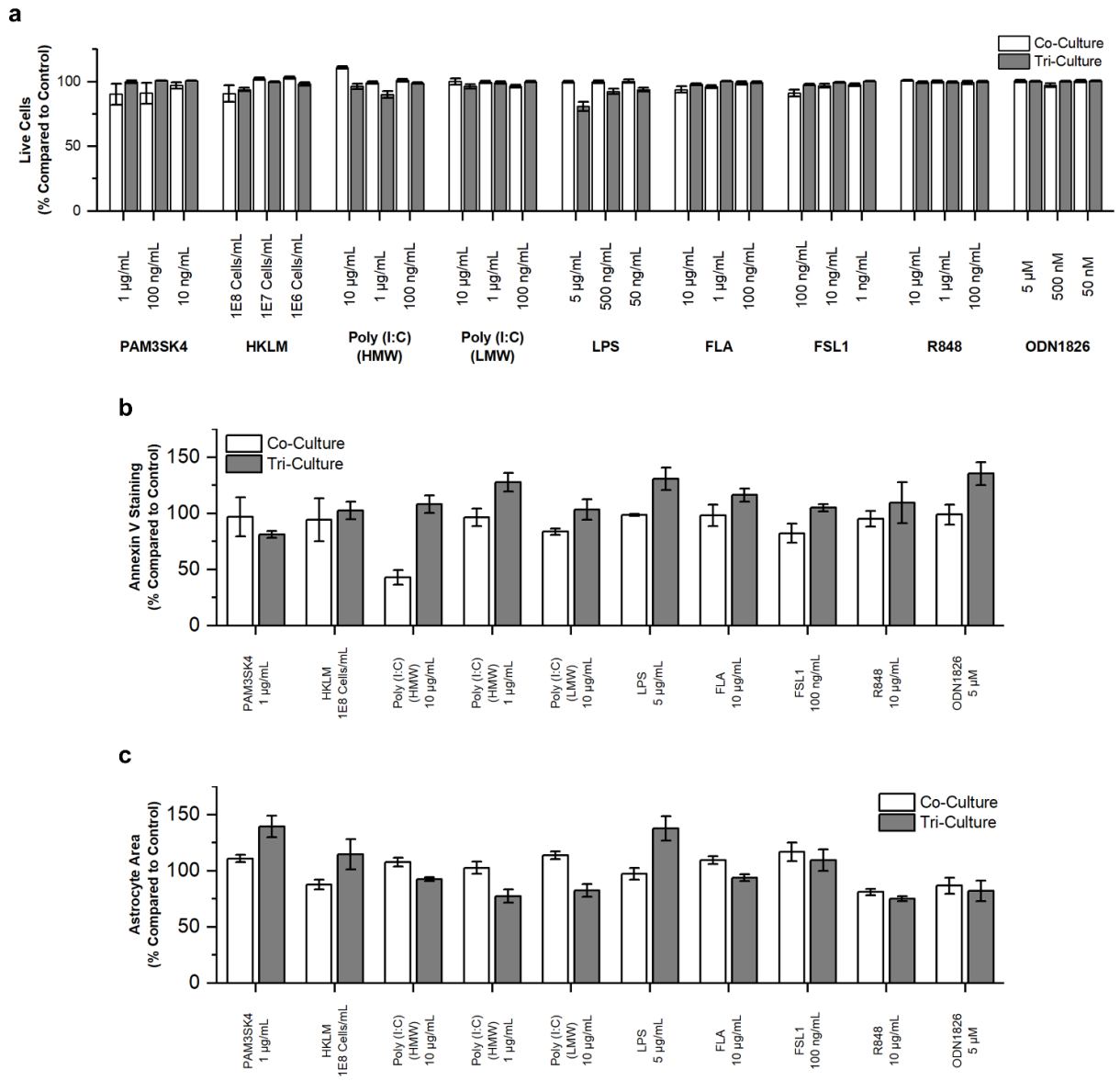

Figure 6.3: Comparison of the change in the number of (a) live cells, (b) Annexin V staining, and (c) astrocyte area between the co- and tri-cultures following TLR agonist treatment normalized to vehicle control.

6.1.3 Influence of TLR Agonists on Glial Cell Morphology

Reactive astrocytes, typically characterized by a hypertrophic morphology, is often used as a marker of neuroinflammation in neurodegenerative [298] and autoimmune disorders [299]. Therefore, we quantified the change in astrocyte area in both the co- and tri-cultures in response to TLR agonist treatment (**Figure 6.4a-c**). Upon exposure to TLR agonists, we did not observe

any significant changes to astrocyte area in the co-cultures (**Figure 6.4d**). However, for the tri-culture, significant astrocyte hypertrophy was evident following treatment with 1 µg/mL PAM3CSK4 (p = 0.033) and 5 µg/mL LPS (p = 0.044) (**Figure 6.4e**). Changes to microglia morphology is another common marker used to identify neuroinflammation, and we have previously shown that in culture, microglia adopt a spread morphology in response to neuroinflammatory stimuli [146]. Therefore, we also quantified the change in microglia morphology in the tri-culture following TLR agonist treatment. We observed a significant increase in microglia area for every treatment condition with the exception of 10 µg/mL HMW poly (I:C) and 10 µg/mL LMW poly (I:C) (**Figure 6.4f**).

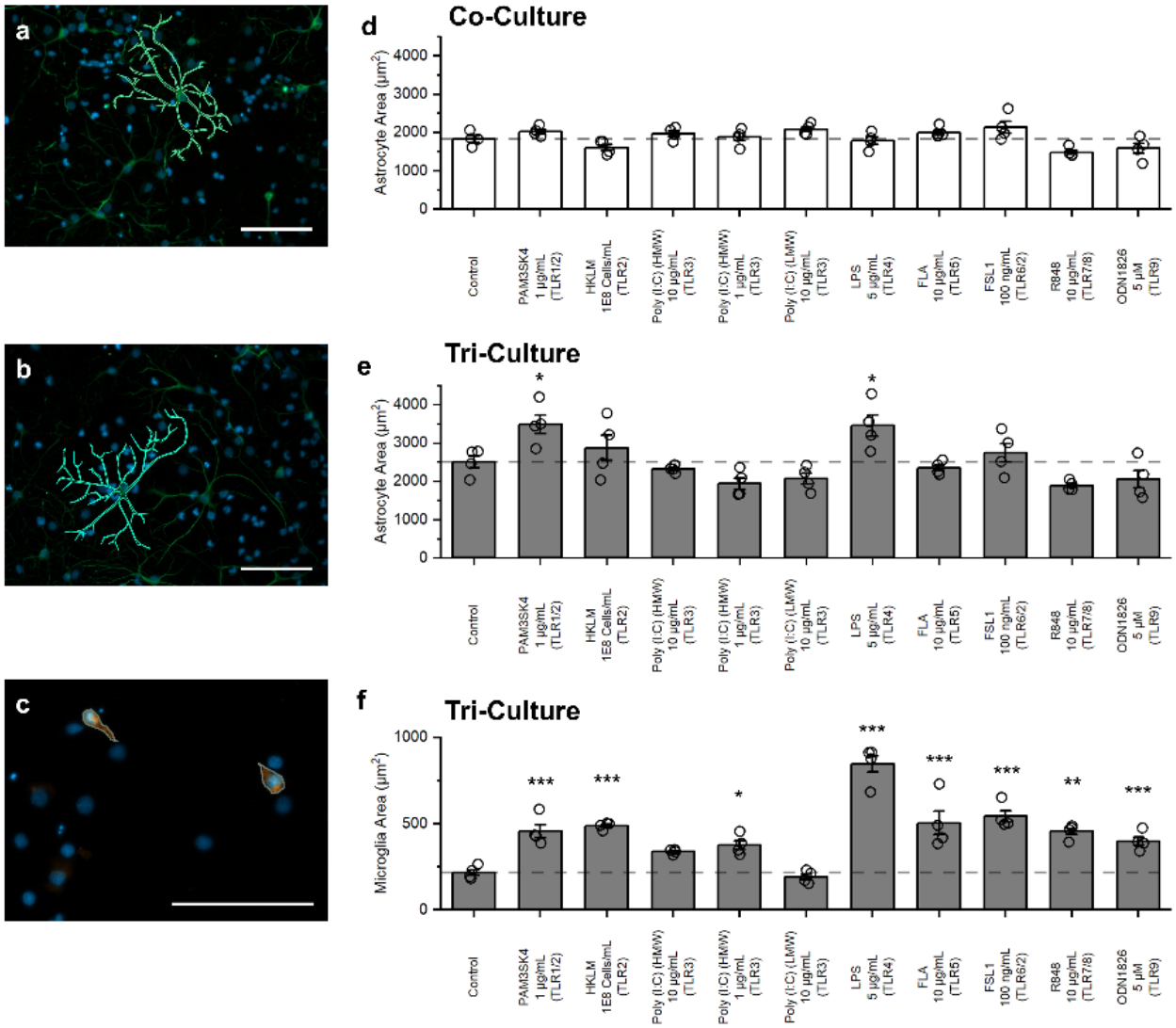

Figure 6.4: Influence on TLR agonist treatment on glial cell morphology. Representative fluorescence images of astrocytes in the (a) co-culture and (b) tri-culture and (c) microglia in the tri-culture at DIV 9 showing the outlining method used to quantify area. Quantification of the average astrocyte area in (d) co-cultures and (e) tri-cultures following 48 h exposure to TLR agonists. (f) Quantification of the average microglia area in the tri-cultures following 48 h exposure to TLR agonists. Data presented as mean ± SEM (n = 4 wells from two independent dissections) with individual data points plotted, *$p < 0.05$, **$p < 0.01$, ***$p < 0.001$ (as determined by a one-way ANOVA followed by Dunnett's test vs vehicle control). Scale bar = 100 µm.

6.2 Comparing the Influence TLR agonist Between Tri-Cultures and Co-Cultures

Previous work has shown that microglia from mice [291] and humans [290] constitutively express mRNA for TLR1-9, and our results suggest that rat microglia also constitutively express TLR1-9. Specifically, following 48 h exposure to TLR agonists, we observed a significant increase

in microglia area indicative of microglia activation [219,220,300,301] for all TLR agonists with the exception of LMW poly(I:C) (Figure 4f). However, both LMW poly(I:C) and HMW poly(I:C) activate TLR3, indicating that microglia respond to TLR3 agonists, but only at specific concentrations, as it has been shown that LMW poly(I:C) has a much lower activation efficiency for TLR3 as compared to HMW poly(I:C) [302]. Additionally, while we observed morphological changes in response to TLR agonists treatments, not all treatments induced further indicators of neuroinflammation such as changes to cell death or apoptosis. Conversely, while it has been suggested that astrocytes express mRNA for TLR1-9 [286,303,304], it has been shown that astrocytes express mRNA for TLR3 at much higher levels than the other TLRs [290]. Similarly, when quantifying the different aspects of neuroinflammation in the co-culture lacking microglia, we only observed changes to cell death and apoptosis in response to TLR3 activation, with no other TLR ligands inducing changes to cell death, apoptosis, or astrocyte morphology. Therefore, while we have not directly quantified the expression levels of different TLRs in the astrocytes and microglia in our cultures, the results from this study suggest that conclusions drawn from mouse and human studies can be extended to our primary rat tri-culture model.

Of all the TLR agonists tested, FLA (TLR5 agonist), FSL1 (TLR6/2 agonist), and ODN1826 (TLR9 agonist) did not show any additional indicators of neuroinflammation in either the co- or tri-cultures beyond changes to microglia morphology. Compared to other TLRs, the role of TLR5 activation in relationship to neuroinflammation and other neurological diseases has received less attention, with much of the research focusing on the expression levels of TLR5 in different CNS cell types and not on the role TLR5 activation may have on neuroinflammation [288,304]. One recent study has shown that activation of TLR5 on microglia induces neural cell loss and apoptosis using a microglia and neuron co-culture [305]. Interestingly, we did not observe the same neurotoxic effects even though we used the same source and concentration of TLR5 agonists for our treatment. One likely cause of this discrepancy may be the difference in the culture methodology, including animal model (rat vs mouse), age (perinatal vs embryonic), and culture

composition (neuron-microglia co-culture vs tri-culture). Another potential reason for the increased neurotoxic features observed by Ifuku *et al.* is that the isolated microglia culture used in their study contained 10% fetal bovine serum (FBS), which has been shown to activate microglia [115], and may be working in combination with the TLR5 activation to produce a more pronounced neurotoxic effect. Activation of TLR9 on microglia has also been shown to induce significant neuronal death *in vivo* [306] that was not observed in our tri-culture. However, this cell death was primarily attributed to the breakdown of the BBB [306], and therefore it is not surprising that the tri-culture was unable to capture this effect.

Activation of TLR4 in microglia by LPS is a well characterized method to induce robust neurotoxic neuroinflammation both *in vitro* [96] and *in vivo* [307]. The results from this study are in line with our previous work showing significant increases in apoptosis and astrocyte and microglia hypertrophy in the tri-culture following exposure to LPS [146]. While we do not observe a statistically significant increase in Annexin V staining in this study, the relative change of Annexin V staining vs control is similar in magnitude to the increase in caspase 3/7 activity in our previous study, and thus the lack of statistical significance in this study ($p = 0.094$) may be a function of the need to control for the familywise error rate (case of multiple of comparisons). In addition, we demonstrate a significant increase in cell death in the tri-culture following 48 h exposure to LPS at concentrations as low as 50 ng/mL confirming that the tri-culture can replicate the robust neuroinflammatory response to LPS treatment seen *in vivo*. Similarly, the response of the co-culture is as expected with no changes to cell death, Annexin V staining, or astrocyte morphology as the culture lacks microglia.

TLR2 has a wide spectrum in recognizing a variety of PAMPs [308], and TLR1 and 6 heterodimerize with TLR2 in further enhancing the recognition of different PAMPs. The heterodimerization has been attributed to an evolutionary mechanism of expanding the ligand recognition spectrum of various cell types to diverse lipopeptide structure of different pathogens [309]. In this study, TLR2 was activated with HKLM, which is a well-known agonist that is used

both for *in vivo* [310] and *in vitro* [311,312] studies. Along with TLR2, the TLR1 and TLR6 heterodimers were activated with PAM3CSK4 and FSL-1 additions to the culture, respectively. We observed an increase trend of cell death in the co-culture with TLR1/2, 2 and 6/2 agonists, whereas the cell death in the corresponding tri-culture groups was negligible except for the tri-culture group treated with the highest concentration of TLR2 agonist. Surprisingly, while cell death was not significant for the tri-culture group treated with TLR1/2 agonist, there was significant astrocyte hypertrophy only for this group (in contrast to the groups treated with TLR 2 and 6/2 agonists). The underlying reasons for these seemingly contradictory phenomena require mechanistic studies and may be due to the dual effects (anti-inflammatory vs pro-inflammatory) of some cytokines secreted as function of TLR activation (e.g., IL-6) [313] and cooperative response of these TLRs exhibiting non-monotonous dependence on agonist concentrations. Importantly, these results highlight that the presence of microglia reveal complex responses in compared to that from neuron-astrocyte co-cultures.

The opposite responses of the co- and tri-cultures to exposure to TLR3 agonist highlights the importance of culture composition on the observed outcomes of neuroinflammatory stimuli. The neuron-astrocyte co-culture shows a significant decrease in cell death and Annexin V staining in following 48 h exposure to 10 µg/mL HMW poly(I:C). This is in line with previous reports that show isolated astrocyte cultures produce neuroprotective cytokines in response to TLR3 activation, and conditioned media from poly(I:C) treated purified astrocyte cultures improved neuron survival in organotypic cultures [289]. Conversely, it has been shown that activation of microglial TLR3 leads to increased production of the pro-inflammatory cytokines TNF-α and IL-6 [314]. Interestingly, the tri-culture was able to capture both the neuroprotective aspect of TLR3 activation on astrocytes and the more neurotoxic aspect of microglia TLR3 activation leading to a non-monotonic change in cell death in response to HMW poly(I:C) concentration in the tri-culture. We observed a significant increase in cell death following treatment with 1 µg/mL HMW poly(I:C), which was not observed at higher (10 µg/mL) treatment concentrations, putatively due to the

neuroprotective aspects of astrocyte TLR3 activation counteracting the neurotoxic aspects of microglia TLR3 activation.

We did not observe a significant change in cell death or astrocyte morphology in either the co- or tri-culture following exposure to R848 (TLR7/8 agonist). However, in the tri-culture we did see a significant increase in Annexin V staining that was not seen in the co-culture. While there has not been much research into the impact of astrocyte TLR7/8 activation [288,304], it has been shown that activation of TLR8 in primary microglia cultures from non-human primates leads to an increase in production of pro-inflammatory cytokines such as TNF-α and IL-12 [315]. Additionally knocking-down (KD) TLR7 in mice lead to a reduction in the production of IL-6 following infections with Japanese encephalitis virus (JEV); however, these mice also showed increased viral load and mortality [316]. It has also been shown that R848 treatment can directly interact with TLR8 receptors on neurons, leading to reduced neurite outgrowth and increased apoptosis [317]. As we did not observe an increase in apoptosis in the co-culture, it is unlikely that direct activation of TLR8 on the neurons was solely responsible for the increase in Annexin V staining in the tri-culture. It is most likely that the increase in proinflammatory factors driven by the activation of microglia TLR7/8 or a combination of the two effects is responsible for the increased apoptosis observed in the tri-culture.

6.3 Conclusions

In this study we demonstrated the importance of microglia on the observed neuroinflammatory response to TLR activation in primary cortical cultures. In response to TLR2, 3, 4, and 7/8, we observed significant neurotoxic responses including increase in cell death and apoptosis in tri-cultures of neurons, astrocytes, and microglia that were not observed in co-cultures of only neurons and astrocytes. The only significant change that we observed in the co-culture was a decrease in cell death and apoptosis in response to TLR3 activation. Future studies comparing changes in cytokine production would further the understanding of the role microglia

play in the neuroinflammatory response to TLR activation. Additionally, comparing the co-activation of different TLRs may also reveal differences in the neuroinflammatory response as previous work has shown unique neuroinflammatory responses to different pairwise combination of TLR agonists [318]. Cell culture models are vital tools to gain a better understanding of cellular and molecular processes underlying many neurological and neurodegenerative disorders. However, it is also critical to recognize the inherent limitations within these models. The use of mixed culture models, such as the tri-culture used in this study, is one method of overcoming some of these limitations. By including neurons, astrocytes, and microglia in a single culture model, we were able to observe the relative influence of all three cell types on the neuroinflammatory response to different TLR agonists. This was particularly apparent in the response to TLR3 activation, in which we observed that microglia and astrocytes play opposing roles in the neuroinflammatory response and depending on the concentration of TLR3 agonist the response of microglia or astrocytes dominated the observed response. Additionally, as the only modification required to establish and maintain the tri-culture is the preparation and use of the specific tri-culture medium, we demonstrate that the tri-culture is well suited for high-throughput experiments. Overall, we have demonstrated that microglia play a significant role in the neuroinflammatory response to TLR activation *in vitro*, and their presence is critical to better replicate the *in vivo* response. Furthermore, we expect that the tri-culture model and the accompanying methods described here will be useful for higher-throughput screening studies that range from neurotoxins to pharmaceuticals.

Chapter 7: Conclusions

Neuroinflammation plays a significant role in nearly all pathological conditions in the CNS including neurodegenerative diseases and psychological disorders. Therefore, there is a critical need to better understand the mechanisms driving neuroinflammatory and neurodegenerative disease progression. However, the high complexity of the CNS and *in vivo* environment makes performing these detailed mechanistic studies extremely challenging. One such technology that can aid in this discovery are organ-on-a-chip platforms, which strike a balance between recapitulating relevant cell-cell interactions found in vivo, while reducing the complexity of the system to allow for more controlled mechanistic studies. Here we discussed our progress in developing an organ-on-a-chip model to study neuroinflammatory and neurodegenerative diseases creating capabilities to study how these disease states are able to propagate to synaptically connected, but anatomically remote regions of the brain.

7.1 Dissertation Findings

In this dissertation we developed the foundation for an organ-on-a-chip platform to better replicate the complexity of neuroinflammation *in vivo*. In particular, we focused on capturing the structural and cellular architecture underlying the propagation and transmission of disease states within the CNS through axonal connections and the important cellular crosstalk between neurons, astrocytes, and microglia that can significantly alter the observed neuroinflammatory response.

We first designed and fabricated a microfluidic device to capture the cellular architecture of anatomically remote, but synaptically connected neural populations. This device was based on compartmentalized neuronal culture devices that were developed for the acute studies of isolated neuron populations [90,127]. These devices consisted of two cell culture chambers connected by a series of microchannels that allows axons to cross through, but physically block the cell bodies of neurons and other glial cells. This creates two distinct neural populations that are synaptically connected, and fluidic isolation of one chamber (primary) can be achieved by increasing the

volume of media in the opposing chamber (secondary), thereby driving a hydrostatic pressure driven flow through the microchannels counteracting any diffusion from the primary chamber to the secondary chamber.

We used multiple theoretical and experimental methods to optimize the microchannel geometries of these devices to enable their use in extended studies of connected mixed neuron-glia populations. We discovered that reducing microchannel height down to 1.5 μm had an outstanding impact on the fluidic properties of the device by significantly reducing the volumetric flow rate through the microchannels that is required for maintaining the fluidic isolation of the primary chamber, and by doing so enable the use of these devices for long-term studies where fluid flow between the chambers can significantly alter the concentration of soluble factors added to the fluidically isolated chamber. Additionally, we found that reducing microchannel height improved the cellular confinement of the devices by reducing the number of cell bodies that can enter the microchannels, while minimally impacting the ability for axons to cross through the channels. The other parameters, such as microchannel width and length and initial seeding density offer additional degrees of freedom in customizing such devices for specific applications, and we condense the effects of all parameters into design to enable researchers to design similar devices to better suit their experimental needs.

We also demonstrated the utility of these devices by engineering a microfluidic neural culture platform with an integrated MEA with microchannels based on the geometries identified by the previous experiments. The engineered device successfully recorded extracellular action potentials from primary rat cortical cells for 59 days *in vitro* with more than on order of magnitude enhancement in signal-to-noise ratio in the microchannels. Additionally, the recordings from electrodes placed within the microchannels showed similar features such as burst duration and ISI within bursts from electrodes placed within the cell culture chambers suggesting that the physical confinement of the microchannels were not impacting the activity of the neurons. These results show that the use of microchannels can improve the fidelity of *in vitro* extracellular

recordings, and that this could be a powerful tool for researchers even if they are not interested in the cellular confinement aspect of the device.

We also developed and characterized a new cell culture model that better mimics the *in vivo* response to a number of neuroinflammatory stimuli, and is also compatible with the previously described microfluidic device. This culture model is established through the use of a new serum-free media formulation that is specifically designed to support neurons, astrocytes, and microglia. We cultured primary cortical cells from neonatal rat pups and demonstrated that this media is capable of supporting a healthy population of neurons, astrocytes, and microglia Additionally, this “tri-culture” may be more representative of the homeostatic *in vivo* environment that more common neuron-astrocyte co-culture models. The tri-culture showed significantly reduced cell death and apoptosis as compared to neuron-astrocyte co-cultures and had an E/I ratio closer to what is observed from *in vivo* recordings from the rat cortex. We attributed this improvement in culture health to the interaction of membrane bound CX3CL1 expressed by neurons and the corresponding receptor (CX3CR1) found on microglia, which has been shown to hold the microglia in a resting state and induce the secretion of the neurotrophic factor IGF-1, which was increased in the tri-culture conditioned media.

We have also demonstrated that the tri-culture better mimics the neuroinflammatory response to a wide range of neuroinflammatory stimuli as compared to neuron-astrocyte co-cultures. In response to LPS the tri-culture displayed many of the classic hallmarks of LPS induced neuroinflammation including an increase in cell death and apoptosis, astrocyte hypertrophy, and the secretion of a number of pro-inflammatory cytokines (e.g., TNF, IL-1α, IL-1β, and IL-6), none of which were observed in LPS-exposed co-cultures. Additionally, we observed a sharp decrease in the spontaneous neural activity within the first 12 hours post LPS exposure. Following mechanical trauma, the tri-culture showed increased caspase 3/7 activity, as compared to the co-culture, along with increased astrocyte migration towards the source of injury. Finally, the

microglia in the tri-culture played a significant neuroprotective role during glutamate-induced excitotoxicity, with significantly reduced neuron loss and astrocyte hypertrophy in the tri-culture.

We also highlighted some of the additional benefits of the relative simplicity of the tri-culture model, with the only modification needed to establish and maintain the tri-culture is the use of a specialized tri-culture medium. We demonstrate the tri-culture's use as a higher-throughput screening platform by examining the response of the tri-culture to a suite of nine TLR ligands at multiple concentrations and demonstrated that microglia play a significant role in the neuroinflammatory response to TLR activation *in vitro*, and their presence is critical to better replicate the *in vivo* response. Finally, we cultured the tri-culture in the microfluidic device and were able to capture high fidelity electrophysiological recordings.

7.2 Future Directions

As the work from this dissertation established the foundation for an organ-on-a-chip system that is capable of modeling the complex neuroinflammatory conditions found *in vivo*, the natural extension of this work is the use of this system to study different neuroinflammatory stimuli with a particular focus on how neuroinflammatory and neurodegenerative disease state are able to propagate to different regions of the brain. One method would be to use the integrated MEA under the interconnecting microchannels to determine if we are able to observe a significant increase in neural activity from the interconnecting axons following the induction of a neuroinflammatory condition in the treatment chamber. If this is found, then it would suggest that increased neural activity or even excitotoxic events may underly the propagation of neuroinflammation, and this dependance could be further confirmed by blocking the propagation of action potentials between the chambers via application of tetrodotoxin [319] and seeing if the transmission of neuroinflammation still occurs. We could also use the results from the initial experiment to determine if there may be some specific electrophysiological features or chances in neural activity that are characteristic of the propagation of neuroinflammation and use electrical

stimulation through the integrated MEA to attempt to mimic that characteristic electrophysiological signal and induce a neuroinflammatory state in the secondary chamber. We could also pharmaceutically block axonal transport via the application of molecules such as brefeldin A [320] to determine if there is an axon transport component required to transmit neuroinflammatory cues.

Preliminary studies using calcium imaging to detect neural activity have demonstrated a strong synaptic connection between the two chambers. After culturing the tri-culture in both chambers of the microfluidic device for 14 DIV, application of 50 µM glutamate to the treatment chamber led to the immediate increase in neural activity in that chamber, which subsequently observed to a lesser degree in the secondary chamber (**Figure 7.1**). Additionally, we observed some evidence of the propagation of neuroinflammation following treatment of the primary chamber with 5 µg/mL LPS, however this was only observed in cultures with low initial seeding densities (< 3 M cells/mL) and was not observed in platforms that were seeded at higher initial concentrations (**Figure 7.2**). However additional studies are needed to confirm these initial results and better characterize the underlying mechanisms driving the propagation of these neuroinflammatory states.

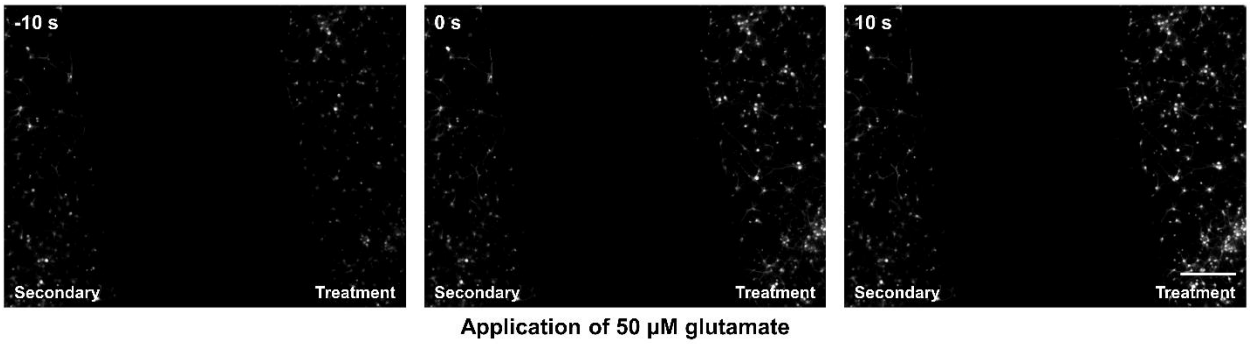

Figure 7.1: Demonstration of the synaptic connectivity between the two tri-culture populations in two synaptically connected chambers in the microfluidic device. Calcium imaging showing the change in fluorescence following the addition of 50 µM glutamate to the treatment chamber at time 0 s. Scale bar: 250 µm.

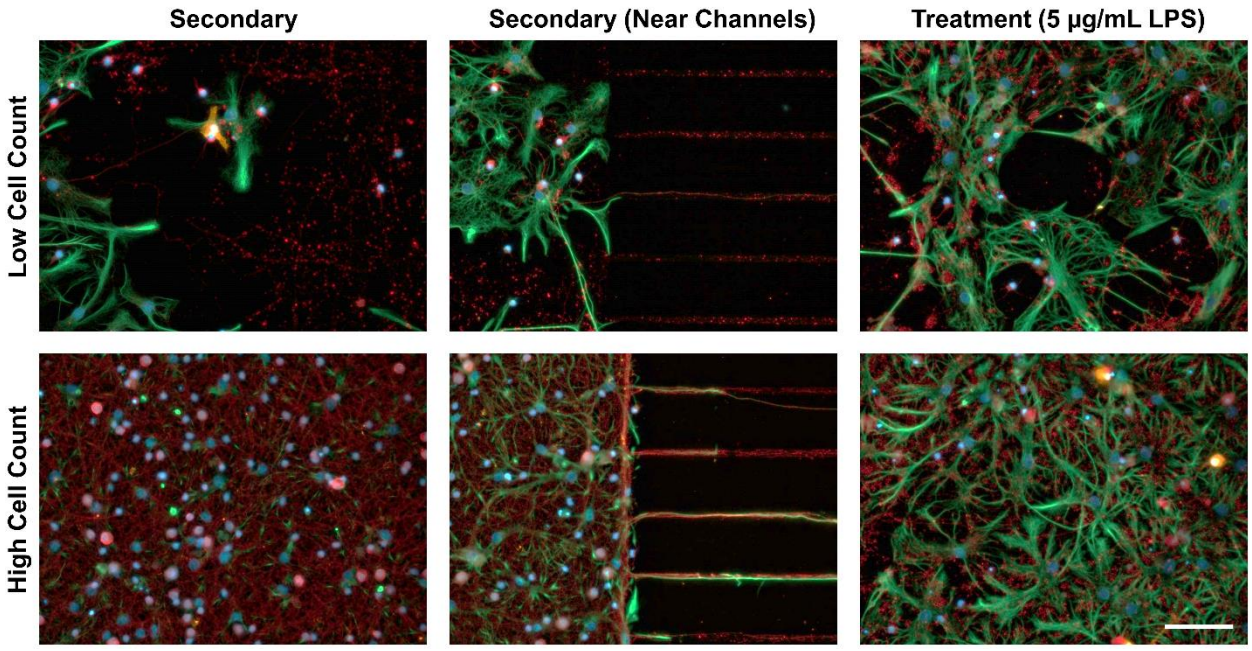

Figure 7.2: Preliminary study demonstrating the propagation of neuroinflammation within our organ-on-a-chip model following a 96 h with of 5 µg/mL LPS. The cultures were immunostained for the three cell types of interest: neurons – anti-βIII-tubulin (red), astrocytes – anti-GFAP (green), microglia – anti-Iba1 (orange) and the general nuclear stain DAPI (blue). Scale bar = 100 µM.

Finally, the tri-culture on its own can be also used to gain a better understanding of the role that neuroinflammation plays in a wide range of CNS conditions including neurodegenerative diseases, autoimmune diseases, and COVID-19 infection. In addition, the studies listed below offer intriguing directions for future research.

1. In addition to neurons, astrocytes, and microglia the CNS contains additional cells associated with neuroinflammation and other pathological states including OPCs, mature oligodendrocytes, and pericytes. The tri-culture already contains a small number of OPCs and we have observed a very small number of mature oligodendrocytes at later timepoints using myelin basic protein staining. Developing a method to increase the population of OPCs and mature oligodendrocytes to physiologically relevant numbers would increase the physiological relevance of the culture.

2. Conversely, it is also important to recognize that the added complexity of maintaining multiple cell types within the culture may not always be necessary. Developing methods to selectively culture subsets and different combinations of CNS cells would be very beneficial to conduct highly directed cellular level experiments and determine the role of different cell types in different neuroinflammatory conditions.
3. We have demonstrated the effectiveness of the tri-culture using primary cells from neonatal rats. In order to increase the relevancy of these models for pharmaceutical and therapeutic applications it would be beneficial to develop similar culture models using human cells.
4. In a similar vein, extending the tri-culture compatibility with primary mouse cells would allow for the use of many transgenic models that are only available in mice.
5. Incorporating the tri-culture into 3D cultures would also improve the overall physiological relevance and enable the study of many processes and morphological changes that are only observable in the 3D environment.
6. Future work could also focus on developing other functional units of the CNS, in particular the neurovascular unit and BBB. Incorporating these models with the enhanced neuroinflammatory tri-culture model would allow researchers to better understand the role of BBB breakdown and CNS specific neuroinflammatory response to different disease states.
7. Additionally, combining these models with the two chambered microfluidic device would create a powerful organ-on-a-chip system that could model the response of multiple brain regions to different neuroinflammatory stimuli and other pathological conditions.

Chapter 8: Publication List and Other Contributions

8.1 Journal Publications

- **Goshi, Noah,** Hyehyun Kim, Alexander Gardner, and Erkin Seker. “The Role of Microglia on the Electrophysiological Response of *in vitro* Cortical Cultures.” *(Submitted to Journal of Neuroinflammation).*
- **Goshi, Noah,** Gregory Girardi, Hyehyun Kim, and Erkin Seker. “Teaching a Biomedical Device Engineering Course: Proposal Development and Research Data-Based Assignments.” *Biomedical Engineering Education. (In press).*
- **Goshi, Noah**, Gregory Girardi, Felipe da Costa Souza, Alexander Gardner, Pamela J. Lein, and Erkin Seker “Influence of Microchannel Geometry on Device Performance and Electrophysiological Recording Fidelity During Long-Term Studies of Connected Neural Populations.” *Lab on a Chip* 22, no. 20 (2022): 3961-3975
- **Goshi, Noah**, Hyehyun Kim, and Erkin Seker. "Primary Cortical Cell Tri-Culture-Based Screening of Neuroinflammatory Response in Toll-like Receptor Activation." *Biomedicines* 10, no. 9 (2022): 2122.
- Palanisamy, Barath, **Noah Goshi**, and Erkin Seker. "Chemically-Gated and Sustained Molecular Transport through Nanoporous Gold Thin Films in Biofouling Conditions." *Nanomaterials* 11, no. 2 (2021): 498.
- **Goshi, Noah**, Rhianna K. Morgan, Pamela J. Lein, and Erkin Seker. "A primary neural cell culture model to study neuron, astrocyte, and microglia interactions in neuroinflammation." *Journal of neuroinflammation* 17 (2020): 1-16.
- Chapman, Christopher AR, **Noah Goshi**, and Erkin Seker. "Multifunctional Neural Interfaces for Closed-Loop Control of Neural Activity." *Advanced Functional Materials* 28, no. 12 (2018): 1703523.

8.2 Conference Presentations

- **Goshi, Noah,** Gregory Girardi, Hyehyun Kim, Felipe da Costa Souza *et al.* "An Organ-on-a-Chip Model to Study Neuroinflammatory and Neurodegenerative Diseases." *UC Davis Neuroengineering and Medicine Symposium*, 2022. ***(Podium Presentation)***.
- **Goshi, Noah,** Gregory Girardi, Hyehyun Kim, Felipe da Costa Souza *et al.* "An Organ-on-a-Chip Model to Study Neuroinflammatory and Neurodegenerative Diseases." *UC Davis Biomedical Engineering Graduate Group Student Symposium*, 2022. ***(Poster)***.
- **Goshi, Noah,** Gregory Girardi, Hyehyun Kim, Felipe da Costa Souza *et al.* "An Organ-on-a-Chip Model to Study Neuroinflammatory and Neurodegenerative Diseases." *31st Annual Biotechnology Training Retreat*, 2022. ***(Podium Presentation)***.
- **Goshi, Noah**, Rhianna Morgan, Pamela Lein, and Erkin Seker. "A Primary Neural Cell Culture Model to Study Neuroinflammation." *Gordon Research Conference on Neuroelectronic Interfaces*, 2022. ***(Poster)***.
- **Goshi, Noah**, Rhianna Morgan, Pamela Lein, and Erkin Seker. "A Primary Neural Cell Culture Model to Study Neuroinflammation." *Biomedical Engineering Society 2020 Annual Meeting*, 2020. ***(Podium Presentation)***.
- **Goshi, Noah**, Rhianna Morgan, Pamela Lein, and Erkin Seker. "A Primary Neural Cell Culture Model to Study Neuroinflammation." *UC Davis Biomedical Engineering Graduate Group Student Symposium*, 2020. ***(Podium Presentation)***.
- **Goshi, Noah**, Rhianna Morgan, Pamela Lein, and Erkin Seker. "A Primary Neural Cell Culture Model to Study Neuron, Astrocyte, and Microglia Interactions in Neuroinflammation." *29th Annual Biotechnology Training Retreat*, 2020. ***(Podium Presentation)***.

- **Goshi, Noah**, Rhianna Morgan, Pamela Lein, and Erkin Seker. “Mechanisms of Neuronal Tranmission of Inflammation to Distal Neuroanatomical Regions.” *28th Annual Biotechnology Training Retreat*, 2019. ***(Podium Presentation)***.

References

1. Corps KN, Roth TL, McGavern DB. Inflammation and neuroprotection in traumatic brain injury. JAMA Neurol. 2015;72:355–62.

2. Jayaraj RL, Azimullah S, Beiram R, Jalal FY, Rosenberg GA. Neuroinflammation: friend and foe for ischemic stroke. J Neuroinflammation. Journal of Neuroinflammation; 2019;16:142.

3. Waisman A, Liblau RS, Becher B. Innate and adaptive immune responses in the CNS. Lancet Neurol [Internet]. Elsevier Ltd; 2015;14:945–55. Available from: http://dx.doi.org/10.1016/S1474-4422(15)00141-6

4. Block F, Dihne M, Loos M. Inflammation in areas of remote changes following focal brain lesion. Prog Neurobiol. 2005;75:342–65.

5. Zhang J, Zhang Y, Xing S, Liang Z, Zeng J. Secondary neurodegeneration in remote regions after focal cerebral infarction: A new target for stroke management? Stroke. 2012;43:1700–5.

6. Xiao P, Gu J, Xu W, Niu X, Zhang J, Li J, et al. RTN4/Nogo-A-S1PR2 negatively regulates angiogenesis and secondary neural repair through enhancing vascular autophagy in the thalamus after cerebral cortical infarction. Autophagy [Internet]. Taylor & Francis; 2022;00:1–20. Available from: https://doi.org/10.1080/15548627.2022.2047344

7. Xing S, Zhang Y, Li J, Zhang J, Li Y, Dang C, et al. Beclin 1 knockdown inhibits autophagic activation and prevents secondary neurodegenerative damage in the ipsilateral thalamus following focal cerebral infarction. Autophagy. 2012;8:63–76.

8. von Monakow C. Lokalisation der Hirnfunktionen [Localization of brain functions]. J fur Psychol Neurol. 1911;17:185–200.

9. Carrera E, Tononi G. Diaschisis : past , present , future. 2014;2408–22.

10. Cao Z, Harvey SS, Bliss TM, Cheng MY, Steinberg GK. Inflammatory Responses in the Secondary Thalamic Injury After Cortical Ischemic Stroke. Front Neurol. 2020;11:1–12.

11. Zhang J, Zhang Y, Xing S. Secondary Neurodegeneration in Remote Regions After Focal

Cerebral Infarction A New Target for Stroke Management ? 2012;1700–5.

12. Heneka MT, Carson MJ, Khoury J El, Landreth GE, Brosseron F, Feinstein DL, et al. Neuroinflammation in Alzheimer's disease. Lancet Neurol. 2015;14:388–405.

13. Heppner FL, Ransohoff RM, Becher B. Immune attack: The role of inflammation in Alzheimer disease. Nat Rev Neurosci. Nature Publishing Group; 2015;16:358–72.

14. Calsolaro V, Edison P. Neuroinflammation in Alzheimer's disease: Current evidence and future directions. Alzheimer's Dement. 2016;12:719–32.

15. Colonna M, Brioschi S. Neuroinflammation and neurodegeneration in human brain at single-cell resolution. Nat Rev Immunol. 2020;20:81–2.

16. Frost GR, Jonas LA, Li YM. Friend, Foe or Both? Immune Activity in Alzheimer's Disease. Front Aging Neurosci. 2019;11:1–20.

17. Henstridge CM, Hyman BT, Spires-Jones TL. Beyond the neuron–cellular interactions early in Alzheimer disease pathogenesis. Nat Rev Neurosci [Internet]. Springer US; 2019;20:94–108. Available from: http://dx.doi.org/10.1038/s41583-018-0113-1

18. Leyns CEG, Holtzman DM. Glial contributions to neurodegeneration in tauopathies. Mol Neurodegener. Molecular Neurodegeneration; 2017;12:1–16.

19. Mawuenyega KG, Sigurdson W, Ovod V, Munsell L, Kasten T, Morris JC, et al. Decreased clearance of CNS β-amyloid in Alzheimer's disease. Science (80-). 2010;330:1774.

20. Ismail R, Parbo P, Madsen LS, Hansen AK, Hansen K V., Schaldemose JL, et al. The relationships between neuroinflammation, beta-amyloid and tau deposition in Alzheimer's disease: A longitudinal PET study. J Neuroinflammation. Journal of Neuroinflammation; 2020;17:1–11.

21. Prokop S, Miller KR, Heppner FL. Microglia actions in Alzheimer's disease. Acta Neuropathol. 2013;126:461–77.

22. Laurent C, Bu L, Blum D. Tau and neuroinflammation : What impact for Alzheimer ' s Disease and Tauopathies ? Biomed J. 2018;41:21–33.

23. Goedert M. Alzheimer’s and Parkinson’s diseases: The prion concept in relation to assembled Ab, tau, and a -synuclein. Science (80-). 2015;349:61–9.

24. Goedert M. Tau proteinopathies and the prion concept [Internet]. 1st ed. Prog. Mol. Biol. Transl. Sci. Elsevier Inc.; 2020. Available from: http://dx.doi.org/10.1016/bs.pmbts.2020.08.003

25. Kametani F, Hasegawa M. Reconsideration of amyloid hypothesis and tau hypothesis in Alzheimer’s disease. Front Neurosci. 2018;12.

26. Seitz RJ, Azari NP, Knorr U, Binkofski F, Herzog H, Freund HJ. The role of diaschisis in stroke recovery. Stroke. 1999;30:1844–50.

27. Craig BT, Carlson HL, Kirton A. Thalamic diaschisis following perinatal stroke is associated with clinical disability. NeuroImage Clin [Internet]. Elsevier; 2019;21:101660. Available from: https://doi.org/10.1016/j.nicl.2019.101660

28. Nagasawa H, Kogure K. Exo-focal postischemic neuronal death in the rat brain. 1990;524:196–202.

29. Dihné M, Grommes C, Lutzenburg M, Witte OW, Block F. Different Mechanisms of Secondary Neuronal Damage in Thalamic Nuclei After Focal Cerebral Ischemia in Rats. 2002;3006–12.

30. Ross DT, Ebner FF. Thalamic retrograde degeneration following cortical injury: An excitotoxic process? Neuroscience. 1990;35:525–50.

31. Watanabe H, Kumon Y, Ohta S, Nakano K, Sakaki S, Matsuda S, et al. Protein synthesis inhibitor transiently reduces neuronal death in the thalamus of spontaneously hypertensive rats following cortical infarction. Neurosci Lett. 1997;233:25–8.

32. Sørensen JC, Dalmau I, Zimmer J, Finsen B. Microglial reactions to retrograde degeneration of tracer-identified thalamic neurons after frontal sensorimotor cortex lesions in adult rats. Exp Brain Res. 1996;112:203–12.

33. Morioka T, Kalehua AN, Streit WJ. Characterization of microglial reaction after middle cerebral artery occlusion in rat brain. J Comp Neurol. 1993;327:123–32.

34. Zhu CZ, Auer RN. Graded hypotension and MCA occlusion duration: Effect in transient focal

ischemia. J Cereb Blood Flow Metab. 1995;15:980–8.

35. Czurkó A, Nishino H. “Collapsed” (argyrophilic, dark) neurons in rat model of transient focal cerebral ischemia. Neurosci Lett. 1993;162:71–4.

36. Butler TL, Kassed C a, Sanberg PR, Willing a E, Pennypacker KR. Neurodegeneration in the rat hippocampus and striatum after middle cerebral artery occlusion. Brain Res [Internet]. 2002;929:252–60. Available from: http://www.ncbi.nlm.nih.gov/pubmed/11864631

37. Viscomi MT, Latini L, Florenzano F, Bernardi G, Molinari M. Minocycline attenuates microglial activation but fails to mitigate degeneration in inferior olive and pontine nuclei after focal cerebellar lesion. Cerebellum. 2008;7:401–5.

38. Bisicchia E, Sasso V, Catanzaro G, Leuti A, Besharat ZM, Chiacchiarini M, et al. Resolvin D1 Halts Remote Neuroinflammation and Improves Functional Recovery after Focal Brain Damage Via ALX/FPR2 Receptor-Regulated MicroRNAs. Mol Neurobiol. Molecular Neurobiology; 2018;55:6894–905.

39. Zhang J, Zhang Y, Xing S, Liang Z, Zeng J. Secondary neurodegeneration in remote regions after focal cerebral infarction: A new target for stroke management? Stroke. 2012;43:1700–5.

40. Nakane M, Tamura A, Sasaki Y, Teraoka A. MRI of secondary changes in the thalamus following a cerebral infarct. Neuroradiology. 2002;44:915–20.

41. Tamura A, Tahira Y, Nagashima H, Kirino T, Gotoh O, Hojo S, et al. Thalamic atrophy following cerebral infarction in the territory of the middle cerebral artery. Stroke. 1991;22:615–8.

42. Nakajima M, Hirano T, Terasaki T, Uchino M. Signal change of the substantia nigra on diffusion-weighted imaging following striatal infarction. Intern Med. 2010;49:65–8.

43. Nakane M, Teraoka A, Asato R, Tamura A. Degeneration of the ipsilateral substantia nigra following cerebral infarction in the striatum. Stroke. 1992;23:328–3332.

44. Xanthos DN, Sandkühler J. Neurogenic neuroinflammation: inflammatory CNS reactions in response to neuronal activity. Nat Rev Neurosci [Internet]. Nature Publishing Group; 2013;15:43–53. Available from: http://www.nature.com/doifinder/10.1038/nrn3617

45. D.G. M, J.C.W. M, M.O. C, P.J. B. Calcitonin gene-related peptide vasodilation of human pulmonary vessels. J Appl Physiol [Internet]. 1989;67:1265–70. Available from: http://www.embase.com/search/results?subaction=viewrecord&from=export&id=L19245057%5Cnhttp://sfx.library.uu.nl/utrecht?sid=EMBASE&issn=01617567&id=doi:&atitle=Calcitonin+gene-related+peptide+vasodilation+of+human+pulmonary+vessels&stitle=J.+APPL.+PHYSIOL.

46. Saria A. Substance P in sensory nerve fibres contributes to the development of oedema in the rat hind paw after thermal injury. Br J Pharmacol. 1984;82:217–22.

47. Ansel JC, Brown JR, Payan DG, Brown MA. Substance P selectively activates TNF-alpha gene expression in murine mast cells. J Immunol [Internet]. 1993;150:4478–85. Available from: http://www.ncbi.nlm.nih.gov/pubmed/7683320

48. Mikami N, Matsushita H, Kato T, Kawasaki R, Sawazaki T, Kishimoto T, et al. Calcitonin Gene-Related Peptide Is an Important Regulator of Cutaneous Immunity: Effect on Dendritic Cell and T Cell Functions. J Immunol [Internet]. 2011;186:6886–93. Available from: http://www.jimmunol.org/cgi/doi/10.4049/jimmunol.1100028

49. Ding W, Stohl LL, Wagner JA, Granstein RD. Calcitonin Gene-Related Peptide Biases Langerhans Cells toward Th2-Type Immunity. J Immunol [Internet]. 2008;181:6020–6. Available from: http://www.jimmunol.org/cgi/doi/10.4049/jimmunol.181.9.6020

50. Ogoshi F, Yin HZ, Kuppumbatti Y, Song B, Amindari S, Weiss JH. Tumor necrosis-factor-alpha (TNF-α) induces rapid insertion of Ca2+-permeable α-amino-3-hydroxyl-5-methyl-4-isoxazole- propionate (AMPA)/kainate (Ca-A/K) channels in a subset of hippocampal pyramidal neurons. Exp Neurol. 2005;193:384–93.

51. Iversen LL, Jessell T, Kanazawa I. Release and metabolism of substance P in rat hypothalamus. Nature. 1976;264:81–3.

52. Rasley A, Bost KL, Olson JK, Miller SD, Marriott I. Expression of functional NK-1 receptors in murine microglia. Glia. 2002;37:258–67.

53. Lieb K, Schaller H, Bauer J, Berger M, Schulze-Osthoff K, Fiebich BL. Substance P and

histamine induce interleukin-6 expression in human astrocytoma cells by a mechanism involving protein kinase C and nuclear factor-IL-6. JNeurochem [Internet]. 1998;70:1577–83. Available from: pm:9523575

54. Abbott NJ, Rönnbäck L, Hansson E. Astrocyte-endothelial interactions at the blood-brain barrier. Nat Rev Neurosci. 2006;7:41–53.

55. Zhao P, Waxman SG, Hains BC. Modulation of Thalamic Nociceptive Processing after Spinal Cord Injury through Remote Activation of Thalamic Microglia by Cysteine – Cysteine Chemokine Ligand 21. 2007;27:8893–902.

56. Verge GM, Milligan ED, Maier SF, Watkins LR, Naeve GS, Foster AC. Fractalkine (CX3CL1) and fractalkine receptor (CX3CR1) distribution in spinal cord and dorsal root ganglia under basal and neuropathic pain conditions. Eur J Neurosci. 2004;20:1150–60.

57. Lindia JA, McGowan E, Jochnowitz N, Abbadie C. Induction of CX3CL1 expression in astrocytes and CX3CR1 in microglia in the spinal cord of a rat model of neuropathic pain. J Pain. 2005;6:434–8.

58. Sokolowski JD, Chabanon-Hicks CN, Han CZ, Heffron DS, Mandell JW. Fractalkine is a “find-me” signal released by neurons undergoing ethanol-induced apoptosis. Front Cell Neurosci. 2014;8:1–10.

59. Clark AK, Malcangio M. Microglial signalling mechanisms: Cathepsin S and Fractalkine. Exp Neurol [Internet]. Elsevier Inc.; 2012;234:283–92. Available from: http://dx.doi.org/10.1016/j.expneurol.2011.09.012

60. Milligan ED, Sloane EM, Watkins LR. Glia in pathological pain: A role for fractalkine. J Neuroimmunol. 2008;198:113–20.

61. Lehnardt S. Innate immunity and neuroinflammation in the CNS: The role of microglia in toll-like receptor-mediated neuronal injury. Glia. 2010;58:253–63.

62. Manson J, Thiemermann C, Brohi K. Trauma alarmins as activators of damage-induced inflammation. Br J Surg. 2012;99:12–20.

63. Crack PJ, Bray PJ. Toll-like receptors in the brain and their potential roles in neuropathology. Immunol Cell Biol. 2007;85:476–80.

64. Andre R, Lerouet D, Kimber I, Pinteaux E, Rothwell NJ. Regulation of expression of the novel IL-1 receptor family members in the mouse brain. J Neurochem. 2005;95:324–30.

65. Hide I, Tanaka M, Inoue A, Nakajima K, Kohsaka S, Inoue K, et al. Extracellular ATP triggers tumor necrosis factor-α release from rat microglia. J Neurochem. 2000;75:965–72.

66. Babcock AA, Kuziel WA, Rivest S, Owens T. Chemokine expression by glial cells directs leukocytes to sites of axonal injury in the CNS. J Neurosci. 2003;23:7922–30.

67. Bachstetter AD, Xing B, de Almeida L, Dimayuga ER, Watterson DM, Van Eldik LJ. Microglial p38α MAPK is a key regulator of proinflammatory cytokine up-regulation induced by toll-like receptor (TLR) ligands or beta-amyloid (Aβ). J Neuroinflammation. 2011;8:1–12.

68. Boje KM, Arora PK. Microglial-produced nitric oxide and reactive nitrogen oxides mediate neuronal cell death. Brain Res. 1992;587:250–6.

69. Long TC, Tajuba J, Sama P, Saleh N, Swartz C, Parker J, et al. Nanosize titanium dioxide stimulates reactive oxygen species in brain microglia and damages neurons in vitro. Environ Health Perspect. 2007;115:1631–7.

70. Yenari MA, Xu L, Xian NT, Qiao Y, Giffard RG. Microglia potentiate damage to blood-brain barrier constituents: Improvement by minocycline in vivo and in vitro. Stroke. 2006;37:1087–93.

71. Ajami B, Bennett JL, Krieger C, McNagny KM, Rossi FMV. Infiltrating monocytes trigger EAE progression, but do not contribute to the resident microglia pool. Nat Neurosci. 2011;14:1142–50.

72. Devetten G, Coutts SB, Hill MD, Goyal M, Eesa M, O'Brien B, et al. Acute corticospinal tract wallerian degeneration is associated with stroke outcome. Stroke. 2010;41:751–6.

73. Domi T, Deveber G, Shroff M, Kouzmitcheva E, MacGregor DL, Kirton A. Corticospinal tract pre-wallerian degeneration: A novel outcome predictor for pediatric stroke on acute MRI. Stroke. 2009;40:780–7.

74. Yu C, Zhu C, Zhang Y, Chen H, Qin W, Wang M, et al. A longitudinal diffusion tensor imaging

study on Wallerian degeneration of corticospinal tract after motor pathway stroke. Neuroimage [Internet]. Elsevier Inc.; 2009;47:451–8. Available from: http://dx.doi.org/10.1016/j.neuroimage.2009.04.066

75. Szydlowska K, Tymianski M. Calcium, ischemia and excitotoxicity. Cell Calcium [Internet]. Elsevier Ltd; 2010;47:122–9. Available from: http://dx.doi.org/10.1016/j.ceca.2010.01.003

76. Beal MF. Mechanisms of excitotoxicity in neurologic diseases. FASEB J. 1992;6:3338–44.

77. Streit WJ, Morioka T, Kalehua AN. MK-801 prevents microglial reaction in rat hippocampus after forebrain ischemia. Neuroreport [Internet]. 1992;3:146–8. Available from: http://journals.lww.com/00001756-199202000-00006

78. Zhang B, Korolj A, Lai BFL, Radisic M. Advances in organ-on-a-chip engineering. Nat Rev Mater [Internet]. Springer US; 2018;3:257–78. Available from: http://dx.doi.org/10.1038/s41578-018-0034-7

79. Zheng F, Fu F, Cheng Y, Wang C, Zhao Y, Gu Z. Organ-on-a-Chip Systems: Microengineering to Biomimic Living Systems. Small. 2016;12:2253–82.

80. Hawkins BT, Davis TP. The Blood-Brain Barrier / Neurovascular Unit in Health and Disease. 2005;57:173–85.

81. Banks WA. The blood brain barrier. Neuroimmune Pharmacol. 2008;21–38.

82. Abbott NJ, Patabendige AAK, Dolman DEM, Yusof SR, Begley DJ. Structure and function of the blood-brain barrier. Neurobiol Dis [Internet]. Elsevier Inc.; 2010;37:13–25. Available from: http://dx.doi.org/10.1016/j.nbd.2009.07.030

83. Kleinman HK, Jacob K. Invasion Assays. Curr Protoc Cell Biol. 1998;00:0–4.

84. Williams-Medina A, Deblock M, Janigro D. In vitro Models of the Blood–Brain Barrier: Tools in Translational Medicine. Front Med Technol. 2021;2:1–20.

85. Maoz BM, Herland A, Fitzgerald EA, Grevesse T, Vidoudez C, Pacheco AR, et al. A linked organ-on-chip model of the human neurovascular unit reveals the metabolic coupling of endothelial and neuronal cells. Nat Biotechnol. 2018;36:865–77.

86. Herland A, Van Der Meer AD, FitzGerald EA, Park TE, Sleeboom JJF, Ingber DE. Distinct contributions of astrocytes and pericytes to neuroinflammation identified in a 3D human blood-brain barrier on a chip. PLoS One. 2016;11:1–21.

87. Park TE, Mustafaoglu N, Herland A, Hasselkus R, Mannix R, FitzGerald EA, et al. Hypoxia-enhanced Blood-Brain Barrier Chip recapitulates human barrier function and shuttling of drugs and antibodies. Nat Commun [Internet]. Springer US; 2019;10:1–12. Available from: http://dx.doi.org/10.1038/s41467-019-10588-0

88. Griep LM, Wolbers F, De Wagenaar B, Ter Braak PM, Weksler BB, Romero IA, et al. BBB on CHIP: Microfluidic platform to mechanically and biochemically modulate blood-brain barrier function. Biomed Microdevices. 2013;15:145–50.

89. Taylor AM, Blurton-jones M, Rhee SW, Cribbs DH, Cotman CW. A microfluidic culture platform for CNS axonal injury , regeneration and transport. 2005;2:599–605.

90. Taylor AM, Rhee SW, Tu CH, Cribbs DH, Cotman CW, Jeon NL. Microfluidic multicompartment device for neuroscience research. Langmuir. 2003;19:1551–6.

91. Peyrin JM, Deleglise B, Saias L, Vignes M, Gougis P, Magnifico S, et al. Axon diodes for the reconstruction of oriented neuronal networks in microfluidic chambers. Lab Chip. 2011;11:3663–73.

92. Virlogeux A, Moutaux E, Christaller W, Genoux A, Bruyère J, Fino E, et al. Reconstituting Corticostriatal Network on-a-Chip Reveals the Contribution of the Presynaptic Compartment to Huntington's Disease. Cell Rep. 2018;22:110–22.

93. Iannielli A, Ugolini GS, Cordiglieri C, Cabassi T, Rasponi M, Broccoli V, et al. Reconstitution of the Human Nigro-striatal Pathway on-a-Chip Reveals OPA1-Dependent Mitochondrial Resource Reconstitution of the Human Nigro-striatal Pathway on-a-Chip Reveals OPA1-Dependent Mitochondrial Defects and Loss of Dopaminergic Synapses. CellReports [Internet]. The Author(s); 2019;29:4646–56. Available from: https://doi.org/10.1016/j.celrep.2019.11.111

94. Guttenplan KA, Liddelow SA. Astrocytes and microglia : Models and tools. J Exp Med.

2018;216:71–83.

95. Harry GJ, Kraft AD. Neuroinflammation and microglia: considerations and approaches for neurotoxicity assessment. Expert Opin Drug Metab Toxicol. 2008;4:1265–77.

96. Liddelow SA, Guttenplan KA, Clarke LE, Bennett FC, Bohlen CJ, Schirmer L, et al. Neurotoxic reactive astrocytes are induced by activated microglia. Nature [Internet]. Nature Publishing Group; 2017;541:481–7. Available from: http://www.nature.com/doifinder/10.1038/nature21029

97. He BP, Wen W, Strong MJ. Activated microglia (BV-2) facilitation of TNF-α-mediated motor neuron death in vitro. J Neuroimmunol. 2002;128:31–8.

98. Yawata I, Takeuchi H, Doi Y, Liang J, Mizuno T, Suzumura A. Macrophage-induced neurotoxicity is mediated by glutamate and attenuated by glutaminase inhibitors and gap junction inhibitors. Life Sci. 2008;82:1111–6.

99. Devinsky O, Vezzani A, Najjar S, Lanerolle NC De, Rogawski MA. Glia and epilepsy : excitability and inflammation. Trends Neurosci [Internet]. Elsevier Ltd; 2013;36:174–84. Available from: http://dx.doi.org/10.1016/j.tins.2012.11.008

100. Taylor DL, Jones F, Chen Seho Kubota ESF, Pocock JM. Stimulation of microglial metabotropic glutamate receptor mGlu2 triggers tumor necrosis factor α-induced neurotoxicity in concert with microglial-derived Fas ligand. J Neurosci. 2005;25:2952–64.

101. Eyo UB, Peng J, Murugan M, Xu P, Margolis DJ, Wu L. Regulation of Physical Microglia – Neuron Interactions by Fractalkine Signaling after Status Epilepticus. 2016;3:1–14.

102. Kato G, Inada H, Wake H, Akiyoshi R, Miyamoto A, Eto K, et al. Microglial contact prevents excess depolarization and rescues neurons from excitotoxicity. Eneuro. 2016;3:1–9.

103. Vinet J, Weering HRJ Van, Heinrich A, Kälin RE, Wegner A, Brouwer N, et al. Neuroprotective function for ramified microglia in hippocampal excitotoxicity. J Neuroinflammation. 2012;9:27.

104. Liu R, Meng X, Yu X, Wang G, Dong Z, Zhou Z. From 2D to 3D Co-Culture Systems : A Review of Co-Culture Models to Study the Neural Cells Interaction. Int J Mol Sci. 2022;23:13116.

105. Haenseler W, Sansom SN, Buchrieser J, Newey SE, Moore CS, Nicholls FJ, et al. A Highly Efficient Human Pluripotent Stem Cell Microglia Model Displays a Neuronal-Co-culture-Specific Expression Profile and Inflammatory Response. Stem Cell Reports [Internet]. ElsevierCompany.; 2017;8:1727–42. Available from: http://dx.doi.org/10.1016/j.stemcr.2017.05.017

106. Xie Z, Smith CJ, Van Eldik LJ. Activated Glia Induce Neuron Death Via MAP Kinase Signaling Pathways Involving JNK and p38. Glia. 2004;45:170–9.

107. Shavali S, Combs CK, Ebadi M. Reactive macrophages increase oxidative stress and alpha-synuclein nitration during death of dopaminergic neuronal cells in co-culture: Relevance to parkinson's disease. Neurochem Res. 2006;31:85–94.

108. Söllvander S, Nikitidou E, Brolin R, Söderberg L, Sehlin D, Lannfelt L, et al. Accumulation of amyloid-β by astrocytes result in enlarged endosomes and microvesicle-induced apoptosis of neurons. Mol Neurodegener [Internet]. Molecular Neurodegeneration; 2016;11:1–19. Available from: http://dx.doi.org/10.1186/s13024-016-0098-z

109. Chavarría C, Rodríguez-Bottero S, Quijano C, Cassina P, Souza JM. Impact of monomeric, oligomeric and fibrillar alpha-synuclein on astrocyte reactivity and toxicity to neurons. Biochem J [Internet]. 2018;475:3153–69. Available from: https://portlandpress.com/biochemj/article/475/19/3153/49813/Impact-of-monomeric-oligomeric-and-fibrillar-alpha

110. Takahashi M, Yamada T, Nakanishi K, Fujita K, Nakajima K, Nobusawa E, et al. Influenza A virus infection of primary cultured cells from rat fetal brain. Park Relat Disord. 1997;3:97–102.

111. Ravichandran V, Major EO, Ibe C, Monaco M, Girisetty M, Hewlett IK. Susceptibility of human primary neuronal cells to Xenotropic Murine Leukemia Virus-related (XMRV) virus infection. Virol J. 2011;8:2–5.

112. Culbert AA, Skaper SD, Howlett DR, Evans NA, Facci L, Soden PE, et al. MAPK-activated Protein Kinase 2 Deficiency in Microglia Inhibits Pro-inflammatory Mediator Release and Resultant Neurotoxicity RELEVANCE TO NEUROINFLAMMATION IN A TRANSGENIC MOUSE

MODEL OF ALZHEIMER DISEASE *. J Biol Chem. 2006;281:23658–67.

113. Gresa-Arribas N, Vieitez C, Dentesano G, Serratosa J, Saura J, Sola C. Modelling Neuroinflammation In Vitro: A Tool to Test the Potential Neuroprotective Effect of Anti-Inflammatory Agents. PLoS One. 2012;7.

114. Roque PJ, Costa LG. Co-culture of Neurons and Microglia. Curr Protoc Toxicol. 2017;74:11–24.

115. Bohlen CJ, Bennett FC, Tucker AF, Collins HY, Mulinyawe SB, Barres BA. Diverse Requirements for Microglial Survival, Specification, and Function Revealed by Defined-Medium Cultures. Neuron [Internet]. Elsevier Inc.; 2017;94:759-773.e8. Available from: http://dx.doi.org/10.1016/j.neuron.2017.04.043

116. Jones E V, Cook D, Murai KK. A Neuron-Astrocyte Co-Culture System to Investigate Astrocyte-Secreted Factors in Mouse Neuronal Development. Astrocytes. Humana Press; 2012. p. 341–52.

117. Efremova L, Schildknecht S, Adam M, Pape R, Gutbier S, Hanf B, et al. Prevention of the degeneration of human dopaminergic neurons in an astrocyte co-culture system allowing endogenous drug metabolism. Br J Pharmacol. 2015;172:4119–32.

118. Ozog MA, Siushansian R, Naus CCG. Blocked Gap Junctional Coupling Increases Glutamate-Induced Neurotoxicity in. J Neuropathol Exp Neurol. 2002;61:132–41.

119. Mizuno T, Kuno R, Nitta A, Nabeshima T, Zhang G, Kawanokuchi J, et al. Protective effects of nicergoline against neuronal cell death induced by activated microglia and astrocytes. Brain Reseach. 2005;1066:78–85.

120. Chapman CAR, Chen H, Stamou M, Biener J, Biener MM, Lein PJ, et al. Nanoporous gold as a neural interface coating: Effects of topography, surface chemistry, and feature size. ACS Appl Mater Interfaces. 2015;7:7093–100.

121. Harry GJ, Kraft AD. Microglia in the developing brain: a potential target with lifetime effects. Neurotoxicology [Internet]. Elsevier B.V.; 2012;33:191–206. Available from:

http://dx.doi.org/10.1016/j.neuro.2012.01.012

122. Coltman BW, Ide CF. Temporal characterization of microglia, IL-1β-like immunoreactivity and astrocytes in the dentate gyrus of hippocampal organotypic slice cultures. Int J Dev Neurosci. 1996;14:707–19.

123. Miller LDP, Mahanty NK, Connor JA, Landis DMD. Spontaneous pyramidal cell death in organotypic slice cultures from rat hippocampus is prevented by glutamate receptor antagonists. Neuroscience [Internet]. 1994;63:471–87. Available from: https://linkinghub.elsevier.com/retrieve/pii/0306452294905444

124. Hailer NP, Järhult JD, Nitsch R. Resting microglial cells in vitro: Analysis of morphology and adhesion molecule expression in organotypic hippocampal slice cultures. Glia. 1996;18:319–31.

125. del Rio JA, Heimrich B, Soriano E, Schwegler H, Frotscher M. Proliferation and differentiation of goal fibrillary acidic protein-immunoreactive goal cells in organotypic slice cultures of rat hippocampus. Neuroscience. 1991;43:335–47.

126. Huuskonen J, Suuronen T, Miettinen R, van Groen T, Salminen A. A refined in vitro model to study inflammatory responses in organotypic membrane culture of postnatal rat hippocampal slices. J Neuroinflammation. 2005;2.

127. Taylor AM, Blurton-Jones M, Rhee SW, Cribbs DH, Cotman CW, Jeon NL. A microfluidic culture platform for CNS axonal injury, regeneration and transport. Nat Methods. 2005;2:599–605.

128. Wayman GA, Bose DD, Yang D, Lesiak A, Bruun D, Impey S, et al. PCB-95 Modulates the Calcium-Dependent Signaling Pathway Responsible for Activity-Dependent Dendritic Growth. Environ Health Perspect. 2012;120:1003–9.

129. Chapman CAR, Wang L, Chen H, Garrison J, Lein PJ, Seker E. Nanoporous Gold Biointerfaces: Modifying Nanostructure to Control Neural Cell Coverage and Enhance Electrophysiological Recording Performance. Adv Funct Mater [Internet]. 2016;1604631:1604631. Available from: http://doi.wiley.com/10.1002/adfm.201604631

130. Kreuz T, Chicharro D, Houghton C, Andrzejak RG, Mormann F. Monitoring spike train synchrony. J Neurophysiol. 2013;109:1457–72.

131. Mulansky M, Kreuz T. PySpike—A Python library for analyzing spike train synchrony. SoftwareX [Internet]. Elsevier B.V.; 2016;5:183–9. Available from: http://dx.doi.org/10.1016/j.softx.2016.07.006

132. Enright HA, Lam D, Sebastian A, Sales AP, Cadena J, Hum NR, et al. Functional and transcriptional characterization of complex neuronal co-cultures. Sci Rep. 2020;10:1–14.

133. Charlesworth P, Cotterill E, Morton A, Grant SGN, Eglen SJ. Quantitative differences in developmental profiles of spontaneous activity in cortical and hippocampal cultures. Neural Dev. 2015;10:1–10.

134. Yuste R. From the neuron doctrine to neural networks. Nat Rev Neurosci. Nature Publishing Group; 2015;16:487–97.

135. Pankevich DE, Altevogt BM, Dunlop J, Gage FH, Hyman SE. Improving and accelerating drug development for nervous system disorders. Neuron [Internet]. Elsevier Inc.; 2014;84:546–53. Available from: http://dx.doi.org/10.1016/j.neuron.2014.10.007

136. Berdichevsky Y, Staley J, Yarmush ML. Building and manipulating neural pathways with microfluidics †. 2010;999–1004.

137. Polanco JC, Li C, Durisic N, Sullivan R, Götz J. Exosomes taken up by neurons hijack the endosomal pathway to spread to interconnected neurons. Acta Neuropathol Commun. Acta Neuropathologica Communications; 2018;6:10.

138. Urrea L, Segura-Feliu M, Masuda-Suzukake M, Hervera A, Pedraz L, García Aznar JM, et al. Involvement of Cellular Prion Protein in α-Synuclein Transport in Neurons. Mol Neurobiol. Molecular Neurobiology; 2018;55:1847–60.

139. Brahic M, Bousset L, Bieri G, Melki R, Gitler AD. Axonal transport and secretion of fibrillar forms of α-synuclein, Aβ42 peptide and HTTExon 1. Acta Neuropathol. Springer Berlin Heidelberg; 2016;131:539–48.

140. Akira S, Takeda K. Toll-like receptor signalling. Nat Rev Immunol. 2004;4:499–511.

141. Takeda S, Wegmann S, Cho H, Devos SL, Commins C, Roe AD, et al. Neuronal uptake and propagation of a rare phosphorylated high-molecular-weight tau derived from Alzheimer's disease brain. Nat Commun. 2015;6.

142. Song HL, Shim S, Kim DH, Won SH, Joo S, Kim S, et al. β-Amyloid is transmitted via neuronal connections along axonal membranes. Ann Neurol. 2014;75:88–97.

143. Samson AJ, Robertson G, Zagnoni M, Connolly CN. Neuronal networks provide rapid neuroprotection against spreading toxicity. Sci Rep [Internet]. Nature Publishing Group; 2016;6:1–11. Available from: http://dx.doi.org/10.1038/srep33746

144. Southam KA, King AE, Blizzard CA, McCormack GH, Dickson TC. Microfluidic primary culture model of the lower motor neuron-neuromuscular junction circuit. J Neurosci Methods [Internet]. Elsevier B.V.; 2013;218:164–9. Available from: http://dx.doi.org/10.1016/j.jneumeth.2013.06.002

145. Bellmann J, Goswami RY, Girardo S, Rein N, Hosseinzadeh Z, Hicks MR, et al. Biomaterials A customizable microfluidic platform for medium-throughput modeling of neuromuscular circuits. Biomaterials [Internet]. Elsevier; 2019;225:119537. Available from: https://doi.org/10.1016/j.biomaterials.2019.119537

146. Goshi N, Morgan RK, Lein PJ, Seker E. A primary neural cell culture model to study neuron, astrocyte, and microglia interactions in neuroinflammation. J Neuroinflammation. Journal of Neuroinflammation; 2020;17:1–16.

147. Tiryaki VM, Ayres VM, Ahmed I, Shreiber DI. Differentiation of reactive-like astrocytes cultured on nanofibrillar and comparative culture surfaces. Nanomedicine. 2015;10:529–45.

148. Fiala JC, Harris KM. Dendrite Structure. Dendrites 2. 1999. p. 1–11.

149. Partadiredja G, Miller R, Oorschot DE. The number, size, and type of axons in rat subcortical white matter on left and right sides: A stereological, ultrastructural study. J Neurocytol. 2003;32:1165–79.

150. Robertson G, Bushell TJ, Zagnoni M. Chemically induced synaptic activity between mixed primary hippocampal co-cultures in a microfluidic system. Integr Biol [Internet]. 2014;6:636–44. Available from: http://xlink.rsc.org/?DOI=C3IB40221E

151. Martin DP, Wallace TL, Johnson EM. Cytosine arabinoside kills postmitotic neurons in a fashion resembling trophic factor deprivation: Evidence that a deoxycytidine-dependent process may be required for nerve growth factor signal transduction. J Neurosci. 1990;10:184–93.

152. Froeter P, Huang Y, Cangellaris O V., Huang W, Dent EW, Gillette MU, et al. Toward intelligent synthetic neural circuits: Directing and accelerating neuron cell growth by self-rolled-up silicon nitride microtube array. ACS Nano. 2014;8:11108–17.

153. Vitzthum L, Chen X, Kintner DB, Huang Y, Chiu SY, Williams J, et al. Study of Na+/H+ exchange-mediated pHi regulations in neuronal soma and neurites in compartmentalized microfluidic devices. Integr Biol. 2010;2:58–64.

154. Pirlo RK, Sweeney AJ, Ringeisen BR, Kindy M, Gao BZ. Biochip/laser cell deposition system to assess polarized axonal growth from single neurons and neuron/glia pairs in microchannels with novel asymmetrical geometries. Biomicrofluidics. 2011;5.

155. Li L, Ren L, Liu W, Wang JC, Wang Y, Tu Q, et al. Spatiotemporally controlled and multifactor involved assay of neuronal compartment regeneration after chemical injury in an integrated microfluidics. Anal Chem. 2012;84:6444–53.

156. Bastiaens A, Sabahi-Kaviani R, Luttge R. Nanogrooves for 2D and 3D Microenvironments of SH-SY5Y Cultures in Brain-on-Chip Technology. Front Neurosci. 2020;14:1–11.

157. Doolin MT, Ornstein TS, Stroka KM. Nuclear deformation in response to mechanical confinement is cell type dependent. Cells. 2019;8:1–17.

158. Le Berre M, Aubertin J, Piel M. Fine control of nuclear confinement identifies a threshold deformation leading to lamina rupture and induction of specific genes. Integr Biol (United Kingdom). 2012;4:1406–14.

159. Behar TN, Smith S V., Kennedy RT, Mckenzi JM, Maric I, Barker JL. GABAB receptors

mediate motility signals for migrating embryonic cortical cells. Cereb Cortex. 2001;11:744–53.

160. Haas MA, Chuckowree JA, Chung RS, Vickers JC, Dickson TC. Identification and characterization of a population of motile neurons in long-term cortical culture. Cell Motil Cytoskeleton. 2007;64:274–87.

161. Lepekhin EA, Eliasson C, Berthold CH, Berezin V, Bock E, Pekny M. Intermediate filaments regulate astrocyte motility. J Neurochem. 2001;79:617–25.

162. Majumdar D, Gao Y, Li D, Webb DJ. Co-culture of neurons and glia in a novel microfluidic platform. J Neurosci Methods [Internet]. Elsevier B.V.; 2011;196:38–44. Available from: http://dx.doi.org/10.1016/j.jneumeth.2010.12.024

163. Park J, Koito H, Li J, Han A. Multi-compartment neuron-glia co-culture platform for localized CNS axon-glia interaction study. Lab Chip. 2012;12:3296–304.

164. Hosmane S, Yang IH, Ruffin A, Thakor N, Venkatesan A. Circular compartmentalized microfluidic platform: Study of axon-glia interactions. Lab Chip. 2010;10:741–7.

165. Lee HU, Nag S, Blasiak A, Jin Y, Thakor N, Yang IH. Subcellular Optogenetic Stimulation for Activity-Dependent Myelination of Axons in a Novel Microfluidic Compartmentalized Platform. ACS Chem Neurosci. 2016;7:1317–24.

166. Accardi M V., Pugsley MK, Forster R, Troncy E, Huang H, Authier S. The emerging role of in vitro electrophysiological methods in CNS safety pharmacology. J Pharmacol Toxicol Methods [Internet]. The Authors; 2016;81:47–59. Available from: http://dx.doi.org/10.1016/j.vascn.2016.03.008

167. Hong N, Joo S, Nam Y. Characterization of Axonal Spikes in Cultured Neuronal Networks Using Microelectrode Arrays and Microchannel Devices. IEEE Trans Biomed Eng. 2017;64:492–8.

168. Pan L, Alagapan S, Franca E, Demarse T, Brewer GJ, Wheeler BC. Large extracellular spikes recordable from axons in microtunnels. IEEE Trans Neural Syst Rehabil Eng. IEEE; 2014;22:453–9.

169. Wang L, Riss M, Buitrago JO, Claverol-tintur E. Biophysics of microchannel-enabled neuron – electrode interfaces. 026010.

170. Lewandowska MK, Bakkum DJ, Rompani SB, Hierlemann A. Recording large extracellular spikes in microchannels along many axonal sites from individual neurons. PLoS One. 2015;10:1–24.

171. Shimba K, Sakai K, Arimatsu K, Kotani K, Jimbo Y. Long term observation of propagating action potentials along the axon in a microtunnel device. Int IEEE/EMBS Conf Neural Eng NER. IEEE; 2013;945–8.

172. Habibey R, Golabchi A, Latifi S, Difato F, Blau A. A microchannel device tailored to laser axotomy and long-term microelectrode array electrophysiology of functional regeneration. Lab Chip. Royal Society of Chemistry; 2015;15:4578–90.

173. Lewandowska MK, Radivojević M, Jäckel D, Müller J, Hierlemann AR. Cortical axons, isolated in channels, display activity-dependent signal modulation as a result of targeted stimulation. Front Neurosci. 2016;10.

174. Brewer GJ, Boehler MD, Leondopulos S, Pan L, Alagapan S, DeMarse TB, et al. Toward a self-wired active reconstruction of the hippocampal trisynaptic loop: DG-CA3. Front Neural Circuits. 2013;7:1–8.

175. Honegger T, Scott MA, Yanik MF, Voldman J. Electrokinetic confinement of axonal growth for dynamically configurable neural networks. Lab Chip. 2013;13:589–98.

176. Call CL, Bergles DE. Cortical neurons exhibit diverse myelination patterns that scale between mouse brain regions and regenerate after demyelination. Nat Commun [Internet]. Springer US; 2021;12. Available from: http://dx.doi.org/10.1038/s41467-021-25035-2

177. Zhou B, Zuo YX, Jiang RT. Astrocyte morphology: Diversity, plasticity, and role in neurological diseases. CNS Neurosci Ther. 2019;25:665–73.

178. Liewald D, Miller R, Logothetis N, Wagner HJ, Schüz A. Distribution of axon diameters in cortical white matter: an electron-microscopic study on three human brains and a macaque. Biol

Cybern. 2014;108:541–57.

179. Ristola M, Sukki L, Azevedo MM. A compartmentalized neuron- oligodendrocyte co-culture device for myelin research : design , fabrication and functionality testing. J Micromechanics Microengineering. 2019;29.

180. Eggen BJL, Raj D, Hanisch U. Microglial Phenotype and Adaptation. J Neuroimmune Pharmacol. 2013;8:807–23.

181. Jensen CJ, Massie A, De Keyser J. Immune players in the CNS: the astrocyte. J Neuroimmune Pharmacol. 2013;8:824–39.

182. Polikov VS, Tresco PA, Reichert WM. Response of brain tissue to chronically implanted neural electrodes. J. Neurosci. Methods. 2005.

183. Li Q, Barres BA. Microglia and macrophages in brain homeostasis and disease. Nat Rev Immunol [Internet]. Nature Publishing Group; 2017;18:225–42. Available from: http://dx.doi.org/10.1038/nri.2017.125

184. Salter MW, Stevens B. Microglia emerge as central players in brain disease. Nat Med [Internet]. Nature Publishing Group; 2017;23:1018–27. Available from: http://dx.doi.org/10.1038/nm.4397

185. Miller SJ. Astrocyte heterogeneity in the adult central nervous system. Front Cell Neurosci. 2018;12:401.

186. Jha MK, Jo M, Kim JH, Suk K. Microglia-Astrocyte Crosstalk: An Intimate Molecular Conversation. Neuroscientist. 2019;25:227–40.

187. Szepesi Z, Manouchehrian O, Bachiller S, Deierborg T. Bidirectional Microglia – Neuron Communication in Health and Disease. Front Cell Neurosci. 2018;12:323.

188. Harry GJ, Kraft AD. Neuroinflammation and microglia: Considerations and approaches for neurotoxicity assessment. Expert Opin Drug Metab Toxicol. 2008;4:1265–77.

189. Luna-Medina R, Cortes-Canteli M, Alonso M, Santos A, Perez-Castillo A. Regulation of inflammatory response in neural cells in vitro by thiadiazolidinones derivatives through

peroxisome proliferator-activated receptor γ activation. J Biol Chem. 2005;280:21453–62.

190. Chapman CAR, Chen H, Stamou M, Biener J, Biener MM, Lein PJ, et al. Nanoporous gold as a neural interface coating: effects of topography, surface chemistry, and feature size. ACS Appl Mater Interfaces. 2015;7:7093–100.

191. von Bartheld CS, Bahney J, Herculano-houzel S. The Search for True Numbers of Neurons and Glial Cells in the Human Brain: A Review of 150 Years of Cell Counting. J Comp Neurol. 2016;524:3865–95.

192. Savchenko VL, Mckanna JA, Nikonenko IR, Skibo GG. Microglia and astrocytes in the adult rat brain: comparative immunocytochemical analysis demonstrates the efficacy of lipocortin 1 immunoreactivity IMMUNOREACTIVITY. Neuroscience. 2000;96:195–203.

193. Lindholm D, Castrdn E, Kiefer R, Zafra F, Thoenen H. Transforming Growth Factor-ßl in the Rat Brain: Increase after Injury and Inhibition of Astrocyte Proliferation. J Cell Biol. 1992;117:395–400.

194. Nishiyama A, Boshans L, Goncalves CM, Wegrzyn J, Patel KD. Lineage, fate, and fate potential of NG2-glia. Brain Res [Internet]. Elsevier; 2016;1638:116–28. Available from: http://dx.doi.org/10.1016/j.brainres.2015.08.013

195. Wellman SM, Kozai TDY. In vivo spatiotemporal dynamics of NG2 glia activity caused by neural electrode implantation. Biomaterials [Internet]. Elsevier Ltd; 2018;164:121–33. Available from: https://doi.org/10.1016/j.biomaterials.2018.02.037

196. Dimou L, Gallo V. NG2-glia and their functions in the central nervous system. Glia. 2015;63:1429–51.

197. Batista CRA, Gomes GF, Candelario-jalil E, Fiebich BL, de Oliveira ACP. Lipopolysaccharide-Induced Neuroinflammation as a Bridge to Understand Neurodegeneration. Int J Mol Sci. 2019;20:2293.

198. Nazem A, Sankowski R, Bacher M, Al-abed Y. Rodent models of neuroinflammation for Alzheimer’s disease. J Neuroinflammation [Internet]. ???; 2015;12:74. Available from: ???

199. Dutta G, Zhang P, Liu B. The lipopolysaccharide Parkinson's disease animal model: mechanistic studies and drug discovery. Fundam Clin Pharmacol. 2008;22:453–64.

200. Henry CJ, Huang Y, Wynne A, Hanke M, Himler J, Bailey MT, et al. Minocycline attenuates lipopolysaccharide (LPS)-induced neuroinflammation, sickness behavior, and anhedonia. J Neuroinflammation. 2008;5:1–14.

201. Wang X, Chen S, Ma G, Ye M, Lu G. Involvement of proinflammatory factors, apoptosis, caspase-3 activation and Ca2+ disturbance in microglia activation-mediated dopaminergic cell degeneration. Mech Ageing Dev. 2005;126:1241–54.

202. Nimmervoll B, White R, Yang J, An S, Henn C, Sun J, et al. LPS-induced microglial secretion of TNFα increases activity-dependent neuronal apoptosis in the neonatal cerebral cortex. Cereb Cortex. 2013;23:1742–55.

203. Schiweck J, Eickholt BJ, Murk K. Important shapeshifter: mechanisms allowing astrocytes to respond to the changing nervous system during development, injury and disease. Front Cell Neurosci. 2018;12:261.

204. Mathews PM, Levy E. Cystatin C in aging and in Alzheimer ' s disease. Ageing Res Rev [Internet]. Elsevier B.V.; 2016;32:38–50. Available from: http://dx.doi.org/10.1016/j.arr.2016.06.003

205. Lewitt MS, Boyd GW. The Role of Insulin-Like Growth Factors and Insulin-Like Growth Factor – Binding Proteins in the Nervous System. Biochem Insights. 2019;12:1–18.

206. Su B, Cai W, Zhang C, Martinez V, Lombet A, Perbal B. The expression of ccn3 (nov)* RNA and protein in the rat central nervous system is developmentally regulated. J Clin Pathol Mol Pathol. 2001;54:184–91.

207. Korecka XJA, Moloney XEB, Eggers XR, Hobo B, Scheffer S, Ras-verloop N, et al. Repulsive Guidance Molecule a (RGMa) Induces Neuropathological and Behavioral Changes That Closely Resemble Parkinson ' s Disease. J Neurosci. 2017;37:9361–79.

208. Rosenstein JM, Krum JM, Ruhrberg C. VEGF in the nervous system. Organogenesis.

2010;6:107–14.

209. Yang Y, Hu W, Jiang S, Wang B, Li Y, Fan C, et al. The emerging role of adiponectin in cerebrovascular and neurodegenerative diseases. Biochem Biophys Acta [Internet]. Elsevier B.V.; 2015;1852:1887–94. Available from: http://dx.doi.org/10.1016/j.bbadis.2015.06.019

210. Schindowski K, Bohlen O Von, Strelau J, Ridder DA, Herrmann O, Schober A, et al. Regulation of GDF-15 , a distant TGF-β superfamily member , in a mouse model of cerebral ischemia. 2011;399–409.

211. Goldmann T, Prinz M. Role of Microglia in CNS Autoimmunity. Clin Dev Immunol. 2013;2013.

212. Ambrosini E, Columba-cabezas S, Serafini B, Muscella A, Aloisi F. Astrocytes are the major intracerebral source of macrophage inflammatory protein-3α/CCL20 in relapsing experimental autoimmune encephalomyelitis and in vitro. Glia. 2003;41:290–300.

213. Jha MK, Lee S, Park DH, Kook H, Park KG, Lee IK, et al. Diverse functional roles of lipocalin-2 in the central nervous system. Neurosci Biobehav Rev [Internet]. Elsevier Ltd; 2015;49:135–56. Available from: http://dx.doi.org/10.1016/j.neubiorev.2014.12.006

214. Yu H, Liu X, Zhong Y. The Effect of Osteopontin on Microglia. Biomed Res Int. 2017;2017.

215. Kothur K, Wienholt L, Brilot F, Dale RC. CSF cytokines/chemokines as biomarkers in neuroinflammatory CNS disorders: A systematic review. Cytokine [Internet]. Elsevier Ltd; 2016;77:227–37. Available from: http://dx.doi.org/10.1016/j.cyto.2015.10.001

216. Papageorgiou IE, Lewen A, Galow L V, Cesetti T, Scheffel J, Regen T, et al. TLR4-activated microglia require IFN- γ to induce severe neuronal dysfunction and death in situ. Proc Natl Acad Sci. 2016;113:10–5.

217. Fernández-Arjona M del M, Grondona JM, Granados-durán P, Fernández-llebrez P, López-ávalos MD. Microglia Morphological Categorization in a Rat Model of Neuroinflammation by Hierarchical Cluster and Principal Components Analysis. Front Cell Neurosci. 2017;11:235.

218. Nakamura Y, Si QS, Kataoka K. Lipopolysaccharide-induced microglial activation in culture: temporal profiles of morphological change and release of cytokines and nitric oxide. Neurosci

Res. 1999;35:95–100.

219. Abd-El-Basset E, Fedoroff S. Effect of Bacterial Wall Lipopolysaccharide (LPS) on Morphology, Motility, and Cytoskeletal Organization of Microglia in Cultures. J Neurosci Reseach. 1995;41:222–37.

220. Persson M, Brantefjord M, Hansson E, Ronnback L. Lipopolysaccharide increases microglial GLT-1 expression and glutamate uptake capacity in vitro by a mechanism dependent on TNF-α. Glia. 2005;51:111–20.

221. Liang C, Park AY, Guan J. In vitro scratch assay: a convenient and inexpensive method for analysis of cell migration in vitro. Nat Protoc. 2007;2:329–33.

222. Faber-Elman A, Solomon A, Abraham JA, Marikovsky M, Schwartz M. Involvement of Wound-associated Factors in Rat Brain Astrocyte Migratory Response to Axonal Injury : In Vitro Simulation. J Clin Invest. 1996;97:162–71.

223. Hirano S, Yonezawa T, Hasegawa H, Hattori S, Greenhill NS, Davis PF, et al. Astrocytes express type VIII collagen during the repair process of brain cold injury. Biochem Biophys Res Commun. 2004;317:437–43.

224. Tecoma E, Monyer H, Goldberg MP, Choi DW. Traumatic Neuronal Injury In Vitro Is Attenuated by NMDA Antagonists. Neruon. 1989;2:1541–5.

225. Donat CK, Scott G, Gentleman SM, Sastre M. Microglial Activation in Traumatic Brain Injury. Front Aging Neurosceince. 2017;9.

226. Gulino M, Kim D, Pané S, Santos SD, Pêgo AP. Tissue response to neural implants: The use of model systems toward new design solutions of implantable microelectrodes. Front Neurosci. 2019;13:1–24.

227. Burda JE, Bernstein AM, Sofroniew M V. Astrocyte roles in traumatic brain injury. Exp Neurol [Internet]. Elsevier Inc.; 2016;275:305–15. Available from: http://dx.doi.org/10.1016/j.expneurol.2015.03.020

228. Wang H, Song G, Chuang H, Chiu C, Abdelmaksoud A, Ye Y, et al. Portrait of glial scar in

neurological diseases. Int J Immunopathol Pharmacol. 2018;31:1–6.

229. Salatino JW, Ludwig KA, Kozai TDY, Purcell EK. Glial responses to implanted electrodes in the brain. Nat Biomed Eng. 2017;1:862–77.

230. Hu F, Ku MC, Markovic D, Dzaye OD, Lehnardt S, Synowitz M, et al. Glioma-associated microglial MMP9 expression is upregulated by TLR2 signaling and sensitive to minocycline. Int J Cancer. 2014;135:2569–78.

231. Hsu JC, Bourguignon LYW, Adams CM, Peyrollier K, Zhang H, Fandel T, et al. Matrix Metalloproteinase-9 Facilitates Glial Scar Formation in the Injured Spinal Cord. J Neurosci. 2008;28:13467–77.

232. Boche D, Cunningham C, Gauldie J, Perry VH. Transforming growth factor-β1-mediated neuroprotection against excitotoxic injury in vivo. J Cereb Blood Flow Metabolosm. 2003;23:1174–82.

233. Luo J, Elwood F, Britschgi M, Villeda S, Zhang H, Ding Z, et al. Colony-stimulating factor 1 receptor (CSF1R) signaling in injured neurons facilitates protection and survival. J Exp Med. 2013;210:157–72.

234. Schousboe A, Waagepetersen HS. Role of astrocytes in glutamate homeostasis: Implications for excitotoxicity. Neurotox Res. 2005;8:221–5.

235. Bonde C, Sarup A, Schousboe A, Gegelashvili G, Zimmer J, Noraberg J. Neurotoxic and neuroprotective effects of the glutamate transporter inhibitor DL-threo-beta-benzyloxyaspartate (DL-TBOA) during physiological and ischemia-like conditions. Neurochem Int. 2003;43:371–80.

236. Masuch A, Shieh CH, van Rooijen N, van Calker D, Biber K. Mechanism of microglia neuroprotection: Involvement of P2X7, TNFα, and valproic acid. Glia. 2016;64:76–89.

237. Arnoux I, Audinat E. Fractalkine Signaling and Microglia Functions in the Developing Brain. Neural Plast. 2015;2015.

238. Paolicelli RC, Bisht K, Tremblay M-ève. Fractalkine regulation of microglial physiology and consequences on the brain and behavior. Front Cell Neurosci. 2014;8:129.

239. Ueno M, Fujita Y, Tanaka T, Nakamura Y, Kikuta J, Ishii M, et al. Layer V cortical neurons require microglial support for survival during postnatal development. Nat Neurosci. Nature Publishing Group; 2013;16:543–51.

240. Bianchi VE, Locatelli V, Rizzi L. Neurotrophic and Neuroregenerative Effects of GH/IGF1. Int J Mol Sci. 2017;18:2441.

241. Naegele M, Martin R. The good and the bad of neuroinflammation in multiple sclerosis [Internet]. 1st ed. Handb. Clin. Neurol. Elsevier B.V.; 2014. Available from: http://dx.doi.org/10.1016/B978-0-444-52001-2.00003-0

242. Hirsch EC, Vyas S, Hunot S. Neuroinflammation in Parkinson's disease. Park Relat Disord. 2012;18:210–2.

243. Simard M, Nedergaard M. The neurobiology of glia in the context of water and ion homeostasis. Neuroscience. 2004;129:877–96.

244. Potter SM, DeMarse TB. A new approach to neural cell culture for long-term studies. J Neurosci Methods [Internet]. 2001;110:17–24. Available from: https://linkinghub.elsevier.com/retrieve/pii/S0165027001004125

245. Kim R, Joo S, Jung H, Hong N, Nam Y. Recent trends in microelectrode array technology for in vitro neural interface platform. Biomed Eng Lett. 2014;4:129–41.

246. Frank CL, Brown JP, Wallace K, Mundy WR, Shafer TJ. Developmental neurotoxicants disrupt activity in cortical networks on microelectrode arrays: Results of screening 86 compounds during neural network formation. Toxicol Sci. 2017;160:121–35.

247. Shafer TJ, Brown JP, Lynch B, Davila-Montero S, Wallace K, Friedman KP. Evaluation of chemical effects on network formation in cortical neurons grown on microelectrode arrays. Toxicol Sci. 2019;169:436–55.

248. Johnstone AFM, Gross GW, Weiss DG, Schroeder OHU, Gramowski A, Shafer TJ. Microelectrode arrays: A physiologically based neurotoxicity testing platform for the 21st century. Neurotoxicology [Internet]. Elsevier B.V.; 2010;31:331–50. Available from:

http://dx.doi.org/10.1016/j.neuro.2010.04.001

249. Gopal K V. Neurotoxic effects of mercury on auditory cortex networks growing on microelectrode arrays: A preliminary analysis. Neurotoxicol Teratol. 2003;25:69–76.

250. Novellino A, Scelfo B, Palosaari T, Price A, Sobanski T, Shafer TJ, et al. Development of micro-electrode array based tests for neurotoxicity: Assessment of interlaboratory reproducibility with neuroactive chemicals. Front Neuroeng. 2011;4:1–14.

251. Charkhkar H, Meyyappan S, Matveeva E, Moll JR, McHail DG, Peixoto N, et al. Amyloid beta modulation of neuronal network activity in vitro. Brain Res [Internet]. Elsevier; 2015;1629:1–9. Available from: http://dx.doi.org/10.1016/j.brainres.2015.09.036

252. Gao F, Gao K, He C, Liu M, Wan H, Wang P. Multi-site dynamic recording for Aβ oligomers-induced Alzheimer's disease in vitro based on neuronal network chip. Biosens Bioelectron [Internet]. Elsevier B.V.; 2019;133:183–91. Available from: https://doi.org/10.1016/j.bios.2019.03.025

253. Amin H, Nieus T, Lonardoni D, Maccione A, Berdondini L. High-resolution bioelectrical imaging of Aβ-induced network dysfunction on CMOS-MEAs for neurotoxicity and rescue studies. Sci Rep. Springer US; 2017;7:1–13.

254. Belle AM, Enright HA, Sales AP, Kulp K, Osburn J, Kuhn EA, et al. Evaluation of in vitro neuronal platforms as surrogates for in vivo whole brain systems. Sci Rep. 2018;8:1–9.

255. Xiang G, Pan L, Huang L, Yu Z, Song X, Cheng J, et al. Microelectrode array-based system for neuropharmacological applications with cortical neurons cultured in vitro. Biosens Bioelectron. 2007;22:2478–84.

256. James CD, Spence AJH, Dowell-Mesfin NM, Hussain RJ, Smith KL, Craighead HG, et al. Extracellular recordings from patterned neuronal networks using planar microelectrode arrays. IEEE Trans Biomed Eng. 2004;51:1640–8.

257. Nam Y, Wheeler BC, Heuschkel MO. Neural recording and stimulation of dissociated hippocampal cultures using microfabricated three-dimensional tip electrode array. J Neurosci

Methods. 2006;155:296–9.

258. Napoli A, Obeid I. Comparative Analysis of Human and Rodent Brain Primary Neuronal Culture Spontaneous Activity Using Micro-Electrode Array Technology. J Cell Biochem. 2016;117:559–65.

259. Odawara A, Saitoh Y, Alhebshi AH, Gotoh M, Suzuki I. Long-term electrophysiological activity and pharmacological response of a human induced pluripotent stem cell-derived neuron and astrocyte co-culture. Biochem Biophys Res Commun [Internet]. Elsevier Inc.; 2014;443:1176–81. Available from: http://dx.doi.org/10.1016/j.bbrc.2013.12.142

260. Heikkilä TJ, Ylä-Outinen L, Tanskanen JMA, Lappalainen RS, Skottman H, Suuronen R, et al. Human embryonic stem cell-derived neuronal cells form spontaneously active neuronal networks in vitro. Exp Neurol [Internet]. Elsevier Inc.; 2009;218:109–16. Available from: http://dx.doi.org/10.1016/j.expneurol.2009.04.011

261. Soscia DA, Lam D, Tooker AC, Enright HA, Triplett M, Karande P, et al. A flexible 3-dimensional microelectrode array for: In vitro brain models. Lab Chip. Royal Society of Chemistry; 2020;20:901–11.

262. Shin H, Jeong S, Lee JH, Sun W, Choi N, Cho IJ. 3D high-density microelectrode array with optical stimulation and drug delivery for investigating neural circuit dynamics. Nat Commun [Internet]. Springer US; 2021;12:1–18. Available from: http://dx.doi.org/10.1038/s41467-020-20763-3

263. Dauth S, Maoz BM, Sheehy SP, Hemphill MA, Murty T, Macedonia MK, et al. Neurons derived from different brain regions are inherently different in vitro: A novel multiregional brain-on-a-chip. J Neurophysiol. 2017;117:1320–41.

264. Goshi N, Girardi G, da Costa Souza F, Gardner A, Lein PJ, Seker E. Influence of microchannel geometry on device performance and electrophysiological recording fidelity during long-term studies of connected neural populations. Lab Chip [Internet]. Royal Society of Chemistry; 2022; Available from: http://xlink.rsc.org/?DOI=D2LC00683A

265. Biffi E, Regalia G, Menegon A, Ferrigno G, Pedrocchi A. The influence of neuronal density and maturation on network activity of hippocampal cell cultures: A methodological study. PLoS One. 2013;8.

266. Wagenaar DA, Pine J, Potter SM. An extremely rich repertoire of bursting patterns during the development of cortical cultures. BMC Neurosci. 2006;7:1–18.

267. Hong S, Dissing-Olesen L, Stevens B. New insights on the role of microglia in synaptic pruning in health and disease. Curr Opin Neurobiol [Internet]. Elsevier Ltd; 2016;36:128–34. Available from: http://dx.doi.org/10.1016/j.conb.2015.12.004

268. Crapser JD, Arreola MA, Tsourmas KI, Green KN. Microglia as hackers of the matrix: sculpting synapses and the extracellular space. Cell Mol Immunol. Springer US; 2021;18:2472–88.

269. Andoh M, Koyama R. Microglia regulate synaptic development and plasticity. Dev Neurobiol. 2021;81:568–90.

270. Flavell SW, Cowan CW, Kim TK, Greer PL, Lin Y, Paradis S, et al. Activity-dependent regulation of MEF2 transcription factors suppresses excitatory synapse number. Science (80-). 2006;311:1008–12.

271. Verstraelen P, Garcia-Diaz Barriga G, Verschuuren M, Asselbergh B, Nuydens R, Larsen PH, et al. Systematic Quantification of Synapses in Primary Neuronal Culture. iScience [Internet]. Elsevier Inc.; 2020;23:101542. Available from: https://doi.org/10.1016/j.isci.2020.101542

272. Lim SH, Park E, You B, Jung Y, Park AR, Park SG, et al. Neuronal synapse formation induced by microglia and interleukin 10. PLoS One. 2013;8:1–13.

273. Wake H, Moorhouse AJ, Jinno S, Kohsaka S, Nabekura J. Resting microglia directly monitor the functional state of synapses in vivo and determine the fate of ischemic terminals. J Neurosci. 2009;29:3974–80.

274. Tremblay MĚ, Lowery RL, Majewska AK. Microglial interactions with synapses are modulated by visual experience. PLoS Biol. 2010;8.

275. Perez-Catalan NA, Doe CQ, Ackerman SD. The role of astrocyte-mediated plasticity in neural circuit development and function. Neural Dev. Neural Development; 2021;16:1–14.

276. Mitchell JF, Sundberg KA, Reynolds JH. Differential Attention-Dependent Response Modulation across Cell Classes in Macaque Visual Area V4. Neuron. 2007;55:131–41.

277. Wang B, Ke W, Guang J, Chen G, Yin L, Deng S, et al. Firing frequency maxima of fast-spiking neurons in human, monkey, and mouse neocortex. Front Cell Neurosci. 2016;10:1–13.

278. Robbins AA, Fox SE, Holmes GL, Scott RC, Barry JM. Short duration waveforms recorded extracellularly from freely moving rats are representative of axonal activity. Front Neural Circuits. 2013;7:181.

279. Sahara S, Yanagawa Y, O'Leary DDM, Stevens CF. The fraction of cortical GABAergic neurons is constant from near the start of cortical neurogenesis to adulthood. J Neurosci. 2012;32:4755–61.

280. Turko P, Groberman K, Browa F, Cobb S, Vida I. Differential dependence of gabaergic and glutamatergic neurons on glia for the establishment of synaptic transmission. Cereb Cortex. 2019;29:1230–43.

281. Miyata S, Nishimura Y, Hayashi N, Oohira A. Construction of perineuronal net-like structure by cortical neurons in culture. Neuroscience. 2005;136:95–104.

282. Lehnardt S, Lachance C, Patrizi S, Lefebvre S, Follett PL, Jensen FE, et al. The Toll-Like Receptor TLR4 Is Necessary for Lipopolysaccharide- Induced Oligodendrocyte Injury in the CNS. J Neurosci. 2002;22:2478–86.

283. Goshi N, Kim H, Seker E. Primary Cortical Cell Tri-Culture-Based Screening of Neuroinflammatory Response in Toll-like Receptor Activation. Biomedicines. 2022;10:2122.

284. Kumar H, Kawai T, Akira S. Toll-like receptors and innate immunity. Biochem Biophys Res Commun [Internet]. Elsevier Inc.; 2009;388:621–5. Available from: http://dx.doi.org/10.1016/j.bbrc.2009.08.062

285. El-Zayat SR, Sibaii H, Mannaa FA. Toll-like receptors activation, signaling, and targeting: an

overview. Bull Natl Res Cent. Bulletin of the National Research Centre; 2019;43.

286. Carpentier PA, Duncan DS, Miller SD. Glial toll-like receptor signaling in central nervous system infection and autoimmunity. Brain Behav Immun. 2008;22:140–7.

287. Kong Y, Le Y. Toll-like receptors in inflammation of the central nervous system. Int Immunopharmacol [Internet]. Elsevier B.V.; 2011;11:1407–14. Available from: http://dx.doi.org/10.1016/j.intimp.2011.04.025

288. Kumar V. Toll-like receptors in the pathogenesis of neuroinflammation. J Neuroimmunol. 2019;332:16–30.

289. Bsibsi M, Persoon-Deen C, Verwer RWH, Meeuwsen S, Ravid R, Van Noort JM. Toll-like receptor 3 on adult human astrocytes triggers production of neuroprotective mediators. Glia [Internet]. 2006;53:688–95. Available from: http://www.unscn.org/en/home/

290. Jack CS, Arbour N, Manusow J, Montgrain V, Blain M, McCrea E, et al. TLR Signaling Tailors Innate Immune Responses in Human Microglia and Astrocytes. J Immunol. 2005;175:4320–30.

291. Olson JK, Miller SD. Microglia Initiate Central Nervous System Innate and Adaptive Immune Responses through Multiple TLRs. J Immunol. 2004;173:3916–24.

292. Serrano R, Coch C, Peters C, Hartmann G, Wesch D, Kabelitz D. Monocyte-dependent co-stimulation of cytokine induction in human γδ T cells by TLR8 RNA ligands. Sci Rep [Internet]. Nature Publishing Group UK; 2021;11:1–13. Available from: https://doi.org/10.1038/s41598-021-94428-6

293. Udayan S, Buttó LF, Rossini V, Velmurugan J, Martinez-Lopez M, Sancho D, et al. Macrophage cytokine responses to commensal Gram-positive Lactobacillus salivarius strains are TLR2-independent and Myd88-dependent. Sci Rep [Internet]. Nature Publishing Group UK; 2021;11:1–16. Available from: https://doi.org/10.1038/s41598-021-85347-7

294. Grubman A, Choo XY, Chew G, Ouyang JF, Sun G, Croft NP, et al. Transcriptional signature in microglia associated with Aβ plaque phagocytosis. Nat Commun. 2021;12.

295. Affram KO, Mitchell K, Symes AJ. Microglial Activation Results in Inhibition of TGF-β-

Regulated Gene Expression. J Mol Neurosci. Journal of Molecular Neuroscience; 2017;63:308–19.

296. Niu T, De Rosny C, Chautard S, Rey A, Patoli D, Groslambert M, et al. NLRP3 phosphorylation in its LRR domain critically regulates inflammasome assembly. Nat Commun [Internet]. Springer US; 2021;12:1–15. Available from: http://dx.doi.org/10.1038/s41467-021-26142-w

297. Allacher P, Baumgartner CK, Pordes AG, Ahmad RU, Schwarz HP, Reipert BM. Stimulation and inhibition of FVIII-specific memory B-cell responses by CpG-B (ODN 1826), a ligand for Toll-like receptor 9. Blood. 2011;117:259–67.

298. Rodríguez JJ, Olabarria M, Chvatal A, Verkhratsky A. Astroglia in dementia and Alzheimer's disease. Cell Death Differ. 2009;16:378–85.

299. Ponath G, Park C, Pitt D. The role of astrocytes in multiple sclerosis. Front Immunol. 2018;9:1–12.

300. Polikov VS, Tresco PA, Reichert WM. Response of brain tissue to chronically implanted neural electrodes. J Neurosci Methods. 2005;148:1–18.

301. Beynon SB, Walker FR. Microglial activation in the injured and healthy brain: What are we really talking about? Practical and theoretical issues associated with the measurement of changes in microglial morphology. Neuroscience [Internet]. IBRO; 2012;225:162–71. Available from: http://dx.doi.org/10.1016/j.neuroscience.2012.07.029

302. Zhou Y, Guo M, Wang X, Li J, Wang Y, Ye L, et al. TLR3 activation efficiency by high or low molecular mass poly I:C. Innate Immun. 2013;19:184–92.

303. Carty M, Bowie AG. Evaluating the role of Toll-like receptors in diseases of the central nervous system. Biochem Pharmacol [Internet]. Elsevier Inc.; 2011;81:825–37. Available from: http://dx.doi.org/10.1016/j.bcp.2011.01.003

304. Aravalli RN, Peterson PK, Lokensgard JR. Toll-like receptors in defense and damage of the central nervous system. J Neuroimmune Pharmacol. 2007;2:297–312.

305. Ifuku M, Hinkelmann L, Kuhrt LD, Efe IE, Kumbol V, Buonfiglioli A, et al. Activation of Toll-like receptor 5 in microglia modulates their function and triggers neuronal injury. Acta Neuropathol Commun [Internet]. BioMed Central; 2020;8:1–19. Available from: https://doi.org/10.1186/s40478-020-01031-3

306. Butchi NB, Woods T, Du M, Morgan TW, Peterson KE. TLR7 and TLR9 trigger distinct neuroinflammatory responses in the CNS. Am J Pathol. 2011;179:783–94.

307. Batista CRA, Gomes GF, Candelario-Jalil E, Fiebich BL, de Oliveira ACP. Lipopolysaccharide-induced neuroinflammation as a bridge to understand neurodegeneration. Int J Mol Sci. 2019;20.

308. Kielian T. Toll-like receptors in central nervous system glial inflammation and homeostasis. J Neurosci Res. J Neurosci Res; 2006;83:711–30.

309. Farhat K, Riekenberg S, Heine H, Debarry J, Lang R, Mages J, et al. Heterodimerization of TLR2 with TLR1 or TLR6 expands the ligand spectrum but does not lead to differential signaling. J Leukoc Biol [Internet]. 2008;83:692–701. Available from: http://doi.wiley.com/10.1189/jlb.0807586

310. Tahtinen S, Tong AJ, Himmels P, Oh J, Paler-Martinez A, Kim L, et al. IL-1 and IL-1ra are key regulators of the inflammatory response to RNA vaccines. Nat Immunol 2022 234. Nature Publishing Group; 2022;23:532–42.

311. Teti E, Golenbock DT, Sundan A, Trude Flo TH, Halaas Ø, Lien E, et al. Human Toll-Like Receptor 2 Mediates. J Immunol Ref. 2022;164:2064–9.

312. McKernan DP, Gaszner G, Quigley EM, Cryan JF, Dinan TG. Altered peripheral toll-like receptor responses in the irritable bowel syndrome. Aliment Pharmacol Ther. John Wiley & Sons, Ltd; 2011;33:1045–52.

313. Rothaug M, Becker-Pauly C, Rose-John S. The role of interleukin-6 signaling in nervous tissue. Biochim Biophys Acta - Mol Cell Res [Internet]. Elsevier B.V.; 2016;1863:1218–27. Available from: http://dx.doi.org/10.1016/j.bbamcr.2016.03.018

314. Town T, Jeng D, Alexopoulou L, Tan J, Flavell RA. Microglia Recognize Double-Stranded RNA via TLR3. J Immunol. 2006;176:3804–12.

315. Zuiderwijk-Sick EA, van der Putten C, Bsibsi M, Deuzing IP, de Boer W, Persoon-Deen C, et al. Differentiation of primary adult microglia alters their response to TLR8-mediated activation but not their capacity as APC. Glia [Internet]. 2007;55:1589–600. Available from: http://www.unscn.org/en/home/

316. Lannes N, Summerfield A, Filgueira L. Regulation of inflammation in Japanese encephalitis. J Neuroinflammation. Journal of Neuroinflammation; 2017;14:1–11.

317. Ma Y, Li J, Chiu I, Wang Y, Sloane JA, Lü J, et al. Toll-like receptor 8 functions as a negative regulator of neurite outgrowth and inducer of neuronal apoptosis. J Cell Biol. 2006;175:209–15.

318. Rosenberger K, Derkow K, Dembny P, Krüger C, Schott E, Lehnardt S. The impact of single and pairwise Toll-like receptor activation on neuroinflammation and neurodegeneration. J Neuroinflammation. 2014;11:1–20.

319. Chong HL, Ruben PC. Interaction between voltage-gated sodium channels and the neurotoxin, tetrodotoxin. Channels. 2008;2:407–12.

320. Campenot RB, Soin J, Blacker M, Lund K, Eng H, MacInnis BL. Block of slow axonal transport and axonal growth by brefeldin A in compartmented cultures of rat sympathetic neurons. Neuropharmacology. 2003;44:1107–17.

Appendix I: Used for Figure 3.1 - Analysis of Microchannel Dimensions in Literature

1. Brofiga, Martina; Pisano, Marietta; Tedesco, Mariateresa; Raiteri, Roberto; Massobrio, Paolo. "Three-dimensionality shapes the dynamics of cortical interconnected to hippocampal networks" JOURNAL OF NEURAL ENGINEERING (2020)
2. Katsikoudi, Antigoni; Ficulle, Elena; Cavallini, Annalisa; Sharman, Gary; Guyot, Amelie; Zagnoni, Michele; Eastwood, Brian J.; Hutton, Michael; Bose, Suchira. "Quantitative propagation of assembled human Tau from Alzheimer's disease brain in microfluidic neuronal cultures" JOURNAL OF BIOLOGICAL CHEMISTRY (2020)
3. Mazzara, Pietro Giuseppe; Muggeo, Sharon; Luoni, Mirko; Massimino, Luca; Zaghi, Mattia; Valverde, Parisa Tajalli-Tehrani; Brusco, Simone; Marzi, Matteo Jacopo; Palma, Cecilia; Colasante, Gaia; Iannielli, Angelo; Paulis, Marianna; Cordiglieri, Chiara; Giannelli, Serena Gea; Podini, Paola; Gellera, Cinzia; Taroni, Franco; Nicassio, Francesco; Rasponi, Marco; Broccoli, Vania. "Frataxin gene editing rescues Friedreich's ataxia pathology in dorsal root ganglia organoid-derived sensory neurons" NATURE COMMUNICATIONS (2020)
4. Bastiaens, Alex; Sabahi-Kaviani, Rahman; Luttge, Regina. "Nanogrooves for 2D and 3D Microenvironments of SH-SY5Y Cultures in Brain-on-Chip Technology" FRONTIERS IN NEUROSCIENCE (2020)
5. Watters, Orla; Connolly, Niamh M. C.; Konig, Hans-Georg; Dussmann, Heiko; Prehn, Jochen H. M.. "AMPK Preferentially Depresses Retrograde Transport of Axonal Mitochondria during Localized Nutrient Deprivation" JOURNAL OF NEUROSCIENCE (2020)

6. Takayama, Yuzo; Kushige, Hiroko; Akagi, Yuka; Suzuki, Yutaka; Kumagai, Yutaro; Kida, Yasuyuki S.. "Selective Induction of Human Autonomic Neurons Enables Precise Control of Cardiomyocyte Beating" SCIENTIFIC REPORTS (2020)
7. Bruyere, Julie; Abada, Yah-Se; Vitet, Helene; Fontaine, Gaelle; Deloulme, Jean-Christophe; Ces, Aurelia; Denarier, Eric; Pernet-Gallay, Karin; Andrieux, Annie; Humbert, Sandrine; Potier, Marie-Claude; Delatour, Benoit; Saudou, Frederic. "Presynaptic APP levels and synaptic homeostasis are regulated by Akt phosphorylation of huntingtin" ELIFE (2020)
8. Asselin, Laure; Alvarez, Jose Rivera; Heide, Solveig; Bonnet, Camille S.; Tilly, Peggy; Vitet, Helene; Weber, Chantal; Bacino, Carlos A.; Baranano, Kristin; Chassevent, Anna; Dameron, Amy; Faivre, Laurence; Hanchard, Neil A.; Mahida, Sonal; McWalter, Kirsty; Mignot, Cyril; Nava, Caroline; Rastetter, Agnes; Streff, Haley; Thauvin-Robinet, Christel; Weiss, Marjan M.; Zapata, Gladys; Zwijnenburg, Petra J. G.; Saudou, Frederic; Depienne, Christel; Golzio, Christelle; Heron, Delphine; Godin, Juliette D.. "Mutations in the KIF21B kinesin gene cause neurodevelopmental disorders through imbalanced canonical motor activity" NATURE COMMUNICATIONS (2020)
9. Wang, Tong; Li, Wei; Martin, Sally; Papadopulos, Andreas; Joensuu, Merja; Liu, Chunxia; Jiang, Anmin; Shamsollahi, Golnoosh; Amor, Rumelo; Lanoue, Vanessa; Padmanabhan, Pranesh; Meunier, Frederic A.. "Radial contractility of actomyosin rings facilitates axonal trafficking and structural stability" JOURNAL OF CELL BIOLOGY (2020)
10. Fujita, Yuki; Nakanishi, Toru; Ueno, Masaki; Itohara, Shigeyoshi; Yamashita, Toshihide. "Netrin-G1 Regulates Microglial Accumulation along Axons and Supports the Survival of Layer V Neurons in the Postnatal Mouse Brain" CELL REPORTS (2020)
11. Vahsen, Bjoern Friedhelm; Ribas, Vinicius Toledo; Sundermeyer, Jonas; Boecker, Alexander; Dambeck, Vivian; Lenz, Christof; Shomroni, Orr; Gomes, Lucas Caldi; Tatenhorst, Lars; Barski, Elisabeth; Roser, Anna-Elisa; Michel, Uwe; Urlaub, Henning;

Salinas, Gabriela; Baehr, Mathias; Koch, Christoph; Lingor, Paul. "Inhibition of the autophagic protein ULK1 attenuates axonal degeneration in vitro and in vivo, enhances translation, and modulates splicing" CELL DEATH AND DIFFERENTIATION (2020)

12. Fantuzzo, Joseph A.; Robles, Denise A.; Mirabella, Vincent R.; Hart, Ronald P.; Pang, Zhiping P.; Zahn, Jeffrey D.. "Development of a high-throughput arrayed neural circuitry platform using human induced neurons for drug screening applications" LAB ON A CHIP (2020)
13. Liu, Jianan; Li, Fangyuan; Wang, Yi; Pan, Limin; Lin, Peihua; Zhang, Bo; Zheng, Yanrong; Xu, Yingwei; Liao, Hongwei; Ko, Giho; Fei, Fan; Xu, Cenglin; Du, Yang; Shin, Kwangsoo; Kim, Dokyoon; Jang, Sung-Soo; Chung, Hee Jung; Tian, He; Wang, Qi; Guo, Wei; Nam, Jwa-Min; Chen, Zhong; Hyeon, Taeghwan; Ling, Daishun. "A sensitive and specific nanosensor for monitoring extracellular potassium levels in the brain" NATURE NANOTECHNOLOGY (2020)
14. Lucci, Cristiano; Mesquita-Ribeiro, Raquel; Rathbone, Alex; Dajas-Bailador, Federico. "Spatiotemporal regulation of GSK3 beta levels by miRNA-26a controls axon development in cortical neurons" DEVELOPMENT (2020)
15. Sundaramoorthy, Vinod; Green, Diane; Locke, Kelly; O'Brien, Carmel M.; Dearnley, Megan; Bingham, John. "Novel role of SARM1 mediated axonal degeneration in the pathogenesis of rabies" PLOS PATHOGENS (2020)
16. Iannielli, Angelo; Ugolini, Giovanni Stefano; Cordiglieri, Chiara; Bido, Simone; Rubio, Alicia; Colasante, Gaia; Valtorta, Marco; Cabassi, Tommaso; Rasponi, Marco; Broccoli, Vania. "Reconstitution of the Human Nigro-striatal Pathway on-a-Chip Reveals OPA1-Dependent Mitochondrial Defects and Loss of Dopaminergic Synapses" CELL REPORTS (2019)
17. Shigeoka, Toshiaki; Koppers, Max; Wong, Hovy Ho-Wai; Lin, Julie Qiaojin; Cagnetta, Roberta; Dwivedy, Asha; Nascimento, Janaina de Freitas; van Tartwijk, Francesca W.;

Strohl, Florian; Cioni, Jean-Michel; Schaeffer, Julia; Carrington, Mark; Kaminski, Clemens F.; Jung, Hosung; Harris, William A.; Holt, Christine E.. "On-Site Ribosome Remodeling by Locally Synthesized Ribosomal Proteins in Axons" CELL REPORTS (2019)

18. Singh, Tanya; Vazquez, Maribel. "Time-Dependent Addition of Neuronal and Schwann Cells Increase Myotube Viability and Length in an In Vitro Tri-culture Model of the Neuromuscular Junction" REGENERATIVE ENGINEERING AND TRANSLATIONAL MEDICINE (2019)
19. Bellmann, Jessica; Goswami, Ruchi Y.; Girardo, Salvatore; Rein, Nelly; Hosseinzadeh, Zohreh; Hicks, Michael R.; Busskamp, Volker; Pyle, April D.; Werner, Carsten; Sterneckert, Jared. "A customizable microfluidic platform for medium-throughput modeling of neuromuscular circuits" BIOMATERIALS (2019)
20. Hyvarinen, Tanja; Hagman, Sanna; Ristola, Mervi; Sukki, Lassi; Veijula, Katariina; Kreutzer, Joose; Kallio, Pasi; Narkilahti, Susanna. "Co-stimulation with IL-1 beta and TNF-alpha induces an inflammatory reactive astrocyte phenotype with neurosupportive characteristics in a human pluripotent stem cell model system" SCIENTIFIC REPORTS (2019)
21. Nagendran, Tharkika; Taylor, Anne Marion. "Unique Axon-to-Soma Signaling Pathways Mediate Dendritic Spine Loss and Hyper-Excitability Post-axotomy" FRONTIERS IN CELLULAR NEUROSCIENCE (2019)
22. Wenzel, Erin D.; Speidell, Andrew; Flowers, Sarah A.; Wu, Chengbiao; Avdoshina, Valeria; Mocchetti, Italo. "Histone deacetylase 6 inhibition rescues axonal transport impairments and prevents the neurotoxicity of HIV-1 envelope protein gp120" CELL DEATH & DISEASE (2019)
23. Vysokov, Nickolai; McMahon, Stephen B.; Raouf, Ramin. "The role of Na-V channels in synaptic transmission after axotomy in a microfluidic culture platform" SCIENTIFIC REPORTS (2019)

24. Lee, Soyeon; Wang, Wei; Hwang, Jinyeon; Namgung, Uk; Min, Kyung-Tai. "Increased ER-mitochondria tethering promotes axon regeneration" PROCEEDINGS OF THE NATIONAL ACADEMY OF SCIENCES OF THE UNITED STATES OF AMERICA (2019)

25. Hixon, Alison M.; Clarke, Penny; Tyler, Kenneth L.. "Contemporary Circulating Enterovirus D68 Strains Infect and Undergo Retrograde Axonal Transport in Spinal Motor Neurons Independent of Sialic Acid" JOURNAL OF VIROLOGY (2019)

26. Costa, Rui O.; Martins, Helena; Martins, Luis F.; Cwetsch, Andrzej W.; Mele, Miranda; Pedro, Joana R.; Tome, Diogo; Jeon, Noo Li; Cancedda, Laura; Jaffrey, Samie R.; Almeida, Ramiro D.. "Synaptogenesis Stimulates a Proteasome-Mediated Ribosome Reduction in Axons" CELL REPORTS (2019)

27. Kamudzandu, M.; Kose-Dunn, M.; Evans, M. G.; Pricker, R. A.; Roach, P.. "A micro-fabricated in vitro complex neuronal circuit platform" BIOMEDICAL PHYSICS & ENGINEERING EXPRESS (2019)

28. Vaquie, Adrien; Sauvain, Alizee; Duman, Mert; Nocera, Gianluigi; Egger, Boris; Meyenhofer, Felix; Falquet, Laurent; Bartesaghi, Luca; Chrast, Roman; Lamy, Christophe Maurice; Bang, Seokyoung; Lee, Seung-Ryeol; Li Jeon, Noo; Ruff, Sophie; Jacob, Claire. "Injured Axons Instruct Schwann Cells to Build Constricting Actin Spheres to Accelerate Axonal Disintegration" CELL REPORTS (2019)

29. Dixon, Angela R.; Horst, Eric N.; Garcia, Jeniffer J.; Ndjouyep-Yamaga, Patricia R.; Mehta, Geeta. "Morphometric and computational assessments to evaluate neuron survival and maturation within compartmentalized microfluidic devices: The influence of design variation on diffusion-driven nutrient transport" NEUROSCIENCE LETTERS (2019)

30. Zheng, Yanrong; Zhang, Xiangnan; Wu, Xiaoli; Jiang, Lei; Ahsan, Anil; Ma, Shijia; Xiao, Ziyu; Han, Feng; Qin, Zheng-Hong; Hu, Weiwei; Chen, Zhong. "Somatic autophagy of axonal mitochondria in ischemic neurons" JOURNAL OF CELL BIOLOGY (2019)

31. Ristola, Mervi; Sukki, Lassi; Azevedo, Maria Manuela; Seixas, Ana Isabel; Relvas, Joao Bettencourt; Narkilahti, Susanna; Kallio, Pasi. "A compartmentalized neuron-oligodendrocyte co-culture device for myelin research: design, fabrication and functionality testing" JOURNAL OF MICROMECHANICS AND MICROENGINEERING (2019)

32. Kamande, Joyce W.; Nagendran, Tharkika; Harris, Joseph; Taylor, Anne Marion. "Multi-compartment Microfluidic Device Geometry and Covalently Bound Poly-D-Lysine Influence Neuronal Maturation" FRONTIERS IN BIOENGINEERING AND BIOTECHNOLOGY (2019)

33. Yokoyama, S.; Otomo, A.; Hadano, S.; Kimura, H.. "An open-type microdevice to improve the quality of fluorescence labeling for axonal transport analysis in neurons" BIOMICROFLUIDICS (2019)

34. Pu, Hongjian; Shi, Yejie; Zhang, Lili; Lu, Zhengyu; Ye, Qing; Leak, Rehana K.; Xu, Fei; Ma, Shubei; Mu, Hongfeng; Wei, Zhishuo; Xu, Na; Xia, Yuguo; Hu, Xiaoming; Hitchens, T. Kevin; Bennett, Michael V. L.; Chen, Jun. "Protease-independent action of tissue plasminogen activator in brain plasticity and neurological recovery after ischemic stroke" PROCEEDINGS OF THE NATIONAL ACADEMY OF SCIENCES OF THE UNITED STATES OF AMERICA (2019)

35. Li, Chao; Zhang, Yi; Levin, Albert M.; Fan, Bao Yan; Teng, Hua; Ghannam, Moleca M.; Chopp, Michael; Zhang, Zheng Gang. "Distal Axonal Proteins and Their Related MiRNAs in Cultured Cortical Neurons" MOLECULAR NEUROBIOLOGY (2019)

36. Goto-Silva, Livia; McShane, Marisa P.; Salinas, Sara; Kalaidzidis, Yannis; Schiavo, Giampietro; Zerial, Marino. "Retrograde transport of Akt by a neuronal Rab5-APPL1 endosome" SCIENTIFIC REPORTS (2019)

37. Klim, Joseph R.; Williams, Luis A.; Limone, Francesco; San Juan, Irune Guerra; Davis-Dusenbery, Brandi N.; Mordes, Daniel A.; Burberry, Aaron; Steinbaugh, Michael J.; Gamage, Kanchana K.; Kirchner, Rory; Moccia, Rob; Casse, Seth H.; Chen, Kuchuan;

Wainger, Brian J.; Woolf, Clifford J.; Eggan, Kevin. "ALS-implicated protein TDP-43 sustains levels of STMN2, a mediator of motor neuron growth and repair" NATURE NEUROSCIENCE (2019)

38. Melamed, Ze'ev; Lopez-Erauskin, Jone; Baughn, Michael W.; Zhang, Ouyang; Drenner, Kevin; YingSun; Freyermuth, Fernande; McMahons, Moira A.; Beccari, Melinda S.; Artates, Jon W.; Ohkubo, Takuya; Rodriguez, Maria; Lin, Nianwei; Wu, Dongmei; Bennetts, C. Frank; Rigos, Frank; Da Cruz, Sandrine; Ravits, John; Lagier-Tourenne, Clotilde; Cleveland, Don W.. "Premature polyadenylation-mediated loss of stathmin-2 is a hallmark of TDP-43-dependent neurodegeneration" NATURE NEUROSCIENCE (2019)
39. Lesniak, Anna; Kilinc, Devrim; Blasiak, Agata; Galea, George; Simpson, Jeremy C.; Lee, Gil U.. "Rapid Growth Cone Uptake and Dynein-Mediated Axonal Retrograde Transport of Negatively Charged Nanoparticles in Neurons Is Dependent on Size and Cell Type" SMALL (2019)
40. Nijssen, Jik; Aguila, Julio; Hoogstraaten, Rein; Kee, Nigel; Hedlund, Eva. "Axon-Seq Decodes the Motor Axon Transcriptome and Its Modulation in Response to ALS" STEM CELL REPORTS (2018)
41. Balaji, Varun; Kaniyappan, Senthilvelrajan; Mandelkow, Eckhard; Wang, Yipeng; Mandelkow, Eva-Maria. "Pathological missorting of endogenous MAPT/Tau in neurons caused by failure of protein degradation systems" AUTOPHAGY (2018)
42. Jia, Longfei; Chopp, Michael; Wang, Lei; Lu, Xuerong; Szalad, Alexandra; Zhang, Zheng Gang. "Exosomes derived from high-glucose-stimulated Schwann cells promote development of diabetic peripheral neuropathy" FASEB JOURNAL (2018)
43. Jia, Longfei; Chopp, Michael; Wang, Lei; Lu, Xuerong; Zhang, Yi; Szalad, Alexandra; Zhang, Zheng Gang. "MiR-34a Regulates Axonal Growth of Dorsal Root Ganglia Neurons by Targeting FOXP2 and VAT1 in Postnatal and Adult Mouse" MOLECULAR NEUROBIOLOGY (2018)

44. Vysokov, Nickolai V.; Silva, John-Paul; Lelianova, Vera G.; Suckling, Jason; Cassidy, John; Blackburn, Jennifer K.; Yankova, Natalia; Djamgoz, Mustafa B. A.; Kozlov, Serguei V.; Tonevitsky, Alexander G.; Ushkaryov, Yuri A.. "Proteolytically released Lasso/teneurin-2 induces axonal attraction by interacting with latrophilin-1 on axonal growth cones" ELIFE (2018)

45. Wang, Ze Zhong; Wood, Matthew D.; Mackinnon, Susan E.; Sakiyama-Elbert, Shelly E.. "A microfluidic platform to study the effects of GDNF on neuronal axon entrapment" JOURNAL OF NEUROSCIENCE METHODS (2018)

46. Van Laar, Victor S.; Arnold, Beth; Howlett, Evan H.; Calderon, Michael J.; St Croix, Claudette M.; Greenamyre, J. Timothy; Sanders, Laurie H.; Berman, Sarah B.. "Evidence for Compartmentalized Axonal Mitochondrial Biogenesis: Mitochondrial DNA Replication Increases in Distal Axons As an Early Response to Parkinson's Disease-Relevant Stress" JOURNAL OF NEUROSCIENCE (2018)

47. Poli, Daniele; Wheeler, Bruce C.; DeMarse, Thomas B.; Brewer, Gregory J.. "Pattern separation and completion of distinct axonal inputs transmitted via micro-tunnels between co-cultured hippocampal dentate, CA3, CA1 and entorhinal cortex networks" JOURNAL OF NEURAL ENGINEERING (2018)

48. Clark, Alex J.; Menendez, Guillermo; AlQatari, Mona; Patel, Niral; Arstad, Erik; Schiavo, Giampietro; Koltzenburg, Martin. "Functional imaging in microfluidic chambers reveals sensory neuron sensitivity is differentially regulated between neuronal regions" PAIN (2018)

49. Jocher, Georg; Mannschatz, Sidney H.; Offterdinger, Martin; Schweigreiter, Ruediger. "Microfluidics of Small-Population Neurons Allows for a Precise Quantification of the Peripheral Axonal Growth State" FRONTIERS IN CELLULAR NEUROSCIENCE (2018)

50. Santhanam, Navaneetha; Kumanchik, Lee; Guo, Xiufang; Sommerhage, Frank; Cai, Yunqing; Jackson, Max; Martin, Candace; Saad, George; McAleer, Christopher W.; Wang,

Ying; Lavado, Andrea; Long, Christopher J.; Hickman, James J.. "Stem cell derived phenotypic human neuromuscular junction model for dose response evaluation of therapeutics" BIOMATERIALS (2018)

51. Urrea, Laura; Segura-Feliu, Miriam; Masuda-Suzukake, Masami; Hervera, Arnau; Pedraz, Lucas; Garcia Aznar, Jose Manuel; Vila, Miquel; Samitier, Josep; Torrents, Eduard; Ferrer, Isidro; Gavin, Rosalina; Hagesawa, Masato; Antonio del Rio, Jose. "Involvement of Cellular Prion Protein in alpha-Synuclein Transport in Neurons" MOLECULAR NEUROBIOLOGY (2018)

52. Polanco, Juan Carlos; Li, Chuanzhou; Durisic, Nela; Sullivan, Robert; Gotz, Jurgen. "Exosomes taken up by neurons hijack the endosomal pathway to spread to interconnected neurons" ACTA NEUROPATHOLOGICA COMMUNICATIONS (2018)

53. Clarkson, Benjamin D. S.; Patel, Misha S.; LaFrance-Corey, Reghann G.; Howe, Charles L.. "Retrograde interferon-gamma signaling induces major histocompatibility class I expression in human-induced pluripotent stem cell-derived neurons" ANNALS OF CLINICAL AND TRANSLATIONAL NEUROLOGY (2018)

54. Virlogeux, Amandine; Moutaux, Eve; Christaller, Wilhelm; Genoux, Aurelie; Bruyere, Julie; Fino, Elodie; Charlot, Benoit; Cazorla, Maxime; Saudou, Frederic. "Reconstituting Corticostriatal Network on-a-Chip Reveals the Contribution of the Presynaptic Compartment to Huntington's Disease" CELL REPORTS (2018)

55. van de Wijdeven, Rosanne; Ramstad, Ola Huse; Bauer, Ulrich Stefan; Halaas, Oyvind; Sandvig, Axel; Sandvig, Ioanna. "Structuring a multi-nodal neural network in vitro within a novel design microfluidic chip" BIOMEDICAL MICRODEVICES (2018)

56. Mills, Richard; Taylor-Weiner, Hermes; Correia, Jorge C.; Agudelo, Leandro Z.; Allodi, Ilary; Kolonelou, Christina; Martinez-Redondo, Vicente; Ferreira, Duarte M. S.; Nichterwitz, Susanne; Comley, Laura H.; Lundin, Vanessa; Hedlund, Eva; Ruas, Jorge L.; Teixeira, Ana I.. "Neurturin is a PGC-1 alpha 1-controlled myokine that promotes motor

neuron recruitment and neuromuscular junction formation" MOLECULAR METABOLISM (2018)

57. Jia, Longfei; Wang, Lei; Chopp, Michael; Li, Chao; Zhang, Yi; Szalad, Alexandra; Zhang, Zheng Gang. "MiR-29c/PRKCI Regulates Axonal Growth of Dorsal Root Ganglia Neurons Under Hyperglycemia" MOLECULAR NEUROBIOLOGY (2018)

58. Sun, Tao; Li, Yuan; Li, Ting; Ma, Huixian; Guo, Yunyun; Jiang, Xingyu; Hou, Ming; Huang, Shuhong; Chen, Zheyu. "JIP1 and JIP3 cooperate to mediate TrkB anterograde axonal transport by activating kinesin-1" CELLULAR AND MOLECULAR LIFE SCIENCES (2017)

59. Bauer, Dirk; Alt, Mira; Dirks, Miriam; Buch, Anna; Heilingloh, Christiane S.; Dittmer, Ulf; Giebel, Bernd; Goergens, Andre; Palapys, Vivien; Kasper, Maren; Eis-Huebinger, Anna M.; Sodeik, Beate; Heiligenhaus, Arnd; Roggendorf, Michael; Krawczyk, Adalbert. "A Therapeutic Antiviral Antibody Inhibits the Anterograde Directed Neuron-to-Cell Spread of Herpes Simplex Virus and Protects against Ocular Disease" FRONTIERS IN MICROBIOLOGY (2017)

60. Nagendran, Tharkika; Larsen, Rylan S.; Bigler, Rebecca L.; Frost, Shawn B.; Philpot, Benjamin D.; Nudo, Randolph J.; Taylor, Anne Marion. "Distal axotomy enhances retrograde presynaptic excitability onto injured pyramidal neurons via trans-synaptic signaling" NATURE COMMUNICATIONS (2017)

61. Habibey, Rouhollah; Latifi, Shahrzad; Mousavi, Hossein; Pesce, Mattia; Arab-Tehrany, Elmira; Blau, Axel. "A multielectrode array microchannel platform reveals both transient and slow changes in axonal conduction velocity" SCIENTIFIC REPORTS (2017)

62. Sakai, Koji; Shimba, Kenta; Kotani, Kiyoshi; Jimbo, Yasuhiko. "A co-culture microtunnel technique demonstrating a significant contribution of unmyelinated Schwann cells to the acceleration of axonal conduction in Schwann cell-regulated peripheral nerve development" INTEGRATIVE BIOLOGY (2017)

63. Peikon, Ian D.; Kebschull, Justus M.; Vagin, Vasily V.; Ravens, Diana I.; Sun, Yu-Chi; Brouzes, Eric; Correa, Ivan R., Jr.; Bressan, Dario; Zador, Anthony M.. "Using high-throughput barcode sequencing to efficiently map connectomes" NUCLEIC ACIDS RESEARCH (2017)

64. Martins, Lus F.; Costa, Rui O.; Pedro, Joana R.; Aguiar, Paulo; Serra, Sofia C.; Teixeira, Fabio G.; Sousa, Nuno; Salgado, Antonio J.; Almeida, Ramiro D.. "Mesenchymal stem cells secretome-induced axonal outgrowth is mediated by BDNF" SCIENTIFIC REPORTS (2017)

65. Jiang, Hai-Fei; Wang, Wei; Jiang, Xuan; Zeng, Wen-Bo; Shen, Zhang-Zhou; Song, Yi-Ge; Yang, Hong; Liu, Xi-Juan; Dong, Xiao; Zhou, Jing; Sun, Jin-Yan; Yu, Fei-Long; Guo, Lin; Cheng, Tong; Rayner, Simon; Zhao, Fei; Zhu, Hua; Luo, Min-Hua. "ORF7 of Varicella-Zoster Virus Is Required for Viral Cytoplasmic Envelopment in Differentiated Neuronal Cells" JOURNAL OF VIROLOGY (2017)

66. Zeng, Wen-Bo; Jiang, Hai-Fei; Gang, Ya-Dong; Song, Yi-Ge; Shen, Zhang-Zhou; Yang, Hong; Dong, Xiao; Tian, Yong-Lu; Ni, Rong-Jun; Liu, Yaping; Tang, Na; Li, Xinyan; Jiang, Xuan; Gao, Ding; Androulakis, Michelle; He, Xiao-Bin; Xia, Hui-Min; Ming, Ying-Zi; Lu, Youming; Zhou, Jiang-Ning; Zhang, Chen; Xia, Xue-Shan; Shu, Yousheng; Zeng, Shao-Qun; Xu, Fuqiang; Zhao, Fei; Luo, Min-Hua. "Anterograde monosynaptic transneuronal tracers derived from herpes simplex virus 1 strain H129" MOLECULAR NEURODEGENERATION (2017)

67. Narula, Udit; Ruiz, Andres; McQuaide, McKinley; DeMarse, Thomas B.; Wheeler, Bruce C.; Brewer, Gregory J.. "Narrow microtunnel technology for the isolation and precise identification of axonal communication among distinct hippocampal subregion networks" PLOS ONE (2017)

68. Yap, Yiing C.; King, Anna E.; Guijt, Rosanne M.; Jiang, Tongcui; Blizzard, Catherine A.; Breadmore, Michael C.; Dickson, Tracey C.. "Mild and repetitive very mild axonal stretch injury triggers cystoskeletal mislocalization and growth cone collapse" PLOS ONE (2017)

69. Zhang, Yi; Chopp, Michael; Liu, Xian Shuang; Katakowski, Mark; Wang, Xinli; Tian, Xinchu; Wu, David; Zhang, Zheng Gang. "Exosomes Derived from Mesenchymal Stromal Cells Promote Axonal Growth of Cortical Neurons" MOLECULAR NEUROBIOLOGY (2017)

70. Suzuki, Koji; Tanaka, Hiroyuki; Ebara, Mitsuhiro; Uto, Koichiro; Matsuoka, Hozo; Nishimoto, Shunsuke; Okada, Kiyoshi; Murase, Tsuyoshi; Yoshikawa, Hideki. "Electrospun nanofiber sheets incorporating methylcobalamin promote nerve regeneration and functional recovery in a rat sciatic nerve crush injury model" ACTA BIOMATERIALIA (2017)

71. Li, Wei; Xu, Zhen; Xu, Bingzhe; Chan, Chung Yuen; Lin, Xudong; Wang, Ying; Chen, Ganchao; Wang, Zhigang; Yuan, Qiuju; Zhu, Guangyu; Sun, Hongyan; Wu, Wutian; Shi, Peng. "Investigation of the Subcellular Neurotoxicity of Amyloid-beta Using a Device Integrating Microfluidic Perfusion and Chemotactic Guidance" ADVANCED HEALTHCARE MATERIALS (2017)

72. Bigler, Rebecca L.; Kamande, Joyce W.; Dumitru, Raluca; Niedringhaus, Mark; Taylor, Anne Marion. "Messenger RNAs localized to distal projections of human stem cell derived neurons" SCIENTIFIC REPORTS (2017)

73. Lombardi, Loredana; Persiconi, Irene; Gallo, Alessandra; Hoogenraad, Casper C.; De Stefano, Maria Egle. "NGF-dependent axon growth and regeneration are altered in sympathetic neurons of dystrophic mdx mice" MOLECULAR AND CELLULAR NEUROSCIENCE (2017)

74. Hong, Nari; Joo, Sunghoon; Nam, Yoonkey. "Characterization of Axonal Spikes in Cultured Neuronal Networks Using Microelectrode Arrays and Microchannel Devices" IEEE TRANSACTIONS ON BIOMEDICAL ENGINEERING (2017)

75. Shimba, Kenta; Sakai, Koji; Kotani, Kiyoshi; Yagi, Tohru; Jimbo, Yasuhiko. "Microtunnel-Electrode Device for Elucidating Axon Features: toward Pharmacological Manipulation of Individual Axons" 2017 8TH INTERNATIONAL IEEE/EMBS CONFERENCE ON NEURAL ENGINEERING (NER) (2017)

76. Cui, Chengcheng; Ye, Xinchun; Chopp, Michael; Venkat, Poornima; Zacharek, Alex; Yan, Tao; Ning, Ruizhou; Yu, Peng; Cui, Guiyun; Chen, Jieli. "miR-145 Regulates Diabetes-Bone Marrow Stromal Cell-Induced Neurorestorative Effects in Diabetes Stroke Rats" STEM CELLS TRANSLATIONAL MEDICINE (2016)

77. Yan, Tao; Venkat, Poornima; Chopp, Michael; Zacharek, Alex; Ning, Ruizhuo; Roberts, Cynthia; Zhang, Yi; Lu, Mei; Chen, Jieli. "Neurorestorative Responses to Delayed Human Mesenchymal Stromal Cells Treatment of Stroke in Type 2 Diabetic Rats" STROKE (2016)

78. Wang, Tong; Martin, Sally; Nguyen, Tam H.; Harper, Callista B.; Gormal, Rachel S.; Martinez-Marmol, Ramon; Karunanithi, Shanker; Coulson, Elizabeth J.; Glass, Nick R.; Cooper-White, Justin J.; van Swinderen, Bruno; Meunier, Frederic A.. "Flux of signalling endosomes undergoing axonal retrograde transport is encoded by presynaptic activity and TrkB" NATURE COMMUNICATIONS (2016)

79. Bomba-Warczak, Ewa; Vevea, Jason D.; Brittain, Joel M.; Figueroa-Bernier, Annette; Tepp, William H.; Johnson, Eric A.; Yeh, Felix L.; Chapman, Edwin R.. "Interneuronal Transfer and Distal Action of Tetanus Toxin and Botulinum Neurotoxins A and D in Central Neurons" CELL REPORTS (2016)

80. Eitan, Erez; Petralia, Ronald S.; Wang, Ya-Xian; Indig, Fred E.; Mattson, Mark P.; Yao, Pamela J.. "Probing extracellular Sonic hedgehog in neurons" BIOLOGY OPEN (2016)

81. Chen, Meifan; Geoffroy, Cedric G.; Wong, Hetty N.; Tress, Oliver; Nguyen, Mallorie T.; Holzman, Lawrence B.; Jin, Yishi; Zheng, Binhai. "Leucine Zipper-bearing Kinase promotes axon growth in mammalian central nervous system neurons" SCIENTIFIC REPORTS (2016)

82. Jia, Longfei; Wang, Lei; Chopp, Michael; Zhang, Yi; Szalad, Alexandra; Zhang, Zheng Gang. "MicroRNA 146a LOCALLY MEDIATES DISTAL AXONAL GROWTH OF DORSAL ROOT GANGLIA NEURONS UNDER HIGH GLUCOSE AND SILDENAFIL CONDITIONS" NEUROSCIENCE (2016)

83. Kim, Hyun Soo; Jeong, Sehoon; Koo, Chiwan; Han, Arum; Park, Jaewon. "A Microchip for High-Throughput Axon Growth Drug Screening" MICROMACHINES (2016)

84. Piccinotti, Silvia; Whelan, Sean P. J.. "Rabies Internalizes into Primary Peripheral Neurons via Clathrin Coated Pits and Requires Fusion at the Cell Body" PLOS PATHOGENS (2016)

85. Carballo-Molina, Oscar A.; Sanchez-Navarro, Andrea; Lopez-Ornelas, Adolfo; Lara-Rodarte, Rolando; Salazar, Patricia; Campos-Romo, Aurelio; Ramos-Mejia, Veronica; Velasco, Ivan. "Semaphorin 3C Released from a Biocompatible Hydrogel Guides and Promotes Axonal Growth of Rodent and Human Dopaminergic Neurons" TISSUE ENGINEERING PART A (2016)

86. Kos, Aron; Wanke, Kai A.; Gioio, Anthony; Martens, Gerard J.; Kaplan, Barry B.; Aschrafi, Armaz. "Monitoring mRNA Translation in Neuronal Processes Using Fluorescent Non-Canonical Amino Acid Tagging" JOURNAL OF HISTOCHEMISTRY & CYTOCHEMISTRY (2016)

87. DeMarse, Thomas B.; Pan, Liangbin; Alagapan, Sankaraleengam; Brewer, GregoryJ.; Wheeler, Bruce C.. "Feed-Forward Propagation of Temporal and Rate Information between Cortical Populations during Coherent Activation in Engineered In Vitro Networks" FRONTIERS IN NEURAL CIRCUITS (2016)

88. Brahic, Michel; Bousset, Luc; Bieri, Gregor; Melki, Ronald; Gitler, Aaron D.. "Axonal transport and secretion of fibrillar forms of alpha-synuclein, A beta 42 peptide and HTTExon 1" ACTA NEUROPATHOLOGICA (2016)

89. Lewandowska, Marta K.; Radivojevic, Milos; Jaeckel, David; Mueller, Jan; Hierlemann, Andreas R.. "Cortical Axons, Isolated in Channels, Display Activity-Dependent Signal Modulation as a Result of Targeted Stimulation" FRONTIERS IN NEUROSCIENCE (2016)

90. Gao, Yandong; Broussard, Joey; Haque, Amranul; Revzin, Alexander; Lin, Tian. "Functional imaging of neuron-astrocyte interactions in a compartmentalized microfluidic device" MICROSYSTEMS & NANOENGINEERING (2016)

91. Takayama, Yuzo; Kida, Yasuyuki S.. "In Vitro Reconstruction of Neuronal Networks Derived from Human iPS Cells Using Microfabricated Devices" PLOS ONE (2016)

92. Ionescu, Ariel; Zahavi, Eitan Erez; Gradus, Tal; Ben-Yaakov, Keren; Perlson, Eran. "Compartmental microfluidic system for studying muscle-neuron communication and neuromuscular junction maintenance" EUROPEAN JOURNAL OF CELL BIOLOGY (2016)

93. Uryu, Daiki; Tamaru, Tomohiro; Suzuki, Azusa; Sakai, Rie; Konishi, Yoshiyuki. "Study of local intracellular signals regulating axonal morphogenesis using a microfluidic device" SCIENCE AND TECHNOLOGY OF ADVANCED MATERIALS (2016)

94. Lei, Yifeng; Li, Jun; Wang, Nuoxin; Yang, Xinglong; Hamada, Yoh; Li, Qizhai; Zheng, Wenfu; Jiang, Xingyu. "An on-chip model for investigating the interaction between neurons and cancer cells" INTEGRATIVE BIOLOGY (2016)

95. Chen, Jieli; Ning, Ruizhuo; Zacharek, Alex; Cui, Chengcheng; Cui, Xu; Yan, Tao; Venkat, Poornima; Zhang, Yi; Chopp, Michael. "MiR-126 Contributes to Human Umbilical Cord Blood Cell-Induced Neurorestorative Effects After Stroke in Type-2 Diabetic Mice" STEM CELLS (2016)

96. Yao, Pamela J.; Petralia, Ronald S.; Ott, Carolyn; Wang, Ya-Xian; Lippincott-Schwartz, Jennifer; Mattson, Mark P.. "Dendrosomatic Sonic Hedgehog Signaling in Hippocampal Neurons Regulates Axon Elongation" JOURNAL OF NEUROSCIENCE (2015)

97. Isomura, Takuya; Shimba, Kenta; Takayama, Yuzo; Takeuchi, Akimasa; Kotani, Kiyoshi; Jimbo, Yasuhiko. "Signal transfer within a cultured asymmetric cortical neuron circuit" JOURNAL OF NEURAL ENGINEERING (2015)

98. Mika, Johann K.; Schwarz, Karin; Wanzenboeck, Heinz D.; Scholze, Petra; Bertagnolli, Emmerich. "Investigation of Neurotrophic Factor Concentrations with a Novel In Vitro Concept for Peripheral Nerve Regeneration" JOURNAL OF NEUROSCIENCE RESEARCH (2015)

99. Usenovic, Marija; Niroomand, Shahriar; Drolet, Robert E.; Yao, Lihang; Gaspar, Renee C.; Hatcher, Nathan G.; Schachter, Joel; Renger, John J.; Parmentier-Batteur, Sophie. "Internalized Tau Oligomers Cause Neurodegeneration by Inducing Accumulation of Pathogenic Tau in Human Neurons Derived from Induced Pluripotent Stem Cells" JOURNAL OF NEUROSCIENCE (2015)

100. Takeda, Shuko; Wegmann, Susanne; Cho, Hansang; Devos, Sarah L.; Commins, Caitlin; Roe, Allyson D.; Nicholls, Samantha B.; Carlson, George A.; Pitstick, Rose; Nobuhara, Chloe K.; Costantino, Isabel; Frosch, Matthew P.; Mueller, Daniel J.; Irimia, Daniel; Hyman, Bradley T.. "Neuronal uptake and propagation of a rare phosphorylated high-molecular-weight tau derived from Alzheimer's disease brain" NATURE COMMUNICATIONS (2015)

101. Li, Yu-Tao; Zhang, Shu-Hui; Wang, Xue-Ying; Zhang, Xin-Wei; Oleinick, Alexander I.; Svir, Irina; Amatore, Christian; Huang, Wei-Hua. "Real-time Monitoring of Discrete Synaptic Release Events and Excitatory Potentials within Self-reconstructed Neuromuscular Junctions" ANGEWANDTE CHEMIE-INTERNATIONAL EDITION (2015)

102. Lin, Shen; Nazif, Kutaiba; Smith, Alexander; Baas, Peter W.; Smith, George M.. "Histone acetylation inhibitors promote axon growth in adult dorsal root ganglia neurons" JOURNAL OF NEUROSCIENCE RESEARCH (2015)

103. Pan, Liangbin; Alagapan, Sankaraleengam; Franca, Eric; Leondopulos, Stathis S.; DeMarse, Thomas B.; Brewer, Gregory J.; Wheeler, Bruce C.. "An in vitro method to manipulate the direction and functional strength between neural populations" FRONTIERS IN NEURAL CIRCUITS (2015)

104. Reginensi, Diego; Carulla, Patricia; Nocentini, Sara; Seira, Oscar; Serra-Picamal, Xavier; Torres-Espin, Abel; Matamoros-Angles, Andreu; Gavin, Rosalina; Teresa Moreno-Flores, Maria; Wandosell, Francisco; Samitier, Josep; Trepat, Xavier; Navarro, Xavier; Antonio del Rio, Jose. "Increased migration of olfactory ensheathing cells secreting the Nogo receptor ectodomain over inhibitory substrates and lesioned spinal cord" CELLULAR AND MOLECULAR LIFE SCIENCES (2015)

105. Kerman, Bilal E.; Kim, Hyung Joon; Padmanabhan, Krishnan; Mei, Arianna; Georges, Shereen; Joens, Matthew S.; Fitzpatrick, James A. J.; Jappelli, Roberto; Chandross, Karen J.; August, Paul; Gage, Fred H.. "In vitro myelin formation using embryonic stem cells" DEVELOPMENT (2015)

106. Markus, Amos; Lebenthal-Loinger, Ilana; Yang, In Hong; Kinchington, Paul R.; Goldstein, Ronald S.. "An In Vitro Model of Latency and Reactivation of Varicella Zoster Virus in Human Stem Cell-Derived Neurons" PLOS PATHOGENS (2015)

107. Calafate, Sara; Buist, Arjan; Miskiewicz, Katarzyna; Vijayan, Vinoy; Daneels, Guy; de Strooper, Bart; de Wit, Joris; Verstreken, Patrik; Moechars, Diederik. "Synaptic Contacts Enhance Cell-to-Cell Tau Pathology Propagation" CELL REPORTS (2015)

108. Renault, Renaud; Sukenik, Nirit; Descroix, Stephanie; Malaquin, Laurent; Viovy, Jean-Louis; Peyrin, Jean-Michel; Bottani, Samuel; Monceau, Pascal; Moses, Elisha; Vignes,

Maeva. "Combining Microfluidics, Optogenetics and Calcium Imaging to Study Neuronal Communication In Vitro" PLOS ONE (2015)

109. Wang, Tong; Martin, Sally; Papadopulos, Andreas; Harper, Callista B.; Mavlyutov, Timur A.; Niranjan, Dhevahi; Glass, Nick R.; Cooper-White, Justin J.; Sibarita, Jean-Baptiste; Choquet, Daniel; Davletov, Bazbek; Meunier, Frederic A.. "Control of Autophagosome Axonal Retrograde Flux by Presynaptic Activity Unveiled Using Botulinum Neurotoxin Type A" JOURNAL OF NEUROSCIENCE (2015)

110. Deglincerti, Alessia; Liu, Yaobin; Colak, Dilek; Hengst, Ulrich; Xu, Guoqiang; Jaffrey, Samie R.. "Coupled local translation and degradation regulate growth cone collapse" NATURE COMMUNICATIONS (2015)

111. Dixon, Angela R.; Philbert, Martin A.. "Morphometric assessment of toxicant induced neuronal degeneration in full and restricted contact co-cultures of embryonic cortical rat neurons and astrocytes: Using m-Dinitrobezene as a model neurotoxicant" TOXICOLOGY IN VITRO (2015)

112. Speranza, Luisa; Giuliano, Teresa; Volpicelli, Floriana; De Stefano, M. Egle; Lombardi, Loredana; Chambery, Angela; Lacivita, Enza; Leopoldo, Marcello; Bellenchi, Gian C.; di Porzio, Umberto; Crispino, Marianna; Perrone-Capano, Carla. "Activation of 5-HT7 receptor stimulates neurite elongation through mTOR, Cdc42 and actin filaments dynamics" FRONTIERS IN BEHAVIORAL NEUROSCIENCE (2015)

113. Lewandowska, Marta K.; Bakkum, Douglas J.; Rompani, Santiago B.; Hierlemann, Andreas. "Recording Large Extracellular Spikes in Microchannels along Many Axonal Sites from Individual Neurons" PLOS ONE (2015)

114. Marquardt, Laura M.; Sakiyama-Elbert, Shelly E.. "GDNF preconditioning can overcome Schwann cell phenotypic memory" EXPERIMENTAL NEUROLOGY (2015)

115. Niederst, Emily D.; Reyna, Sol M.; Goldstein, Lawrence S. B.. "Axonal amyloid precursor protein and its fragments undergo somatodendritic endocytosis and processing" MOLECULAR BIOLOGY OF THE CELL (2015)

116. Sakai, Koji; Shimba, Kenta; Kotani, Kiyoshi; Jimbo, Yasuhiko. "Microfabricated multi-electrode device for detecting oligodendrocyte-regulated changes in axonal conduction velocity" 2015 37TH ANNUAL INTERNATIONAL CONFERENCE OF THE IEEE ENGINEERING IN MEDICINE AND BIOLOGY SOCIETY (EMBC) (2015)

117. Selfridge, Aaron; Hyun, Nicholas; Chiang, Chai-Chun; Reyna, Sol M.; Weissmiller, April M.; Shi, Linda Z.; Preece, Daryl; Mobley, William C.; Berns, Michael W.. "Rat embryonic hippocampus and induced pluripotent stem cell derived cultured neurons recover from laser-induced subaxotomy" NEUROPHOTONICS (2015)

118. Habibey, Rouhollah; Golabchi, Asiyeh; Latifi, Shahrzad; Difato, Francesco; Blau, Axel. "A microchannel device tailored to laser axotomy and long-term microelectrode array electrophysiology of functional regeneration" LAB ON A CHIP (2015)

119. Chiang, Hao; Ohno, Nobuhiko; Hsieh, Yu-Lin; Mahad, Don J.; Kikuchi, Shin; Komuro, Hitoshi; Hsieh, Sung-Tsang; Trapp, Bruce D.. "Mitochondrial fission augments capsaicin-induced axonal degeneration" ACTA NEUROPATHOLOGICA (2015)

120. Tong, Ziqiu; Segura-Feliu, Miriam; Seira, Oscar; Homs-Corbera, Antoni; Antonio Del Rio, Jose; Samitier, Josep. "A microfluidic neuronal platform for neuron axotomy and controlled regenerative studies" RSC ADVANCES (2015)

121. Ashrafi, Ghazaleh; Schlehe, Julia S.; LaVoie, Matthew J.; Schwarz, Thomas L.. "Mitophagy of damaged mitochondria occurs locally in distal neuronal axons and requires PINK1 and Parkin" JOURNAL OF CELL BIOLOGY (2014)

122. Wu, Kong-Yan; He, Miao; Hou, Qiong-Qiong; Sheng, Ai-Li; Yuan, Lei; Liu, Fei; Liu, Wen-Wen; Li, Guangpu; Jiang, Xing-Yu; Luo, Zhen-Ge. "Semaphorin 3A activates the

guanosine triphosphatase Rab5 to promote growth cone collapse and organize callosal axon projections" SCIENCE SIGNALING (2014)

123. Gluska, Shani; Zahavi, Eitan Erez; Chein, Michael; Gradus, Tal; Bauer, Anja; Finke, Stefan; Perlson, Eran. "Rabies Virus Hijacks and Accelerates the p75NTR Retrograde Axonal Transport Machinery" PLOS PATHOGENS (2014)

124. Yap, Yiing C.; Dickson, Tracey C.; King, Anna E.; Breadmore, Michael C.; Guijt, Rosanne M.. "Microfluidic culture platform for studying neuronal response to mild to very mild axonal stretch injuryn" BIOMICROFLUIDICS (2014)

125. Tran, Hien T.; Chung, Charlotte Hiu-Yan; Iba, Michiyo; Zhang, Bin; Trojanowski, John Q.; Luk, Kelvin C.; Lee, Virginia M. Y.. "alpha-Synuclein Immunotherapy Blocks Uptake and Templated Propagation of Misfolded alpha-Synuclein and Neurodegeneration" CELL REPORTS (2014)

126. Pan, Liangbin; Alagapan, Sankaraleengam; Franca, Eric; DeMarse, Thomas; Brewer, Gregory J.; Wheeler, Bruce C.. "Large Extracellular Spikes Recordable From Axons in Microtunnels" IEEE TRANSACTIONS ON NEURAL SYSTEMS AND REHABILITATION ENGINEERING (2014)

127. Otsmane, Belkacem; Moumen, Anice; Aebischer, Julianne; Coque, Emmanuelle; Sar, Chamroeun; Sunyach, Claire; Salsac, Celine; Valmier, Jean; Salinas, Sara; Bowerman, Melissa; Raoul, Cedric. "Somatic and axonal LIGHT signaling elicit degenerative and regenerative responses in motoneurons, respectively" EMBO REPORTS (2014)

128. Brewer, Bryson M.; Shi, Mingjian; Edd, Jon F.; Webb, Donna J.; Li, Deyu. "A microfluidic cell co-culture platform with a liquid fluorocarbon separator" BIOMEDICAL MICRODEVICES (2014)

129. Tegenge, Million Adane; Rajbhandari, Labchan; Shrestha, Shiva; Mithal, Aditya; Hosmane, Suneil; Venkatesan, Arun. "Curcumin protects axons from degeneration in the setting of local neuroinflammation" EXPERIMENTAL NEUROLOGY (2014)

130. Saito, Atsushi; Takayama, Yuzo; Moriguchi, Hiroyuki; Kotani, Kiyoshi; Jimbo, Yasuhiko. "Induced Current Pharmacological Split Stimulation System for Neuronal Networks" IEEE TRANSACTIONS ON BIOMEDICAL ENGINEERING (2014)

131. Tang-Schomer, Min D.; Davies, Paul; Graziano, Daniel; Thurber, Amy E.; Kaplan, David L.. "Neural circuits with long-distance axon tracts for determining functional connectivity" JOURNAL OF NEUROSCIENCE METHODS (2014)

132. Park, Jaewon; Kim, Sunja; Park, Su Inn; Choe, Yoonsuck; Li, Jianrong; Han, Arum. "A microchip for quantitative analysis of CNS axon growth under localized biomolecular treatments" JOURNAL OF NEUROSCIENCE METHODS (2014)

133. Deleglise, Berangere; Magnifico, Sebastien; Duplus, Eric; Vaur, Pauline; Soubeyre, Vanessa; Belle, Morgane; Vignes, Maeva; Viovy, Jean-Louis; Jacotot, Etienne; Peyrin, Jean-Michel; Brugg, Bernard. "beta-amyloid induces a dying-back process and remote trans-synaptic alterations in a microfluidic-based reconstructed neuronal network" ACTA NEUROPATHOLOGICA COMMUNICATIONS (2014)

134. Dujardin, Simon; Lecolle, Katia; Caillierez, Raphaelle; Begard, Severine; Zommer, Nadege; Lachaud, Cedrick; Carrier, Sebastien; Dufour, Noelle; Auregan, Gwennaelle; Winderickx, Joris; Hantraye, Philippe; Deglon, Nicole; Colin, Morvane; Buee, Luc. "Neuron-to-neuron wild-type Tau protein transfer through a trans-synaptic mechanism: relevance to sporadic tauopathies" ACTA NEUROPATHOLOGICA COMMUNICATIONS (2014)

135. Song, Ha-Lim; Shim, Sungbo; Kim, Dong-Hou; Won, Se-Hoon; Joo, Segyeong; Kim, Sudong; Jeon, Noo Li; Yoon, Seung-Yong. "beta-Amyloid Is Transmitted via Neuronal Connections along Axonal Membranes" ANNALS OF NEUROLOGY (2014)

136. Robertson, Graham; Bushell, Trevor J.; Zagnoni, Michele. "Chemically induced synaptic activity between mixed primary hippocampal co-cultures in a microfluidic system" INTEGRATIVE BIOLOGY (2014)

137. Tong, Ziqiu; Seira, Oscar; Casas, Cristina; Reginensi, Diego; Homs-Corbera, Antoni; Samitier, Josep; Antonio Del Rio, Jose. "Engineering a functional neuro-muscular junction model in a chip" RSC ADVANCES (2014)

138. Rage, Florence; Boulisfane, Nawal; Rihan, Khalil; Neel, Henry; Gostan, Thierry; Bertrand, Edouard; Bordonne, Remy; Soret, Johann. "Genome-wide identification of mRNAs associated with the protein SMN whose depletion decreases their axonal localization" RNA (2013)

139. Tsantoulas, Christoforos; Farmer, Clare; Machado, Patricia; Baba, Katsuhiro; McMahon, Stephen B.; Raouf, Ramin. "Probing Functional Properties of Nociceptive Axons Using a Microfluidic Culture System" PLOS ONE (2013)

140. Sauer, Brian M.; Schmalstieg, William F.; Howe, Charles L.. "Axons are injured by antigen-specific CD8(+) T cells through a MHC class I- and granzyme B-dependent mechanism" NEUROBIOLOGY OF DISEASE (2013)

141. Brewer, Gregory J.; Boehler, Michael D.; Leondopulos, Stathis; Pan, Liangbin; Alagapan, Sankaraleengam; DeMarse, Thomas B.; Wheeler, Bruce C.. "Toward a self-wired active reconstruction of the hippocampal trisynaptic loop: DG-CA3" FRONTIERS IN NEURAL CIRCUITS (2013)

142. Southam, Katherine A.; King, Anna E.; Blizzard, Catherine A.; McCormack, Graeme H.; Dickson, Tracey C.. "Microfluidic-primary culture model of the lower motor neuron-neuromuscular junction circuit" JOURNAL OF NEUROSCIENCE METHODS (2013)

143. Deleglise, Berangere; Lassus, Benjamin; Soubeyre, Vaneyssa; Alleaume-Butaux, Aurelie; Hjorth, Johannes J.; Vignes, Maeva; Schneider, Benoit; Brugg, Bernard; Viovy, Jean-Louis; Peyrin, Jean-Michel. "Synapto-Protective Drugs Evaluation in Reconstructed Neuronal Network" PLOS ONE (2013)

144. Saito, Atsushi; Saito, Aki; Moriguchi, Hiroyuki; Kotani, Kiyoshi; Jimbo, Yasuhiko. "Localized Induced Current Stimulation to Neuronal Culture Using Soft Magnetic Material" ELECTRONICS AND COMMUNICATIONS IN JAPAN (2013)

145. Sun, Tao; Yu, Nuo; Zhai, Lu-Kai; Li, Na; Zhang, Chao; Zhou, Liang; Huang, Zhuo; Jiang, Xing-Yu; Shen, Ying; Chen, Zhe-Yu. "c-Jun NH2-terminal Kinase (JNK)-interacting Protein-3 (JIP3) Regulates Neuronal Axon Elongation in a Kinesin- and JNK-dependent Manner" JOURNAL OF BIOLOGICAL CHEMISTRY (2013)

146. Ben M'Barek, Karim; Pla, Patrick; Orvoen, Sophie; Benstaali, Caroline; Godin, Juliette D.; Gardier, Alain M.; Saudou, Frederic; David, Denis J.; Humbert, Sandrine. "Huntingtin Mediates Anxiety/Depression-Related Behaviors and Hippocampal Neurogenesis" JOURNAL OF NEUROSCIENCE (2013)

147. Swanger, Sharon A.; He, Yuncen A.; Richter, Joel D.; Bassell, Gary J.. "Dendritic GluN2A Synthesis Mediates Activity-Induced NMDA Receptor Insertion" JOURNAL OF NEUROSCIENCE (2013)

148. Cusack, Corey L.; Swahari, Vijay; Henley, W. Hampton; Ramsey, J. Michael; Deshmukh, Mohanish. "Distinct pathways mediate axon degeneration during apoptosis and axon-specific pruning" NATURE COMMUNICATIONS (2013)

149. Zhang, Yi; Ueno, Yuji; Liu, Xian Shuang; Buller, Benjamin; Wang, Xinli; Chopp, Michael; Zhang, Zheng Gang. "The MicroRNA-17-92 Cluster Enhances Axonal Outgrowth in Embryonic Cortical Neurons" JOURNAL OF NEUROSCIENCE (2013)

150. Liot, Geraldine; Zala, Diana; Pla, Patrick; Mottet, Guillaume; Piel, Matthieu; Saudou, Frederic. "Mutant Huntingtin Alters Retrograde Transport of TrkB Receptors in Striatal Dendrites" JOURNAL OF NEUROSCIENCE (2013)

151. Zala, Diana; Hinckelmann, Maria-Victoria; Saudou, Frederic. "Huntingtin's Function in Axonal Transport Is Conserved in Drosophila melanogaster" PLOS ONE (2013)

152. Taylor, Anne Marion; Wu, Jason; Tai, Hwan-Ching; Schuman, Erin M.. "Axonal Translation of beta-Catenin Regulates Synaptic Vesicle Dynamics" JOURNAL OF NEUROSCIENCE (2013)

153. Sgro, Allyson E.; Bajjalieh, Sandra M.; Chiu, Daniel T.. "Single-Axonal Organelle Analysis Method Reveals New Protein-Motor Associations" ACS CHEMICAL NEUROSCIENCE (2013)

154. Barbati, Alexander C.; Fang, Cheng; Banker, Gary A.; Kirby, Brian J.. "Culture of primary rat hippocampal neurons: design, analysis, and optimization of a microfluidic device for cell seeding, coherent growth, and solute delivery" BIOMEDICAL MICRODEVICES (2013)

155. Wu, Jessica W.; Herman, Mathieu; Liu, Li; Simoes, Sabrina; Acker, Christopher M.; Figueroa, Helen; Steinberg, Joshua I.; Margittai, Martin; Kayed, Rakez; Zurzolo, Chiara; Di Paolo, Gilbert; Duff, Karen E.. "Small Misfolded Tau Species Are Internalized via Bulk Endocytosis and Anterogradely and Retrogradely Transported in Neurons" JOURNAL OF BIOLOGICAL CHEMISTRY (2013)

156. Shimba, Kenta; Sakai, Koji; Arimatsu, Kazuyuki; Kotani, Kiyoshi; Jimbo, Yasuhiko. "Long Term Observation of Propagating Action Potentials along the Axon in a Microtunnel Device" 2013 6TH INTERNATIONAL IEEE/EMBS CONFERENCE ON NEURAL ENGINEERING (NER) (2013)

157. Nguyen, Thanh D.; Hogue, Ian B.; Cung, Kellye; Purohit, Prashant K.; McAlpine, Michael C.. "Tension-induced neurite growth in microfluidic channels" LAB ON A CHIP (2013)

158. Honegger, Thibault; Scott, Mark A.; Yanik, Mehmet F.; Voldman, Joel. "Electrokinetic confinement of axonal growth for dynamically configurable neural networks" LAB ON A CHIP (2013)

159. Hallfors, Nicholas; Khan, Asif; Dickey, Michael D.; Taylor, Anne Marion. "Integration of pre-aligned liquid metal electrodes for neural stimulation within a user-friendly microfluidic platform" LAB ON A CHIP (2013)

160. Ngoc-Duy Dinh; Chiang, Ya-Yu; Hardelauf, Heike; Baumann, Jenny; Jackson, Emily; Waide, Sarah; Sisnaiske, Julia; Frimat, Jean-Philippe; van Thriel, Christoph; Janasek, Dirk; Peyrin, Jean-Michel; West, Jonathan. "Microfluidic construction of minimalistic neuronal co-cultures" LAB ON A CHIP (2013)

161. Grigoryan, Sergei; Kinchington, Paul R.; Yang, In Hong; Selariu, Anca; Zhu, Hua; Yee, Michael; Goldstein, Ronald S.. "Retrograde axonal transport of VZV: kinetic studies in hESC-derived neurons" JOURNAL OF NEUROVIROLOGY (2012)

162. Butko, Margaret T.; Yang, Jin; Geng, Yang; Kim, Hyung Joon; Jeon, Noo Li; Shu, Xiaokun; Mackey, Mason R.; Ellisman, Mark H.; Tsien, Roger Y.; Lin, Michael Z.. "Fluorescent and photo-oxidizing TimeSTAMP tags track protein fates in light and electron microscopy" NATURE NEUROSCIENCE (2012)

163. Walker, Breset A.; Ji, Sheng-Jian; Jaffrey, Samie R.. "Intra-Axonal Translation of RhoA Promotes Axon Growth Inhibition by CSPG" JOURNAL OF NEUROSCIENCE (2012)

164. Freundt, Eric C.; Maynard, Nate; Clancy, Eileen K.; Roy, Shyamali; Bousset, Luc; Sourigues, Yannick; Covert, Markus; Melki, Ronald; Kirkegaard, Karla; Brahic, Michel. "Neuron-to-neuron transmission of alpha-synuclein fibrils through axonal transport" ANNALS OF NEUROLOGY (2012)

165. Li, Li; Ren, Li; Liu, Wenming; Wang, Jian-Chun; Wang, Yaolei; Tu, Qin; Xu, Juan; Liu, Rui; Zhang, Yanrong; Yuan, Mao-Sen; Li, Tianbao; Wang, Jinyi. "Spatiotemporally Controlled and Multifactor Involved Assay of Neuronal Compartment Regeneration after Chemical Injury in an Integrated Microfluidics" ANALYTICAL CHEMISTRY (2012)

166. Lu, Xi; Kim-Han, Jeong S.; O'Malley, Karen L.; Sakiyama-Elbert, Shelly E.. "A microdevice platform for visualizing mitochondrial transport in aligned dopaminergic axons" JOURNAL OF NEUROSCIENCE METHODS (2012)

167. Fujiwara, Takeshi; Morimoto, Koji. "Cooperative effect of p150Glued and microtubule stabilization to suppress excitotoxicity-induced axon degeneration" BIOCHEMICAL AND BIOPHYSICAL RESEARCH COMMUNICATIONS (2012)

168. Kobayashi, Mariko; Wilson, Angus C.; Chao, Moses V.; Mohr, Ian. "Control of viral latency in neurons by axonal mTOR signaling and the 4E-BP translation repressor" GENES & DEVELOPMENT (2012)

169. Kim, Hyung Joon; Park, Jeong Won; Byun, Jae Hwan; Poon, Wayne W.; Cotman, Carl W.; Fowlkes, Charless C.; Jeon, Noo Li. "Quantitative Analysis of Axonal Transport by Using Compartmentalized and Surface Micropatterned Culture of Neurons" ACS CHEMICAL NEUROSCIENCE (2012)

170. Yang, In Hong; Gary, Devin; Malone, Misti; Dria, Stephen; Houdayer, Thierry; Belegu, Visar; Mcdonald, John W.; Thakor, Nitish. "Axon Myelination and Electrical Stimulation in a Microfluidic, Compartmentalized Cell Culture Platform" NEUROMOLECULAR MEDICINE (2012)

171. Hosmane, Suneil; Tegenge, Million Adane; Rajbhandari, Labchan; Uapinyoying, Prech; Kumar, Nishant Ganesh; Thakor, Nitish; Venkatesan, Arun. "Toll/Interleukin-1 Receptor Domain-Containing Adapter Inducing Interferon-beta Mediates Microglial Phagocytosis of Degenerating Axons" JOURNAL OF NEUROSCIENCE (2012)

172. Ueno, Masaki; Hayano, Yasufumi; Nakagawa, Hiroshi; Yamashita, Toshihide. "Intraspinal rewiring of the corticospinal tract requires target-derived brain-derived neurotrophic factor and compensates lost function after brain injury" BRAIN (2012)

173. Wang, Ling; Riss, Michael; Buitrago, Jennifer Olmos; Claverol-Tinture, Enric. "Biophysics of microchannel-enabled neuron-electrode interfaces" JOURNAL OF NEURAL ENGINEERING (2012)

174. Zhang, Yanqing; Bekku, Yoko; Dzhashiashvili, Yulia; Armenti, Stephen; Meng, Xiaosong; Sasaki, Yo; Milbrandt, Jeffrey; Salzer, James L.. "Assembly and Maintenance of Nodes of

Ranvier Rely on Distinct Sources of Proteins and Targeting Mechanisms" NEURON (2012)

175. Park, Jaewon; Koito, Hisami; Li, Jianrong; Han, Arum. "Multi-compartment neuron-glia co-culture platform for localized CNS axon-glia interaction study" LAB ON A CHIP (2012)

176. Takayama, Yuzo; Moriguchi, Hiroyuki; Kotani, Kiyoshi; Suzuki, Takafumi; Mabuchi, Kunihiko; Jimbo, Yasuhiko. "Network-wide integration of stem cell-derived neurons and mouse cortical neurons using microfabricated co-culture devices" BIOSYSTEMS (2012)

177. Hosie, Katherine A.; King, Anna E.; Blizzard, Catherine A.; Vickers, James C.; Dickson, Tracey C.. "Chronic excitotoxin-induced axon degeneration in a compartmented neuronal culture model" ASN NEURO (2012)

178. Volpicelli-Daley, Laura A.; Luk, Kelvin C.; Patel, Tapan P.; Tanik, Selcuk A.; Riddle, Dawn M.; Stieber, Anna; Meaney, David F.; Trojanowski, John Q.; Lee, Virginia M. -Y.. "Exogenous alpha-Synuclein Fibrils Induce Lewy Body Pathology Leading to Synaptic Dysfunction and Neuron Death" NEURON (2011)

179. Shi, Peng; Scott, Mark A.; Ghosh, Balaram; Wan, Dongpeng; Wissner-Gross, Zachary; Mazitschek, Ralph; Haggarty, Stephen J.; Yanik, Mehmet Fatih. "Synapse microarray identification of small molecules that enhance synaptogenesis" NATURE COMMUNICATIONS (2011)

180. Pan, Liangbin; Alagapan, Sankaraleengam; Franca, Eric; Brewer, Gregory J.; Wheeler, Bruce C.. "Propagation of action potential activity in a predefined microtunnel neural network" JOURNAL OF NEURAL ENGINEERING (2011)

181. Cohen, Michael S.; Orth, Carlos Bas; Kim, Hyung Joon; Jeon, Noo Li; Jaffrey, Samie R.. "Neurotrophin-mediated dendrite-to-nucleus signaling revealed by microfluidic compartmentalization of dendrites" PROCEEDINGS OF THE NATIONAL ACADEMY OF SCIENCES OF THE UNITED STATES OF AMERICA (2011)

182. Andres, Robert H.; Horie, Nobutaka; Slikker, William; Keren-Gill, Hadar; Zhan, Ke; Sun, Guohua; Manley, Nathan C.; Pereira, Marta P.; Sheikh, Lamiya A.; McMillan, Erin L.; Schaar, Bruce T.; Svendsen, Clive N.; Bliss, Tonya M.; Steinberg, Gary K.. "Human neural stem cells enhance structural plasticity and axonal transport in the ischaemic brain" BRAIN (2011)

183. Hur, Eun-Mi; Yang, In Hong; Kim, Deok-Ho; Byun, Justin; Saijilafu; Xu, Wen-Lin; Nicovich, Philip R.; Cheong, Raymond; Levchenko, Andre; Thakor, Nitish; Zhou, Feng-Quan. "Engineering neuronal growth cones to promote axon regeneration over inhibitory molecules" PROCEEDINGS OF THE NATIONAL ACADEMY OF SCIENCES OF THE UNITED STATES OF AMERICA (2011)

184. Pirlo, R. K.; Sweeney, A. J.; Ringeisen, B. R.; Kindy, M.; Gao, B. Z.. "Biochip/laser cell deposition system to assess polarized axonal growth from single neurons and neuron/glia pairs in microchannels with novel asymmetrical geometries" BIOMICROFLUIDICS (2011)

185. Danzer, Karin M.; Ruf, Wolfgang P.; Putcha, Preeti; Joyner, Daniel; Hashimoto, Tadafumi; Glabe, Charles; Hyman, Bradley T.; McLean, Pamela J.. "Heat-shock protein 70 modulates toxic extracellular alpha-synuclein oligomers and rescues trans-synaptic toxicity" FASEB JOURNAL (2011)

186. Arundell, Martin; Perry, V. Hugh; Newman, Tracey. A.. "Integration of a macro/micro architectured compartmentalised neuronal culture device using a rapid prototyping moulding process" LAB ON A CHIP (2011)

187. Peyrin, Jean-Michel; Deleglise, Berangere; Saias, Laure; Vignes, Maeva; Gougis, Paul; Magnifico, Sebastien; Betuing, Sandrine; Pietri, Mathea; Caboche, Jocelyne; Vanhoutte, Peter; Viovy, Jean-Louis; Brugg, Bernard. "Axon diodes for the reconstruction of oriented neuronal networks in microfluidic chambers" LAB ON A CHIP (2011)

188. Hosmane, Suneil; Fournier, Adam; Wright, Rika; Rajbhandari, Labchan; Siddique, Rezina; Yang, In Hong; Ramesh, K. T.; Venkatesan, Arun; Thakor, Nitish. "Valve-based

microfluidic compression platform: single axon injury and regrowth" LAB ON A CHIP (2011)

189. Kilinc, Devrim; Peyrin, Jean-Michel; Soubeyre, Vanessa; Magnifico, Sebastien; Saias, Laure; Viovy, Jean-Louis; Brugg, Bernard. "Wallerian-Like Degeneration of Central Neurons After Synchronized and Geometrically Registered Mass Axotomy in a Three-Compartmental Microfluidic Chip" NEUROTOXICITY RESEARCH (2011)

190. Taylor, Anne M.; Dieterich, Daniela C.; Ito, Hiroshi T.; Kim, Sally A.; Schuman, Erin M.. "Microfluidic Local Perfusion Chambers for the Visualization and Manipulation of Synapses" NEURON (2010)

191. Vitzthum, Lucas; Chen, Xinzhi; Kintner, Douglas B.; Huang, Yu; Chiu, Shing-Yan; Williams, Justin; Sun, Dandan. "Study of Na+/H+ exchange-mediated pH(i) regulations in neuronal soma and neurites in compartmentalized microfluidic devices" INTEGRATIVE BIOLOGY (2010)

192. Hosmane, Suneil; Yang, In Hong; Ruffin, April; Thakor, Nitish; Venkatesan, Arun. "Circular compartmentalized microfluidic platform: Study of axon-glia interactions" LAB ON A CHIP (2010)

193. Berdichevsky, Yevgeny; Staley, Kevin J.; Yarmush, Martin L.. "Building and manipulating neural pathways with microfluidics" LAB ON A CHIP (2010)

194. Shi, Peng; Nedelec, Stephane; Wichterle, Hynek; Kam, Lance C.. "Combined microfluidics/protein patterning platform for pharmacological interrogation of axon pathfinding" LAB ON A CHIP (2010)

195. Zhang, Kai; Osakada, Yasuko; Vrljic, Marija; Chen, Liang; Mudrakola, Harsha V.; Cui, Bianxiao. "Single-molecule imaging of NGF axonal transport in microfluidic devices" LAB ON A CHIP (2010)

196. Park, Jaewon; Koito, Hisami; Li, Jianrong; Han, Arum. "Microfluidic compartmentalized co-culture platform for CNS axon myelination research" BIOMEDICAL MICRODEVICES (2009)

197. Shulga, Anastasia; Blaesse, Anne; Kysenius, Kai; Huttunen, Henri J.; Tanhuanpaa, Kimmo; Saarma, Mart; Rivera, Claudio. "Thyroxin regulates BDNF expression to promote survival of injured neurons" MOLECULAR AND CELLULAR NEUROSCIENCE (2009)

198. Stoothoff, Will; Jones, Phillip B.; Spires-Jones, Tara L.; Joyner, Daniel; Chhabra, Ekta; Bercury, Kathryn; Fan, Zhanyun; Xie, Hong; Bacskai, Brian; Edd, Jon; Irimia, Daniel; Hyman, Bradley T.. "Differential effect of three-repeat and four-repeat tau on mitochondrial axonal transport" JOURNAL OF NEUROCHEMISTRY (2009)

199. Blurton-Jones, Mathew; Kitazawa, Masashi; Martinez-Coria, Hilda; Castello, Nicholas A.; Mueller, Franz-Josef; Loring, Jeanne F.; Yamasaki, Tritia R.; Poon, Wayne W.; Green, Kim N.; LaFerla, Frank M.. "Neural stem cells improve cognition via BDNF in a transgenic model of Alzheimer disease" PROCEEDINGS OF THE NATIONAL ACADEMY OF SCIENCES OF THE UNITED STATES OF AMERICA (2009)

200. Hengst, Ulrich; Deglincerti, Alessia; Kim, Hyung Joon; Jeon, Noo Li; Jaffrey, Samie R.. "Axonal elongation triggered by stimulus-induced local translation of a polarity complex protein" NATURE CELL BIOLOGY (2009)

201. Yang, In Hong; Siddique, Rezina; Hosmane, Suneil; Thakor, Nitish; Hoeke, Ahmet. "Compartmentalized microfluidic culture platform to study mechanism of paclitaxel-induced axonal degeneration" EXPERIMENTAL NEUROLOGY (2009)

202. Taylor, Anne M.; Berchtold, Nicole C.; Perreau, Victoria M.; Tu, Christina H.; Jeon, Noo Li; Cotman, Carl W.. "Axonal mRNA in Uninjured and Regenerating Cortical Mammalian Axons" JOURNAL OF NEUROSCIENCE (2009)

203. Berdichevsky, Yevgeny; Sabolek, Helen; Levine, John B.; Staley, Kevin J.; Yarmush, Martin L.. "Microfluidics and multielectrode array-compatible organotypic slice culture method" JOURNAL OF NEUROSCIENCE METHODS (2009)

204. Kim, Young-tae; Karthikeyan, Kailash; Chirvi, Sajal; Dave, Digant P.. "Neuro-optical microfluidic platform to study injury and regeneration of single axons" LAB ON A CHIP (2009)

205. Liu, Wendy W.; Goodhouse, Joseph; Jeon, Noo Li; Enquist, L. W.. "A Microfluidic Chamber for Analysis of Neuron-to-Cell Spread and Axonal Transport of an Alpha-Herpesvirus" PLOS ONE (2008)

206. Bergen, Jamie M.; Pun, Suzie H.. "Analysis of the intraceltular barriers encountered by nonviral gene carriers in a model of spatially controlled delivery to neurons" JOURNAL OF GENE MEDICINE (2008)

207. Cui, Bianxiao; Wu, Chengbiao; Chen, Liang; Ramirez, Alfredo; Bearer, Elaine L.; Li, Wei-Ping; Mobley, William C.; Chu, Steven. "One at a time, live tracking of NGF axonal transport using quantum dots" PROCEEDINGS OF THE NATIONAL ACADEMY OF SCIENCES OF THE UNITED STATES OF AMERICA (2007)

208. Sutton, Michael A.; Taylor, Anne M.; Ito, Hiroshi T.; Pham, Anh; Schuman, Erin M.. "Postsynaptic decoding of neural activity: eEF2 as a biochemical sensor coupling miniature synaptic transmission to local protein synthesis" NEURON (2007)

209. Millet, Larry J.; Stewart, Matthew E.; Sweedler, Jonathan V.; Nuzzo, Ralph G.; Gillette, Martha U.. "Microfluidic devices for culturing primary mammalian neurons at low densities" LAB ON A CHIP (2007)

210. Ding, JQ; Allen, E; Wang, W; Valle, A; Wu, CB; Nardine, T; Cui, BX; Yi, J; Taylor, A; Jeon, NL; Chu, S; So, Y; Vogel, H; Tolwani, R; Mobley, W; Yang, YM. "Gene targeting of GAN in mouse causes a toxic accumulation of microtubule-associated protein 8 and impaired retrograde axonal transport" HUMAN MOLECULAR GENETICS (2006)

211. Park, Jeong Won; Vahidi, Behrad; Taylor, Anne M.; Rhee, Seog Woo; Jeon, Noo Li. "Microfluidic culture platform for neuroscience research" NATURE PROTOCOLS (2006)

Appendix II

In **Appendix II** detailed experimental protocols are given.

Primary Rat Cortical Tri-Culture

1. Prepare Stock Solutions
    a. 0.1% w/v BSA (Bovine Serum Albumin) Solution
        i. Prepare ~50 mL of 0.1% w/v BSA solution in PBS+ and sterile filter.
        ii. Store at 4ºC
    b. 100 µg/mL IL-34 Solution
        i. Add 100 µL of 0.1% w/v BSA solution to a 10 µg vial of lyophilized IL-34 (R&D Systems, 5195-ML)
        ii. Store between -20ºC and -70ºC
    c. 10 µg/mL TGF-β Solution
        i. Add 200 µL of 0.1% BSA solution to a 2 µg vial of lyophilized TGF-β (Peprotech, 100-35B)
        ii. Store between -20ºC and -70ºC
    d. 1.5 mg/mL Cholesterol Solution
        i. Prepare a 1.5 mg/mL solution of cholesterol (Avanti Polar Lipids ,7000000) in absolute ethanol.
        ii. Store between -20ºC and -70ºC
    e. Plating Media (PM)
        i. Combine 500 mL Neurobasal A, 50 mL heat-inactivated horse serum, 10 mL of B27 supplement, 10 mL of 1 M HEPES pH 7.5, and 5 mL GlutaMax (all from ThermoFisher) and sterile filter.
        ii. Aliquot and store at -80ºC
    f. Growth Media (GM)

i. Combine 500 mL Neurobasal A, 10 mL of B27 supplement, and 5 mL GlutaMax (all from ThermoFisher) and sterile filter.

ii. Aliquot and store at -80ºC

2. Prepare Tri-Culture Media (25 mL)
    a. Combine 25 mL GM with 25 µL IL-34 solution, 5 µL TGF-β solution, and 25 µL cholesterol solution and sterile filter.
    b. Store at 4ºC. *Note: At 4°C if tri-culture media is stored longer than 1 week, the number of microglia decreases significantly. It is important to make fresh media each week during the duration of the culture. Using the following feeding protocol the media will last for 2 media changes; it is recommended to calculate the amount of media required for the week and adjust the recipe accordingly*
3. Substrate Preparation
    a. Cover Poly-L-Lysine coated substrates with PM for at least 4 h at 37ºC and 5% CO_2 (preferably overnight).
4. Plate Cells in PM (Media volume is given for 12 well plates)
    a. Gather cells following a perinatal rap pup dissection (cortex).
    b. Dilute cells from the stock solution in PM to an adequate density for plating
    c. Aspirate the PM from the samples and replace with 500 µL of the cell dilution.
    d. Spread cells over the surface of the wells by sliding back and forth and side to side.
    e. Place samples into an incubator at 37°C and 5% CO_2 for 4 hours to allow for attachment.
    f. Remove the samples from the incubator and place them back into BSC.
    g. Aspirate PM from the samples.
    h. Replace with 500 µL of tri-culture media.
    i. Place samples back in incubator at 37°C and 5% CO_2.

5. Culture Maintenance (Media volume is given for 12 well plates)
    a. At day *in vitro* 3
        i. Replenish the tri-culture media by adding 500 µL of fresh, warmed tri-culture media to each well.
    b. At day *in vitro* 7
        i. Aspirate 500 µL of tri-culture media from each well.
        ii. Replenish the tri-culture media by adding 500 µL of fresh, warmed tri-culture media to each well.
    c. Repeat every 3-4 days through the culture duration.

Microfluidic Device Fabrication

1. Fabricate MEA
    a. Clean 500 µm thick borosilicate glass wafers (University Wafers) via sequential 2 min sonication in acetone, isopropyl alcohol, and deionized water.
    b. Dehydration bake the cleaned wafer at 150ºC for 5 min.
    c. Pattern the trace layer using the negative photoresist NR9-1500PY (Futurrex).
    d. Sputter deposit a 250 nm-thick Au layer over a 160 nm-thick Cr adhesion layer and lift-off to reveal the patterned traces.
    e. Deposit a 250 nm-thick layer of SiO_2 via PECVD to serve as the insulation layer.
    f. Pattern S1813 (Microposit) to define the electrode sites, and briefly immerse in buffered oxide etch to open the insulation layer. *Note: This immersion time will need to be determined based on the size of the openings and thickness of SiO_2.*
    g. Check that the electrode sites are fully opened using a profilometer (Bruker Dektak XT).
    h. Cover with wafer with S1813 to protect the surface, dice the wafer, and remove the S1813 with acetone to obtain completed MEAs.

2. Microfluidic Master Mold Fabrication
    a. Clean a 500 µm thick Si wafer via sequential 2 min sonication in acetone, isopropyl alcohol, and deionized water.
    b. Dehydration bake the cleaned wafer at 150ºC for 5 min.
    c. Pattern alignment marks with S1813 and sputter with an 160 µm-thick layer of Cr.
    d. Lift-off the S1813 with acetone to reveal the Cr alignment marks.
    e. Pattern the microchannels with SU-8 6005 (Kayaku Advanced Materials) spun to the appropriate thickness. *Note: Spin speeds will be dependent on the desired height of the microchannels. For 1.5 µm channels spin at 8000 rpm for 45 s.*
    f. Pattern the cell culture chambers with SU-8 2050 spun to a thickness of 75 µm.
    g. Hard bake the mold for 1 h at 250ºC to improve the longevity of the mold.
    h. Confirm the heights of the features using a profilometer.
3. Soft Lithography
    a. Fix the master mold in a 100 mm Ø petri dish with double sided tape.
    b. Mix 70 mL of PDMS (1:10 curing agent to PDMS by weight; Slygard 184) and place in a vacuum chamber for 1 h to remove air bubbles. *Note: Only the first pour of PDMS requires 70 mL in order to completely fill the petri dish, subsequent pours should only require ~35 mL as only the portion above the master mold needs to be filled.*
    c. Pour over master mold and place back into the vacuum chamber for 30 min to remove air bubbles.
    d. Cure PDMS on a hot plate at 95ºC for 1.5 h.
4. Integradted Microfluidic and MEA Device Assembly.
    a. Cut out PDMS from master mold and trim excess PDMS to form the final platform.
    b. Punch out the fluidic ports using a 3 mm Ø biopsy punch.

c. Remove any particles from the PDMS platform using clear tape and clean with 70% EtOH and dry under nitrogen flow.
d. Clean the corresponding MEA using 70% EtOH and dry under nitrogen flow.
e. Treat the PDMS platform (feature side up) and MEA with air plasma at 10 W for 2 min.
f. Remove from the air plasma chamber and cover both the PDMS platform and MEA with 70% EtOH.
g. Place the PDMS platform over the MEA and align the microchannels over the electrodes under a dissection microscope.
h. Place the aligned device in a vacuum chamber for 1 h to remove the EtOH solution and permanently bond the PDMS platform to the MEA.
i. Treat the bonded devices with air plasma at 30 W for 10 min to make the surfaces hydrophilic and sterilize the devices.
j. Quickly transfer to the BSC and fix 8 mm Ø glass cloning cylinders over the fluidic ports using vacuum grease.
k. Add PLL solution into the microfluidic device and incubate for 4 h at 37°C and 5% CO_2.
l. Wash each device 6x with sterile DI water and cover with PM until use.

ImageJ Macros

The following macros were used during image analysis.

Cell count using DAPI at 100x magnification

```
macro "Full IsoData Analysis" {
    G_Sdir = getDirectory("Choose a Directory ");
    list = getFileList(G_Sdir);
    for(i=0; i< list.length ;i++) {
```

```
                Analysis(list[i]);
        }
}

function Analysis(img_filename) {
        fullpath_image = G_Sdir + img_filename;
        open(fullpath_image);
        sourceID = getImageID();
        imageTitle=getTitle();
        run("Split Channels");
        selectWindow("C1-"+imageTitle);
        close();
        selectWindow("C2-"+imageTitle);
        close();
        selectWindow("C3-"+imageTitle);
        close();
        selectWindow("C4-"+imageTitle);
        run("Subtract Background...", "rolling=50");
        run("Auto Threshold", "method=IsoData");
        run("Median...", "radius=2");
        run("Watershed");
        run("Analyze Particles...", "size=50-Infinity summarize");
        close();
}
```

Astrocyte and neurite % area coverage

```
macro "Full IsoData Analysis" {
	G_Sdir = getDirectory("Choose a Directory ");
	list = getFileList(G_Sdir);
	for(i=0; i< list.length ;i++) {
		Analysis(list[i]);
	}
}

function Analysis(img_filename) {
	fullpath_image = G_Sdir + img_filename;
	open(fullpath_image);
	sourceID = getImageID();
	for(i=1; i<5; i++) {
		Stack.setChannel(i);
		run("Subtract Background...", "rolling=50");
		run("Auto Threshold", "method=Huang");
		run("8-bit");
		run("Median...", "radius=2");
		run("Analyze Particles...", "summarize");
	}
	close();
}
```

Synaptic Puncta Count

```
macro "Full IsoData Analysis" {
	G_Sdir = getDirectory("Choose a Directory ");
```

```
	list = getFileList(G_Sdir);
	for(i=0; i< list.length ;i++) {
		Analysis(list[i]);
	}
}

function Analysis(img_filename) {
	fullpath_image = G_Sdir + img_filename;
	open(fullpath_image);
	sourceID = getImageID();
	imageTitle=getTitle();
	run("Split Channels");
	selectWindow("C1-"+imageTitle);
	close();
	selectWindow("C4-"+imageTitle);
	close();
	selectWindow("C2-"+imageTitle);
	run("Subtract Background...", "rolling=50");
	run("Auto Threshold", "method=Moments white");
	run("Median...", "radius=2");
	selectWindow("C3-"+imageTitle);
	run("Subtract Background...", "rolling=50");
	run("Auto Threshold", "method=Moments white");
	run("Median...", "radius=2");
	imageCalculator("AND create", "C2-"+imageTitle,"C3-"+imageTitle);
	selectWindow("C2-"+imageTitle);
```

```
        run("Convert to Mask");
        run("Watershed");
        selectWindow("C3-"+imageTitle);
        run("Convert to Mask");
        run("Watershed");
        selectWindow("Result of C2-"+imageTitle);
        run("Convert to Mask");
        run("Watershed");
        selectWindow("C2-"+imageTitle);
        run("Analyze Particles...", "size=0.1-Infinity summarize overlay");
        close();
        selectWindow("C3-"+imageTitle);
        run("Analyze Particles...", "size=0.1-Infinity summarize overlay");
        close();
        selectWindow("Result of C2-"+imageTitle);
        run("Analyze Particles...", "size=0.05-Infinity summarize overlay");
        close();
}
```

Statistical Analysis

Generalized R codes used for statistical analyses are given below.

Hierarchical linear regression analysis

```
# Import Data
Aggrigate_Data_Full_R <- read_excel("data file")
View(Aggrigate_Data_Full_R)
```

```
Aggrigate_Data_Full_R$Nuclei <- Aggrigate_Data_Full_R$Channel_Total +
Aggrigate_Data_Full_R$Oppo_Total

#Plot all columns to check for normality
par(mfcol=c(3,3))
hist(Aggrigate_Data_Full_R$Seeding, main = "Seeding")
hist(Aggrigate_Data_Full_R$Height, main = "Height")
hist(Aggrigate_Data_Full_R$Width, main = "Width")
hist(Aggrigate_Data_Full_R$Length, main = "Length")
hist(Aggrigate_Data_Full_R$Axon, main = "Axon")
hist(Aggrigate_Data_Full_R$Dendrite, main = "Dendrite")
hist(Aggrigate_Data_Full_R$Astrocyte, main = "Astrocyte")
hist(Aggrigate_Data_Full_R$Channel_Total, main = "Nuceli in Channel")
hist(Aggrigate_Data_Full_R$Oppo_Total, main = "Nuclei Crossing Channel")

#Normalize data
normalize <- function(x){
  return((x-min(x))/(max(x)-min(x)))
}
Aggrigate_Data_Full_R$Seeding_norm <- normalize(Aggrigate_Data_Full_R$Seeding)
Aggrigate_Data_Full_R$Height_norm <- normalize(Aggrigate_Data_Full_R$Height)
Aggrigate_Data_Full_R$Width_norm <- normalize(Aggrigate_Data_Full_R$Width)
Aggrigate_Data_Full_R$Length_norm <- normalize(Aggrigate_Data_Full_R$Length)
Aggrigate_Data_Full_R$Axon_norm <- normalize(Aggrigate_Data_Full_R$Axon)
Aggrigate_Data_Full_R$Dendrite_norm <- normalize(Aggrigate_Data_Full_R$Dendrite)
Aggrigate_Data_Full_R$Astrocyte_norm <- normalize(Aggrigate_Data_Full_R$Astrocyte)
```

```
Aggrigate_Data_Full_R$Channel_Total_norm <-
normalize(Aggrigate_Data_Full_R$Channel_Total)
Aggrigate_Data_Full_R$Oppo_Total_norm <- normalize(Aggrigate_Data_Full_R$Oppo_Total)
Aggrigate_Data_Full_R$Nuclei_norm <- normalize(Aggrigate_Data_Full_R$Nuclei)

#Generate normalized data frame
Norm_data <- Aggrigate_Data_Full_R %>% select(Seeding_norm, Height_norm, Width_norm,
Length_norm, Axon_norm, Dendrite_norm, Astrocyte_norm, Channel_Total_norm,
Oppo_Total_norm, Nuclei_norm)

#Axon analysis (This code can be repeated for other features)
Axon_model <- lm(Axon_norm ~ Seeding_norm + Height_norm + Length_norm + Width_norm,
data = Norm_data)
Axon_best <- ols_step_best_subset(Axon_model)
plot(Axon_best)
Axon_best
Am0 <- lm(Axon_norm ~ 1, data = Norm_data)
Am1 <- lm(Axon_norm ~ Seeding_norm, data = Norm_data)
Am2 <- lm(Axon_norm ~ Seeding_norm + Width_norm, data = Norm_data)
Am3 <- lm(Axon_norm ~ Seeding_norm + Width_norm + Length_norm, data = Norm_data)
Am4 <- lm(Axon_norm ~ Seeding_norm + Width_norm + Length_norm + Height_norm, data =
Norm_data)
anova(Am0)
anova(Am1, Am2, Am3, Am4)
summary(Am1)
summary(Am2)
```

```
summary(Am3)

summary(Am4)
```

Linear mixed effects model to analyze electrophysiological features

```
# Import Data

ActR <- read_excel("data file")

View(ActR)


# Analyze data

lmer_fit <- lmer(Burst ~ Culture*bs(Time) + (1 | ID), data = ActR)

em <- ref_grid(lmer_fit,

               at = list(

                 Culture = c("Co", "Tri"),

                 Time = c(7, 10, 14, 17, 21),

                 ~ Burst | Time

               ))

contrast(em, "pairwise", adjust = NULL)
```